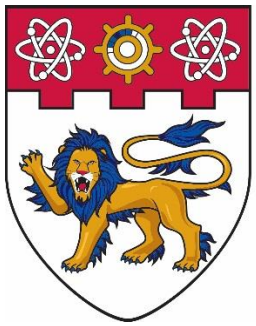

NANYANG TECHNOLOGICAL UNIVERSITY
SINGAPORE

TRANSPORT AND FATE OF SILVER NANOPARTICLES IN THE AQUATIC ENVIRONMENT

W. W. B. I. P. M. FERNANDO
Interdisciplinary Graduate School
Nanyang Environment and Water Research Institute

TRANSPORT AND FATE OF SILVER NANOPARTICLES IN THE AQUATIC ENVIRONMENT

W. W. B. I. P. M. FERNANDO

Interdisciplinary Graduate School
Nanyang Environment and Water Research Institute

A thesis submitted to the Nanyang Technological University in partial fulfillment of the requirement for the degree of
Doctor of Philosophy

2019

Statement of Originality

I hereby certify that the work embodied in this thesis is the result of original research, is free of plagiarised materials, and has not been submitted for a higher degree to any other University or Institution.

05. 08. 2019

. . . . . .

Date

. . . . . .

W.W.B.I.P.M. FERNANDO

Supervisor Declaration Statement

I have reviewed the content and presentation style of this thesis and declare it is free of plagiarism and of sufficient grammatical clarity to be examined. To the best of my knowledge, the research and writing are those of the candidate except as acknowledged in the Author Attribution Statement. I confirm that the investigations were conducted in accord with the ethics policies and integrity standards of Nanyang Technological University and that the research data are presented honestly and without prejudice.

05. 08. 2019

. . . . . .

Date

. . . . . .

Assoc. Prof. Zhou Yan

Authorship Attribution Statement

This thesis contains material from four paper(s) published in the following peer-reviewed journal(s) where I was the first author.

Chapter 5 is published as Fernando, I., & Zhou, Y. (2019). Impact of pH on the stability, dissolution and aggregation kinetics of silver nanoparticles. *Chemosphere, 216*, 297-305.
The contributions of the co-authors are as follows:

- Assoc. Prof Zhou Yan provided the initial project direction and revised the manuscript drafts.
- I designed the study, performed all the laboratory work at the Advanced Environmental Biotechnology Centre (AEBC) and School of Civil and Environmental Engineering, analyzed the data and prepared the manuscript.
- All microscopy, including sample preparation, was conducted by me in the Facility for Analysis, Characterization, Testing and Simulation.

Chapter 6 is published as Fernando, I., & Zhou, Y. (2019). Concentration dependent effect of humic acid on the transformations of silver nanoparticles. *Journal of Molecular Liquids*, 284, 291-299.
The contributions of the co-authors are as follows:

- Assoc. Prof Zhou Yan provided the initial project direction and revised the manuscript drafts.
- I designed the study, performed all the laboratory work at the Advanced Environmental Biotechnology Centre (AEBC) and School of Civil and Environmental Engineering, analyzed the data and prepared the manuscript.
- All microscopy, including sample preparation, was conducted by me in the Facility for Analysis, Characterization, Testing and Simulation.

Chapter 4 is published as Fernando, I., Qian, T. & Zhou, Y. (2019), Long term impact of surfactants & polymers on the colloidal stability, aggregation and dissolution of Silver Nanoparticles. *Environmental Research*, 179, 108781.

The contributions of the co-authors are as follows:

- Assoc. Prof Zhou Yan provided the initial project direction and revised the manuscript drafts.
- Dr. Qian Tinting helped in the analysis of FTIR results.
- I designed the study, performed all the laboratory work at the Advanced Environmental Biotechnology Centre (AEBC) and School of Civil and Environmental Engineering, analyzed the data and prepared the manuscript.
- All microscopy, including sample preparation, was conducted by me in the Facility for Analysis, Characterization, Testing and Simulation.

Chapter 7 is published as Fernando, I., Lu, D. & Zhou, Y., Interactive influence of extracellular polymeric substances (EPS) and electrolytes on the colloidal stability of silver nanoparticles. *Environmental Science: Nano*.

The contributions of the co-authors are as follows:

- Assoc. Prof Zhou Yan provided the initial project direction and revised the manuscript drafts.
- Ms. Lu Dan helped in EPS characterization and statistical correlation.
- I designed the study, performed all the laboratory work at the Advanced Environmental Biotechnology Centre (AEBC) and School of Civil and Environmental Engineering, analyzed the data and prepared the manuscript.

05. 08. 2019

. . . . . .

Date

. . . . . .

W.W.B.I.P.M. FERNANDO

Acknowledgement

I would like to express my sincere gratitude to my dear supervisor, Assoc. Prof. Zhou Yan, for all her support, guidance and motivation rendered to succeed in my post graduate studies.

I am grateful to my co-supervisor Dr. Eileen Fong and Mentor Prof. Liu Yu and the members of the Thesis Advisory Committee (TAC) for their kind support given to me whenever requested.

I would also like to thank Nanyang Environment and Water Research Institute (NEWRI) and Interdisciplinary Graduate School (IGS) for supporting me in financial means to continue on my graduate studies.

I would also like to thank Dr. Tay Yee Yan, Dr. Dong Feng and Dr. Qian Tingting for their support during my PhD journey. Furthermore, I would also like to thank Zhu Wenyu, Yan Wangwang, Wu Dan, Desmond and Lu Dan my research group members for extending support and helping hand whenever it was requested.

The administration and technical support given by Ms Hera Adam, the laboratory staff at Advanced Environment and Biotechnology Centre (AEBC), Ms. Maria Chong and Ms. Pearlyn Shee at the Central Environmental Science and Engineering Laboratory (CESEL), Environment Laboratory in School of Civil and Environmental Engineering (CEE) and Facility for Analysis, Characterization, Testing and Simulation at School of Materials Science and Engineering (MSE) is highly appreciated and I am very grateful for their tremendous efforts in helping me during my research study.

Last but not least, my special appreciation and thanks would go to my family, my parents for their affection, care and understanding when I stay far away from home. I would like to thank my husband, Hasith Karunasekera for his love, continuous understanding, trust and encouragement during the most stressful period of my life.

Abstract

The invention of new materials to enhance various product qualities has grabbed the consumer attention. Among them, engineered nanoparticles play a pivotal role due to their different physical and chemical characteristics. Silver nanoparticles (AgNPs), recorded as widely used in consumer products due to its unique antimicrobial properties undergo different transformations when present in the aquatic environment. The transformations of AgNPs will vary according to their physical properties and the chemical properties of the solution matrix they are present. The physical properties governing the transformations include size, shape, structure and the surface coatings. The chemical properties determining the transformation of AgNPs include pH, ionic strength, dissolved organic matter and extracellular polymeric substances. Understanding the transformations of AgNPs is important in predicting the transport and fate of the AgNPs in the environment and design adequate removal mechanisms.

This thesis investigates the impact of different chemical properties of the matrix including solution pH, humic acid, protein, polysaccharides and extracellular polymeric substances on the transformations of AgNPs including aggregation, dissolution and colloidal stability. Freshly synthesized uncoated AgNPs were used during all the experiments to avoid the possible interferences resulting from the coatings and other chemicals. When assessing the impact of these factors the prominence was given to study the environmentally relevant conditions either in the natural environment or wastewater, which will provide important implications on the fate of AgNPs in the respective pathways. Furthermore, the long-term stability induced by the surfactants and polymers, which are used as coating agents in the transport and storage of AgNPs was also assessed. Commonly used surfactants and polymers representing the different categories were used in the experiments. Multitude of characterization and analytical techniques were used during the experiments including spectrometry, DLS, ICP-MS, TEM, EDX and FTIR. Finally, the suitability of a burgeoning technique, liquid cell transmission electron microscopy to track the time resolved changes in the transformations of the AgNPs was developed. The results obtained during the study provide an overview on the impact of the above-mentioned factors on the temporal changes in the transformations of the AgNPs in the aquatic matrices. The conclusions obtained during the study are important in predicting the transport and fate of AgNPs in

the water, hence, the behavior of the engineered NPs in the aquatic environment. The insights obtained during the study can be utilized in assessing the life cycle of AgNPs and subsequently their overall impact on the nature.

Table of Contents

List of figures

List of tables

List of Acronyms

AE	Attachment Efficiency
AgNPs	Silver Nanoparticles
BSA	Bovine Serum Albumin
CCC	Critical Coagulation Concentration
DLS	Dynamic Light Scattering
DLVO theory	Derjaguin-Landau-Verwey-Overbeek Theory
DOM	Dissolved Organic Matter
EDS	Energy Dispersive Spectroscopy
EPM	Electrophoretic mobility
EPS	Extracellular Polymeric Substances
FE-SEM	Field Emission Scanning Electron Microscopy
FTIR	Fourier Transform Infra-Red Spectroscopy
HA	Humic Acid
HRT	Hydraulic Retention Time
ICP-OES	Inductively Coupled Plasma-Optical Emission Spectroscopy
ICP-MS	Inductively Coupled Plasma-Mass Spectroscopy
NOM	Natural Organic Matter
NPs	Nanoparticles
NTA	Nanoparticle Tracking Analysis
ROS	Reactive Oxygen Species
SA	Sodium Alginate
SPR	Surface Plasmonic Response
SRT	Sludge Retention Time
TEM	Transmission Electron Microscopy
TOC	Total Organic Carbon
WWTP	Waste Water Treatment Plant
XDLVO Theory	Extended Derjaguin-Landau-Verwey-Overbeak Theory
XPS	X-Ray Photoelectron Spectroscopy

List of Publications

Journal Papers

1. Fernando, I., & Zhou, Y. (2019). Impact of pH on the stability, dissolution and aggregation kinetics of silver nanoparticles. *Chemosphere*, *216*, 297-305.

2. Fernando, I., & Zhou, Y. (2019). Concentration dependent effect of humic acid on the transformations of silver nanoparticles. *Journal of Molecular Liquids*, 284, 291-299.

3. Fernando, I., Qian T. & Zhou, Y. (2019) Long term impact of surfactants & polymers on the colloidal stability, aggregation and dissolution of Silver Nanoparticles. *Environmental Research*, 179, 108781.

4. Fernando, I., Lu D. & Zhou, Y. (2020) Interactive influence of extracellular polymeric substances (EPS) and electrolytes on the colloidal stability of silver nanoparticles. *Environment Science: Nano.*

5. Fernando, I., & Zhou, Y.: Impact of Polysaccharides and Protein on the colloidal stability of silver nanoparticles. – Under preparation

6. Fernando, I., Tay, Y. Y., Karunasekera, H. & Zhou, Y.: pH induced interactions of AgNPs in the aquatic matrices observed using in situ liquid cell transmission electron microscopy. – Under preparation

1 Introduction

This chapter provides a brief overview on the background, objectives and contributions of the study followed by the organization of the thesis.

1.1 Background

The rapid increase in the utilization of nanoparticles (NPs) especially in consumer products have paved way for them to leach into the aquatic environments. The seepage of NPs into the aquatic environments has resulted in their presence in the natural aquatic bodies and wastewater treatment plants (WWTP). From hundred types of NPs used in manufacturing consumer products, silver nanoparticles (AgNPs) play a pivotal role being recorded as the type of NPs that is highly used. When the AgNPs are present in the water, they tend to undergo a variety of transformations such as aggregation, dissolution, sedimentation and precipitation. These transformations vary depending on a number of different physical and chemical factors including pH, ionic strength, dissolved organic matter, extracellular polymeric substances and the characteristics of the NPs such as shape, structure, size, and surface coating. Due to these complexities, it is difficult to use the traditional theories of colloidal science only to predict the transformations of AgNPs. Therefore, this study focuses on studying the impacts of different environmental factors on the aggregation, dissolution and the colloidal stability of AgNPs and their effect on the transport and fate of AgNPs in the aquatic environment.

1.2 Objectives and Scope

The main objectives of this study include :

(1) To evaluate the impact of surfactants and polymers, which are used as coatings during the transport and storage of NPs, on the temporal changes of the colloidal stability of AgNPs

(2) To examine the effect of pH, ionic strength, dissolved organic matter (DOM) : Humic acid, proteins and polysaccharides and extracellular polymeric substances on the colloidal stability of AgNPs

(3) To assess the suitability of an emerging technique, in situ liquid cell transmission electron microscopy on tracking the time resolved changes in the transformations of AgNPs

1.3 Major contributions of the study

1. Cetyl trimethyl ammonium bromide (CTAB), Tween 20, polyvinyl pyrrolidone (PVP) and polyethylene glycol (PEG) are among the commonly used surfactants and polymers to stabilize AgNPs. The cationic surfactant, CTAB was able to produce a monomodal particle size distribution in a prolonged period without

affecting dissolution. In the presence of Tween 20, a non-ionic surfactant, dissolution was promoted in the long run and the particles were preserved with minimal aggregation. In the presence of the polymers, PVP and PEG, the particle structure was not affected even though dissolution was observed. The interactions of AgNPs with surfactants and polymers could significantly affect their transformations and fate in the aquatic environment

2. The solution pH modifies the surface charge and the oxidative dissolution of AgNPs. As a result, the particle behavior varied in acidic and alkaline conditions. The particle size decreased with the increasing pH at a given time frame resulting in lower aggregation in the higher pH regime and increased particle stability. These results have been further proved with the direct evidence obtained using time resolved in situ imaging acquired through Liquid cell transmission electron microscopy (LCTEM). Furthermore, the magnitude of the impact of the pH on the particle properties is higher than the impact of the dissolved oxygen concentration. The derived empirical formulae reflect that the AgNP oxidation depends on both dissolved oxygen and protons while the AgNP dissolution increasing with the increase of either of these. Overall, our results highlight the impact of the solution pH on the evolution of the properties of AgNPs over the time.
3. Influence of humic acid (HA) concentration (0–250mg/L) on the colloidal stability and dissolution of AgNPs was evaluated. AgNPs underwent oxidative dissolution and aggregation disturbing their colloidal stability. In the HA concentration range of 1–20 mg/L, HA stabilized AgNPs due to the inhibition of the release of ionic Ag ensuring the persistence of AgNPs in the aquatic environment for a longer period. At higher concentrations of HA (20–250mg/L) in the soil environment, AgNPs were wrapped by the HA molecules, increasing the hydrodynamic diameter of the AgNPs. Due to the suppression of dissolution of AgNPs, primary particles remained stable in the environment for a prolonged period with no change in the primary particle size and morphology. Furthermore, it was observed that ionic Ag in the solution can be reduced to form fresh, secondary AgNPs at the lower levels of HA in the aquatic environment, in the presence of sunlight.
4. The colloidal stability of AgNPs was significantly affected by the electrolytes following the Derjaguin-Landau-Verwey-Overbeek (DLVO) theory. Lower

critical coagulation concentration (CCC) for AgNPs was observed in divalent electrolytes. Three types of EPS namely, soluble EPS (SB- EPS), loosely bound EPS (LB-EPS) and tightly bound EPS (TB-EPS) extracted from activated sludge, were added into electrolytes that containing AgNPs to investigate the potential different impacts on AgNPs transformation. Overall, the presence of all types of EPS reduced the aggregation rate and increased the CCC values in $NaNO_3$ and low concentrations of $Ca(NO_3)_2$ (0.05 – 10 mM) solutions. When the $NaNO_3$ concentration was above 12 mM, the attachment efficiency of the AgNPs was below one, depicting that EPS adsorbed on AgNPs leading to steric repulsion, and effectively stabilizing the AgNP suspension. However, the presence of EPS increased the AgNPs aggregation rate at high $Ca(NO_3)_2$ concentrations (10 – 40 mM), which can be caused due to the aggregation of the dissolved EPS via intermolecular bridging linking the AgNPs and aggregates together. Among the three types of EPS used in the study, LB-EPS effectively stabilized the AgNPs irrespective of the electrolyte mainly due to the low presence of the hydrophilic dissolved organic matter in LB-EPS.

5. Influence of the polysaccharides and protein on the colloidal stability and dissolution of AgNPs was evaluated in a series of long-term experiments. Sodium alginate (SA) as a model polysaccharide and bovine serum albumin (BSA) as a model protein were used in the experiments in variable concentrations. SA and BSA stabilized the AgNPs via two different mechanisms. An increase in the hydrodynamic diameter was observed in the presence of both the organic compounds, even though aggregation was not observed. The surface modification of AgNPs induced by SA reduced the AgNP dissolution. However, the SA coating was not permanent, as SA lacks the ability to produce strong ionic Ag ligands. In the presence of BSA, ionic Ag released by the AgNPs were chelated by the constituents in the BSA molecule, followed by coating the AgNPs. Due to the BSA's high affinity towards ionic Ag, it was chemically adsorbed on the AgNP surface. As such, increased dissolution was observed in the presence of BSA. Therefore, both SA and BSA modified the AgNP surface and increased the colloidal stability. In summary, the stability of AgNPs is higher in the presence of protein compared to the polysaccharides.

1.4 Organization of the thesis

This thesis consists of ten chapters as mentioned below.

(1) Chapter 1 presents a brief introduction on the background and the objectives of this study.
(2) Chapter 2 presents a comprehensive literature review, covering an overview on the current knowledge and the future research needs.
(3) Chapter 3 presents the details about the materials used during the experiments and the experimental methods which are common to the chapters with experimental results.
(4) Chapter 4 investigates the impact of different surfactants and polymers on the long-term colloidal stability of AgNPs.
(5) Chapter 5 presents the study on the impact of pH on the aggregation of AgNPs in the aquatic environment.
(6) Chapter 6 consists of the study assessing the concentration dependent impact of humic acid on the transformations of AgNPs.
(7) Chapter 7 discusses about the interactive influence of electrolytes and the extracellular polymeric substances on the colloidal stability of AgNPs.
(8) Chapter 8 focuses on understanding the impact of protein and polysaccharide on the temporal changes of the colloidal stability of AgNPs using sodium alginate (SA) and bovine serum albumin (BSA) as a model polysaccharide and protein respectively.
(9) Chapter 9 investigates the application of a novel technique, liquid cell transmission electron microscopy to evaluate the time resolved changes in the interactions of AgNPs in the aquatic matrix.
(10) Chapter 10 summarizes the major findings of this study and provides recommendations for future investigation.

2 Literature Review

This chapter provides a comprehensive literature review on the research topic to understand the knowledge gap and to decide on the research directions.

2.1 Background

Due to the industrialization and mass scale production in the past decade, NPs are now widely utilized in many products. They are used in paints, catalysts, coatings, cosmetics, skin cream, biomedicine, toothpaste and many other applications. Unique physical and chemical characteristics, which include optical, electrical and magnetic properties make the utilization of NPs ideal in manufacturing industries. Moreover, NPs have been used as a semiconductor, fuel cell electrolyte, UV absorber, antioxidant, polishing and coating chemical. NPs have been utilized vividly in consumer products, such as anti-bactericide coating, sunscreen and other industrial, military and medical applications. The commercialization and industrialization of NPs have made the release of these compounds to the surrounding environments. Recently, studying the fate and transport of NPs in the environment has attracted the attention of researchers [1]. NPs can inhibit the biodegradation, nitrification and anaerobic digestion process[2],[3]. Agglomeration and adsorption of NPs are the main mechanisms that play a major role in the transformation of NPs in the aquatic environment [4].

From hundred types of NPs used in manufacturing consumer products, AgNPs play a pivotal role being recorded as the type of NPs that is highly used in manufacturing consumer products such as cosmetics and clothing due to their unique antimicrobial properties. When the AgNPs are present in the aquatic environment, they tend to undergo a variety of transformations such as aggregation, dissolution, sedimentation, and precipitation. The degree of these transformations varies depending on a number of different physical factors such as shape, structure, size, and surface coating and chemical factors including the solution pH, ionic strength, dissolved organic matter (DOM) and extracellular polymeric substances (EPS). Among the other factors that affect the transport and fate of AgNPs in the aquatic environment, the chemical speciation [5, 6] and the surface charge of the AgNPs play an important role, which will affect their chemical and biological interactions in the matrix [7, 8]. In order to vividly address these complexities, it is not sufficient to use only the traditional theories of colloidal science and experimental methods to predict the transformations of AgNPs. Hence, this review addresses the current theoretical and experimental knowledge on understanding the impact of different factors on the aggregation of AgNPs in the aquatic environment and proposes future directions for research.

2.2 Importance of AgNPs

Silver (Ag) is considered as a naturally occurring type B soft metal [9, 10], which is widely known for its admirable antimicrobial activities [11, 12], predominantly due to the release of ionic Ag in the aquatic environment [13, 14]. Even though ionic Ag is considered as one of the most toxic components in the fresh water environment [15], its derivatives are widely used for different applications in the health industry. Silver Nitrate ($AgNO_3$) and Silver Sulphadiazine (SSD) [16] are commonly used in medicinal products to treat or prevent diseases[17] caused by microorganisms such as bacteria [18], fungi [19] and virus [20].

Due to its strong antimicrobial performance, it is listed as a toxic heavy metal by most of the environmental regulating authorities [21, 22]. For example, the US EPA has set the maximum level for Ag in drinking water as 0.1mg/L and the permissible level for aquatic life in freshwater and salt water as 3.2 μg/L and 1.9 μg/L respectively [23, 24]. The leachate with a Ag concentration higher than 5mg/L is considered as hazardous during the Toxicity Characteristic Leaching Procedure (TCLP) [25]. Not only in United States, but also the countries in the other parts of the world have declared safe occupational Ag exposure limits. For example, in Austria and Japan the Permissible Exposure Limit (PEL) for Ag in air is 0.01 mg/m^3 and 0.1 mg/m^3 in United Kingdom, Australia and Sweden [26].

Among the types of NPs which are highly used in the industrial applications, AgNPs play a major role. These are widely used as delivery or antimicrobial agents in day to day consumer products such as clothes, dietary supplements and food packaging [27]. The reason for higher usage include its strong antibacterial activity due to the higher specific surface area [28] and the release of ionic Ag during the dissolution [29]. According to a market survey done on the global application of AgNPs:[30], it is estimated that the market of AgNPs will increase up to US$ 2,415.5 Million by 2023, which will potentially increase its release to the environment as well.

AgNPs also termed as nano Ag is basically, zero valent (Ag^0) particles with a size of 1-100 nm [31] in at least one of its dimensions [32-34]. Apart from the dimensions, AgNPs come in different morphologies such as spheres, rods and cubes [35-37]. AgNPs are

usually synthesized using chemical reduction methods where a Ag salt such as Silver nitrate ($AgNO_3$) [13, 38, 39], Silver perchlorate ($AgClO_4$) [40] or Silver tetrafluoroborate ($AgBF_4$) [40, 41] is reduced using ethylene glycol [42], ethanol [43], glucose [39] or Sodium borohydride ($NaBH_4$) [12, 44]. In order to prevent aggregation during the synthesis of AgNPs, coating agents or stabilizers such as polyvinyl pyrolidone (PVP) [42, 45], polysaccharide [46], polyvinyl alcohol (PVA) [14], polyethylene glycol (PEG) [47] or citrate [48] are commonly used. Rather than that, several other methods such as electrochemical reduction [49], irradiation [50] and biological reduction [51] can also be utilized in the synthesis of AgNPs.

During the transport and storage of AgNPs, its colloidal stability should be maintained to avoid aggregation, as the generation of larger aggregates results in a loss of its antibacterial activity [52, 53]. Therefore, different types of surfactants and polymers are used to coat AgNPs to avoid aggregation during the transport and storage. However, the long-term stability of AgNP dispersions, in different surfactants and polymers have barely discussed and compared.

Even though AgNPs are manufactured using different methods, eventually they are released to sewage [34], wastewater treatment plant [54], solid waste treatment facilities or natural aquatic systems [4]. According to Kaegi et al. [55], AgNPs undergo different transformations throughout the process of wastewater treatment and hence released to the natural environment in a different form. Therefore, there is a great concern that AgNPs when present in higher concentration can be harmful to aquatic life. In order to understand the extent of harmful effects, it is vital to understand the different mechanisms associated with the interactions of AgNPs in the aquatic environment.

2.3 Interactions of AgNPs in the aquatic environment

The commonly observed interactions of AgNPs are dissolution, precipitation, aggregation and formation of complexes. During the dissolution, AgNPs tend to release ionic Ag to the solution [56], [57]. The rate and extent of dissolution of AgNPs will depend on their physicochemical properties which include shape [58], size [59], concentration [60] and surface functionalization or coating [61]. Apart from that the solution temperature also plays a major role in the dissolution of AgNPs since it requires

energy [62]. When AgNPs are introduced to a system, it will take several seconds to minutes to even days to reach a stable condition. As described by Kittler et al., the small changes which the NPs undergo are often neglected during the classical analytical methods such as microscopy and spectroscopy. This is due to their insensitivity to the release of ions as the particle diameter undergoes minor changes during the dissolution [56].

If there are any anions such as chlorides, sulphides etc. present in the aquatic matrix, there is a higher tendency for AgNPs to form precipitates. The details on the solubility product and the enthalpy of formation of common Ag precipitates are mentioned in the Table 2.1.

Table 2.1 Details about common Silver precipitates

Silver precipitate	**Solubility product (K_{sp}) at 25°C**	**Enthalpy of Formation (ΔH_f^0 at 25°C, kJmol^{-1})**
Silver chloride (AgCl)	1.77×10^{-10}	-127
Silver sulphide (Ag_2S)	8×10^{-51}	-31.8
Silver bromide (AgBr)	5.35×10^{-13}	-100.4
Silver iodide (AgI)	8.52×10^{-17}	-62.4
Silver sulphate (Ag_2SO_4)	1.20×10^{-5}	-717.2
Silver carbonate (Ag_2CO_3)	8.46×10^{-12}	-506.1
Silver chromate (Ag_2CrO_4)	1.1×10^{-12}	-712
Silver iodate ($AgIO_3$)	3×10^{-8}	-166.24

*Source : [63-65]

According to the information presented in the
Table 2.1, most of these precipitates possess a low solubility product constant and a low enthalpy of formation. This indicates that the formation of these types of precipitates requires only a low concentration of the particular ions and low energy. When the precipitates are formed during in the aquatic systems, they tend to sediment to the bottom of the system. Due to the formation of layers [66], the flow of water can be interrupted and result in adverse conditions. Kaegi et al. [67] in the study on effect of silver chloride formed from AgNPs has mentioned about the different transformations

undergone by the Ag precipitates and their effect on the microbial growth[13]. Furthermore, another study shows the differential abilities of the common precipitate, silver chloride in the water [68].

AgNPs tend to form complexes with different types of ions and ligands [69]. Even though this topic is not discussed vividly by the researchers, there are some studies on the effect of the formation of complexes with proteins [70], metal ions [71] etc. The threat which can be posed to human health and the environment due to the different formations by the AgNPs has been discussed by Panyala et al. [72]. The property of formation of complexes of Ag has been utilized by the industries in manufacturing different types of antimicrobial agents which are used as antibiotics and in many other applications [73-75].

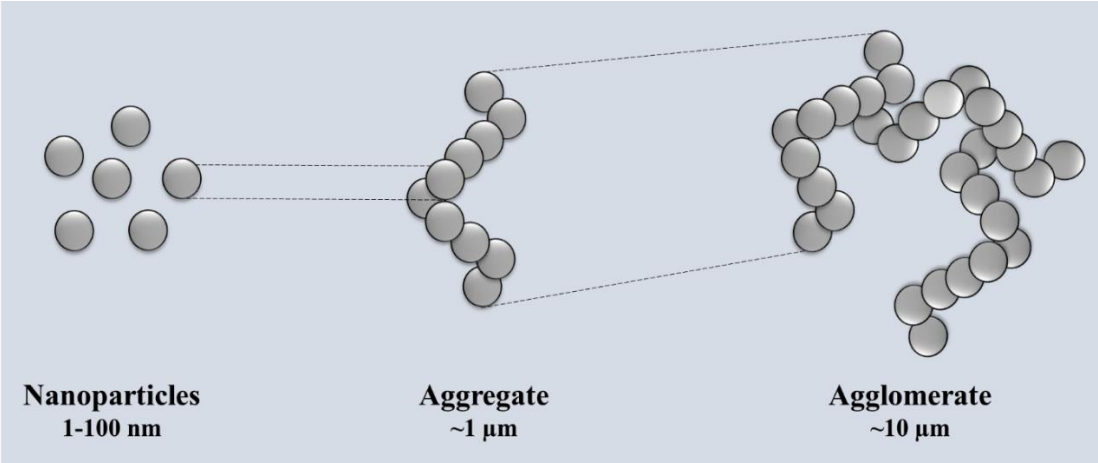

Figure 2.1 Difference of Aggregation and Agglomeration of NPs.

Aggregation is also considered as one of the major transformations that takes place when the AgNPs are introduced in to the aquatic systems. The difference between the aggregation and agglomeration can be clearly seen in the Figure 2.1. Aggregation as shown in Figure 2.1, which takes place between particles in the size of 1-100 nm, is a process where NPs tend to form clusters (~1µm) due to the different interactions such as electrostatic attraction and hydrogen bonding[76]. The sets of aggregates then tend to form agglomerates due to Van der Waals forces which is in the size range of 1-100 µm. The extent of aggregation depends on a series of factors which have been discussed in the next chapters. Recently studying the aggregation behavior and the colloidal stability of AgNPs has attracted the attention of many researchers [7, 77]. From the

previously mentioned transformations of AgNPs, aggregation is the least understood and discussed topic, which makes it important to study the mechanisms involved with it.

2.4 Aggregation of NPs

When present in environmental or engineered systems NPs can be considered as dispersions of primary particles, which tend to form aggregates or clusters up to several microns in size [78] due to the interactions among them. Therefore, the aggregation of NPs is important in determining the reactivity, toxicity, risk, transport and fate in the environment [76]. Many recent studies have directed their attention towards understanding the phenomenon of aggregation in the aquatic environment, even though it was not considered critical previously. The researchers have started applying the colloidal science principles based on the Derjaguin-Landau-Verwey-Overbeak (DLVO) Theory to understand the aggregation of NPs in different conditions. Furthermore, particles released to the aquatic environment undergo different degrees of aggregation due to the different conditions in the solution matrix governed by pH, dissolved ions, DOM, EPS etc.

2.4.1 Types of aggregation

Nanoparticle	Brownian	Shear-induced	Shear-induced	Turbulent
↔	↔	↔	↔	
Surface forces	Aggregation	restructuring	Aggregation	reacting flow
<1nm	1-100 nm	0.1-10 μm	0.01 – 10 mm	0.01-1 m
Quantum	Molecular	Brownian	Direct Numerical	Quantum
Chemistry	Simulations	Dynamics	Simulations	Chemistry

Figure 2.2 Aggregation of NPs.

Aggregation of NPs occur, when physical processes bring the particle surfaces in contact with each other and a short range of thermodynamic reactions allow the particles to attach to each other. As clearly shown in Figure 2.2, for particles <100nm in size, the long-range forces between the individual NPs are controlled by the Brownian diffusion. When two NPs are in contact with each other, it can result either in attachment or

repulsion. In the context of DLVO Theory[79], this phenomenon can be understood with reference to short range thermodynamic interactions.

There are two types of aggregation namely, homo-aggregation and hetero-aggregation, which can occur in the natural environment with respect to the NPs. Homo-aggregation is the aggregation of two or many particles of the same species. It can be mainly observed in homogeneous particle suspensions that are usually used in laboratory studies to make useful correlations with the theories such as DLVO Theory[80].

In the real environment, there are different kinds of particles present and compared to them the number of NPs will be less. Therefore, the NPs present tend to form attachments with these different kinds of particles such as clay. Hence, this process of formation of aggregates between dissimilar particles is referred to as hetero-aggregation and it is the most important type of aggregation when considering about the manufactured NPs in aquatic systems.

2.4.2 Theory of aggregation

2.4.2.1 Sticking Coefficient (α)

The probability that two particles get attached to each other is given by the sticking coefficient, which is also termed as attachment efficiency (AE) and denoted by α. When α=1, sticking occurs 100% of the time and when α=0.5, sticking occurs 50% of the time. Initial particles attach (α=1) will form large dendritic aggregates, whereas particles sticking only after several collisions (α<1) will tend to form denser and less dendritic aggregates [81].

2.4.2.2 Fractal Dimension (D_f)

Fractal dimension is a concept that is used to describe the aggregate structure. The value of the Fractal Dimension usually falls within the range of 1 – 3, where 1 denotes a line and 3 a sphere, which have been derived from Euclidean dimensions. The values 1, 2 and 3 denote a straight line (eg: x^1), a flat surface (eg: x^2) and a volume (eg: x^3) respectively. Fractal structures in the ideal form will be always self-similar. Under the experimental conditions, homo-aggregation produces aggregates with reasonably

predictable fractal dimensions [82]. Hetero-aggregation usually produces natural fractals which are statistically self-similar over a limited range of length scale making the aggregation state more difficult to predict. But as shown in Figure 2.2, fractal dimensions provide a quantitative interpretation for the aggregation happened in the aquatic environment where the size is greater than 1 nm. The physical properties of the aggregates can influence the bioavailability, toxicity and the reactive surface area. Hence it is important to study the aggregate structure when predicting the fate, transport and toxicity of NP aggregation.

2.4.2.3 DLVO Theory

The total of the attractive and repulsive forces governs the NP attachment according to the classical DLVO theory [83]. It further suggests that these two forces predominantly determine the interactions between the NPs. They are named as attractive van der Waals (vdW) and electro-static double layer (EDL) forces. The Eqn. (2.1) below, shows the vdW attraction experienced by two spheres in suspension [84].

$$\frac{V_{VDW}}{kT} = -\frac{A}{6kT}\left[\frac{2a^2}{s(4a+s)} + \frac{2a^2}{(2a+s)^2} + ln\frac{s(4a+s)}{(2a+s)^2}\right] \qquad (2.1)$$

Since this equation calculates the attraction between two spherical particles, expanded theoretical approaches are required to assess the behavior of the available different types of NPs with different shapes. [85]

EDL depends on the surface charge of the particles the solution chemistry of the surrounding matrix. The radius of the diffuse layer from the surface is governed by the ionic strength of the solution, which gives an indication of the ions present in the solution. High ionic strength compresses the EDL, whereas reduced ionic strength suggests that the EDL ion cloud extends far away from the NPs. The Eqn. (2.2), mentioned below is an expression for two charged spheres in suspension [84].

$$\frac{V_{EDL}}{kT} = \frac{64\pi nkT}{\kappa}\frac{(a+\delta)^2}{(s+2a)}\left[tanh\left(\frac{ze\Psi_d}{4kT}\right)\right]^2 exp^{-\kappa(s-2\delta)} \qquad (2.2)$$

$$where \quad \kappa = \left[\frac{\sum_i^N e^2 z_i^2 n_i}{a_{rs} a_o kT}\right]^{\frac{1}{2}} \tag{2.3}$$

The addition of Eqn. (2.1) and (2.2) sums up the vdW and EDL potentials to decide if the forces are net attractive ($-V_T$) or net repulsive ($+V_T$). In the context of engineered NPs, most of them will have an organic coating. Therefore, only the classical DLVO forces are not enough to predict their aggregation behaviour. Steric repulsive forces ($V_T + V_{ELAS}$) resulting from polymeric or organic coatings may only have a net attraction. Therefore, coated NPs may aggregate reversibly [86], which has a significant impact on the fate and transport of NPs. All these additional forces are collectively known as extended DLVO (XDLVO) forces and are summarized in Table 2.2.

Table 2.2 Extended DLVO forces contributing to the aggregation of NPs

Force	Equations	Origin
Magnetic attraction	$V_M = \frac{-8\pi\mu_0 M_s^2 a^3}{9\left(\frac{s}{a}+2\right)^3}$	Aligning electron spins [87]
Hydrophobic (Lewis acid-base)	$\frac{V_{AB}}{surface\ area} = \Delta G_{s_0}^{AB} exp\left(\frac{s_0 - s}{\lambda}\right)$	Entropic penalty of separating hydrogen bonds in water [79, 88]
Osmotic repulsion	$2d \le s \Longrightarrow \left\{\frac{V_{OSM}}{kT} = 0\right\}$ $d \le s < 2d \Longrightarrow \left\{\frac{V_{OSM}}{kT} = \frac{a4\pi}{\nu_1}\phi_p^2\left(\frac{1}{2}-\chi\right)\left(d-\frac{s}{2}\right)^2\right\}$ $s < d \Longrightarrow \left\{\frac{V_{OSM}}{kT} = \frac{a4\pi}{\nu_1}\phi_p^2\left(\frac{1}{2}-\chi\right)d^2\left(\frac{s}{2d}-\frac{1}{4} - ln\left(\frac{s}{d}\right)\right)\right\}$	Concentration of ions between two particles [89], [90], [91, 92]
Elastic-steric repulsion	$d \le s \Longrightarrow \left\{\frac{V_{elas}}{kT} = 0\right\}$ $d > s$ $\Longrightarrow \left\{\frac{V_{elas}}{kT} = \left(\frac{2\pi a}{M_w}\phi_p d^2 \rho_p\right)\left\{\frac{s}{d} ln\left[\frac{s}{d}\left(\frac{3-\frac{s}{d}}{2}\right)^2\right]\right\}\right.$ $\left. - 6ln\left(\frac{3-\frac{s}{d}}{2}\right) + 3\left(1+\frac{s}{d}\right)\right\}$	Molecules on the NP surfaces resist the loss of entropy due to the compactness [89], [90], [91, 92]
Bridging attraction	NA	Surface molecules bridge to other particles [93, 94]

*where; a:average particle radius; d:thickness of "brush" polymer layer (~δ); χ:Flory-Huggins solvency parameter; $\Delta G_{s_0}^{AB}$:free energy of acid base interaction between particles at distance s_0; A:Hamaker Constant; ε:relative permittivity of water (=78.5 $C.V^{-1}m^{-1}$); ε_o:permittivity of a vacuum (=8.854 x 10^{-12}); e:elementary charge of an electron; κ:inverse Debye length; δ:Stern layer thickness; k:Boltzmann constant;

λ:decay length for acid–base interactions (=0.6 nm); M_s:saturation magnetization; μ_o:vacuum permeability; M_W:molecular weight of polyelectrolyte; n:number concentration of ion pairs; ρ_p:density of polymer; Ψ_d:diffuse potential (~zeta potential); s:distance between the interacting surfaces; s_0:minimum equilibrium separation distance (=0.158 nm); T:absolute temperature; φ_p:volume fraction of polymer in "brush"; v_1:volume of solvent molecule; z:electrolyte valence.

2.5 Challenges to study the impact of NP aggregation

The phenomenon of aggregation demonstrates that several forces with different nature and origin govern its kinetics. In addition to that, engineered NPs present a combination of challenges to these theories due to their size, chemical composition, structure, shape and the surface coatings.

2.5.1 Particle Size

Due to the smaller size of NPs, there is a conflict with the fundamental assumptions of DLVO theory. When the particles become smaller, its surface curvature is too small hence assumed it is flat. Therefore, this is one of the key challenges faced in applying DLVO theory to NPs. Furthermore, when the particle size decreases most of the atoms will be on the surface which can affect the electron arrangement, surface charge and reactivity. Recent research suggests that the redistribution of the atoms and the charge cloud on the surface of the NPs strongly influence their reactivity [95]. Furthermore, He et al. [96] has showed that the particle size is inversely proportional to the measured point of zero charge (PZC). At the same ionic strength, smaller NPs aggregate faster than the larger NPs [96] suggesting the impact of polydispersity in engineered NPs on their aggregation behavior.

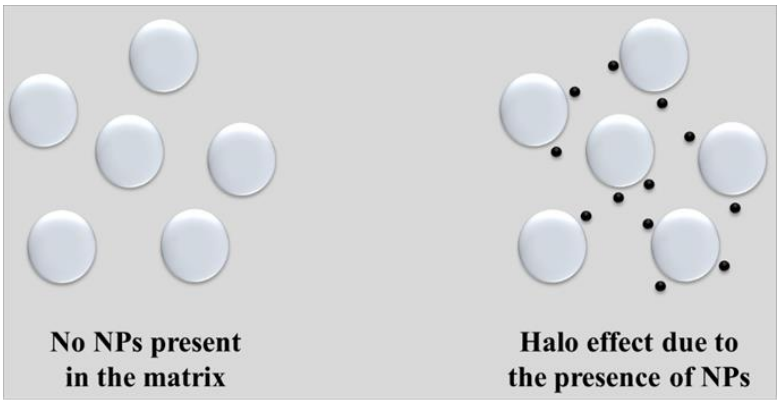

Figure 2.3 "Halo" effect of NPs.

“Halo” stabilization is another effect caused due to the size of the NPs. During this phenomenon, the electrostatic repulsion between two approaching micrometer sized particles are governed by the nano-sized materials. This phenomenon hinders the flocculation of the particles by keeping them far beyond the range of DLVO attractive forces as shown in Figure 2.1. Studies on this phenomenon reveals that the resultant poly dispersity presents a challenge in understanding the aggregation behavior of the dispersions[80].

2.5.2 Chemical Composition

In the colloidal science, the chemical composition is denoted by the Hamaker constant. It governs the vdW attractions, saturation magnetization which governs the magnetic attractions, hydrophobicity, which governs the hydrophobic interactions [88] and the surface charge, which governs the EDL interactions (Eqn. (2.2)) [97]. Particles with a higher Hamaker constant shows a greater tendency for aggregation compared to the particles with a lower Hamaker constant. The origin of vdW attractions is permanent or induced dipoles. Therefore, a material with electronic or molecular structure that favours generation of permanent or induced dipoles generally has a higher Hamaker constant.

The composition and morphology of NPs too challenge the DLVO explanations of aggregation. NPs with a higher surface potential have a lower aggregation tendency compared to the NPs with a lower surface potential. The chemical composition of NPs changes its surface potential by dissociation or ion adsorption via surface atoms [97]. As a result, the surface charge of bare, uncoated NPs is governed partially by the type of atoms on the surface of the NPs.

The studies performed so far reveals that the presence of coatings, core-shell structures and chemical transformations impart charges to NP surfaces. These charge sources or combinations are not considered in the colloidal science. Therefore, to get a comprehensive understanding about the environmental fate of NPs it is indeed important to understand the types of transformations that NPs undergo during manufacturing, usage and disposal.

2.5.3 Shape

One of the primary assumptions in the DLVO theory is that all the particles present are spherical. This assumption is valid for ideal colloid systems but not for the engineered NPs which come in a variety of nano-spherical shapes, triangles, icosahedrons, ellipses, rhombohedrons, spindles, rods, tubes etc. Variation in the shape makes complications in the calculations using conventional DLVO and XDLVO[98]. The changes in the NP shape will affect both the vDW and EDL forces [99],[100].

Recent research shows that the shape of the NPs can theoretically control aggregation under different orientations. Accordingly, it is evident that the NPs in different shapes pose a challenge to colloidal science in understanding their aggregation behavior. Even though, non-conventional theories such as surface element integration [99], may consider the interfacial forces in irregular shapes i.e. ellipsoids, they are unable to explain the characteristics due to unique and diverse types of NP shapes.

2.5.4 Surfactants and Macromolecular Surface coatings

Surface coatings such as polymers, surfactants and polyelectrolytes are used to coat the NPs during the manufacturing process to enhance their dispersion stability and surface functionality. The surfactants adsorbed or covalently bonded to NPs prevent the aggregation and enhance the colloidal stability of NPs. It occurs as a result of the increased surface charge and electrostatic repulsion or the reduction in the interfacial energy between the NPs and the solvent [101].

In contrast to the surfactants, polymers or organic macromolecules too are considered as surface active agents with a higher molecular weight. Unlike surfactants, polymers or their repeating monomer units adsorb to NPs at different places along the polymer chain making the adsorption of polymers stronger and relatively irreversible.

The magnitude of the electro steric repulsion is governed by the surface excess (adsorbed mass of polymers per unit surface area of a NP), density, molecular weight of the polymer, solution composition and thickness of the adsorbed layer thickness (Table 2.2). The interactions with surfactants and polymers are very complex and often kinetically controlled rather than considering their thermodynamic equilibrium. The

scientific evidence to describe the adsorbed mass and layer conformation is not sufficient. Added to that, these depend on the conditions of the surrounding matrix of NPs such as pH and ionic strength. Therefore, predicting the behavior of NPs coated with surfactants, polymers and organic macro molecules remains challenging.

2.6 Factors affecting the aggregation of AgNPs

Common uses of AgNPs such as laundering, and skin cleansing can be the major pathway for AgNPs to enter the aquatic environment. Due to the potential toxicity of AgNPs towards microorganisms, significant efforts are taken to identify the physical and chemical parameters that control the behavior of AgNPs in the aquatic environment. The chemistry of Ag and ionic Ag species will govern the fate of AgNPs, even though different systems will have their own specificities in terms of composition and targeted organisms. Therefore, it is important to evaluate the phenomena deeply via studying model systems before transferring the knowledge to applied cases [5].

AgNPs entering the natural aquatic environments are susceptible to variable temperature, light illumination, pH, dissolved oxygen concentration, ionic strength, concentration and composition of natural organic matter (NOM) and EPS. These parameters have the potential to differentially impact the colloidal stability of AgNPs. Furthermore, they influence the dissolution of AgNPs to produce ionic Ag, which primarily depends on the proton and molecular oxygen concentration. Among the potential transformations of AgNPs entering the natural aquatic environment, the least investigated are those influenced by EPS and NOM.

2.6.1 pH

pH or the concentration of H^+ ions plays a pivotal role in the aggregation AgNPs. Different research approaches have been used to test the impact of pH on the aggregation of AgNPs, but up to today they have not been able to distinguish the exact role of pH in the aggregation of AgNPs [102].

The potential for the transformations of AgNPs in the aquatic environment is governed by the different properties of the matrix [7, 69, 103], including varying acidity, salt

content, and biological media [77]. Varying acidity or the level of pH plays a major role, controlling several other factors such as ionic strength and DOM. Prior studies have examined the dissolution and aggregation [104] of AgNPs in different environmental conditions, but only a few have focused on the aggregation kinetics [105, 106].

According to a study by Tai et al. [105], it has been mentioned that the rate of aggregation of the AgNPs have been increased with the increasing acidity. For this experiment, citrate coated 20nm AgNPs have been used within the pH range of pH 2.9 to 6.4, using Nitric acid to adjust the pH. It has been recorded that the study has been carried up to 19h with a rapid change observed in the first 10 mins of exposure to the acid. Even though, Nitric acid has been used to adjust the pH the study does not clearly mention about the procedure used to avoid the oxidation of the AgNPs to ionic Ag. Furthermore, it is mentioned that the study has been done up to 19h, but the study is not carried out to observe the change continuously with the time, rather it contains details about the results taken in different time intervals.

The study by Peretyazhko et al. [106] has observed the dissolution accompanied aggregation of chemically synthesized AgNPs coated with thiol functionalized methoxyl polyethylene glycol (PEGSH) in different sizes of 6, 9, 13 and 70 nm in the neutral water at pH 7 and pH 3. Acetic acid has been used to adjust the pH in the pH 3 solution. Similar to Tai et al.'s [105] experimental procedure, this study also have been performed for 80 days while measuring the number concentration in different time intervals from days to weeks. This study has been unable to observe the aggregation behavior of the AgNPs but reported that there is a significant size change in 6nm particles. The change observed in this case, may not exactly be the phenomenon of aggregation, but may be due to the re-deposition of ionic Ag on the AgNPs which is attributed as another process named Ostwald ripening [107].

Another recent study by Axson et al. [27], has been able to observe the effect of pH on the aggregation kinetics of AgNPs. This study has simulated the gastric fluid conditions in which the pH varies from 2 to 5, to observe the effect of pH on the aggregation. The experiment has been performed for AgNPs of different sizes (20nm and 110 nm) with different coatings (citrate and PVP). Hydrochloric acid has been used to adjust the pH during these experiments. The study has been able to report that the tendency towards

aggregation increases with increasing acidity, but it has not evaluated the behavioral change with the time.

Furthermore, many researchers have mentioned that the change in pH in the solution or the aquatic matrix can have different impacts on the aggregation of AgNPs [108]. As mentioned in his review by Reidy et al.[109], there is a very limited number of research carried out to investigate the effect of pH on the rate of aggregation of AgNPs. The studies have mainly looked at highly acidic or basic conditions rather than the natural environmental conditions which is vital for a better understanding on the effect of aggregation of the AgNPs in the aquatic systems.

It is necessary to investigate the aggregation behavior of AgNPs within the pH of 6 – 7.5 which is commonly found in the natural environment. Due to the higher rate of aggregation of AgNPs it is needed to be tracked in a timely manner.

2.6.2 Ionic strength

Different types of ions in varying concentrations in the aquatic environment play a critical role in the aggregation of AgNPs. Anions such as chlorides (Cl^-), nitrates, sulphates and hydroxides and cations like Sodium, Calcium, Potassium and Aluminium are among the commonly available. When AgNPs are released into the water, part of it tend to form Ag+ ions [27] which can in turn form precipitates with most of the anions such as Cl^- and sulphates due to their low solubility constant and enthalpy of formation [67]. Up to date, different studies have focused their attention to investigate the effect of ionic strength on the aggregation of AgNPs [102, 110, 111], but only a few of them have been able to highlight the importance of the anions in the matrix during the mechanism of aggregation [7, 57, 112, 113].

In the study by Jiang et al. [113], it is mentioned that the AgNPs pose a great sensitivity towards the different types of inorganic anions like chloride, bromide, iodide, thiocyanate, fluoride, sulphate, nitrate and perchlorate and cations like Zinc(II), Cadmium(II) and Copper (II). Ag nanoplates of 70 nm have been used for the study to observe the interaction with different ions. The results obtained in the study attributed that the shift in the SPR peak observed is mainly due to the change in the surface charge

of the particles determined by the interactions between the AgNPs and the respective ions in the matrix. The study has also urged the need of a complete study on the variation of the aggregation due to the ionic strength. Usually in the open environment there are many different ions prevalent in the aquatic systems. This study has only observed the effect on aggregation via an individual type of ion. Therefore, to simulate the real environment, there is a need to carry out the experiments with a multitude of anions and cations.

Li and Zhu et al. [114], has observed that AgNPs show an accelerated reactivity towards hydrochloric acid, which is not observed with bulk Ag in their study. Chemically synthesized NPs in different sizes (2-18nm with the average being 8.2 nm) and different coatings (Polyvinyl pyrolidine (PVP) and polyacrylamide (PAM)) have been used for the study and the results have been discussed based on the amount of insoluble precipitate of AgCl generated as the product of the reaction. The study has attributed this higher reactivity of AgNPs to the formation of Silver (I) ions in the system. But the study has not been able to clearly distinguish the reason for this higher reactivity of AgNPs which is not observed in bulk Ag or coarse-grained Ag thus highlighted the need to understand this mechanism which is of equal importance in theoretical and technological studies.

The study by Li et al. [115] has been able to look at the aggregation kinetics of AgNPs with different coatings (trisodium citrate, Tween 80 and sodium dodecyl sulfate (SDS)) and in different types of electrolytes (Sodium chloride (NaCl), Sodium nitrate ($NaNO_3$), and Calcium chloride ($CaCl_2$)) with varying concentrations. The results of the study has reported that the aggregation kinetics of the AgNPs with the different ionic strength is consistent with the DLVO theory [116, 117]. The conclusion of this study reveals that the surface coatings contribute to the transformations of AgNPs in the aquatic environment and can act as a barrier towards aggregation, as a result of detachment from the AgNPs. Therefore, during our experiments, uncoated AgNPs were used in order to avoid the effect of other disturbing factors which help to assess the true behavior of AgNPs.

Botasini et al. [118], has reported that the aggregation of AgNPs is influenced by the presence of Cl^- in the medium. This study has been performed using chemically

synthesized AgNPs of the size range from 10-20nm with starch as the capping agent. The study has reported that the AgNPs are stabilized against Cl^- by the cumulative impact of starch coating and high pH. The results of the study also highlight the need to analyze the state of AgNPs in the natural environment, since Cl^- is ubiquitous in aquatic systems and it may pose a challenge doubt on the utilization of products with AgNPs. According to the literature, the need to understand the mechanism associated with the different ions available in the aquatic matrix and the aggregation of AgNPs is highlighted.

2.6.3 Dissolved Organic matter

When engineered NPs with different surface coatings are introduced into the aquatic environment, their expected surface modification is hindered by organic and inorganic ligands prevalent in the matrix [7, 45, 119].

The most common natural organic ligands available in the aquatic systems include reduced thiol (-SH), which is a functional group in cysteine, -COOH, which is a functional group in organic acids, amino acids and vitamins, derivatives of humic [120, 121] and fulvic [122] acids with different aliphatic and aromatic groups including R-OH, -COOH, -OH, $-OCH_3$ and $–NH_2$. Among others, carbohydrates, which is a product of metabolic and decomposition process are also put into the category of organic ligands available in the aquatic environment [123]. Previous studies have demonstrated that the addition of purified, naturally extracted NOM at low concentrations decreases homo-aggregation rates hence increase the colloidal stability of AgNPs. This is applicable to both electrostatically stabilized and sterically stabilized AgNPs [45, 124, 125].

Pokhrel et al. [126], has investigated the colloidal stability of chemically synthesized citrate capped AgNPs of size 56.5±19.2 nm, in the presence of L-cysteine, dissolved organic carbon and trolox, which is an antioxidant. Aggregation was only observed in the presence of dissolved organic carbon. The study reported that the rate of aggregation increased with the increasing concentration of dissolved organic carbon. However, the study does not quantify the extent of aggregation in the presence of DOM thus has focused more on the effects of toxicity of AgNPs in the presence of organic ligands opening new directions for the future research.

According to Gunsolus et al. [127], the previous studies were focused on the impact of NOM on the stability and dissolution of AgNPs, which can be attributed to the high heterogeneity of NOM and the properties of AgNPs. This study has focused on the effect of humic and fulvic acid on the colloidal stability of AgNPs in the aquatic systems. It has observed the behavior of chemically synthesized AgNPs capped with citrate and PVP of size 12.1 ± 2.4 and 15.5 ± 4.1 nm respectively when exposed to NOM, Suwanee river Humic and Fulvic acid and Pony Lake Fulvic acid. The study has focused more towards evaluating the toxicity behavior of AgNPs when exposed to NOM. At the same time the study reported that the rate of aggregation of AgNPs in aquatic systems with organic matter depends on the chemical composition of the NOM.

According to Wirth et al. [128], the combined effect of EPS and NOM stand as a barrier for aggregation increasing the colloidal stability. The study used commercial PVP capped AgNPs in the size range of 20-50 nm. The results obtained in the previous studies [129-132] were further proved by this study reporting that the rate of dissolution increased with the decreasing particle size. Furthermore, dissolved ionic Ag tends to form complexes with the HA decreasing the amount of ionic Ag available in the system. Even though the research has been conducted in investigating the different mechanisms of interactions between NOM and the dissolution and aggregation kinetics of AgNPs in aquatic systems, the relationship between the NOM and the AgNP aggregation has not been clearly identified. Therefore, the need to understand the kinetics of interactions of AgNPs and NOM in aquatic matrices is important.

HA which accounts for a large portion among DOM in natural aquatic and soil environment[133], plays a vital role in the DOM mediated transformations of AgNPs [134]. According to Yin et al [135], the reduction phenomenon took place through generating free radicals of superoxide anions with the interaction between oxygen and the phenolic groups in HA. However, Hou et al [136] suggested that the reaction was independent of oxygen and instead corresponded to the charge transfer of the ligand to the metal between Ag and HA complexes. In addition, sunlight exposure seems to affect the AgNP stability as well. Yu et al. [137], reported that AgNPs were more stable in HA than those without HA with sunlight exposure.

When considering the natural environment, HA presents in both the aquatic environment and soil environment in varying concentrations. Even though, several studies have assessed the impact of HA on AgNPs, the concentration in different environments which differentiate the transformations of AgNPs is not clearly presented. Furthermore, most of the studies previously used commercially available NPs with different coatings which can induce multiple effects on the stability of the AgNPs. The coatings are most likely to detach from the AgNP surface once entering the environment [138]. Thus, the studies using commercial AgNPs may not be able to reveal the true fate of AgNPs in the environment.

2.6.4 Extracellular Polymeric Substances

EPS is complex mixture comprising of polysaccharides, protein, nucleic acids, fats and inorganic substances. Polysaccharides and Protein are the main constituents in EPS and account for 70–80% of the total organic carbon (TOC) content of EPS [139]. EPS contain aliphatic and aromatic monomers in their protein fractions. Hydrophobic chains in the polysaccharide parts and many polar functional groups [140, 141] are also present in EPS. Due to the impact of EPS on the interactions, it is important to study its impact on the aggregation of AgNPs as well. Even though the adaptative and defense mechanisms to cope with AgNPs are poorly understood, previous work with other toxic heavy metals suggests that EPS secreted by bacteria could play a significant protective role [142]. Bacteria can secrete and embed themselves in EPS that are comprised mostly of polysaccharides and protein [143, 144].

According to Kang et al. [145], the structural components in EPS such as protein and polysaccharides is responsible for ionic Ag reduction and immobilization, which affects the colloidal stability of AgNPs. Yet, the mechanism of EPS modified aggregation of AgNPs is not clearly understood. Zhou et al. [146], also reported that the EPS has different interactions with AgNPs, which vary according to the particle properties such as size and the capping agent and the type of EPS. This study has reported the impact of EPS on dissolution and the ionic Ag releasing kinetics but not about the colloidal stability or aggregation. Wang et al. [147], has discussed about the interactions of NPs with EPS as well as the aggregation behavior of the NPs affected by the EPS. Most of the studies up to date on the interactions between EPS and AgNPs, focused

predominantly on their antibacterial properties rather than the aggregation behavior. Therefore, the impact of EPS on the aggregation of AgNPs needs to be clearly understood.

2.7 Novel technologies to study the interactions of NPs

Studying the interactions of NPs in aquatic systems is a very challenging task. The conventional methods used to study the effect on the morphology and the composition of NPs such as TEM, SEM have not been able to build up a clear picture on the real-time interactions of NPs when they are present in the aquatic systems. The advantages and disadvantages of using the existing techniques have been listed in the Table 2.3.

Table 2.3 Comparison of the different techniques used in the NP characterization

Technique	Advantages	Disadvantages
DLS	• Measure quickly and conveniently • Easier sample preparation • Measure the samples in a broader range of size from nanometers to micrometers	• Prefer monodispersed samples • Measure the hydrodynamic size of the particles rather than the direct size • Difficult to measure the diluted samples • Cause a large error when measuring small NPs
TEM	• Require a small amount of sample • Measure the size and shape of the particles with higher accuracy • Observe the structure at nano level • Visualize the interactions between the NPs and other compounds	• Require a large amount of time to count the particles from image analysis • Cause disturbances due to the artefacts occurred during sample drying and fixation • Analyze only the samples in solid state
SEM	• Measure the size and shape of larger NPs with accuracy • Observe the three-dimensional structure of particles at nanometer resolution	• Require a higher amount of time for sample preparation and image capture • Cause potential artefacts • Measure only larger NPs with size greater than 20 nm
AFM	• Measure the size distribution roughly at nanometer level • Measure the samples in complex environments	• Cannot observe the detailed structure • Cause disturbances due to the artefacts occur when fixing the samples
FFF	• Measure the hydrodynamic size of samples in complex environments with reliability • Measure poly-dispersed samples in liquid form	• Need standards for the calibration • Consume a lot of time and complex to optimize the operation
DCS	• Measure the hydrodynamic size of liquid samples with high accuracy • Can use to measure the thickness of the surface coating of the particles provided that a good experiment design is available	• Need standards for the calibration • Measure samples with size larger than 3 nm • High accuracy can be obtained only with concentrated samples • Require higher operation time to measure smaller NPs
spICP-MS	• Detect low concentrations of samples in the range of µg/L • Measure the number and size distribution of the samples at the same time • Measure poly dispersed samples with high precision • Require small sample volume	• Have the size limitation of 20nm • Complicated parameter setting • Need validation with standards • Lack of selectivity to detect different NPs with different elemental compositions
SERS	• Characterize the nanoparticle size, concentration, aggregation state and reaction with molecules • Sensitive and selective molecular sensing of nanomaterials	• Careful operation of the instrument due to the hazardous exposure due to the radiation • Difficulty to optimize the parameters

*AFM: Atomic force microscopy; SERS: Surface enhanced Raman Spectroscopy; FFF: Field flow fractionation; spICP-MS: single particle inductively coupled plasma mass spectroscopy

Considering the limitations of the existing techniques, the attention of the researchers has been directed to try out novel techniques to quantify the interactions especially the aggregation of NPs. Some of the emerging techniques that has been utilized during the recent research studies have been mentioned below with a brief explanation on their performance.

2.7.1 Nanoparticle Tracking Analysis (NTA)

NTA is a technique which uses the properties of both the Brownian Motion and light scattering to generate the particle size distribution of a sample in liquid suspension [148]. This instrument provides high resolution particle size, concentration while a fluorescence mode provides specific results for labelled particles. The equipment provides real time monitoring of the subtle changes in the characteristics of the particles in the solution confirmed by visual validation. This is a technique which enable simultaneous measurement of multiple variables, which in turn saves time and sample volume. It requires minimal sample preparation and consumables, which reduces the day to day running cost as well.

2.7.2 Lab on a chip experiments

“Lab on a chip or microfluidic device” is a recently introduced technology which has been able to draw the attention of many researchers. Microfluidic device is a miniaturized platform which can be utilized to simulate the effect of chemical reactions with increased speed and reliability and reduced sample consumption and cost [149]. This is a technology which can also be used to model precise, high throughput and automatic analysis of chemical processes. Compared to the conventional laboratory experiments, the advantages of using microfluidics for research include shorter reaction time, high mixing efficiency, higher heat transfer coefficient, controllable residence time, small reactor volume and high surface to volume ratio [149].

2.7.3 In situ TEM imaging

In situ electron microscopy is a technique used to investigate a sample's response to a stimulus in real time using the transmission electron microscopy. With the high energy stored in the beam of electrons which is used to image the sample, the sample can be damaged and result in poor readings. Therefore, this new technique enables the user to get high resolution images, while the sample is in the specimen chamber. Another advantage of this method is the ability to capture images through time induced changes and modifications.

2.8 Conclusions

Different interactions of the AgNPs that take place when present in aquatic systems pave their way to the different mechanisms associated with the aggregation kinetics. The phenomena that can take place include oxidative dissolution, formation of a passivating layer and erosion of this layer by other chemical species, re-deposition of Ag and formation of bridging materials between particles that lead to their aggregation. Oxidation that occurs in the metallic Ag core plays an essential step in the action mechanism of AgNPs. When oxidizers are present in the system in abundance i.e atmospheric O_2, AgNPs tend to form ionic Ag and thus be an effective Ag source in forming precipitates. Even though not very active Ag^0, too brings advantages to the system which include being an object that diffuses as one entity comprising of thousands of Ag atoms.

The action mechanism of AgNPs is highly dependent on physical properties including size, shape and the surface properties including the different coatings used in the commercial products. Smaller NPs having a higher specific surface area exhibits a higher dissolution rate. Therefore, it tends to avoid aggregation, since aggregation lowers the effective specific surface and result in sedimentation. Different types of chemical species including anions and cations, NOM and EPS present in the matrix can also have an impact on the aggregation of AgNPs. The effects vary in a range resulting in higher or lower rate of aggregation. Therefore, when carrying out research on those aspects, there should be proper attention given in sample preparation and preparing the medium for the system, since there will be unquantified effects to the results due to the multitude of species. When arriving at a conclusion, the researchers need to pay

attention to the influence by the other species present in the matrix and should make it clear whether what species were exactly present in the matrix and be aware of their consequences.

2.9 Future research needs

According to the literature review, it was revealed that the exact mechanism leading to the interactions of AgNPs is not properly understood. Due to the strong antibacterial properties of Ag and its derivatives, researchers have mostly concentrated on studying the antibacterial effects of AgNPs rather than the interactions of them in the aquatic systems. This suggests the need for future research as mentioned in this section.

It is necessary to introduce a reliable and accurate method of assessment to quantify the AgNP uptake and characterization in the aquatic systems in a time resolved manner. This will help to generate a clear picture of the interactions and associated mechanisms of AgNPs. Most of the studies so far were carried out in different time intervals but not in a continuous time frame which has paved way to a dearth of data in the first 30 mins after introducing the AgNPs to the aquatic system. Even though, some researchers have mentioned that the highest reactivity of AgNPs is observed in the first 10 mins after the introduction. Therefore, it is necessary to carry out the experiment in a continuous time frame to evaluate the reactivity and the kinetics of AgNPs.

When studying about AgNPs, there are many segments to consider which include the effects due to pure AgNPs, ionic Ag and Ag^0. When AgNPs are introduced into aquatic systems, part of them will convert into ionic Ag. Therefore, there is a need for a proper methodology to distinguish the individual and combined effects due to dissolved ionic Ag and AgNPs.

As reported, the aggregation kinetics of AgNPs are affected by the properties and the constituents of the aquatic matrix which include pH, ionic strength, DOM and EPS. But the role of each of these factors in the process of aggregation is barely understood according to the best of the authors' knowledge. When we consider pH, many have considered the behavior only in extreme conditions where pH range from 1-5, but not in the real open environment where the pH is around 6.5-7.5. Due to the presence of

ions in the aquatic system, there is a need to study the impact of different cations and anions on the aggregation phenomena. DOM and EPS are complex factors of which the impact on the aggregation vary according to the type, medium and time. Therefore, it is suggested that there is a necessity to understand their impacts on the aggregation in a time resolved manner.

In most of the studies carried up to date, the researchers have used AgNPs capped with various coatings rather than bare AgNPs. Usually the coatings are added to avoid aggregation during the storage and transportation. Therefore, when using the coated AgNPs for the studies, it will be unable to acquire a proper understanding on the kinetics of aggregation as most of the studies have mentioned that very limited aggregation is observed with differently coated AgNPs. Therefore, it is required to perform the experiments using bare AgNPs to clearly understand the aggregation behavior.

Even though research has been carried out on different impacts of AgNPs on different species, the attention given to the study of kinetics of these reactions is not sufficient. Therefore, there exists a need to have quantitative results on kinetics of AgNPs during the processes such as uptake, localization, particle degradation/dissolution, aggregation and the intervention with different biological products such as bacteria, virus and fungi. The information obtained in these terms will be a guideline to carry out further research digging into minute areas on of the colloidal stability of AgNPs.

Furthermore, the available conventional analytical methods are not sufficient to distinguish the kinetics of aggregation due to the various properties of the aquatic matrix. Therefore, there is a need to utilize high end technology such as Nanoparticle Tracking Analysis (NTA) [148], Lab on a chip experiments [150] to investigate the behavior of AgNPs with respect to the aggregation when present in the solutions without affecting the morphology of the aggregates.

Therefore, the objectives of this thesis are to:

(1) evaluate the impact of surfactants and polymers, which are used as coatings during the transport and storage of AgNPs, on the temporal changes of the colloidal stability of AgNPs

(2) examine the effect of pH, ionic strength, dissolved organic matter (DOM) : Humic acid, proteins and polysaccharides and extracellular polymeric substances on the colloidal stability of AgNPs

(3) To assess the suitability of an emerging technique, in situ liquid cell transmission electron microscopy on tracking the time resolved changes in the transformations of AgNPs

3 Materials and Methods

This chapter presents the details of the common materials and experimental methods used during the research studies mentioned in the subsequent chapters. The common analytical techniques used during the experiments have been mentioned in detail in this chapter.

3.1 Materials

Analytical grade silver nitrate (99.8%) (Sigma- Aldrich) and sodium borohydride (Alfa Aesar) were purchased in the powder form and used without further purification. Analytical grade nitric acid (98%) and the other chemicals used in the experiments were bought from Sigma Aldrich. The de-ionized water used during the experiments was obtained through a Milli-Q water system (Millipore) with a resistivity of 18.2 MΩ.cm. The solutions used in the process of synthesis was purified via filtering through 0.22 μm cellulose ester membrane syringe filters. The glassware and labware used in the process of synthesis were adequately cleaned and stored under dust-free conditions prior to use.

3.2 Synthesis of AgNPs

The AgNPs used in the experiment were synthesized through an oxidation reduction method using silver nitrate and sodium borohydride. Detailed procedure on the synthesis with mechanism is mentioned in Figure 3.1. High ionic strength in the liquid phase will cause aggregation [115, 151] during AgNP synthesis, which can lead to failure in the synthesis of AgNPs [152]. Therefore, low initial $AgNO_3$ and $NaBH_4$ concentration is essential to reduce the solution ionic strength. Increasing the $NaBH_4/AgNO_3$ concentration ratio will enable more BH_4^- to be available in the solution hence stabilize uncoated AgNPs [153]. Three batches of AgNPs were prepared to evaluate the reproducibility and the results show production method was highly reliable Figure 3.2.

3.2.1 Mechanism of reduction of $AgNO_3$ with $NaBH_4$ to produce AgNPs

Briefly, 0.12 mM silver nitrate solution was added to 3 mM sodium borohydride solution, of which the concentration was 25 times excess. The mixture was then vigorously stirred at 1200 rpm for one hour at room temperature (25 ± 2 °C). The solution container was then covered with aluminum foil and stored under 4ºC till further usage.

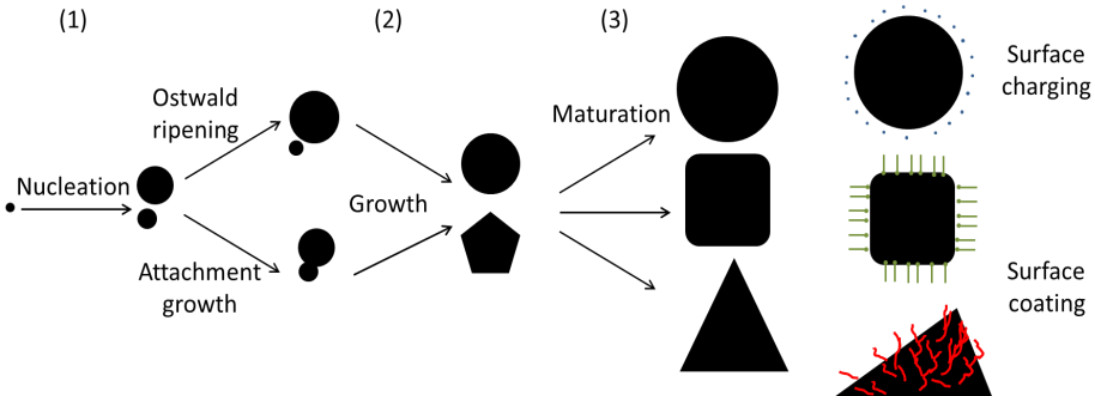

Figure 3.1 The Mechanism of formation of AgNPs.

During the process of synthesis, (1) Silver ions are reduced to form metallic Ag as nuclei in different sizes (nucleation). (2) Then the nuclei will grow into relatively large AgNPs, which is controlled by Ostwald ripening and attachment growth. These Ag nanocrystals may have different morphologies with a relatively narrow size distribution. (3) If there are more Ag+ reduced to atomic Ag, the AgNPs will grow further to generate mature NPs in various shapes under the control of capping agents. Finally, ions (for charging) and large molecules (for coating) are attached to the surface of NPs for stabilization. The equations mentioned below illustrate the reactions involved during the process of synthesis.

Reactions involved:

$$AgNO_{3(aq)} + NaBH_{4(aq)} + 3H_2O_{(aq)} \rightarrow Ag_{(s)} + \frac{7}{2}H_{2(g)} + H_3BO_{3(aq)} + NaNO_{3(aq)} \quad (3.1)$$

$$Ag^+ + e^- \rightarrow Ag \quad E^{\Theta}(298\ K) = 0.7992\ V \quad (3.2)$$

$$BH_4^-{}_{(aq)} + 3H_2O_{(aq)} \rightarrow H_3BO_{3(aq)} + \frac{7}{2}H_{2(g)} \quad (3.3)$$

$$H_3BO_{3(aq)} + H_2O_{(aq)} \rightarrow B(OH)_4^- + H^+ \quad \text{pKa} = 9.2 \quad (3.4)$$

3.2.2 Reproducibility of the synthesis method of AgNPs

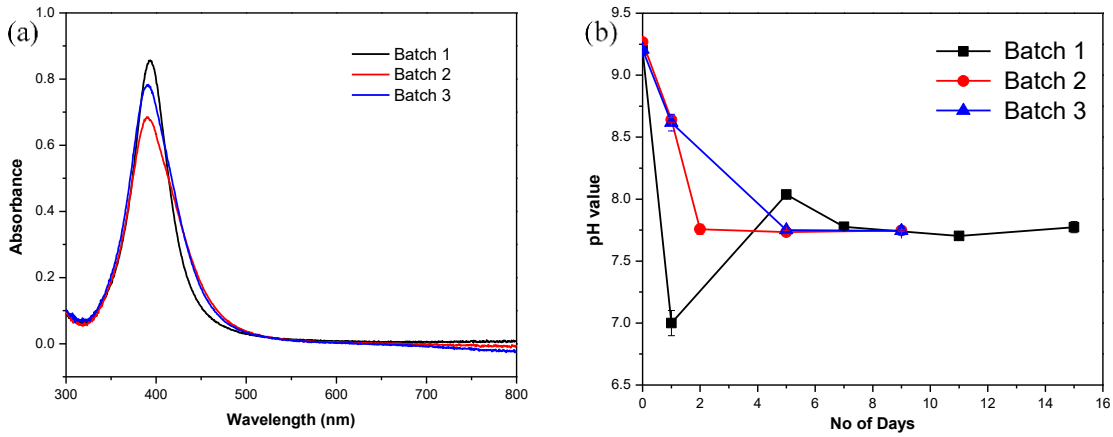

Figure 3.2 (a) The UV vis spectrum among different batches (b) Change of pH among the batches.

According to the results showed in the graphs in Figure 3.2, it can be observed that the SPR peak of the AgNPs remained around 391 ± 2 nm for the AgNPs synthesized in different batches. Furthermore, a narrow SPR spectrum has been observed for all the three batches. The solution pH of the three batches was fluctuating during the first few days and after day 5, it was observed to be stabilized and continued at a constant value. These results suggest that the method we used to synthesize the AgNPs in reproducible and the particle properties of different batches will be similar.

3.3 AgNP Characterization

3.3.1 UV-vis Spectrometry

UV-vis Spectrometry (Shimadzu UV- 4201 PC UV vis spectro-photometer, UK) was used to measure the localized surface plasmon resonance (SPR) of the AgNPs over the wavelength in the range of 300 – 800 nm.

3.3.2 Particle size

The particle size distribution of the AgNPs was measured by Dynamic Light Scattering (DLS) using a Zetasizer Nano (Malvern Instruments, UK) with a 1 cm optical cell. Each measurement was averaged over 10 runs of 2-3 mins each on which the Dispersion

Technology Software V4.20 (Malvern Instruments Ltd.) was utilized to fit both single and multiple exponential algorithms to each autocorrelation function [154].

3.3.3 Zeta Potential measurement

Zeta potential of the synthesized AgNPs and the experimental samples at different conditions was measured using Zetasizer Nano (Malvern Instruments, UK) at 25 ± 2 $^{\circ}$C.

3.3.4 Total silver concentration

The total Ag concentration of the synthesized AgNP stock solutions was measured by the acid digestion method. Briefly, 0.5 ml of 70% nitric acid with 0.5 ml of AgNP stock solution was incubated at 60 $^{\circ}$C for 12 hours. The digested solution was then diluted with DI water to a known volume with 1% (w/v%) HNO_3 solution. The dissolved Ag+ was quantified by an inductively coupled plasma optical emission spectrometer (ICP-OES, Perkin Elmer Instruments).

3.3.5 Dissolver silver concentration

The dissolved ionic Ag in the synthesized AgNPs and the experimental samples was quantified after removing the suspending AgNPs and the method used is described in 3.3.5.1.

3.3.5.1 Determining the centrifugation time for the separation of AgNPs and ionic Ag

To determine the optimum centrifugation time to obtain the ionic Ag concentration, a series of experiments were carried out. AgNP aliquots of 1 ml obtained from the parent solution were centrifuged at 10000 g at 4^{o}C for 0, 0.25, 0.5, 1, 2, 3, 4, 5 hours respectively. After the centrifugation, the samples were taken out and the supernatant and the sediment were separated and mixed with 70 % HNO_3 acid at a volume ratio of 1:1. Then the samples were stored at -20^{o}C for 24 hours. The chilled samples were diluted with DI water at a volume ratio of 1:70 to a HNO_3 concentration of 1% (w/v%) before being measured by the ICP-OES. The measurements were acquired in triplicates.

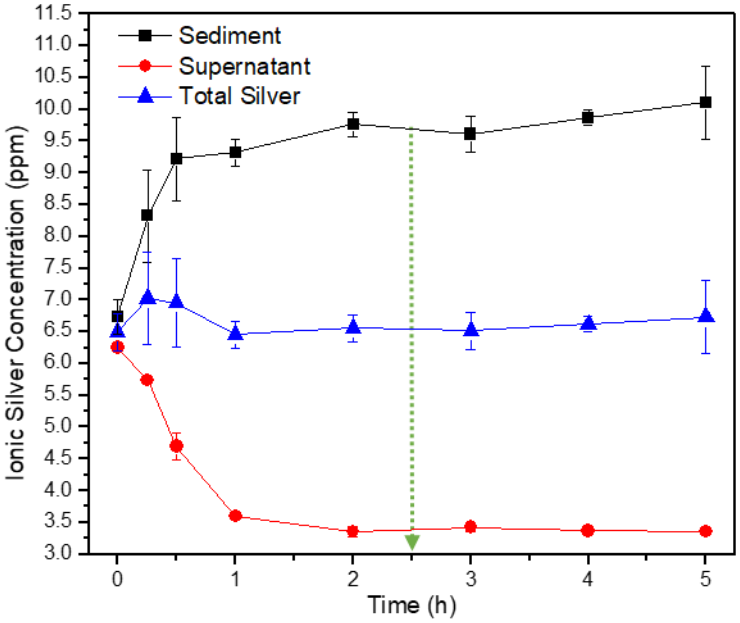

Figure 3.3 Dissolution and Sedimentation kinetics of AgNPs with time

The results obtained have been marked in Figure 3.3. Total silver is calculated with the formula mentioned in Eqn. (3.5).

$$\begin{pmatrix}\text{Total Ag}\\ \text{Concentration}\\ \text{in the}\\ \text{solution}\end{pmatrix} = \frac{1}{2}\left\{\begin{pmatrix}\text{Ionic Ag}\\ \text{Concentration}\\ \text{in the}\\ \text{supernatant}\end{pmatrix} + \begin{pmatrix}\text{Ionic Ag}\\ \text{Concentration}\\ \text{in the}\\ \text{sediment}\end{pmatrix}\right\} \qquad (3.5)$$

According to the Figure 3.3, it is evident that after 2 hours of centrifugation, the Ag concentration in all the three phases almost reached the equilibrium level and remained constant throughout the rest of the experiment at different time intervals. Therefore, it was decided to use 2.5 hours as the centrifugation time for the experimental samples to obtain the ionic Ag concentration.

Briefly, samples were centrifuged for 2.5 hours at 10000 g at 4 $^{\circ}$C to remove AgNPs (Figure 3.3). The supernatant from the centrifuged samples was transferred to different tubes and 70 % (w/v%) HNO_3 acid was added at a volume ratio of 1:1. Before measurement, the samples were diluted with DI water at a volume ratio of 1:70 to a HNO_3 concentration of 1% (w/v%). The ionic Ag concentration was determined by the ICP-OES. The measurements were acquired in triplicates and the reported value was the average of the three measurements.

3.3.6 TEM sample preparation and imaging

Morphology, size and the energy dispersive x-ray spectroscopy (EDX) analysis of the AgNPs was observed using transmission electron microscopy (TEM) without solely relying on the hydrodynamic behaviour. The preparation of the TEM grids was done by the centrifugation method that can remove many artifacts that disturb the conventional drop deposition on the grid [155]. This method ensures that the aggregation in the native solution can be identified clearly without any drying effects caused due to traditional drop deposition TEM grid preparation. Sample vials were shaken vigorously and 3 ml [156] of the sample was transferred to a polypropylene vial where particles were deposited directly on to the 200 mesh Cu grids (Latech Ltd. Singapore) via centrifugation. Images of the particles were obtained using a JEOL 2010 UHR TEM operated at 220 kV. A beam convergence angle of 10.8 m.rad and a nominal spot size of 0.7 nm was maintained at the probe . Images were recorded using a detector angle of 100 m.rad and processed using the Digital Micrograph software (GATAN Inc.).

3.3.7 FTIR spectrometry

To assess the possible attachment mechanisms and to get a qualitative interpretation of the bonds newly created and disappeared, Fourier Transform Infra-Red (FTIR) spectrometry was conducted. FTIR spectra were obtained on a spectrometer (Perkin Elmer, Frontier Series) equipped with Mercury Cadmium Telluride (MCT)-(MIR) liquid nitrogen-cooled detector and Spectrum processing software. The FTIR spectrum was acquired in the 4000-600 cm^{-1} region with a resolution of 16 cm^{-1}.

4 Long term impact of surfactants & polymers on the colloidal stability of AgNPs

This chapter presents the details of the study conducted to evaluate the long-term temporal changes in the colloidal stability of AgNPs induced by the surfactants and polymers. Section 4.1 is an introduction to the chapter with a brief overview of the study followed by the detailed experimental methods in the section 4.2. Results obtained during the experiments with a discussion on the same can be found in the section 4.3 with the conclusions mentioned in the section 4.4.

4.1 Introduction

The stability of AgNPs in the aqueous dispersions can be enhanced through two different types of protection mechanisms. First mechanism is based on the steric repulsion, which occurs in the presence of polymers and nonionic surfactants, stabilizing the particles via binding in the interface [157-159]. The polymers which are used to induce steric stabilization include polyethylene glycol (PEG) [160], polyvinyl alcohols (PVA) [161], polyvinyl pyrrolidone (PVP) [162, 163], polyacrylamides [164] and polyurethanes (PU) [165]. The non-ionic surfactants adsorb at the surface of NPs in a more compact mode and create an excellent stabilizing effect [166] when compared to the polymers. The commonly used non-ionic surfactants include Brij, Tween and Triton X-100 [167].

The second stabilization mechanism is based on the electrostatic repulsion. Upon the addition of the ionic surfactant, the surface charge of the dispersed phase will be enhanced, which electrostatically protect the NPs. Sodium dodecyl sulfate (SDS) [168] and cetyltrimethylammonium chloride or bromide (CTAC, CTAB) [169, 170] have been widely used as anionic and cationic surfactants respectively in many studies as stabilizing agents [169, 171]. For instance, Chen et al. [172] proposes a mechanism of bonding of SDS molecules on the particle surface. According to that mechanism, a double layer was formed around the surface of the NPs with hydrophilic tails directed outward [172]. In this case, it was possible to produce stable AgNP dispersions using SDS, which was stable at least for one month.

Even though the surfactants and polymers were used as agents in obtaining stable NP dispersions, their impact on the fate of NPs during the long term storage is barely discussed, which has attracted the attention in the recent years [138, 173-175]. The main reason for the rise of interest in this research area is the detachment of coatings when the coated NPs are stored for a long-term. Most of the previous studies have evaluated the short term or immediate effect of the surfactants on the NP dispersions and highlighted the need for studying the long-term effect of surfactants and polymers [176]. Studying the possible impacts of surfactants and polymers on the AgNPs is important when considering their fate during the long-term storage.

During this study, four different types of polymers and surfactants were used to evaluate their impact on monodispersed, freshly synthesized uncoated AgNPs in a series of long-term experiments. The changes in the hydrodynamic diameter, zeta potential and the localized surface plasmonic resonance (SPR) was measured to assess the colloidal stability of uncoated AgNPs. Rates of ionic Ag release were also determined to understand the potential impacts of the polymers and surfactants on the dissolution of AgNPs. Firstly, the short-term effects of the surfactants and polymers upon mixing with AgNPs were assessed followed by the experiments to evaluate the long-term effect.

4.2 Experimental methods

4.2.1 Preparation of stock solutions

CTAB stock solution was prepared by dissolving 36.4 mg of 99 % CTAB in 100 ml of DI water via vigorous mixing on a magnetic stirrer to obtain a concentration of approximately 1 m.moldm^{-3} (364 mg/L). Tween 20 solution was prepared by dissolving 71 mg of Tween 20 in 100 ml of DI water via vigorous stirring for an hour to obtain a stock solution with the concentration of 1 m.moldm^{-3} (523 mg/L). 1 g of PVP 10 was dissolved in 100 ml of DI water via ultra-sonication for 60 minutes to obtain a stock solution with a concentration of 1 m.moldm^{-3}. 0.8 g of PEG 8000 was dissolved in 100 ml of DI water via ultra-sonication for 75 minutes to obtain a stock solution with a concentration of 1 m.moldm^{-3}. CTAB was used to assess the behavior of ionic surfactants and Tween 20 as a non-ionic surfactant. Both PEG and PVP were used as polymers during the experiments.

4.2.2 Stability experiments

To assess the individual influence of the compounds, samples were prepared with different concentrations of CTAB, Tween 20, PVP and PEG to obtain a final concentration of 0, 0.05, 0.1, 0.2, 0.25, 0.3, 0.4 and 0.5 m.moldm^{-3}. The range of concentration has been selected to mimic the levels frequently observed in the day to day applications [177, 178]. The stability of these samples was analyzed using UV vis spectrometry and dynamic light scattering on 0, 1 h, 1, 5, 10, 20, 25, 30, 45 and 90 days. The dissolved ionic Ag concentration in the samples during the experimental period was monitored to assess the impact of the surfactants and the polymers on the dissolution of

AgNPs. Images obtained using the transmission electron microscopy (TEM), Fourier Transform Infrared Spectroscopy (FTIR) spectra and the results obtained for the zeta potential in the presence and absence of surfactants and polymers were used to explain the reasons for the variations in stability observed in the UV vis, DLS and ionic Ag results. Furthermore, the stability of the pure AgNPs and AgNPs with DI water (no surfactants or polymers) were also compared with the samples in the presence of surfactants/polymers to understand the distinct effect of surfactants and polymers.

4.3 Results and Discussion

4.3.1 AgNPs characterization

The average size of the synthesized AgNPs was 31 ± 0.1322 nm. More than 84% of the particles were between 10 and 50 nm (Figure 4.1). The particles were reasonably monodispersed in the suspension and had a spherical shape (Figure 4.1(a)) with a yellow colour in the solution (Figure 4.1(b)). The size value obtained using DLS was the maximum size based on the intensity distribution (39.86 ± 4.3516 nm) (Figure 4.1(c)). The synthesized AgNPs exhibited a characteristic peak at the wavelength of 392 ± 2 nm in the UV-Vis absorption spectrum with a maximum absorbance of 0.734 (Figure 4.1(d)). The total Ag concentration of the synthesized AgNPs was 5.872 ± 0.034 mg/L, with an ionic Ag concentration of 2.265 ± 0.002 mg/L. pH and zeta potential of the stock AgNP solution was 8.04 and -28.64 ± 1.6 mV respectively.

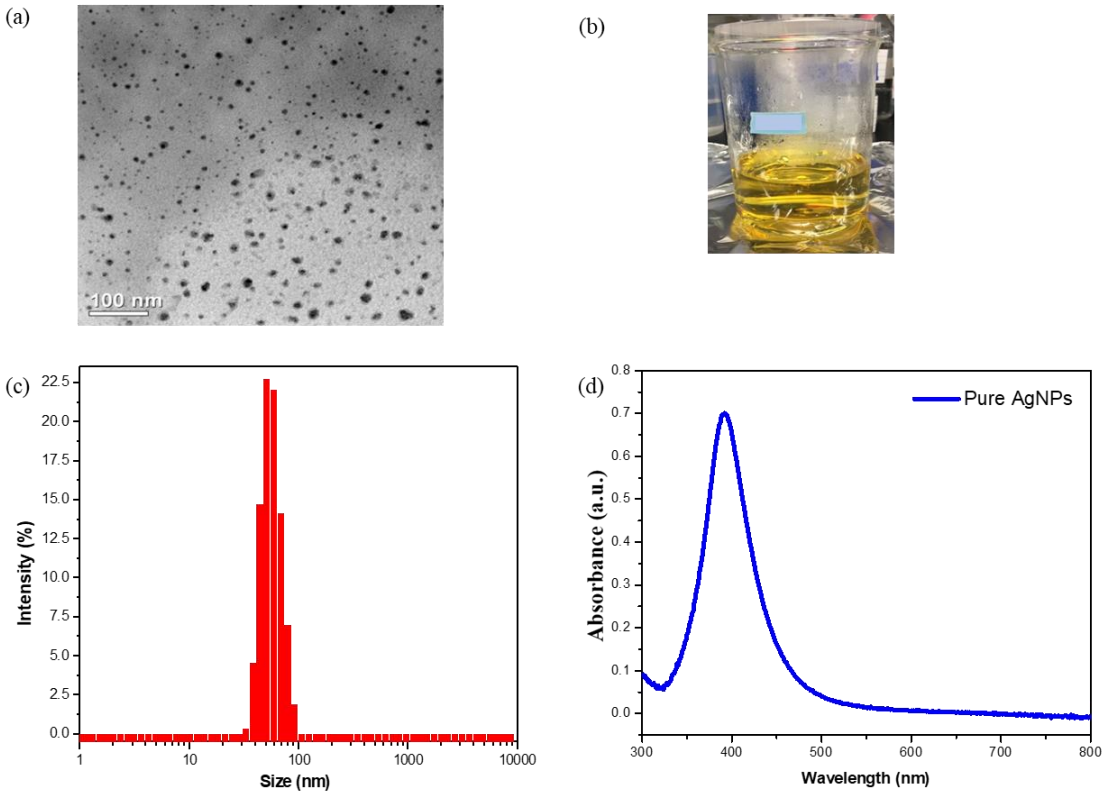

Figure 4.1 Characterization of the synthesized particles (a) Morphology by the TEM (b) Photo of the AgNP suspension (c) Size distribution of the suspension by DLS (d) UV vis absorption spectrum

4.3.2 Evaluation of the AgNP stability

The aggregation of the AgNPs with different surfactants and polymers was evaluated with a method combining UV vis spectrometry and DLS. After 1-hour incubation, the UV-vis spectrum of the aqueous suspension of pure AgNPs exhibits an absorption peak at 392 nm, which corresponds to the surface plasmon resonance (SPR) peak of AgNPs (Figure 4.2). The SPR absorption at the characteristic wavelength, decreased from 0.69 to 0.32 upon the addition of pure DI water.

According to the UV-vis results, the characteristic wavelength and the peak absorbance of AgNPs were changed depending on the type of surfactant or polymer and its concentration in the short-term. With the addition of CTAB, the SPR peak wavelength shifted from 392.7 nm (0 mM CTAB) to 412 nm (0.5 mM CTAB) (Figure 4.2(a)), with an increase in the peak absorbance from 0.32 (0 mM CTAB) to 0.38 (0.5 mM CTAB) (Figure 4.3(a)). Upon the addition of the Tween 20, the peak absorbance wavelength

shifted from 392.2 nm (0 mM Tween 20) to 404.8 nm (0.5 mM Tween 20) (Figure 4.2(b)), with no obvious change in the peak absorbance (Figure 4.3(b)). With the increase in the concentration of PVP, the peak absorbance wavelength shifted from 392.7 (0 mM PVP) nm to 413.4 nm (0.5 mM PVP) with almost no change in the peak absorbance (Figure 4.2(c), Figure 4.3(c)). In the presence of PEG, there was a slight shift in the characteristic peak, observed with the increasing PEG concentration (Figure 4.2(d)). The peak absorbance at the characteristic wavelength has slightly reduced from 0.32 (0 mM PEG) to 0.314 (0.5 mM PEG) (Figure 4.3(d)). However, the peak absorbance at the characteristic wavelength increased up to PEG concentration of 0.1 mM and then decreased (Figure 4.2(d)). The red shift observed in the presence of surfactants/polymers suggest that the particles were changed to a different form with a new characteristic wavelength corresponding to the peak absorbance. All the pure surfactant and polymer solutions, including CTAB, Tween 20, PVP and PEG displayed no absorption in the wavelength region of 300–800 nm [177]. Thus, the intensity of absorbance peak at the characteristic wavelength represents the concentration of AgNPs in the presence of the surfactants and polymers.

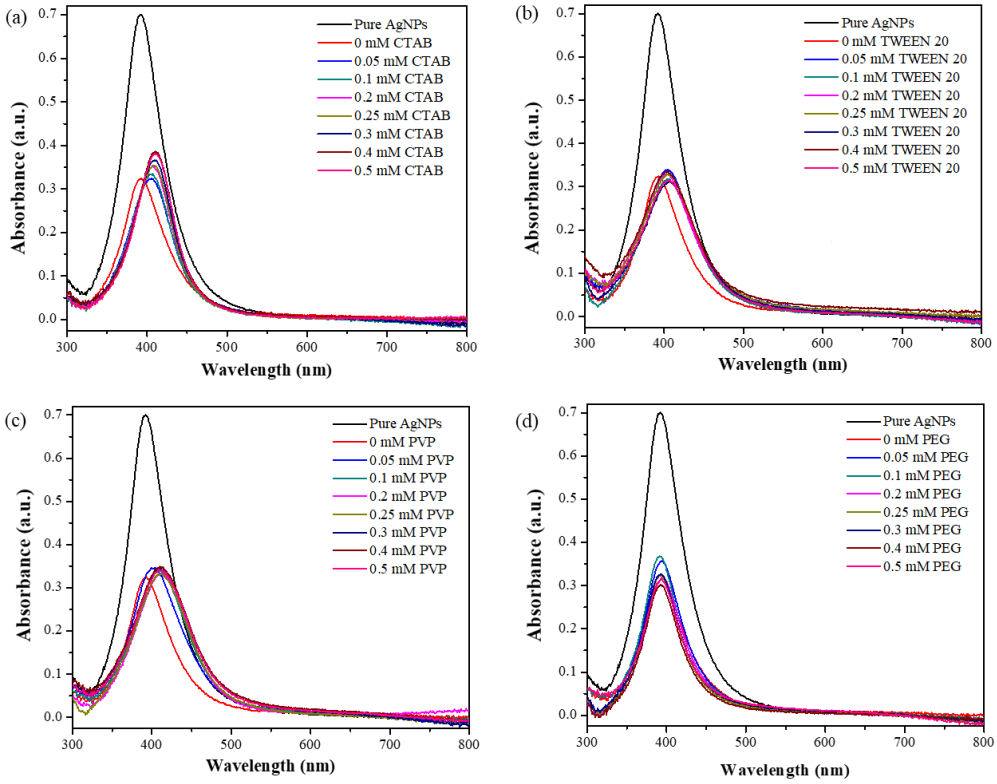

Figure 4.2 Change in the UV vis spectrum of AgNPs with concentration for (a) CTAB (b) Tween 20 (c) PVP and (d) PEG after 1 h of incubation. AgNP concentration: 5 mg/L.

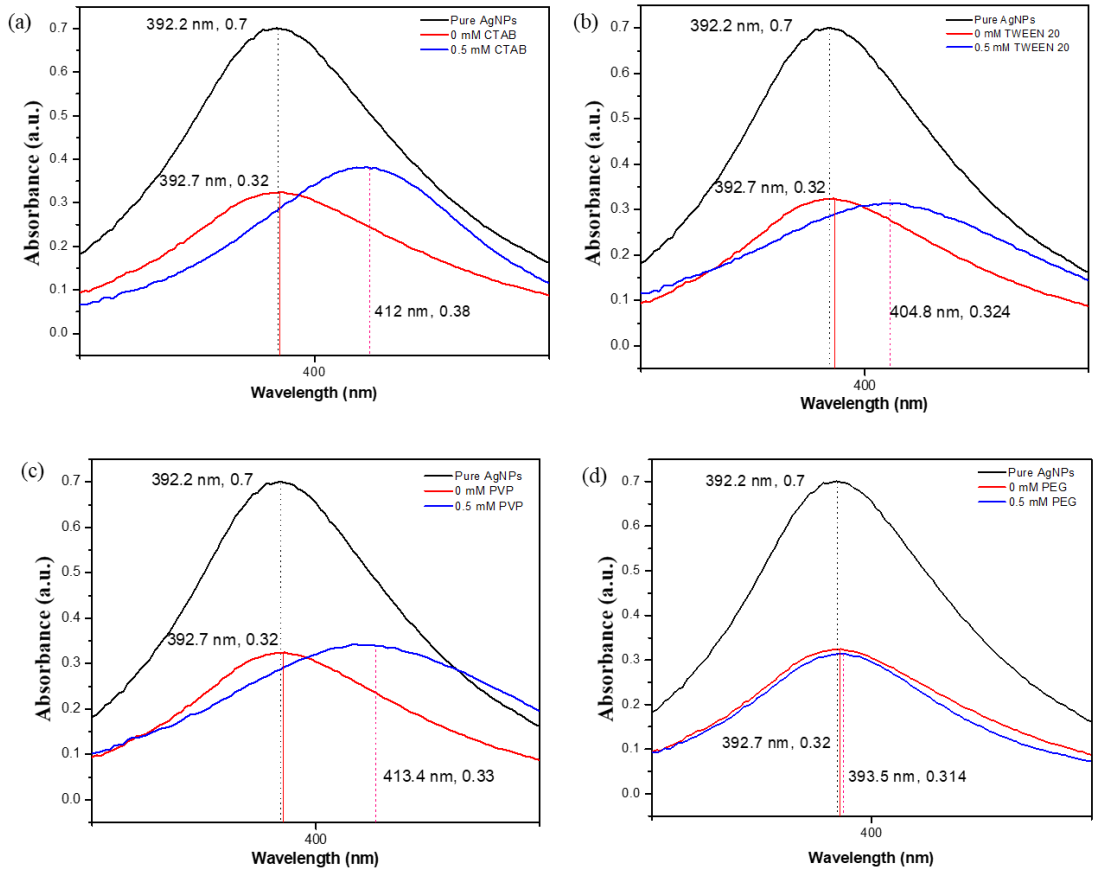

Figure 4.3 Change in the UV vis spectrum of AgNPs with concentration for (a) CTAB (b) Tween 20 (c) PVP and (d) PEG

The change of the particle size of the samples was investigated using DLS. The particle size distribution of the AgNPs in the solutions changed with the surfactant/polymer concentration, creating destabilization among the mono dispersed pure AgNPs (Figure 4.4). The particle size distribution observed in the low concentrations of CTAB (0.05 mM and 0.2 mM) after 1 h of incubation was almost monomodal like the pure AgNPs except for some minor peaks observed around the diameter of 10 nm (Figure 4.4(a)). At higher CTAB concentration of 0.5 mM several peaks can be observed in the particle size distribution. This observation implies that with the increase in the CTAB concentration the particle size of the solution changed and hence resulted in a redistribution of the particle size. In the presence of 0.05 mM Tween 20, the mono modal particle size distribution of AgNPs changed to a particles size distribution with two obvious modes (Figure 4.4(b)). When the Tween 20 concentration was further increased, the mode at the higher diameter gradually decreased and moved to the left,

depicting a decrease in the particle size. When PVP was added to the system, the particle size distribution changed with more peaks observed in the lower diameter region (Figure 4.4(c)). When the concentration of PVP in the system increased up to 0.5 mM, the particle size distribution was widened, with three peaks observed at 5, 11 and 100 nm. In the presence of PEG, the average particle size increased at 0.05 mM and then decreased gradually with the increasing PEG concentration (Figure 4.4(d)).

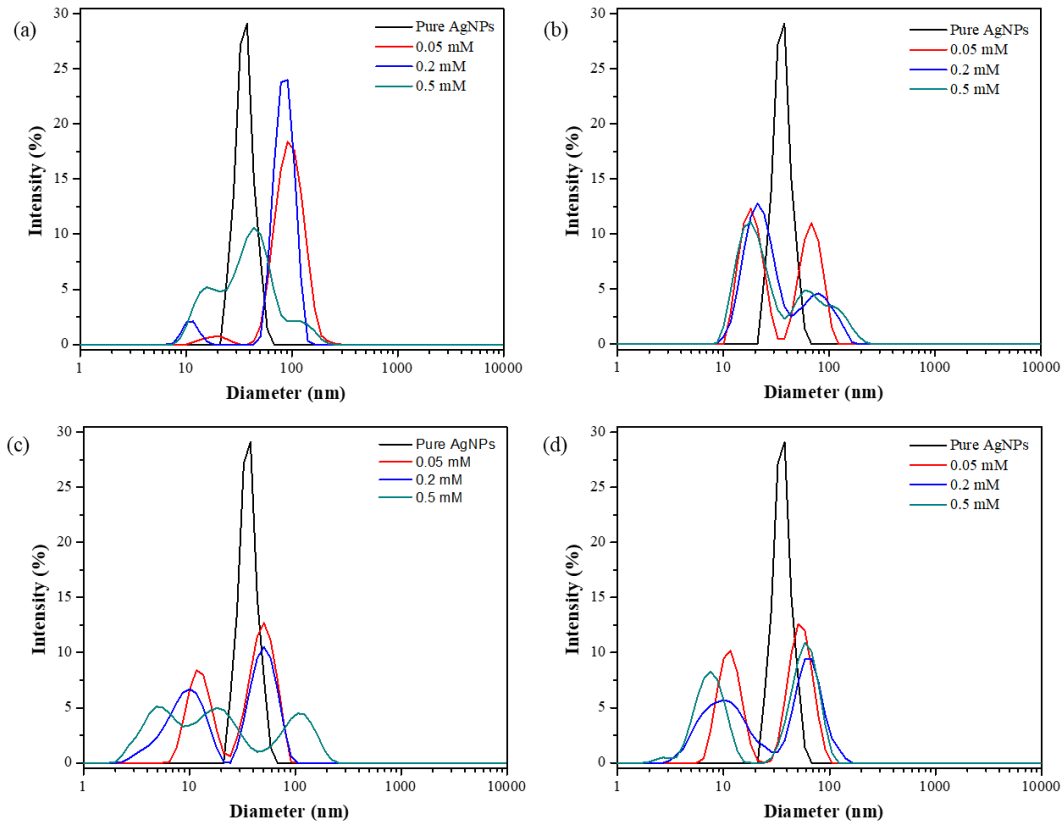

Figure 4.4 Change in the particle size distribution of AgNPs with concentration for (a) CTAB (b) Tween 20 (c) PVP and (d) PEG after 1 h of incubation. AgNP concentration: 5 mg/L.

The increase in the particle size upon addition of surfactants or polymers can be due to two reasons: the first one being aggregation occurred in the solution due to the ionic substances and the second one being the coating induced by the surfactants or polymers on the uncoated AgNPs. The emergence of the peaks below 10 nm can be due to the dissolution occurred in the AgNP solution. In Figure 4.2 & Figure 4.4, the short-term effects on the AgNPs due to the addition of surfactants or polymers were observed after

1 h of incubation to understand the effect of surfactants and polymers on the short-term/instant transformations of AgNPs and to provide a basis for the long term study. The short-term results provide an overview on the fate of AgNPs in the presence of surfactants and polymers at initial stage. To completely assess the impact of surfactants and polymers on the AgNPs, it is important to observe their long-term behaviour as well. Hence the long-term study to evaluate the impact of surfactants and polymers on the AgNPs was designed and carried out.

0.2 mM was selected as the representative concentration of surfactants and polymers for long-term study as it is above the critical micelle concentration of surfactants and polymers [173]. The particle size distribution obtained with the variation in time at a constant surfactant or polymer concentration of 0.2 mM, is compared with the profile of pure AgNPs and 0 mM surfactants/polymers in Figure 4.5. According to the particle size distribution obtained for pure AgNPs (Figure 4.5(a)), the particle size started to change after 1 d of incubation resulting in an increase in the average particle size. The particle size further changed at the prolonged period, resulting in several peaks at the time points of 45 and 90 days, deviating from the initial mono modal particle size distribution. The particle size had the highest recorded at the time point of 90 days. In the presence of DI water without surfactants/polymers (Figure 4.5(b)), the particle size started to change upon the mixing with DI water. The monomodal particle size distribution obtained for pure AgNPs changed to a particle size distribution with several peaks. The emergence of different peaks changed throughout the experimental period, implying that the storage of AgNPs in their original solution and DI water is not stable when considering their long-term stability.

Several peaks appeared and disappeared over the course of time in Tween 20, PVP and PEG samples (Figure 4.5(d), (e) & (f)), compared to the scenario under pure AgNPs and in the DI water (Figure 4.5(a) & (b)). According to the results, the change in the particle size distribution of the pure AgNPs is less compared to the change in the particle size distribution of AgNPs + DI water mixture. This observation is due to the fact that the uncoated AgNPs are stable on its own for some time, and when present in the DI water their surrounding matrix change resulting in hindering the stability of pure AgNPs. The instability of AgNPs in the DI water results in the change of the particle properties producing a different particle size distribution with time. However, clean single modal

particle size distribution can be observed in the presence of 0.2 mM CTAB during the experimental period (Figure 4.5(c)). Furthermore, the particle size in the presence of CTAB is higher compared to the other test conditions. Intensity of the peaks observed above 100 nm, in the presence of CTAB is evident, while the peaks above 100 nm in the other conditions is negligible. Furthermore, it can be observed that the size kept increasing with the time (Figure 4.5(c)) in the presence of CTAB. On the other hand, it can be observed that the peaks below 10 nm have gradually decreased in the presence of Tween 20 (Figure 4.5(d)) but increased in the presence of polymers with time (Figure 4.5(e) & (f)), which suggests that the dissolution of AgNPs to ionic Ag took place continuously throughout the experimental period in polymer solution.

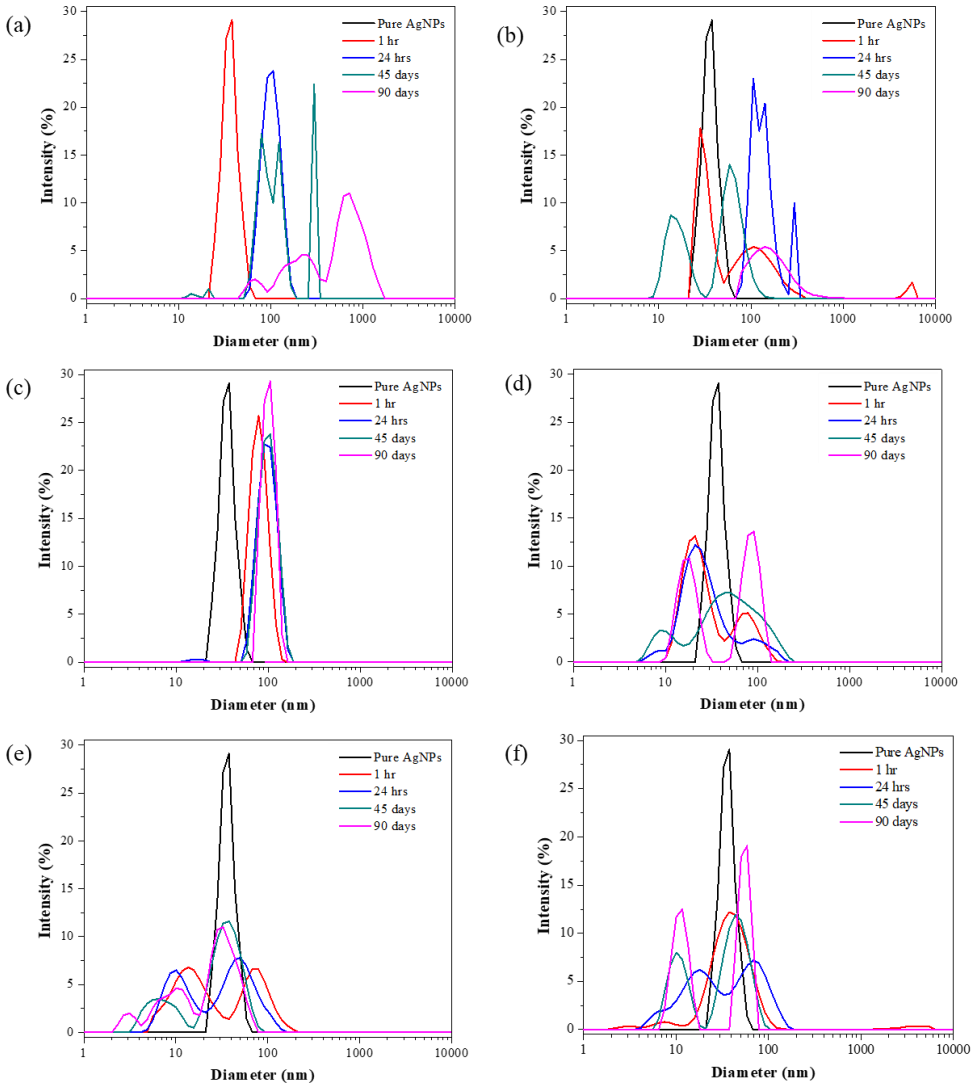

Figure 4.5 Change in the particle size distribution of AgNPs with time for (a) only AgNPs (b) 0 mM surfactant/polymer (c) CTAB (0.2 mM) (d) Tween 20 (0.2 mM) (e) PVP (0.2 mM) and (f) PEG (0.2 mM). AgNP concentration: 5 mg/L.

The results described above on the change in the particle size distribution with the different surfactants and polymers with time can be further proved with the observation made in the UV vis spectrum recorded with time as shown in the Figure 4.6. In the presence of CTAB, particles tend to aggregate with time as well even though the particle size distribution is mono modal (Figure 4.6(a)). TEM imaging was carried out to observe the aggregation process and to study the stabilization of the AgNPs in the presence of different surfactants/polymers.

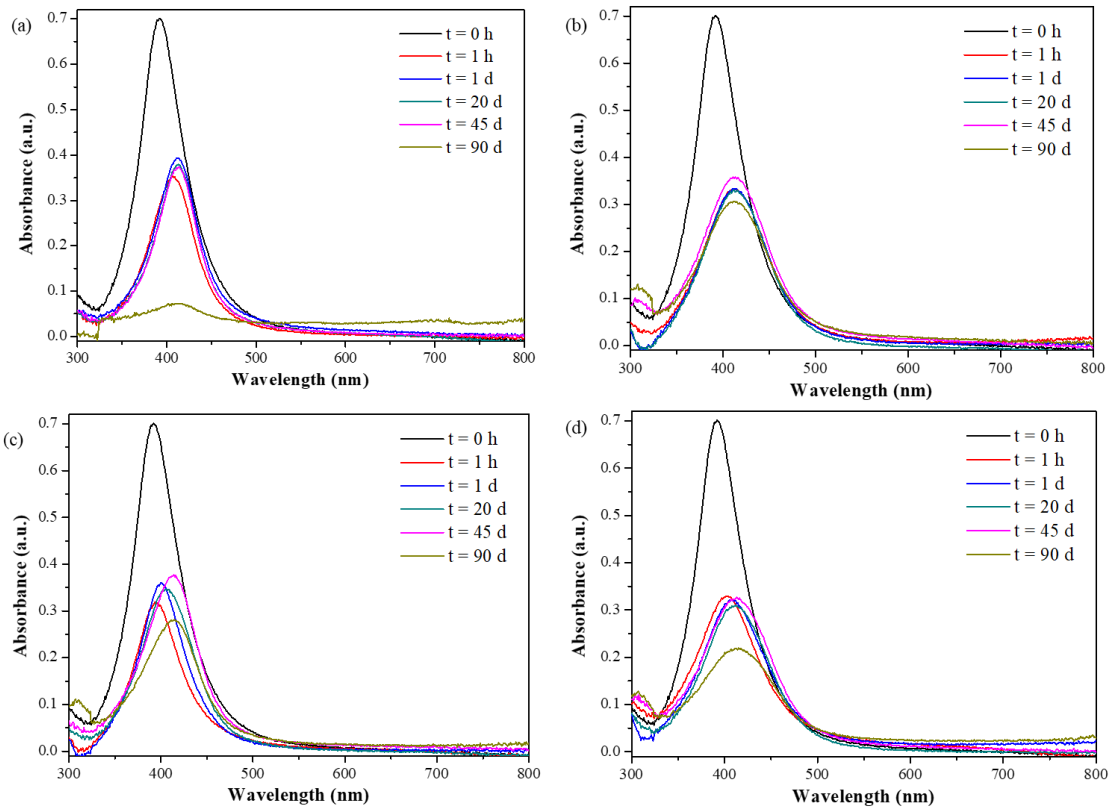

Figure 4.6 Change in the UV vis spectrum of AgNPs with time for (a) CTAB (0.25 mM) (b) Tween 20 (0.25 mM) (c) PVP (0.25 mM) and (d) PEG (0.25 mM). AgNP concentration: 5 mg/L.

The images obtained on day 1 and day 45 are shown in Figure 4.7. Compared to the TEM images of the pure AgNP, the particle morphology and dispersion are very different with the presence of surfactant and polymers. The morphology of AgNPs dispersed in CTAB solution changed distinctly after the incubation for 1 day, which is illustrated by the original structure of AgNPs being corroded partly or entirely, with the appearance of many NPs. At a prolonged period (45 days), CTAB further stabilized the

particles and resulted in stable particles in the solution (Figure 4.7(g)), also as shown by the monomodal particle size distribution obtained Figure 4.5(c). In the presence of Tween 20, individual and non- aggregated particles were observed (Figure 4.7(c)). As observed in the particle size distribution (Figure 4.5(d)), the tendency for aggregation in the prolonged period in the presence of Tween 20 can be observed in the TEM images obtained after 45 days of incubation (Figure 4.7(h)). A similar phenomenon to CTAB was observed in the case of PVP, which could account for the facilitated dissolution of AgNPs in the solution. It can be visualized in the images as the particles are spotted dark black and there is some grey coloured spot around that, which is due to dissolution. This result is further confirmed by the results obtained for the particle size distribution where many smaller particles are observed than bigger particles (Figure 4.5(e)). However, the particles were isolated as well as aggregated (Figure 4.7(i)) after a prolonged period resulting in a multimodal particle size distribution as observed in Figure 4.5(e). AgNPs retained their intact particle structure and the morphology did not change significantly after 1 d of incubation with PEG (Figure 4.7(e)). After longer period, slight aggregation was observed (Figure 4.7(j)), which is consistent with the multi modal particle size distribution observed at Figure 4.5(f). When comparing the TEM images obtained at different time points, the AgNPs are more likely to be intact in the presence of the surfactants and polymers compared to the scenario in the absence of surfactants and polymers. More TEM images obtained at different magnifications are included in Figure 4.8.

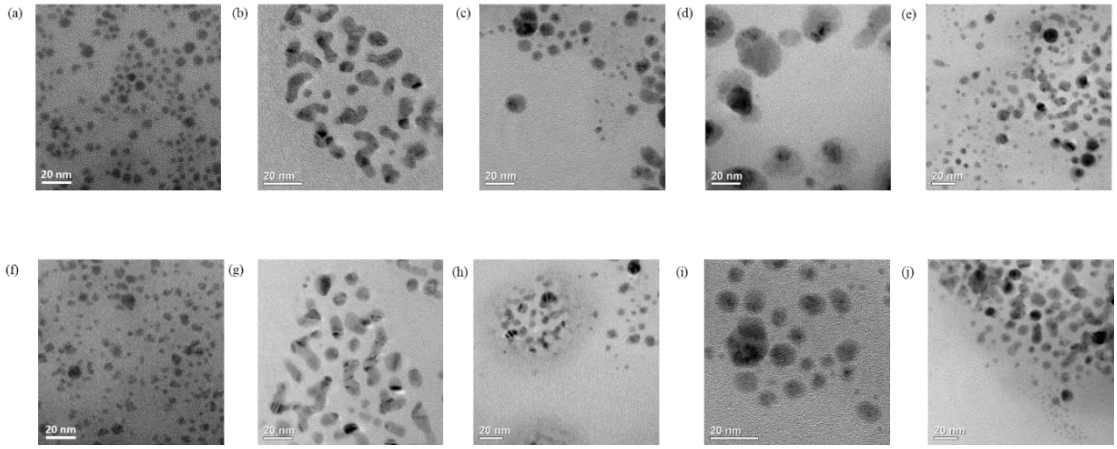

Figure 4.7 TEM images of the AgNP solutions in the (a,f) absence of surfactants/polymers and in the presence of (b,g) CTAB (0.2 mM) (c,h) Tween 20 (0.2 mM) (d,i) PVP (0.2 mM) and (e,j) PEG (0.2 mM) obtained after 1 day and 45 days of incubation respectively. AgNP concentration: 5 mg/L.

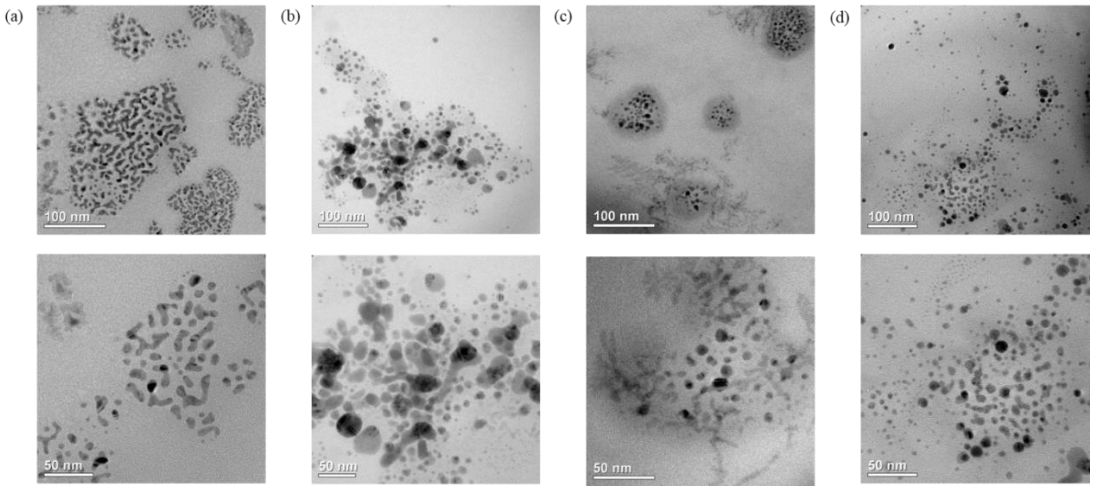

Figure 4.8 TEM images of the AgNP solutions in the presence of (a) CTAB (0.2 mM) (b) Tween 20 (0.2 mM) (c) PVP (0.2 mM) and (d) PEG (0.2 mM) obtained after 1 d of incubation at different magnifications. AgNP concentration : 5 mg/L.

4.3.3 Change in the ionic Ag concentration

The results obtained for the ionic Ag concentration of the AgNP dispersions in the presence of different surfactants and polymers are shown in the Figure 4.9. According to Figure 4.9, the ionic Ag concentration increased with the increasing surfactant or

polymer concentration. The ionic Ag concentration observed in the presence of Tween 20 was higher than that of CTAB (Figure 4.9(a) & (b)). In the presence of polymers, the ionic Ag concentration observed in the presence of PVP was lower than in the presence of PEG, at lower concentrations. When the polymer concentrations further increased, the ionic Ag concentration in the presence of PVP is higher than that of PEG (Figure 4.9(c) & (d)). When the time factor is considered in the dissolution, it can be observed that the dissolution increased with the time in the presence of both the surfactants and polymers in the initial points of time and became stable during the prolonged period up to 90 days.

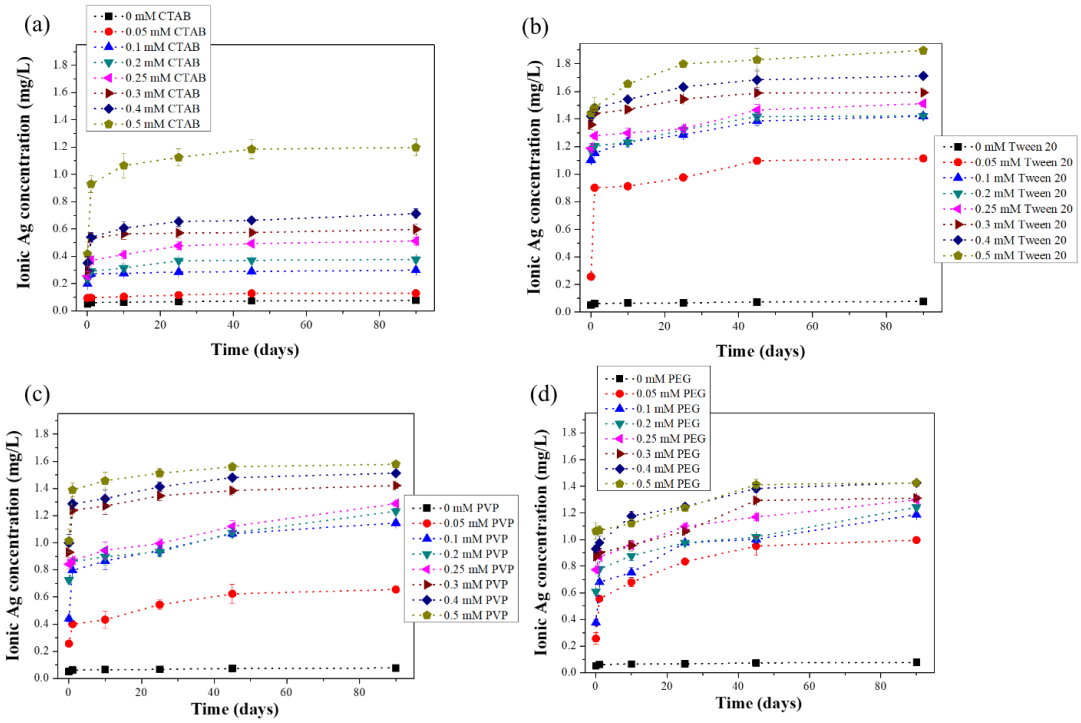

Figure 4.9 Change in the ionic Ag concentration of AgNPs with the time in the presence of different concentrations of (a) CTAB (b) Tween 20 (c) PVP and (d) PEG during long term experiments. AgNP concentration: 5 mg/L.

Interactions of the surfactants or polymers with the AgNP surface can be further understood from the critical coagulation concentration (CCC) value obtained from the simplified calculations of the effective charge of the compounds that induces the aggregation process. The DLVO theory predicts the CCC value by considering the repulsive electrostatic interactions and the van der Waals attractions [97]. This prediction can be approximated as mentioned in Eqn. (4.1):

$$CCC = \frac{87 \times 10^{-40}}{z^6 A^2} \quad (4.1)$$

where z represents the charge of the counterion of the added electrolyte and A stands for the Hamaker constant in Joules for CCC in moles per liter. As the best estimation for the value of Hamaker constant for an interacting pair of AgNPs, the value of 39×10^{-20} J has been determined experimentally using the atomic force microscopy (AFM) method [177]. The zeta potential varied with the type and concentration of surfactants and polymers (Figure 4.10).

The zeta potential of AgNPs reflects the surface electric potential and has a significant impact on the stability of AgNPs as mentioned in the Eqn. (4.1), which governs the CCC, when the Hamaker constant is a constant for a single type of NPs. The zeta potential of pristine AgNPs was −28.64 mV, suggesting that they were negatively charged, and there was a repulsive force between the AgNPs. As shown in Figure 4.10, the zeta potential of AgNPs decreased in the solution of Tween 20, PVP and PEG, but increased distinctly in the presence of the cationic surfactant CTAB. In addition, the zeta potential increased with an increase in the concentration of the cationic surfactant (Figure 4.10(a)). The increase in the zeta potential could result in a significant decrease in the CCC (Eqn. (4.1)) and eventually in the electrostatic repulsion between the surfactants and the surface of AgNPs. This phenomenon consequently promotes the attachment of the cationic surfactants to the AgNP surfaces via electrostatic attractive interaction, and then neutralize part of the negative charges.

In the presence of surfactants, the zeta potential differed on the basis whether they are ionic or non-ionic. When the CTAB concentration increased, zeta potential also increased with a positive value resulting in more positive surface charge, since CTAB is a cationic surfactant (Figure 4.10(a)). In the presence of the non-ionic, Tween 20, the zeta potential decreased with the increasing Tween 20 concentration (Figure 4.10(b)). The zeta potential of the AgNP solutions decreased with the increase in the PVP concentration (Figure 4.10(c)), resulting in a more stable solution as exhibited with the results obtained for the SPR peak and the particle size distribution. With the increase in the PEG concentration, the zeta potential increased up to 0.2 mM and then decreased with the further increase in the polymer concentration (Figure 4.10(d)).

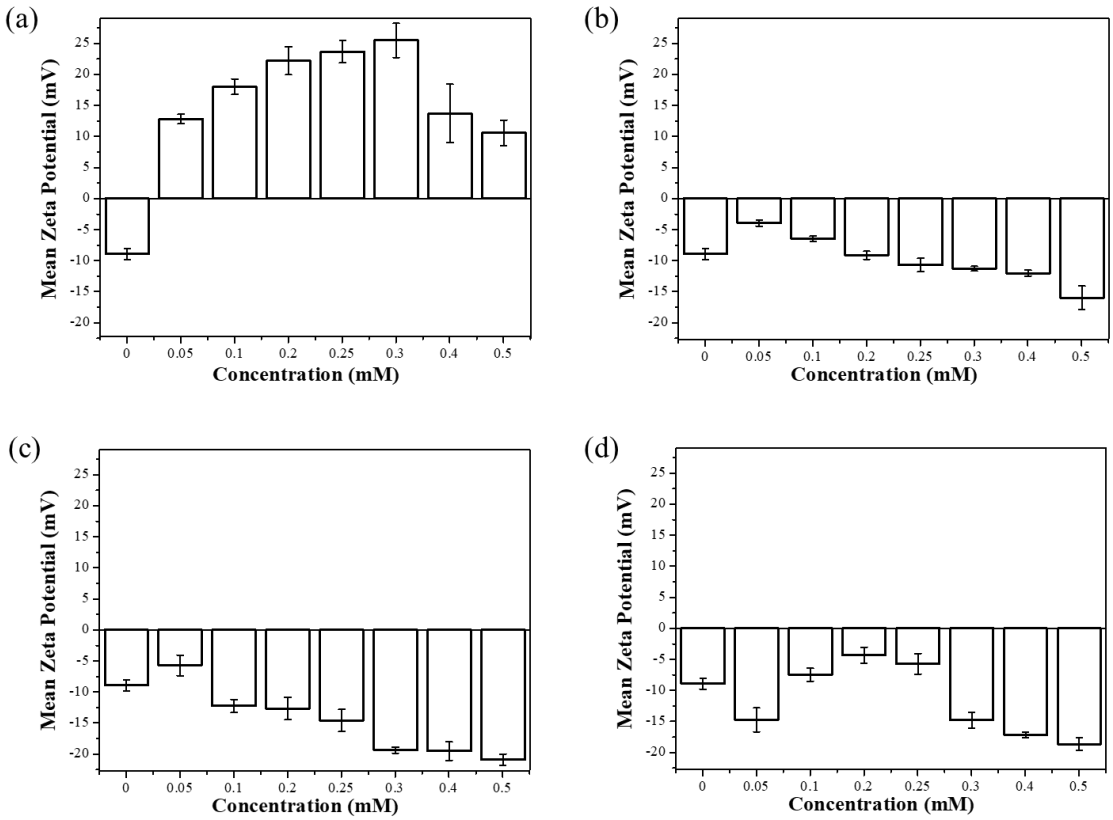

Figure 4.10 Change in the zeta potential for (a) CTAB, (b) Tween 20, (c) PVP and (d) PEG after 1 h of incubation. AgNP concentration: 5 mg/L.

When considering the zeta potential distribution of AgNPs dispersed in the different surfactants and polymers, the most stable distribution was obtained in the presence of CTAB with a mode around -50 mV. The zeta potential distribution for pure AgNPs displayed several peaks, and they were reduced to one or two peaks upon addition of different surfactants or polymers (Figure 4.11). The zeta potential of the solution did not show any obvious change during the long-term experiments.

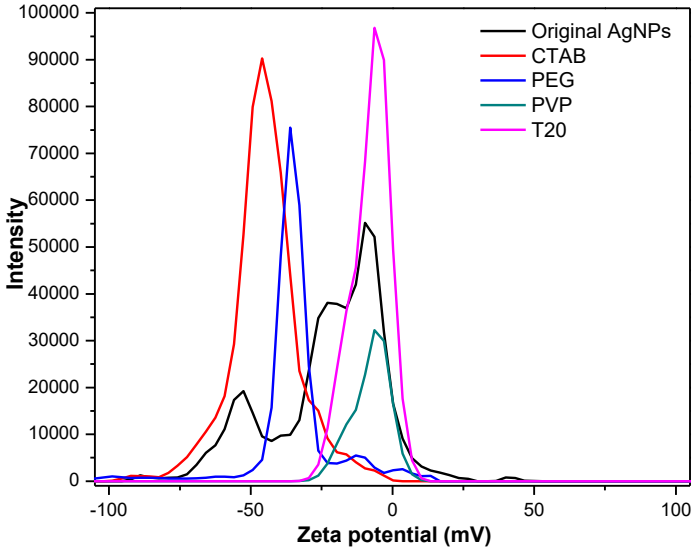

Figure 4.11 Change in the zeta potential distribution of AgNPs in the presence of different surfactants and polymers after 1 h of incubation. AgNP concentration: 5 mg/L.

Figure 4.12 shows the FTIR spectra of studied surfactants and polymers and the mixtures of AgNPs and the studied surfactants and polymers. The characteristic peaks of CTAB (Figure 4.12(a)) can be observed at 2915 cm^{-1} (asymmetric -CH_2 stretching), 2845 cm^{-1} (symmetric -CH_2 stretching)[179], 2285 cm^{-1} (C-H stretching), 1562 cm^{-1} (C-C stretching), 1398 cm^{-1} (C-H bending vibration)[180], and 710 cm^{-1} (C-H stretching) [181]. Most of these peaks observed in the spectrum of CTAB has disappeared in the spectrum of AgNP and CTAB mixture. This phenomenon could be due to the suppressed vibration of chemical bonds of CTAB molecule as a result of the interaction between CTAB and AgNPs.

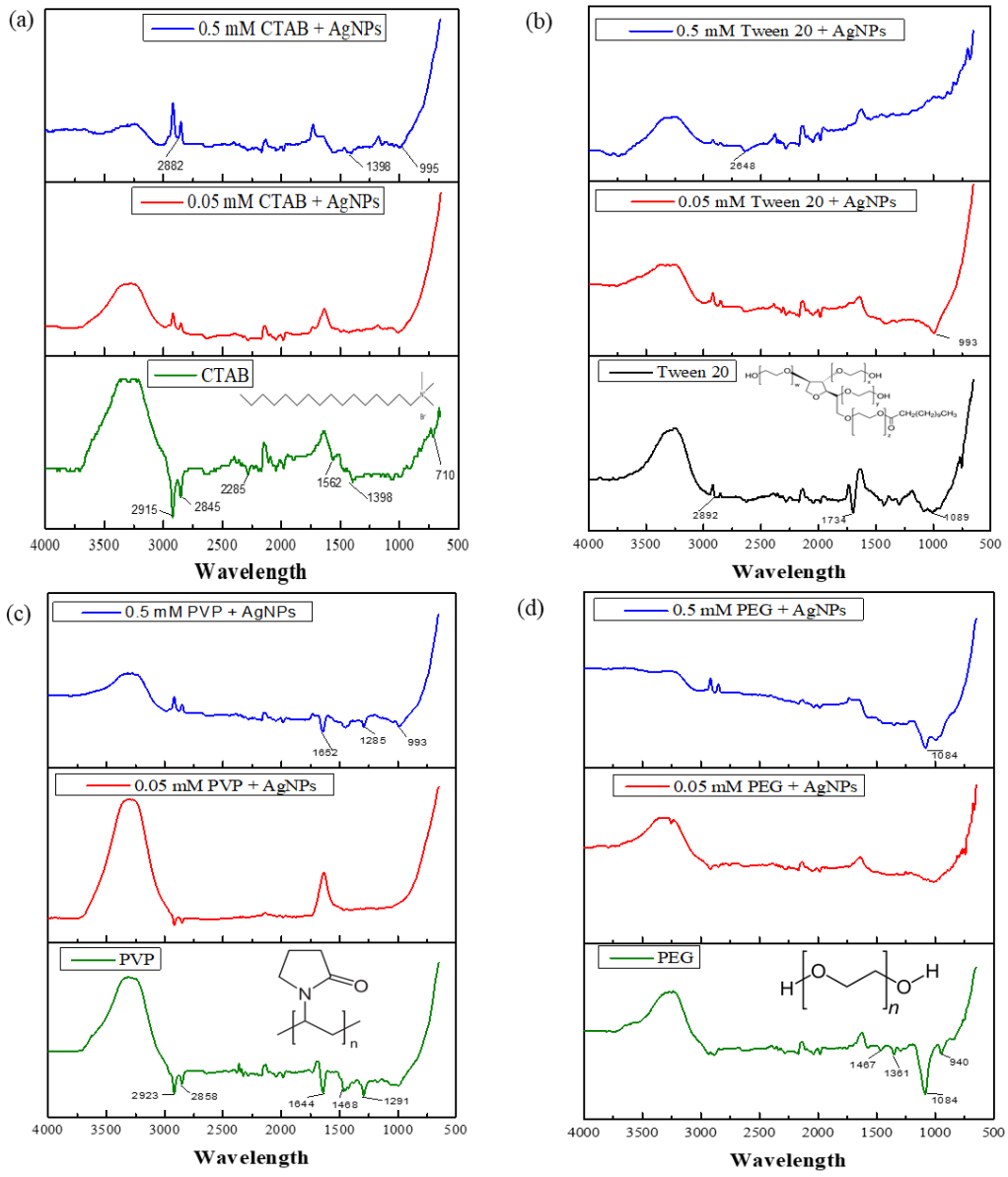

Figure 4.12 Change in the FTIR spectrum of the AgNP solutions as a function of (a) CTAB (b) Tween 20 (c) PVP and (d) PEG concentration

The FTIR spectrum of Tween 20 is shown in Figure 4.12(b). Absorption peaks have been observed at 2892 cm^{-1} (asymmetric and symmetric -CH_2 stretching vibrations) , 1734 cm^{-1} (-RCOOR group), 1089 cm^{-1} (stretch vibration of -CH_2-O-CH_2-) in the FTIR spectrum of Tween 20 [182, 183] as shown in Figure 4.12(b). Most of these peaks have disappeared in the spectrum of the mixture of Tween 20 and AgNPs. At low concentration of Tween 20 (0.5 mM), an absorption peak at 993 cm^{-1} has emerged due to the blue shift of absorption band for the stretch vibrations of -CH_2-O-CH_2-. At higher concentration, these peaks have disappeared yet a relatively small peak can be observed

at 2648 cm^{-1} , which can be due to the blue shift of asymmetric and symmetric methylene stretching vibrations of Tween 20 in the presence of AgNPs [182].

Absorption bands in the regions, 2950–2920 cm^{-1} and 1420 –1430 cm^{-1} were observed in the FTIR spectrum (Figure 4.12 (c)) obtained for PVP, which correspond to the $–CH_2$ and –CH groups of the polymer respectively. More peaks were observed at 1,291 (C-N) and 1,644 (C=O) cm^{-1} [184]. In the FTIR spectrum obtained for AgNP and PVP mixture, the typical $-CH_2$ bands in PVP were observed. Furthermore, the peaks corresponding to C-N and C=O in PVP have shifted to 1285 and 1652 cm^{-1} respectively. The peak shift observed in the mixtures can be attributed to the formation of coordination bonds between the N or O atoms in the PVP molecules with AgNPs [185].

The spectrum of PEG was shown in Figure 4.12(d). the peaks at 1467 and 1361 cm^{-1} are attributed to $-CH_2-$ Scissoring vibration [186] and $-CH_2-$ rocking vibration, respectively. The peaks at 1084 and 940 cm^{-1} belong to C-O-C stretching [186]. The peaks observed in PEG disappear in the spectrum of AgNPs in the presence of 0.05 mM PEG. The peak observed at 1084 cm^{-1} in the spectrum of AgNPs and PEG (0.5 mM) mixture is attributed to the binding of C–C–O and C–C–H groups with AgNPs [187] as shown in Figure 4.12(d).

The results obtained using the zeta potential and FTIR further provide evidence that the AgNPs are differently affected by the type and the concentration of surfactants and polymers. In the presence of CTAB, positive zeta potential values suggest the formation of micelle clusters closer to the NP surface stabilizing the AgNPs and this was also illustrated by the FTIR spectra (Figure 4.12(a)). No possible creation or loss of bonds other than the inherent bonds were identified in the FTIR spectra with presence of Tween 20, due to the fact that the Tween 20 is a non-ionic surfactant (Figure 4.12(b)). In the presence of polymers, i.e. PVP and PEG, the FTIR spectra show the coordination bonds between the polymers and AgNPs (Figure 4.12(c) & (d)).

4.3.4 Impact of surfactants and polymers

In the presence of the cationic surfactant, CTAB, there was no evidence of immediate aggregation revealed in the AgNP dispersions (Figure 4.2(a) & Figure 4.4(a)). However,

when the AgNP dispersion was incubated with CTAB for a longer period up to 90 days, a decrease in the absorbance at the characteristic wavelength was observed (Figure 4.6(a)), maintaining a mono modal particle size distribution (Figure 4.5(a)). The stabilizing effect of CTAB in obtaining a mono modal particle size distribution can be related to two effects. First, according to the DLVO theory, stability is improved by a significant increase in the absolute value of the surface charge of NPs as reflected in the increase of the zeta potential (Figure 4.10(a)). Even though the electrostatic stabilization is of greater importance, the effect of the proposed double layer structure should also be considered. The combined effects induced by CTAB resulted in a monomodal particle size distribution of the AgNPs. Therefore, even at a low concentration of CTAB (0.05 mM), AgNPs were stabilized into a mono modal particle size distribution (Figure 4.4(a)). CTAB coating on the AgNPs suppressed the release of ionic Ag. Hence, the concentration of dissolved ionic Ag was less during the long-term incubation compared to the other surfactants and polymers.

In the presence of the non-ionic surfactant, Tween 20, the particles were less stable compared to the particles in the presence of CTAB (Figure 4.4(b), Figure 4.5(b) & Figure 4.9(b)). Even though a slow aggregation process was observed after the first 1 h, it was not strengthened further at a prolonged period. Contrary to the rate of aggregation, a higher dissolution was observed in the presence of Tween 20 (Figure 4.5(b) & Figure 4.9(b)). A secondary peak was observed around the wavelength of 500 nm after 1 hour (Figure 4.6(b)), which corresponds to the formation of weakly interactive AgNP aggregates [188]. These weak interactions between the AgNPs and Tween 20 demonstrates the stabilization of the AgNPs by Tween 20 as observed in the TEM images (Figure 4.7(c), (h) & Figure 4.8 (b)). The improvement in the AgNPs stability induced by Tween 20 as compared to the condition of without surfactant/polymer is mainly related to steric stabilization, which can be linked to the reorganization of the surface structure. The stabilizing effect induced in the presence of Tween 20 can also be observed from the slower growth of the size of the aggregates over time (Figure 4.5(b)). The stabilization effect induced by Tween 20, can be occurred due to the weak adsorption of the molecules onto the AgNP surface [97]. The weaker stabilization observed in the presence of Tween 20 can be occurred due to the structural behavior of the molecules reflected in the hydrophilic-lipophilic balance (HLB) value. The HLB value is from 0-20 for non-ionic surfactants and approximately 15 for Tween

20 [189]. When the HLB value is higher, the surfactants tend to exhibit less effective stabilization and tend to become hydrophilic [190].

In the presence of polymers, PVP and PEG, a different bonding mechanism on the surface of the AgNPs was observed due to the differences in physical and chemical properties between the two types. The PVP group bonded strongly on the AgNP surface using the nitrogen atom in the molecule [163] (Figure 4.12 (c)), and PEGs weakly bonded on to the AgNP surface through the oxygen atom [177] (Figure 4.12 (d)). Higher amount of dissolution took place in the presence of PVP as revealed by the peaks observed below 10 nm in the particle size distribution (Figure 4.4(c) & Figure 4.5(c)). This can be due to the interconnection of the AgNPs through the molecular chains of a weak polymer in the tail mode. The slow aggregation of AgNPs, initiated immediately by PVP is similar to the flocculation which is a reversible process [124, 163, 191, 192]. Due to the weak interactions with the AgNP surface, PEG molecules can be easily replaced by other molecules compared to PVP molecules. PEG group polymers exhibit a marginal influence on the colloidal stability and the aggregation in the aqueous dispersions of AgNPs (Figure 4.4(d), Figure 4.5(d) & Figure 4.9(d)). This could be attributed to the formation of a surface layer on the surface of AgNPs by PEG, hence the other molecules such as water cannot penetrate through the adsorption layer of the AgNPs.

4.4 Conclusion

The mono dispersed, uncoated AgNPs were freshly synthesized using an oxidation-reduction method and used during the study in the presence of different surfactants and polymers to assess the colloidal stability, physical phenomena of aggregation and dissolution. According to the results obtained using a multitude of techniques, it was found that the surfactants stabilize the AgNPs better than the polymers and assist in obtaining a monomodal particle size distribution. From the two surfactants used during the experiments, CTAB being a cationic surfactant showed promising characteristics as a suitable stabilizer which can preserve the synthesized AgNPs for an extended period with less dissolution, compared to the others. The results obtained during this study provide an improved interpretation on the impact of surfactants and polymers on the

temporal changes of the AgNPs during their fate and transformations in the aquatic matrices.

.

5 Impact of solution pH on the colloidal stability of AgNPs

This chapter discusses the impact of the solution pH on the colloidal stability of AgNPs. Section 5.1 is an introduction to the study. Detailed experimental methods used are described in the section 5.2. Section 5.3 presents the results obtained during the study followed by an extensive discussion in the section 5.4. Key conclusions derived during the study are summarized in the section 5.5.

5.1 Introduction

The environmental conditions where nano silver is suspended play a key role in governing the transformations of the AgNPs [102]. The factors affecting the environmental chemical conditions include pH [27], ionic strength [7], dissolved oxygen, dissolved organic matter [127] and microbial extracellular polymeric substances (EPS) [145]. Of which, pH is one of the most important parameters governing the physical and chemical status [76]. Altering the liquid pH can influence the surface charge and the extent of dissolution of AgNPs, which eventually determines the fate of the AgNPs [7].

Although there has been extensive research on the fate of AgNPs in the aquatic environment, the emphasis on the impact of pH on the aggregation and dissolution of AgNPs in environmentally relevant conditions is minimal. When the pH is considered, the environmental conditions usually observed are pH 5-8. Several studies focused on how extreme low pH would change the properties of AgNPs or how pH change would affect AgNPs in short term incubation conditions [7, 27, 77, 104-106]. The pH range of 5-8 has not been vividly investigated. Further, in most cases, the AgNPs used in the studies are commercially available particles or particles with different types of surface coatings. It should be noted that the coatings are likely detached from the surface once exposed to open environment [193]. Such detachment may also affect the true changes occurred.

In the highly acidic environment, the physical and chemical properties of the AgNPs can be modified and can affect their final form, fate and transformation in the environment [103]. When exposed to environment, AgNPs may undergo different changes in their state, surface charge and morphology. Since the major transformation of AgNPs was observed to occur within several minutes of exposure to acid [194], the modifications have not been fully understood resulting in a lack of knowledge on these processes. For example, in the highly acidic environment, different degrees of particle growth have been observed in which the transformation proposed to occur via a step by step process: first via aggregation from the loss of coating followed by the release of ionic silver and finally the formation of precipitates such as silver chloride [194]. An initial time point of measurement was normally after 10 mins in most of the previous

studies, implying that there is a deficiency of data within a key time frame during which particles undergo their most rapid transformation [105, 106], making the use of previous data challenging in interpretation of these phenomena.

This study provides an improved interpretation on how the solution pH altered the properties of particles over the time, due to its impact on the particle size and dissolved silver concentration. It can be further influenced by the dissolved oxygen as well according to the derived empirical formulae. In summary, the results provide an insight into how the particle properties of AgNPs change as they age in the aquatic matrices and suggest how the particles evolve in the acidic and alkaline pH conditions.

5.2 Experimental methods

5.2.1 Stability of AgNPs under different pH

A series of samples was prepared from the pure AgNP stock solution to evaluate the changes over a period of 24 days. pH was varied in the range of 4-9 in the short-term experiments (up to 1 hour) and 5-8 in the long-term (0-24 days) experiments. Aliquots of 10% (w/v%) HNO_3 or 10% (w/v%) NaOH were used to adjust the pH value to the desired target. All the experiments were carried out in the ambient environment at 25 ± 2 $^{\circ}$C and analyzed in 2 min, 10 min, 20 min and 1 hour for short term experiments and in 1 hour, 24 hours, 7 days and 24 days for long term experiments. Before measurement, the samples were thoroughly mixed for approximately 1 min in screw capped 50 ml centrifuge tubes kept at room temperature (25± 2 $^{\circ}$C). Each type of experimental sample was prepared in triplicate; therefore, the result represents the average of these three samples.

LCTEM experiments were carried out using a Poseidon 210 liquid fluid holder (Protochips Inc.) with liquid cell e-chips containing silicon nitride (Si_3N_4) membrane with a thickness of 50 nm using a JEOL 2010 HR TEM operated at 200 kV. Parallel beam TEM mode was used to record the in-situ images with a dwell time of 0.2 s per frame and hundreds of frames for each sequence [195]. Freshly synthesized AgNPs was used with 10 % (w/v%) HNO_3 acid to investigate the aggregation phenomena in the acidic condition (pH ~ 5.5) and the DI water to investigate the aggregation phenomena in the neutral conditions.

Dissolution of the AgNPs induced by the irradiation of the electron beam in the DI water can be observed in some instances. However, recrystallization of dissolved ions was not observed during the experimental conditions. This dissolution of AgNPs under these conditions will vary on different factors such as irradiation time, dose rate and beam strength. All the images presented in this chapter were acquired under the experimental conditions where no obvious dissolution was occurred.

5.2.2 Stability of AgNPs under different oxygen concentrations

It should be noted that dissolved oxygen (DO) level is a parameter that cannot be ignored when investigating the pH effect. To evaluate the stability of the synthesized AgNPs under different DO levels, three samples were prepared. The first sample was exposed to the ambient environment where there would be atmospheric oxygen exchange with the sample. The second sample was sparged with N_2 and capped immediately after N_2 sparging, and the capped sample was kept at the ambient environment. There would be some oxygen dissolved when the cap was opened for sampling. The third sample was sparged with N_2, capped and kept in the anaerobic chamber. All the samples were covered with aluminium foil to avoid the impact of light on the AgNPs. The SPR peak, pH, zeta potential and the particle size of the three samples were monitored for two weeks and the results are mentioned in Fig. S10-12.

5.3 Results

5.3.1 Characterization of the synthesized AgNPs

The average size of the synthesized AgNPs was 26 ± 1.248 nm. TEM results show the diameters of more than 81% of the counted AgNPs ranged between 10-50 nm. The particles were reasonably monodispersed in the suspension and had a spherical shape (Figure 5.1(a)) with a light-yellow color in the solution (Figure 5.1(b)). The size value obtained using DLS was the peak size based on the intensity distribution (36.76 ± 5.172 nm) (Figure 5.1(c)). The synthesized NPs showed a characteristic peak at the wavelength of 391 ± 2 nm in the UV-Vis absorption spectrum with a peak-absorbance of 0.726 (Figure 5.1(d)). The total silver concentration of the synthesized AgNPs was 5.929 ± 0.025 mg/L with a dissolved silver concentration of 2.278 ± 0.004 mg/L. The

pH and the zeta potential of the pure AgNP stock solution was reported to be 8.03 and -29 ± 1.9 mV respectively.

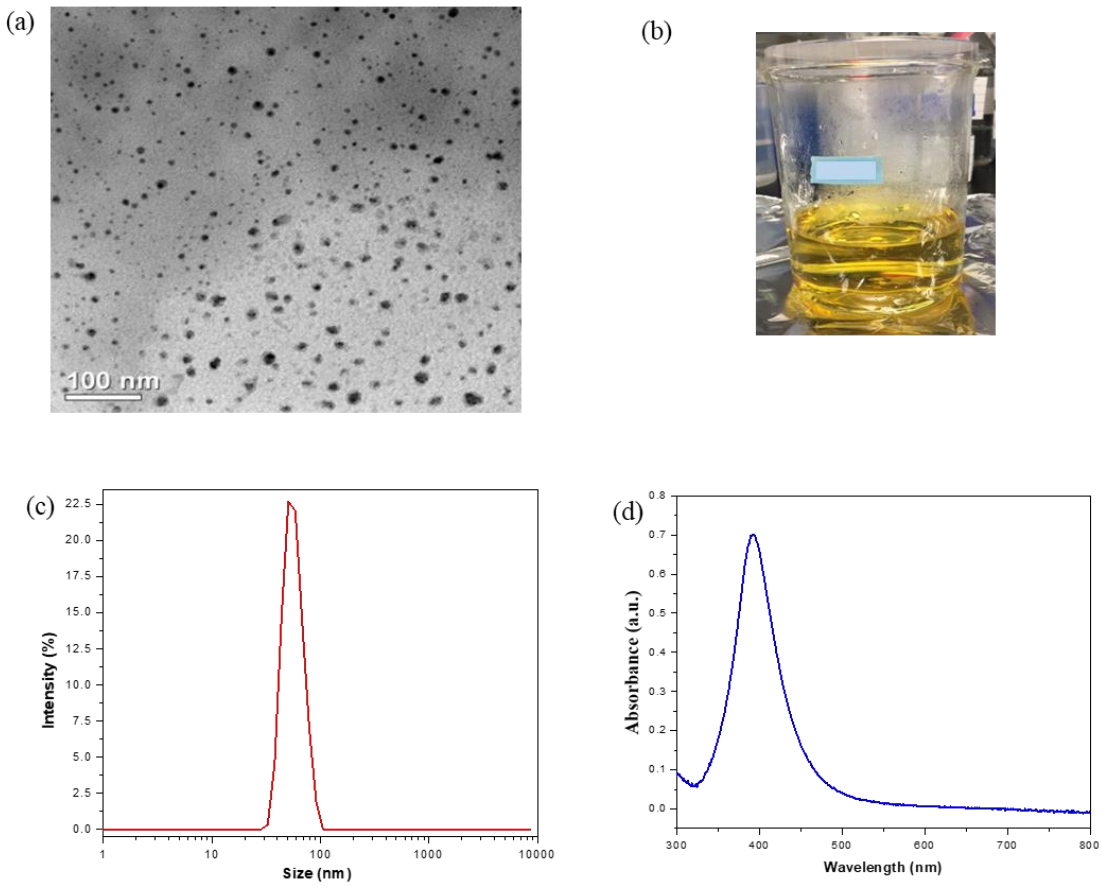

Figure 5.1 Characterization of the synthesized particles (a) Morphology by the TEM (b) Photo of the AgNP suspension (c) Size distribution of the suspension by DLS (d) UV vis absorption spectrum.

5.3.2 Short-term pH impact

The peak absorbance at the characteristic wavelength (391 ± 2 nm for AgNPs) implies the concentration of AgNPs in the solution [196]. The freshly synthesized AgNPs (also denoted as pure AgNPs) displayed a clean and relatively narrow SPR with a peak absorbance of 0.701 at 391 nm (Figure 5.2). The introduction of acid lowered the SPR peak to 0.15 and 0.35 at pH 5 and 6 respectively (Figure 5.2(a) & (b)). In the condition of pH 7, where no acid or base was added and only diluted with DI water, the SPR was reduced from original 0.701 to 0.342 due to the dilution hence causing hindrance to the solution matrix of pure AgNPs (Figure 5.2(c)). At pH 8 (minor pH adjustment from pure

AgNPs solution), the SPR reduced from 0.701 to 0.61 after 2 minutes and remained almost stable for the rest 1 hour of evaluation (Figure 5.2(d)).

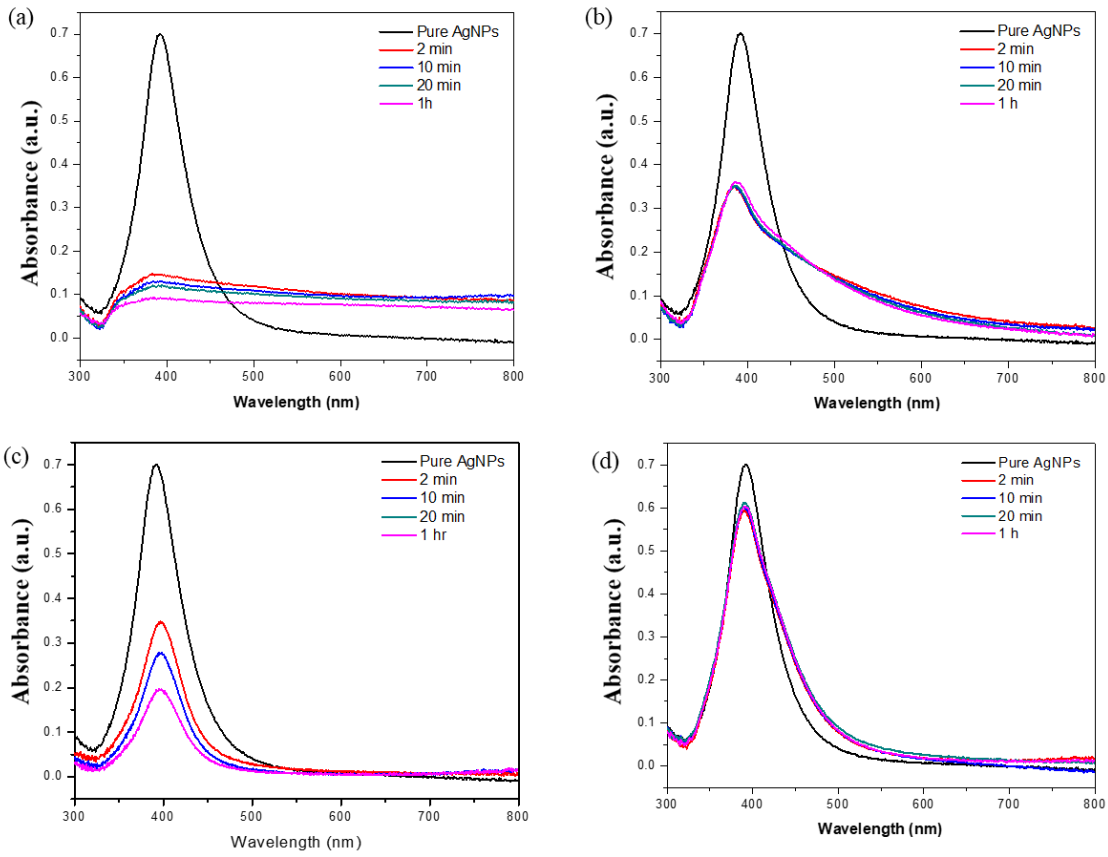

Figure 5.2 Short-term changes in the UV vis spectrum at (a) pH 5 (b) pH 6 (c) pH 7 and (d) pH 8.

Rapid size change in the AgNPs was observed in the first few minutes (Figure 5.3 (a)). From a z average size of 36.76 nm (mode 38.32 nm), the particle size increased to a z average (z avg) size of 433.2 nm within 1 hour, when the solution pH was changed to pH 4. Similarly, the rate of change of z avg diameter was also changed within this 1-hour time (Table 5.2). The largest size was observed at pH 4, and the size gradually decreased with the increasing pH.

The size values obtained at different pH were further confirmed by the results obtained from UV vis spectrum (Figure 5.3(b)) and the particle size distribution (Figure 5.3(c)). The UV vis spectrum shows a significant decrease in the absorbance from 0.701 to 0.19 at pH 7 within 1 hr. The peak absorbance further decreased with the decreasing pH

(Figure 5.3(b)), meantime, a considerable peak absorbance was visible at the wavelength from 500 - 600 nm. It has been reported that 500 - 600 nm is the wavelength used for characterization of AgNP aggregates[197]. Thus, significant amount of AgNP aggregates may appear under low pH conditions. For the solution with the pH in the alkaline region, the decrease in the absorbance was far less compared to the acidic region suggesting that the solution was more stabilized in the alkaline pH. When pH was above 8, the peak absorbance wavelength shifted slightly to the right (Figure 5.3(b)), while maintaining the peak absorbance almost at a constant level regardless of the pH value. The particle size distribution at acidic pH shifted to the right with the peaks in between 300-400 nm (Figure 5.3(c)) suggesting that the particles were destabilized in the acidic conditions and larger sized particles were formed due to the increased particle aggregation [102]. In contrast, the particles in the alkaline conditions became more stable with a particle size distribution similar as pure AgNPs (Figure 5.3(c), Table 5.1). The dissolved silver concentration shows a decreasing trend with the increasing pH (Figure 5.3(d)).

Above observation provides evidence that the short-term aggregation kinetics of the AgNPs is dependent on the solution pH. A higher rate of change was observed in the lower pH at pH 4 (Table 5.2). With the increasing pH, the rate of change decreased depicting that the rate of aggregation was higher in the acidic region compared to alkaline region (Table 5.2). The phenomenon of aggregation could be divided into two main phases [76]. The first phase was where the faster rate of aggregation occurs, which corresponded to the aggregation of individual AgNPs into smaller clusters. During the second phase these smaller clusters came together to form larger clusters which happened in a lower rate. As shown in Figure 5.3(a), this phenomenon took place in the acidic region whereas in the alkaline region or in higher pH, particle size remained almost constant during the experimental period of 1 hour.

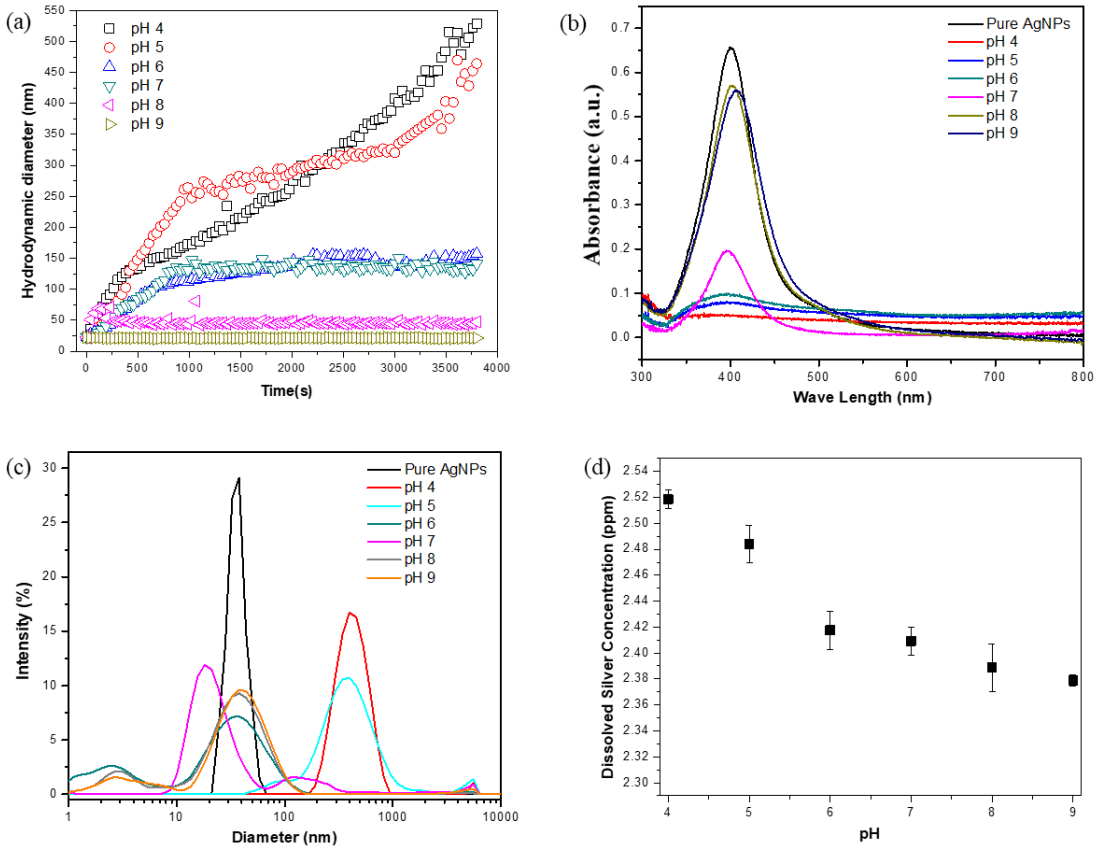

Figure 5.3 Change in the (a) aggregation kinetics (b) UV vis spectrum (c) particle size distribution and (d) dissolved silver concentration during 1 hour.

5.3.3 Long-term pH impact

pH 5, 6, 7 and 8 were chosen for the long-term study. The results show that the SPR peak decreased with the time for all pH conditions with significant changes occurred at pH 5, 6 and 7 (Figure 5.4(a), (b) and (c)) and the highest rate of change occurred in pH 5. At pH 8, there was a red shift in the peak absorbance but the SPR shifted back slightly at the later stage and remained above 0.6 (Figure 5.4(d)).

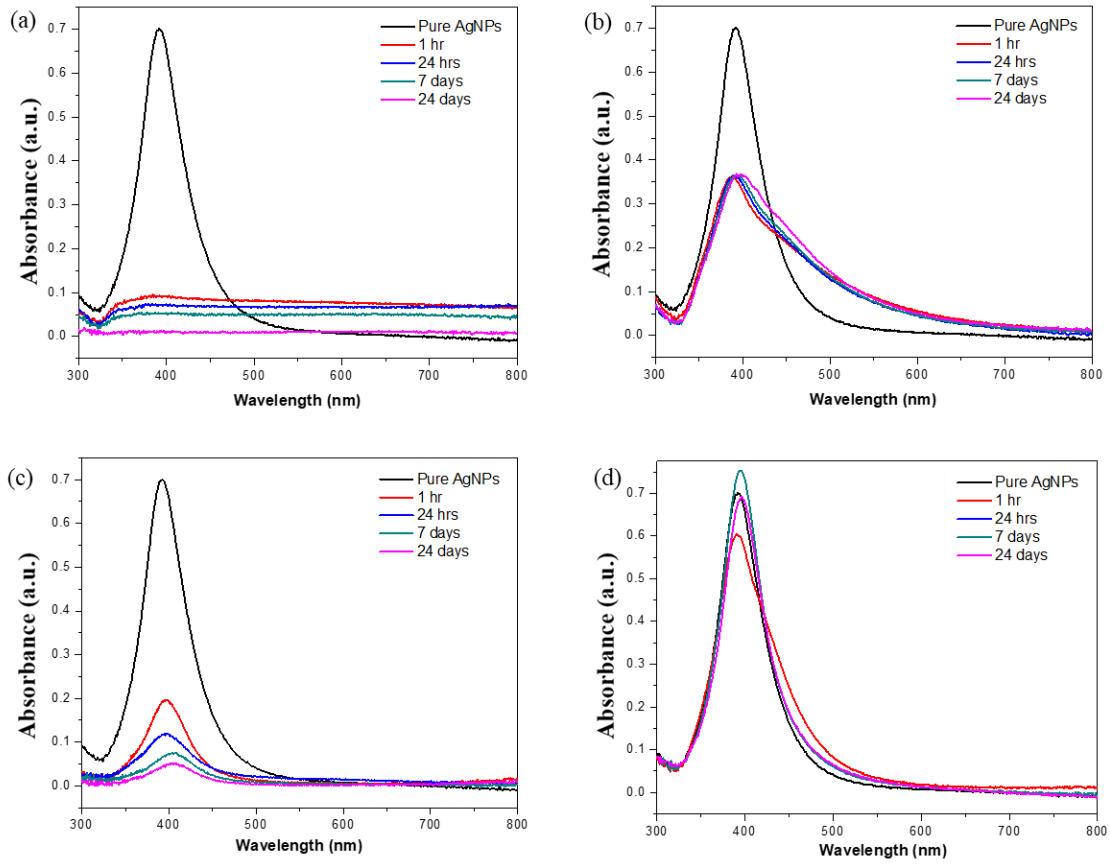

Figure 5.4 Change in the UV vis spectrum at (a) pH 5 (b) pH 6 (c) pH 7 and (d) pH 8

Table 5.1 Hydrodynamic diameter[a] under different pH conditions.

Experimental sample	1 hour			24 hours			7 days			24 days		
	mode	z avg	PdI	mode	z avg	PdI	mode	z avg	PdI	mode	z avg	PdI
Pure AgNPs	38.32	36.76	0.384							40.12	37.8	0.19
pH 4	396.1	433.2	0.271									
pH 5	342	324.1	0.36	396.1	433.2	0.271	458.7	506.5	0.18	531.2	522.7	0.275
pH 6	37.84	41.92	0.545	58.77	68	0.584	78.21	76.3	0.526	91.28	84.2	0.546
pH 7	18.17	75.15	0.375	50.75	47.8	0.505	68.06	69.2	0.576	83.4	82.4	0.524
pH 8	28.21	22.57	0.565	21.04	20.33	0.512	24.81	24.66	0.423	29.41	27.46	0.467
pH 9	24.36	19.44	0.58									

[a]The hydrodynamic diameters and the polydispersity index values have been derived from an average of 10 replicate scans during the measurements.

The particle size distribution in the acidic condition (Figure 5.5(a)) shows that most of the particles were larger (peak at 342 nm) than in the pure AgNPs after the first hour. TEM imaging (Figure 5.6) displays the AgNPs in aggregated clusters which could be attributed to the solution destabilization and subsequent aggregation. The results indicate that the aggregation took place within the first hour in a faster rate, then remained relatively stable after 24 hours. Over the extended period, more particles evolved into larger particles. This peak then remained largely unchanged although there was some increase in a small number of much larger aggregates at approximately 4000 nm. In the neutral and alkaline pH conditions, the particle size remained below 100 nm throughout the experimental period (Figure 5.5(c) & (d)). TEM images obtained for pH 8 depict more stabilized individual particles compared to the images obtained at the acidic conditions (Figure 5.6).

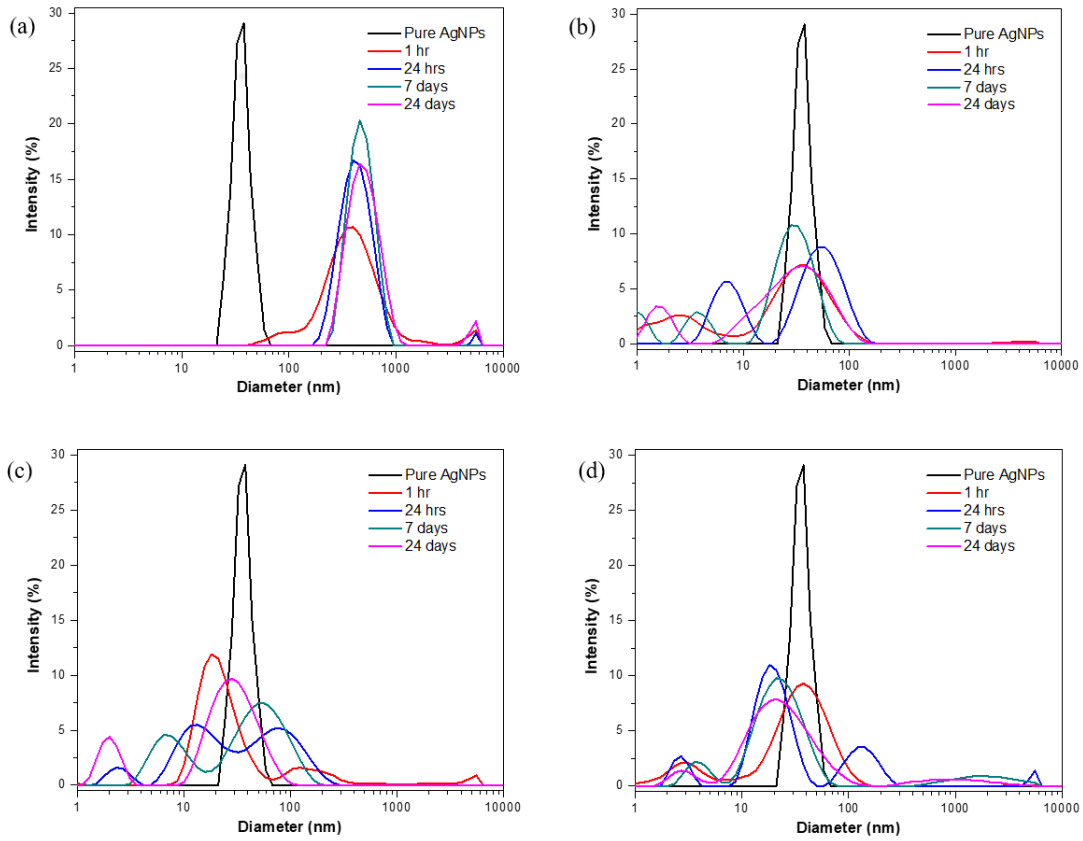

Figure 5.5 Change in the particle size distribution at (a) pH 5 (b) pH 6 (c) pH 7 and (d) pH 8.

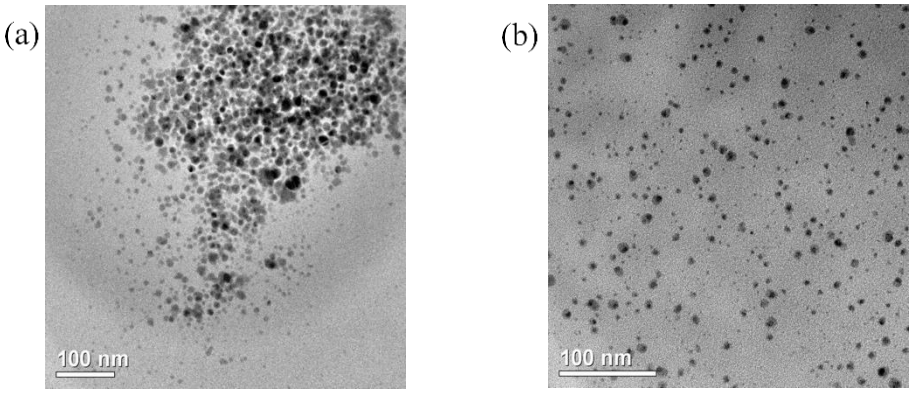

Figure 5.6 TEM images obtained at (a) pH 5 & (b) pH 8.

The zeta potential results obtained for solutions at different pH after 24 hours incubation can be found in Figure 5.7. The results support the results obtained using DLS and UV vis and show that during the alkaline conditions the particles were relatively stable than in the acidic conditions due to the re-stabilization occurred by the negatively charged hydroxyl ions resulting in negative zeta potential. The positive yet the less than 25 mV zeta potential value obtained at pH 5, shows the degree of de-stability occurred in the acidic conditions, due to the addition of protons into the solution which hindered the stability of negatively charged AgNPs in the solution.

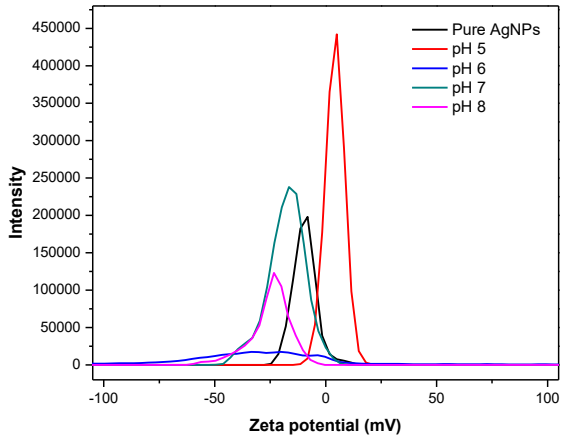

Figure 5.7 Change in the zeta potential at different pH.

The increase in the dissolved silver concentration at pH 5 and 6 (Figure 5.8(a) & (b)) was probably due to the ionic silver released from AgNPs or due to the oxidative dissolution of AgNPs [106]. On the other hand, Ag+ concentration at pH 7 and 8

decreased with the time (Figure 5.8 (c) & (d)). The degree of the dissolution of ionic silver from AgNPs reduced with the increasing pH (Table 5.2). To verify the potential precipitation, EDX analysis of the samples were carried out and the results are mentioned in Figure 5.9 & Table 5.3. The EDX results reveal that there was no precipitation observed in pH 5, 6 and 8.

Table 5.2 Summary of the calculated rate values obtained under different conditions

pH	Absorption Kinetics (a.u.)				Dissolution Kinetics (ppm)		Aggregation Kinetics (nm)	
	Short term		Long term					
	Rate[b]	R^2	Rate[b]	R^2	Rate[b]	R^2	Rate[b]	R^2
4							9426.2	0.9617
5	1.2961	0.9401	0.0030	0.9190	0.0396	0.9111	4890.2	0.9561
6	0.5762	0.9927	0.0002	0.9149	0.0304	0.9106	1503.4	0.9396
7	0.8964	0.9642	0.0028	0.9584	0.0271	0.9768	25.9	0.9038
8	0.2886	0.9485	0.0001	0.9015	0.0176	0.9238	8.6	0.9261
9							1.7	0.9132

[b] the values mentioned are the rates of change per day in the respective category.

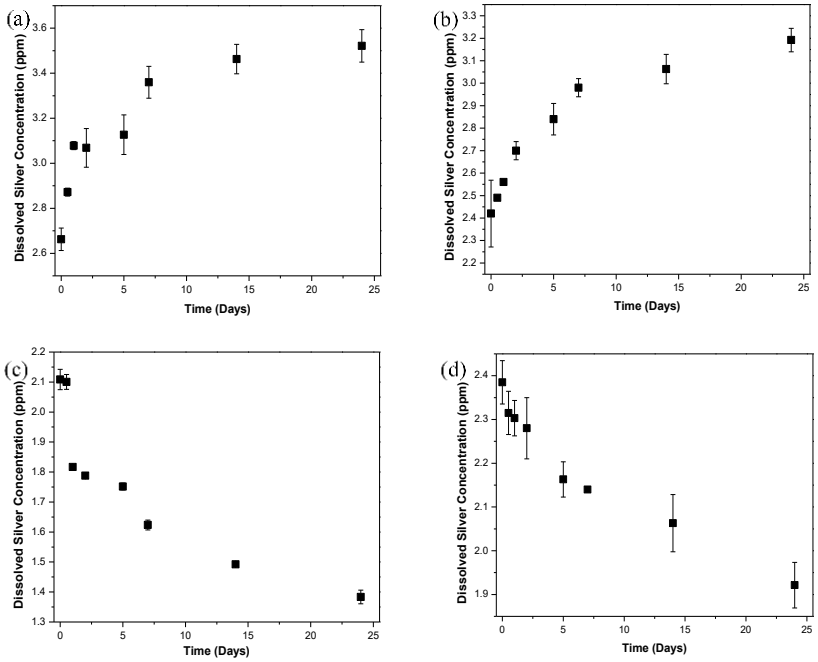

Figure 5.8 Change in the dissolved silver concentration with time at (a) pH 5 (b) pH 6 (c) pH 7 & (d) pH 8.

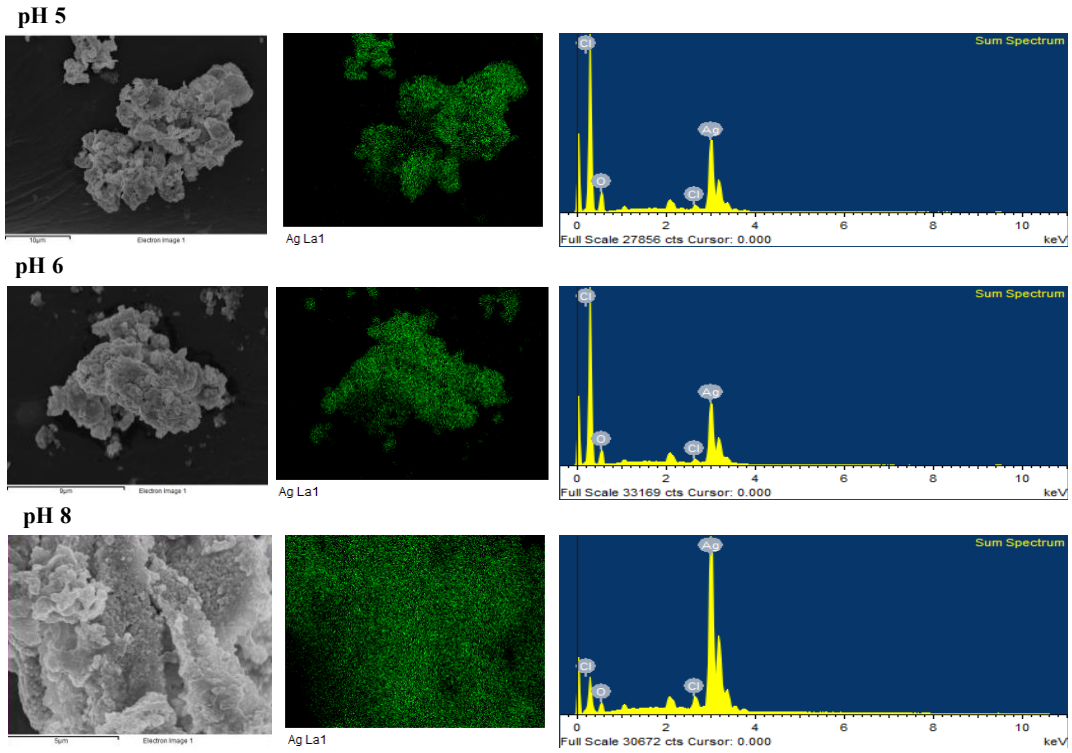

Figure 5.9 EDX analysis of samples at pH 5, 6 and 8.

Table 5.3 Elemental Composition of the samples

Element	pH 5		pH 6		pH 8	
	Weight (%)	Atomic (%)	Weight (%)	Atomic (%)	Weight (%)	Atomic (%)
O	25.60	69.48	23.20	66.64	9.44	40.63
Cl	0.69	0.84	0.74	0.96	1.21	2.35
Ag	73.71	29.68	76.06	32.40	89.35	57.02
Total	100	100	100	100	100	100

5.3.4 In-situ imaging of AgNP aggregation

The aggregation of AgNPs under acidic and neutral conditions was observed using in-situ TEM imaging. The time series TEM images were processed and illustrated in the Figure 5.10. In the acidic conditions, all the particles present within the frame aggregated within 85.8s (Figure 5.10- upper row). On the other hand, there were individual particles in the frame without attaching to the aggregates that previously formed after 175s in the neutral condition (Figure 5.10- lower row). According to these

time series images it is further evident that the rate of aggregation is higher in the acidic conditions compared to the neutral conditions.

In the Figure 5.10, the aggregates formed in each frame were circled in red. According to the time series images, the time taken for two single particles to aggregate was 34.6 s and 64.5 s under acidic and natural conditions, respectively. However, the time required for a single particle to aggregate into an already formed aggregate was shorter (22.6 s and 24.9 s under acidic and natural conditions, respectively). This implies the energy barrier that the single particles need to overcome may be higher compared to the same for a cluster or an aggregate[198]. This can be clearly viewed in the videos showing the movement of particles in neutral and acidic solution (SI Movie 1 & 2).

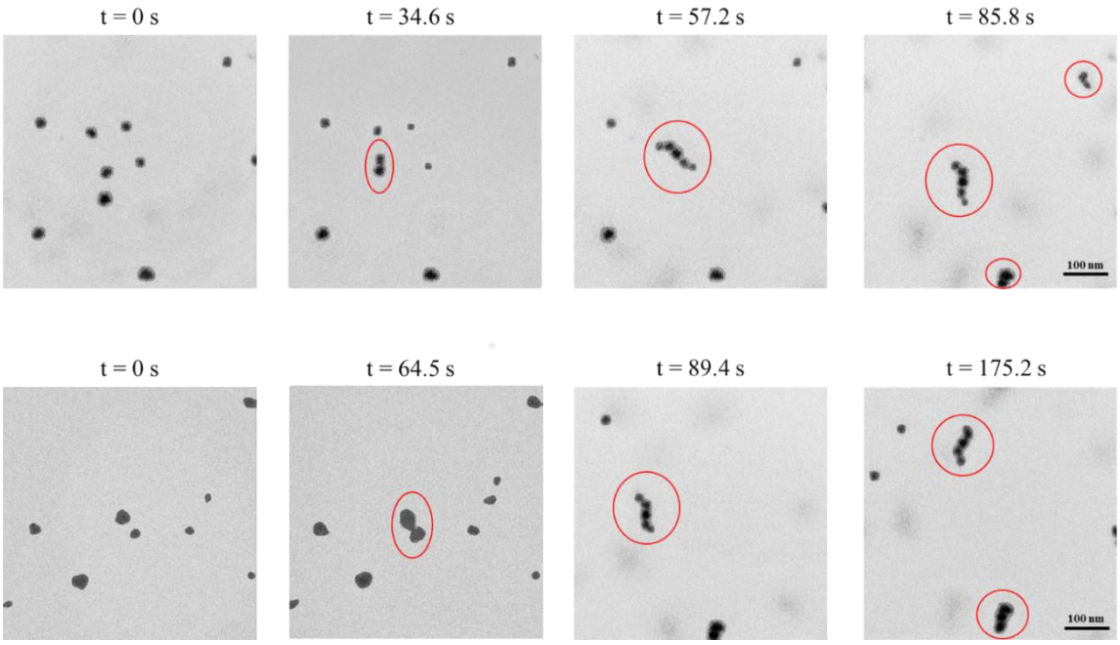

Figure 5.10 Formation of AgNPs aggregates in the time series in acidic condition (upper row) and neutral condition (lower row).

5.4 Discussion

The aging process of the spherical, freshly synthesized uncoated AgNPs during the short -term experiments took place at a higher rate of reaction compared to the same during the long term experiments (Table 5.2), while aggregation dominated the short term transformations. Understanding the impact of the pH will not be completed without studying the potential impact of the DO in the solution matrix. Therefore, the DO effect

has also been discussed in terms of aggregation and dissolution during this study (Figure 5.11-Figure 5.13). However, the results reveal that the impact of DO during the short-term experiments was negligible compared to the impact during the long-term study. The individual and the cumulative impact of DO and pH on the oxidative dissolution and aggregation are discussed in detail in this section.

The results show that the AgNPs were relatively more stable in the reduced oxygen conditions than in the ambient conditions (Figure 5.11). The change in the SPR was less in the suboxic condition compared to the ambient condition after 15 days of incubation. Under the ambient conditions, the SPR reduced from 0.88 to 0.48 (Figure 5.11a).

Under the anaerobic conditions, the peak absorbance was not changed in the first day but after 5 days it was reduced from 0.88 to 0.76 with a shift in the peak to the right and remained stable over the rest of the two weeks (Figure 5.11c). The peak shift implies that the concentration of AgNPs in its original form decreased and the particles stabilized in the anaerobic environment [196]. Considering all the observation under these three conditions, it is evident that the highest rate of stability was observed in the anaerobic conditions. The observation was further proved by the TEM images obtained under different conditions (Figure 5.12). The change of the pH and the particle size distribution of the AgNPs in different DO conditions can be found in Figure 5.13.

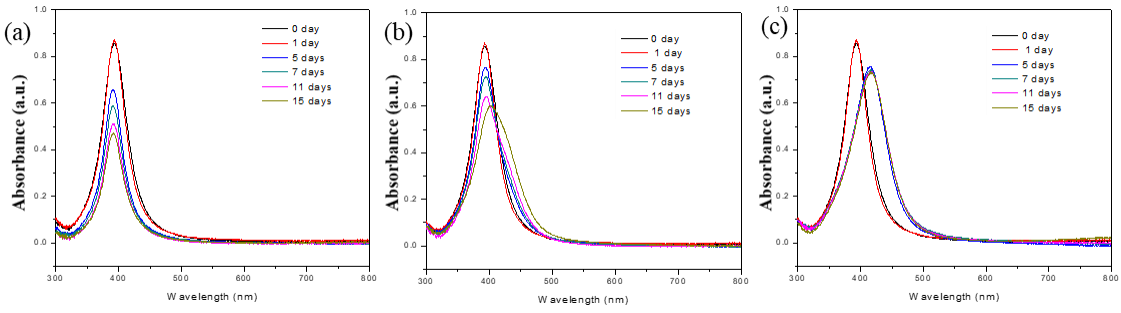

Figure 5.11 Change in the UV vis spectrum in the (a) ambient condition (b) suboxic condition and (c) anaerobic condition.

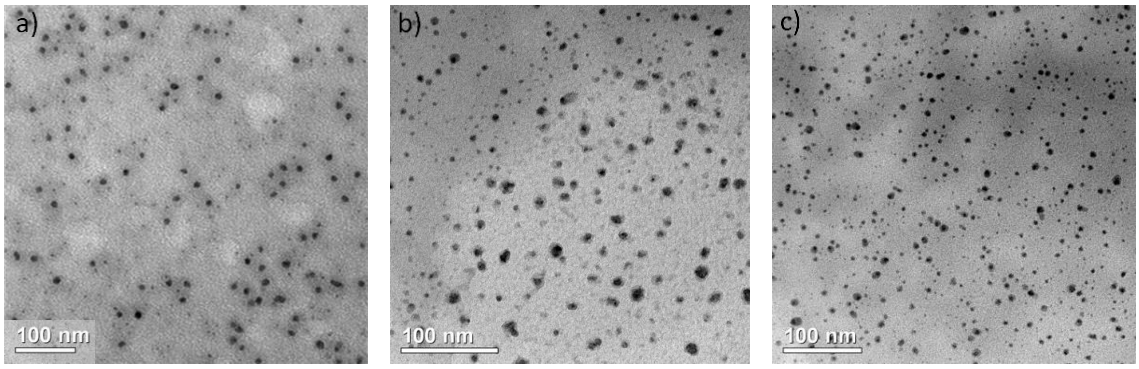

Figure 5.12 TEM images obtained in the (a) ambient condition (b) suboxic condition and (c) anaerobic condition.

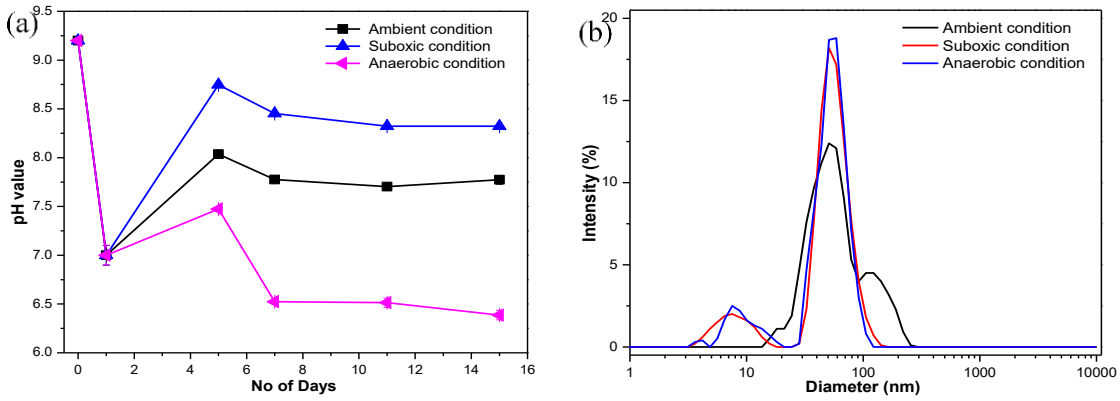

Figure 5.13 (a) Change of the pH in different DO conditions (b) Change of the particle size distribution in different DO condition.

In this study, it was assumed that the dissolved oxygen level in all the samples remained constant (saturated level) and the impact from DO was minor compared to that from pH. To verify the hypothesis, the stability of pure AgNPs without pH adjustment was monitored over 15 days (Figure 5.13(a)). The SPR peak change of the pure AgNPs was used as a baseline to illustrate the DO (sole factor) impact on AgNPs (Figure 5.14). The SPR curves obtained from various pH were normalized with the peak absorbance of pure AgNPs on respective days (e.g. day 1). This is to eliminate the changes caused by background DO and reflect the true effect of pH. A set of the normalized curves obtained on day 1 are shown in the Figure 5.15. The results confirmed that the change in the SPR caused by pH was evidently significant compared to the change caused by DO. This

information clearly depicts that the impact of pH on the aggregation hence the colloidal stability of AgNPs was higher compared to the impact of DO.

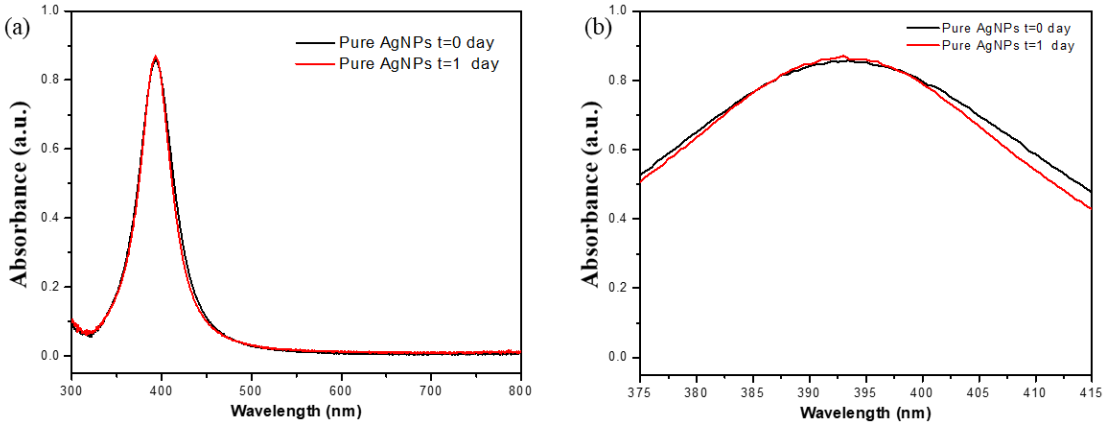

Figure 5.14 (a) Change of the SPR of the pure AgNPs (b) Enhanced image of the change of the SPR of the pure AgNPs.

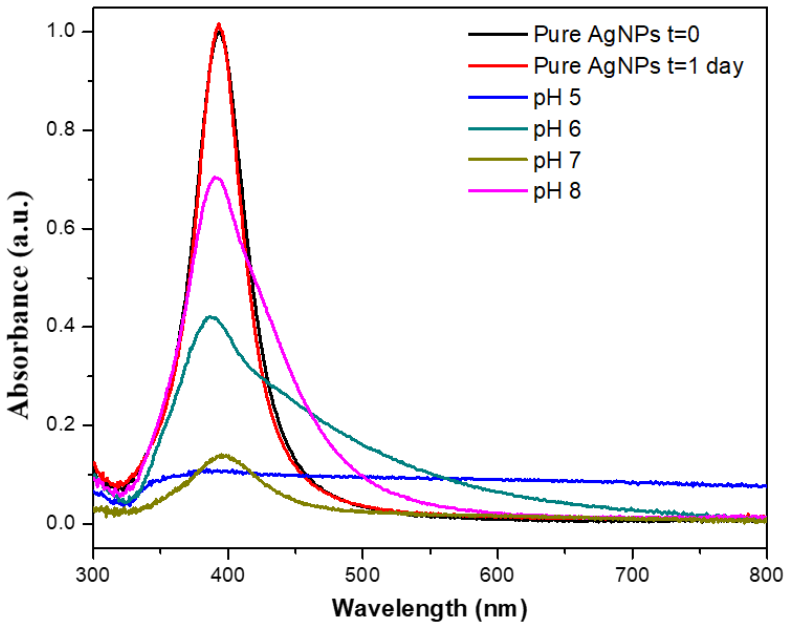

Figure 5.15 Normalized curve to distinct between the impact of dissolved oxygen and pH.

The oxidative dissolution of AgNPs in the solution takes place with the reactions where the metallic Ag is oxidized by oxygen and subsequently reacts with protons (Eqn. (5.1), (5.2)) [106, 199] .

$$4Ag_{(s)} + O_2 \rightarrow 2Ag_2O_{(s)} \quad (5.1)$$

$$Ag_2O_{(s)} + 2H^+ \rightarrow 2Ag^+ + H_2O \quad (5.2)$$

As illustrated in the Eqn. (5.1) the oxygen concentration plays a critical role in the dissolution of AgNPs. During the experiments, it was assumed that the oxygen concentration was kept constant, since DI water was used from the same source and all the experiments were conducted in the ambient environment. The overall reaction took place in the solution can be illustrated as in Eqn. (5.3). It shows that the DO and solution pH directly contribute to the dissolved silver concentration.

$$4Ag_{(s)} + O_2 + 4H^+ \rightarrow 4Ag^+ + 2H_2O \quad (5.3)$$

The hard sphere collision theory can be utilized to determine the dissolution kinetics of AgNPs [59]. According to the theory, rate (γ_{Ag^+}) of ionic silver (Ag^+) release during the overall oxidation of $Ag_{(s)}$ to Ag^+ from the above reaction is shown in the Eqn. (5.4).

$$\gamma_{Ag^+} = \frac{3}{4}\left(\frac{8\pi k_B T}{m_B}\right)^{1/2} \rho^{-1} exp\left(\frac{-E_a}{k_B T}\right) r^{-1}[O_2]^{0.5}[H^+]^2[Ag] \quad (5.4)$$

where k_B is the Boltzmann constant; T is the absolute temperature (K); m_B is the molecular weight of the reactant B (g/mol), which is either oxygen or protons in this case; ρ is the density of the AgNPs (g/cm^3); E_a is the activation energy (J); r is the particle radius (nm); $[O_2]$ and $[H^+]$ are the molar concentrations (mol/L) of dissolved oxygen and hydrogen ions; and $[Ag]$ is the mass concentration of silver in the system (g/L).

At a fixed time, temperature (25 ± 2 °C), DO, $[Ag]$, the original particle size of the samples, m_B and r can be considered as constants. If the results were to be compared across with different pH, Eqn. (5.4) can be rearranged with the following expression:

$$\gamma_{Ag^+} = k[H^+]^2 \quad (5.5)$$

with

$$k = \frac{3}{4}\left(\frac{8\pi k_B T}{m_B}\right)^{1/2} \rho^{-1} exp\left(\frac{-E_a}{k_B T}\right) r^{-1}[O_2]^{0.5}[Ag] \quad (5.6)$$

According to the Eqn. (5.5), the rate of dissolution of AgNPs is proportional to the $[H^+]^2$. This indicates that a minor increase in the H^+ concentration can result in a higher rate of dissolution. This is evident from the results obtained, which shows that with the decreasing pH, the dissolved silver concentration increased in a higher rate (Table 5.2), compared to the higher pH. These observations are in consistence with the previous results [56, 59, 106] and demonstrate that the rate of dissolution will increase with the decreasing pH. The complete dissolution of the AgNPs will occur only when the pH is further lowered or at a longer exposure period.

Based on the SPR peak obtained for the pure AgNPs (Figure 5.1(d)), it can be confirmed that the initial surface of the AgNPs was free of an oxide layer. With the exposure to different pH, the oxide layer of the AgNPs has been changed. According to the EDX results, an increasing trend in the oxygen concentration with the decreasing pH has been observed (Table 5.3). It is possible that the low pH and high DO induced the formation of an oxide layer during the incubation. Therefore, it is confirmed that dissolution of AgNPs was pH dependent, which is related to the dissolution of this silver oxide (Ag_2O) layer (Eqn. (5.2)). The dissolution of the oxide layer may expose metallic silver, which also exhibits pH dependent dissolution (Eqn. (5.3)) [59].

The decrease in SPR normally reflects the change in particle size or morphology [200]. This study reveals that the particle morphology remained spherical regardless of aggregation (Figure 5.6), while only particle size changed. Further, the AgNP concentration at the lower pH was reduced, reflecting a reduction in the stability of the particles. Both particle size and dissolved silver increased under lower pH. The results obtained on the impact of pH on the aggregation and dissolution of AgNPs, were consistent with the previous work [57, 106, 124].

Aggregation of AgNPs takes place when the kinetic energy of the Brownian motion overcomes the energy barrier between the NPs. The energy barrier would be reduced in acidic solution as the NPs become essentially neutral [7] due to the addition of positive charged protons to the negative charged AgNPs. Using in-situ TEM imaging, this study demonstrates that the rate of aggregation increased with the introduction of the protons. The process of aggregation took place with the introduction of protons to the AgNPs in

the aquatic solution. The external protons introduced to the system deteriorated the electron cloud around the particles and attracted the electrons towards them, and eventually destabilized AgNPs [79]. However, in the alkaline conditions, the AgNPs were more stable in solution, since the hydroxyl ions with the negative charge strengthened the negative charges among the AgNPs, hence, the repulsion force increased among the particles. When the hydroxyl ions were introduced to the system of AgNPs in the aquatic solution, they were repelled by the negatively charged AgNPs. This in turn strengthened the electron cloud around the particles and restabilized the electron cloud which enhanced the stability of the particles in the solution. The mechanisms took place in acidic and alkaline conditions are graphically summarized in the Figure 5.16(a) & (b).

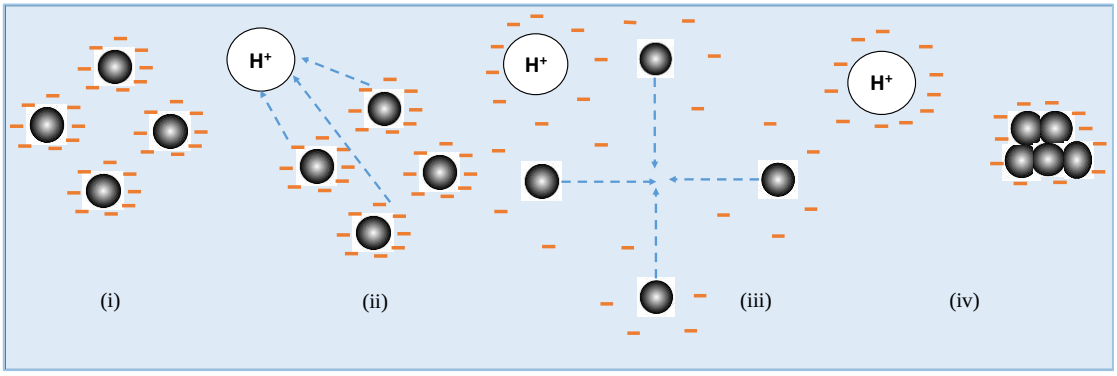

Figure 5.16 (a) Mechanism involved in the change of the particle size with pH in acidic region

(i) AgNPs in the aquatic solution (ii) Introduction of a proton to the system (iii) Deterioration of the electron cloud around the particles and attraction of the electrons towards the proton (iv) Formation of the aggregates by the destabilized AgNPs which is enhanced by the increasing amount of protons

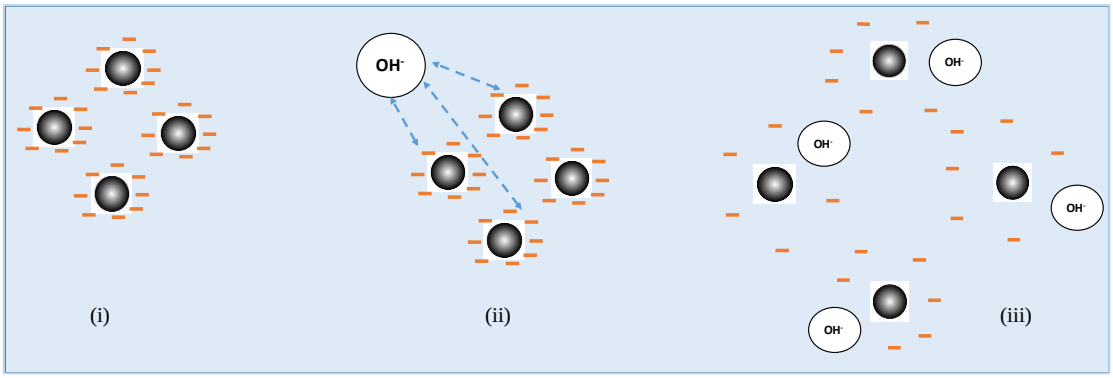

Figure 5.17 (b) Mechanism involved in the change of the particle size with pH in alkaline region

(i) AgNPs in the aquatic solution (ii) Introduction of a hydroxyl ion to the system (iii) Enhancement of the electron cloud around the particles and restabilization of the electron cloud which will enhance the stability of the particles in the solution

During this study, we conducted a series of experiments to get a better understanding on how the properties of AgNPs change over time as a function of pH. This indicates a deviation from the previous research with AgNPs that were conducted under different conditions. Therefore, the outcome of this study provides an insight into the fate of the AgNPs. It will also help to identify the conditions under which the studies conducted with freshly synthesized AgNPs can be confidentially extended to explain such behavior in the environment.

5.5 Conclusions

This study demonstrates the time resolved changes in the properties of uncoated AgNPs as they were exposed to different pH conditions in the aquatic environment. The particles were freshly synthesized and utilized in the study to allow the monitoring and understanding on the aging process of the particles. It was observed that pH had a strong influence on the properties of the AgNPs, as it governed the surface charge of AgNPs hence aggregation (Figure 5.3) and oxidative dissolution (Figure 5.8). It was found that AgNPs were dominantly affected by the pH under the phenomena of aggregation and dissolution. At acidic and neutral pH, the particles were destabilized resulting in higher rate of aggregation. In the alkaline conditions, the particles were re-stabilized due to the presence of hydroxyl ions resulting in more stable suspensions. The short-term results reveal that the impact of DO on the fate of the AgNPs is negligible compared to the

effect of pH, and aggregation dominate the initial transformation. During the long-term study, the aging process of particles happens at a lower rate compared to the short-term study but provide distinct trends in the particle properties in terms of oxidative dissolution and aggregation as a function of pH and DO. These results provide an insight to understand the impact of solution pH on the aging of negatively charged AgNPs, which is important to assess the transport and fate of engineered as well as natural NPs and eventually their impact on the environment.

6 Concentration dependent effect of humic acid on the transformations of AgNPs

This chapter presents the findings investigating the concentration dependent effect of humic acid on the transformations of AgNPs. Section 6.1 provides an overview to the study. Specific experimental methods used in this study are mentioned in the section 6.2. Section 6.3 discusses the results obtained and the insights from the study that can be applicable to the environment with a summary of finding at the end.

6.1 Introduction

The interactions between AgNPs with different environmental constituents can have variable impacts on stability, dissolution and toxicity of AgNPs [36, 103]. These environmental constituents include ligands that bind Ag^{+}, such as NH_3, Cl^{-}, S^{2-} and thiols, cations that can destabilize AgNPs such as Mg^{2+} and Ca^{2+}, as well as the biological macromolecules and dissolved organic matter (DOM) such as humic acid (HA), proteins and polysaccharides which can stabilize AgNPs [103, 201-205].

DOM is known as an agent in improving the stability and reducing the aggregation of AgNPs [206, 207] by reducing the release of ionic Ag [208]. These studies focused on the role of DOM in the transformations of particle properties [8, 209] or release of Ag^{+} [210]. Recent studies [135, 206, 211] have stated that DOM can reduce the ionic Ag in the presence of sunlight in natural water bodies like rivers containing DOM [121, 135, 136]. However, the complexity [212] of DOM and their behavior in the environment make the understanding the fate of AgNPs difficult.

The main objective of this study is to understand the concentration dependent role of HA on the stability and dissolution of AgNPs in the simulated natural environment. In the natural aquatic environment the HA concentration ranges from 0-20 mg/L [206] and 0 – 250 mg/L in the soil environment [213]. The experiments were carried out for a period of 150 days with freshly synthesized uncoated AgNPs in a HA concentration range of 0 – 250 mg/L.

Briefly, aggregation and dissolution of AgNPs in the presence of different HA concentrations, was evaluated as a function of time. Then, an in-depth study was designed and carried out to investigate the impact of light irradiation on the stability of AgNPs in the presence of HA. Particle size distribution (PSD), zeta potential, localized surface plasmonic resonance, dissolved silver concentration, transmission electron microscopy (TEM) and energy dispersive X-ray spectroscopy (EDX) were utilized to assess the colloidal stability of AgNPs. This study provides an important overview on the evaluation of the long-term stability of the AgNPs in the presence of different concentrations of HA in the environment, using freshly synthesized uncoated AgNPs.

6.2 Experimental Methods

6.2.1 Long-term stability of AgNPs

Different concentrations of HA (0, 1, 5, 10, 20, 50, 100, 150, 200 and 250 mg/L) which is abundant in soils and aquatic environment[57] was prepared from the stock solution as mentioned in 6.2.2. The stability of AgNPs (5 mg/L) incubated with various concentrations of HA was analyzed using UV vis spectroscopy and dynamic light scattering. The samples were kept in screw capped tubes and stored under the ambient temperature (25 ± 2 ºC) in the indoor lab environment (with a light intensity ~ 500 lux) and analyzed on 0, 1, 6, 14, 21, 35, 40, 48, 70, 100 and 150 days.

6.2.2 Preparation of stock solutions

Humic acid stock solution was prepared by dissolving 15.2 mg of humic acid (Sigma-Aldrich) in 50 ml of DI water via vigorous mixing in the dark to obtain a concentration of approximately 300 mg/L (actual 304 mg/L as HA and 161 mg/L as DOC). The resulting solution was filtered through a 0.45 µm membrane filter.

6.2.3 Impact of sunlight on the AgNPs in the presence of HA

The lighting conditions of the samples were simulated by exposing the samples to the artificial sunlight from a solar simulator of 1.5 AM (Newport Inc., USA) with a Xenon arc lamp of 300 W (light intensity ~ 10000 lux). During the study, eight hours of light exposure per day was selected as it approximated the conditions in the natural environment[214] and the temperature was maintained at 35 ± 2 ºC. The wavebands were controlled into a specific range of 420–630 nm (visible light), which approximated that of real sunlight using dichroic mirrors. The positioning of the samples was adjusted accordingly to make sure that all the samples received equal exposure to light. AgNPs (5 mg/L) were incubated with different concentrations of HA (0, 1, 5, 10, 20 mg/L) in the 250 mL beakers to simulate the natural aquatic environmental concentrations[211] for two weeks. After exposure to the simulated sunlight the beakers were covered with transparent lids, hence the water loss due to the evaporation is considered negligible. The dissolved oxygen concentration of the samples was around 4.8 ± 0.2 mg/L. To assess the impact of AgNP concentration and ionic Ag concentration, experiments were also conducted at (1) AgNP concentration of 10 mg/L with 1 mg/L HA and (2) ionic Ag

(5 mg/L) only at HA concentration of 1, 5, 10 and 20 mg/L. The experiments were conducted again in the dark conditions by completely covering the solution containers with aluminum foil to exclude the interaction with light. The chemical concentration and operating conditions were similar to the experiments under sunlight. At pre-set time intervals, sample aliquots were collected and analyzed for UV vis spectrum, dissolved silver concentration and pH.

6.3 Results and Discussion

6.3.1 Characterization of synthesized AgNPs

TEM images show that the particles were well dispersed in the solution and generally spherical in shape (Figure 6.1) with an average particle size of 22 ± 0.674 nm. A characteristic peak with an absorbance of 0.926 was obtained at the wavelength of 392 ± 2 nm in the UV-Vis absorption spectrum. The intensity weighted average size obtained using DLS was 32.72 ± 2.214 nm. The total silver concentration of the parent solution was 5.829 ± 0.015 mg/L with a dissolved silver concentration of 2.072 ± 0.002 mg/L. The pH and zeta potential of the parent solution was 8.02 and -28.4 ± 1.6 mV, respectively.

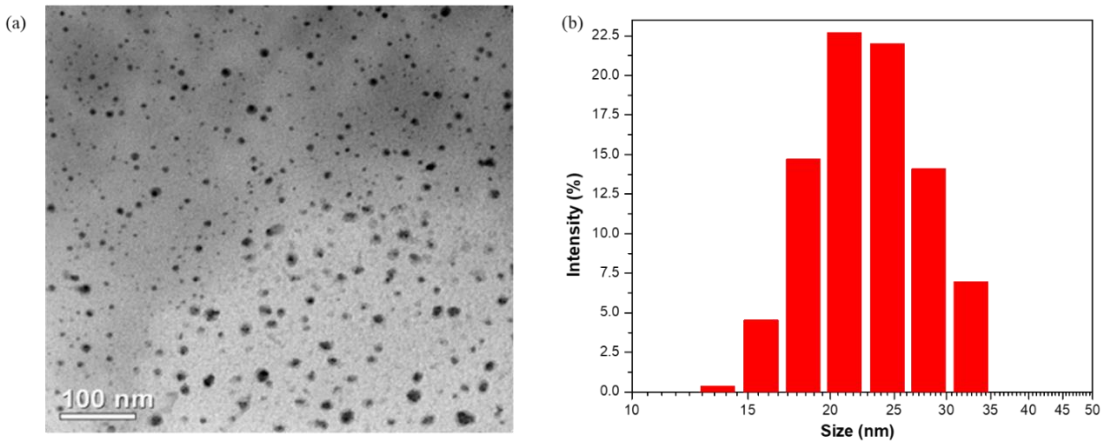

Figure 6.1 Characterization of the synthesized particles (a) Morphology by the TEM and (b) Particle Size distribution of the AgNPs.

6.3.2 Colloidal stability of AgNPs in the presence of HA

Upon the mixing of HA with pure AgNPs, the peak absorbance wavelength shifted from 392 nm to 412 nm with a decrease in absorbance (Figure 6.2(a)). With the increase in

the HA concentration, the absorbance at 412 nm increased from 0.329 to 1.337 (Figure 6.3). Inter-particle bridging among the AgNPs at increased HA concentrations (≥20 mg/L) subsequently resulted in larger particles [215], which was correlated to an increase in the hydrodynamic diameter of the AgNPs (Figure 6.2(b)). For example, the average hydrodynamic diameter increased from 32.72 nm at 0 mg/L HA to 460 nm at 250 mg/L HA. The results observed in the UV vis spectrum is consistent with the change recorded using DLS (Figure 6.2(a) & (b)). Compared to no HA addition case, the particle diameter was almost doubled upon the addition of HA at 1 mg/L (Figure 6.2(b)). At the HA concentration of 10 mg/L (Figure 6.2(b)), the particle diameter was increased by more than 100 nm and further increased with the increase in the concentration. Delay et al. [216] also reported similar particle size change during the absorption of organic materials present in the lake water. The change in the diameter of AgNPs observed with the increasing HA concentration exhibits the different effects caused due to the change in the concentration (0 - 250 mg/L) of HA. Up to the concentration of 20 mg/L, there was an increase in the particle diameter compared to the no HA condition, but the increase was lower compared to the observation above 20 mg/L. Again, there was another remarkable increase in size at HA concentration of 250 mg/L.

20 mg/L and 200 mg/L HA were selected as representative concentrations of the natural aquatic environment and soil environment, respectively. PSD of AgNPs in 20 and 200 mg/L of HA solutions was compared in Figure 6.2(c). The PSD is relatively monomodal for both HA concentrations. The distribution curve shifted to the right depicting an increase in the size of the AgNPs when the HA concentration was changed from 20 mg/L to 200 mg/L, which is consistent with the observed average hydrodynamic diameter. The ionic Ag concentration recorded with the concentration of HA (Figure 6.2(d)) at 1 h shows that the ionic Ag concentration increased with the HA concentration with a relatively similar concentration when HA concentration was above 20 mg/L.

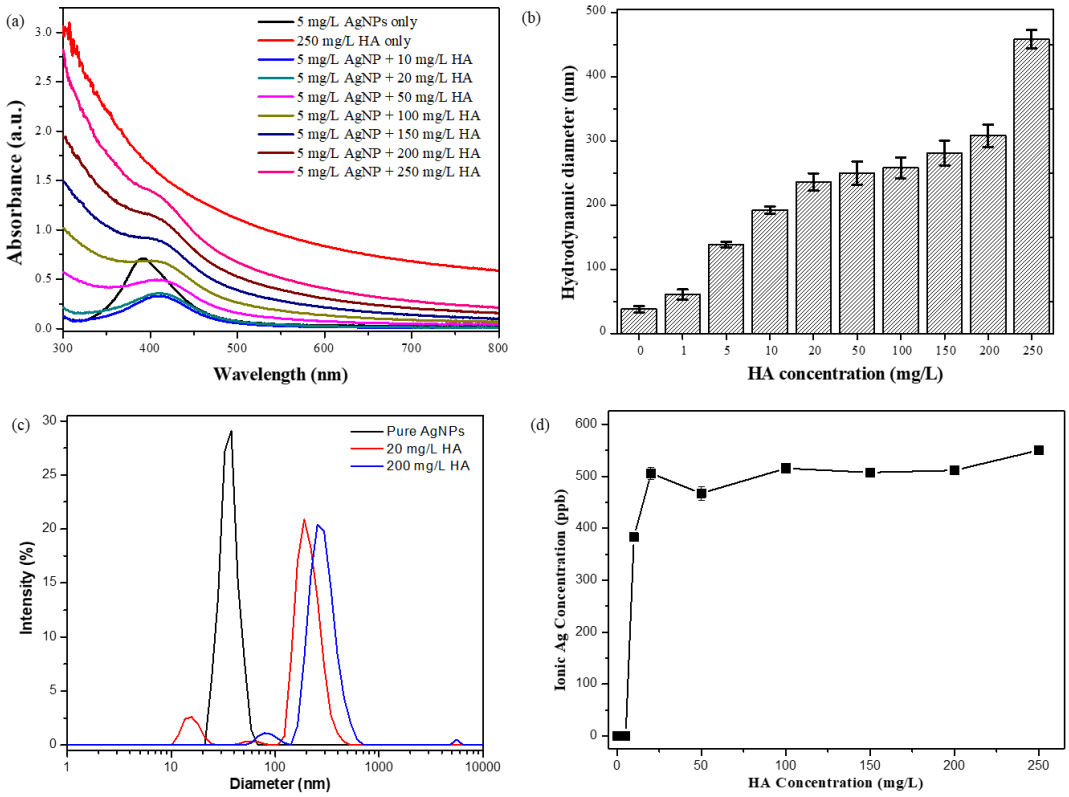

Figure 6.2 (a) UV-vis absorption spectrum and (b) average hydrodynamic diameter of the AgNPs after 1 h incubation with different concentrations of HA. (c) PSD of AgNPs after 1 h incubation with HA concentrations of 0, 20 and 200 mg/L and (d) Change in the ionic Ag concentration with the HA concentration after 1 h of incubation. AgNP concentration: 5 mg/L.

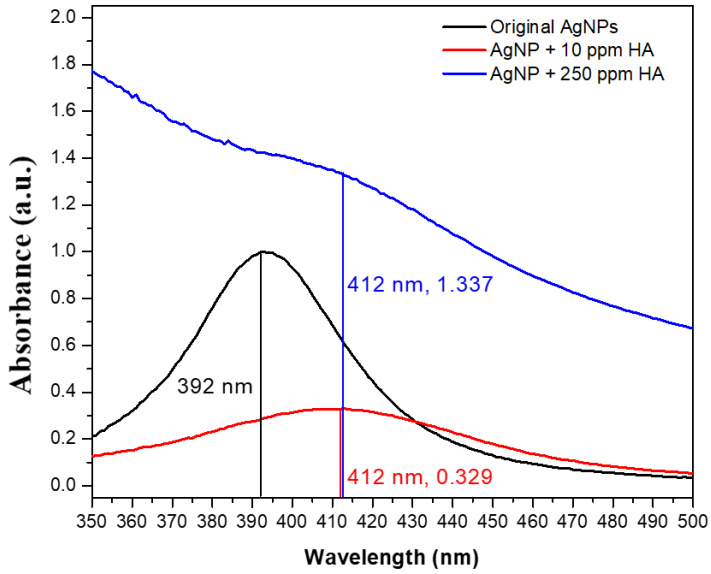

Figure 6.3 Peak shift in the localized surface plasmon resonance (SPR) spectra of AgNPs with variable concentrations of HA.

HA can alter the zeta potential and the conductivity of the solution given being a polyelectrolyte solution with a mixture of carboxylic type and phenolic type groups. HA shows a gradual increase in the negative zeta potential with the increasing concentration due to the higher dissociation of protons at higher concentrations (Figure 6.4(a)). It has been reported that the carboxylic type groups are responsible for this behavior at lower pH and phenolic type groups are expected to contribute more at higher pH values [217]. The negative charge that develops due to this phenomenon, leads to the development of a double layer which is further affected by the ions in the system, in this case the ionic Ag from AgNPs. Therefore, the concentration of HA will affect zeta potential and conductivity, which in turn affects the AgNP surface charge and conductivity when present together.

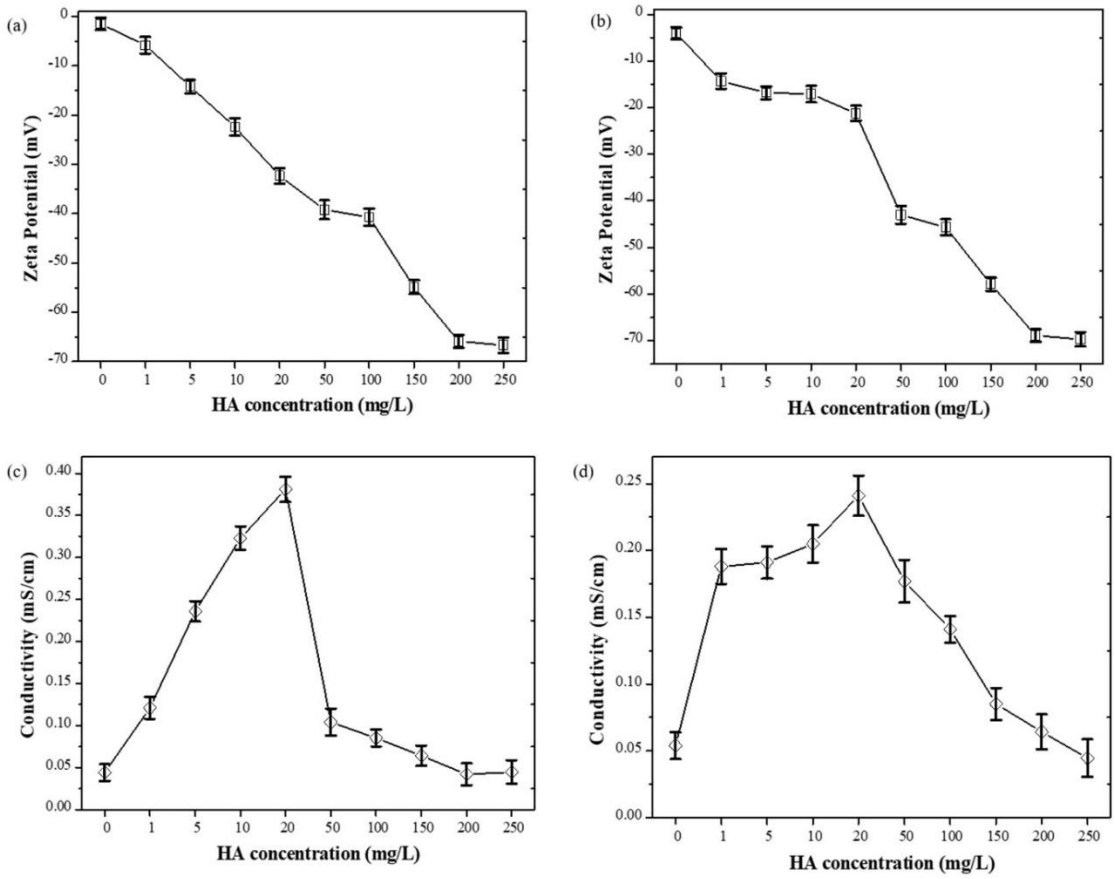

Figure 6.4 (a) Change in the zeta potential and (c) conductivity of HA solutions with the change of HA concentration (b) Change in the zeta potential and (d) conductivity of AgNPs in the presence of different concentrations of HA after 1 h incubation, AgNP concentration: 5 mg/L.

Figure 6.4(a) presents the change in the zeta potential of the HA solutions with the HA concentration. The results show that with the increasing HA concentration, the negative zeta potential of the solution increased. The conductivity profile of HA (Figure 6.4(c)) shows that the conductivity of HA solution increased up to 20 mg/L and then decreased afterwards. Although the zeta potential continuously decreased with the HA concentration, the conductivity at higher HA concentrations was closer to that of lower concentrations. The mono valent ionic Ag has a low affinity for the reactive groups present in the HA but can be present in the double layer as counter ions. At near neutral pH values, approximately half of the groups in the HA are dissociated. Therefore, the net negative charge and the associate cation binding will increase with the HA concentration.

Figure 6.4(b) shows the zeta potential results of AgNPs in the presence of different concentrations of HA. A decrease towards negative zeta potential was again observed upon the increase in the HA concentration. This implies that the HA-AgNP interactions can increase the AgNP stability at higher HA concentrations. Observation of mono modal zeta potential distribution with an increased intensity further proves the fact that the AgNPs became stable at higher HA concentrations (Figure 6.5). As AgNPs carry negative charge at the surface, the zeta potential had more negative value at the same HA concentration with and without the presence of AgNPs.

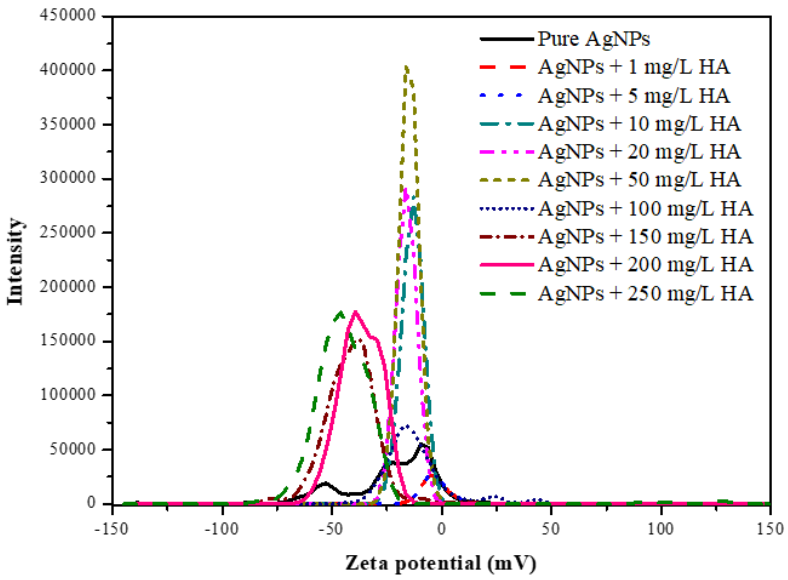

Figure 6.5 Change in the zeta potential distribution with the HA concentration in AgNP-HA mixtures after 1 h incubation, AgNP concentration: 5 mg/L.

HA can be bound to AgNPs via two different mechanisms. One way is the specific binding of protons to reactive sites on the particles and the other way is governed by the properties of the double layer. However, the results we obtain is the cumulative effect of the two parts. The double layer formed depends on the type of the metal ions present in the system and is evaluated through the change in the zeta potential measured experimentally [217]. Since the pure AgNPs are negatively charged, the addition of HA will result in an increased negative zeta potential due to the adsorption of negatively charged HA molecules. The resulting stabilization of AgNPs can be interpreted as an electrostatic effect in which the charge reversal of surfaces prevents the aggregation and increases the repulsive double layer interactions. If steric stabilization would play a significant role, one would expect a different relationship between zeta potential and stability[218] for the AgNPs in the presence of HA. Thus, these results clearly indicate that the stabilizing effect of adsorbed HA is purely electrostatic by adding negative charge to the AgNP surfaces and the concentration of HA plays a critical role in governing the transformations of AgNPs.

According to the results obtained above, it can be concluded that with the increase in the HA concentration, the AgNPs become relatively stable in the presence of HA in the short-term incubation period up to 1 h. When considering the colloidal stability of AgNPs, time factor also plays an important role. Therefore, to assess the impact of time, AgNPs were incubated with different concentration of HA for a period of 150 days and the results are mentioned in Figure 6.6.

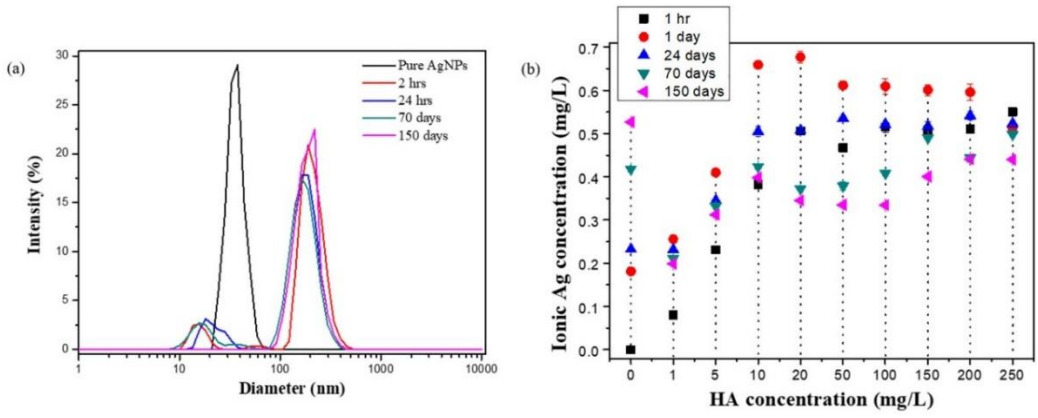

Figure 6.6 (a) Change in the PSD of AgNP solution incubated with 20 mg/L HA with time and (b) dissolved silver concentration at different time intervals after incubation with different concentrations of HA, AgNP concentration: 5 mg/L.

Since 20 mg/L is the HA concentration which separates the two environments it has been selected as the representative concentration to discuss on the PSD. The peak of the PSD shifted from the initial 36 nm to 201.3 nm upon mixing 20 mg/L of HA with the pure AgNPs (Figure 6.6(a)). Then the peak remained relatively stable and steady over the duration of the experiment up to 150 days, with a slight change in the polydispersity index (Table 6.1) and the percentage peak intensity. The arrangement of the distribution remained virtually unaffected during the incubation period. The observed stability of the PSD suggests that the AgNP structures remained unchanged in the presence of HA. It should be noted that there was a second minor peak appeared on the left of the main peak, and this peak disappeared after long term incubation. The reason for the change of this peak will be discussed later.

Table 6.1 Observed z-Average hydrodynamic diameter (z-d_H, nm) and polydispersity Index Measurements for the experimental mixtures**

	2 h			24 h			70 days			150 days		
	Mode	z-d_H	PdI	Mode	z-d_H	PdI	mode	z-d_H	PdI	mode	z-d_H	PdI
S1	201.3	193.7	0.326	283.4	264.9	0.338	309.6	304	0.383	250.3	225.2	0.293
S2	208.4	204.2	0.308	187.0	179.1	0.438	251.2	241.9	0.377	247.5	240.6	0.356
S3	119.8	116.3	0.196	119.1	108.2	0.188	101.2	98.84	0.216	119.9	111.6	0.189
S4	412.9	407.8	0.433	374.0	371.4	0.431	257.6	240.3	0.329	222.7	216	0.333
S5	422.1	411.7	0.523	612.2	563.7	0.555	342.3	327.8	0.401	364.4	359.1	0.376
S6	302.3	298.1	0.405	412.3	382.5	0.618	1348	1330	0.903	396.2	360.8	0.668
S7	462.3	451.7	0.223	712.2	663.7	0.455	542.3	427.8	0.301	464.4	459.1	0.276

**Hydrodynamic diameter and polydispersity index values usually derived from an average of 10 replicate scans. The mode values shown have been obtained for the dominant distribution in each case; modes have not been tabulated for secondary peaks in polymodal dispersions.
***The samples mentioned above are ; S1 – HA (10 mg/L); S2 – HA (20 mg/L) ; S3 – HA (50 mg/L); S4 – HA (100 mg/L); S5 – HA (150 mg/L); S6 – HA (200 mg/L); S7 – HA (250 mg/L). AgNP concentration - 5 mg/L.

Dissolved silver concentration in each AgNP-HA mixture was monitored during the incubation period of 150 days. Remarkable differences in the ionic Ag concentration (Figure 6.6(b)) in each HA solution and the rate of dissolution (Table S2) was recorded. During the first 24 h, we observed that the instant release of ionic Ag upon addition of HA (Figure 6.6(b)), whereas the release of ionic Ag was minor with no HA. Less ionic Ag was released with the increased HA concentration in the first 24 hours. After 24 hours, ionic Ag concentration decreased at a given HA concentration with time. On the

other hand, the ionic Ag concentration increased with the time at no HA condition. Long term tracking shows there was not much variation on ionic Ag concentration at higher HA concentrations (e.g. 200 and 250 mg/L). In the lower concentration range of HA, the dissolution of AgNPs decreased with the time in prolonged periods at the same HA concentration.

Table 6.2 Summary of the dissolution kinetics* in the presence of HA

Concentration	Rate of dissolution	
mg/L	Rate	R^2
10	5.1421	0.9633
20	4.6035	0.9420
50	4.1326	0.9126
100	4.5611	0.9499
150	4.6353	0.9566
200	3.4439	0.8999
250	2.7082	0.9598

*The units of the dissolution rate mentioned above is $mg.L^{-1}.day^{-1}$.

The rate of dissolution (γ_{Ag^+}) was obtained using the nonlinear least square function using the following equations.

$$\gamma_{Ag^+} = k[Ag] \tag{6.1}$$

$$k = \frac{3}{4}\left(\frac{8\pi k_B T}{m_B}\right)^{1/2} \rho^{-1} exp\left(\frac{-E_a}{k_B T}\right) r^{-1}[O_2]^{0.5}[H^+]^2 \tag{6.2}$$

$$[Ag^+]_t = ([Ag^+]_{total})\left(1 - e^{-kt}\right) \tag{6.3}$$

where k_B is the Boltzmann constant; T is the absolute temperature (K); m_B is the molecular weight of the reactant B (g/mol), which is either oxygen or protons in this case; ρ is the density of the AgNPs (g/cm^3); E_a is the activation energy (J); r is the particle radius (nm); $[O_2]$ and $[H^+]$ are the molar concentrations (mol/L) of dissolved oxygen and hydrogen ions; and $[Ag]$ is the mass concentration of silver in the system

(g/L); $[Ag^+]_t$ and $[Ag^+]_{total}$ is the concentration of dissolved Ag at time t and the total dissolved Ag concentration respectively. k is the pseudo first order rate constant.

Higher HA concentrations generally led to lower ionic Ag releasing rates (Table 6.2). This observation reflected the potential of HA in reducing ionic Ag to AgNPs [135, 136, 216, 219]. According to the results, the behavior of HA varied with the concentration in different environments. It was also noted that HA wrapped the AgNPs and coat the AgNPs at higher HA concentrations (Figure 6.7). Such coating may reduce the contact of AgNPs with surrounding aquatic environment thus reduce the oxidative dissolution of AgNPs. Meantime, the coating also resulted in an increase in the size as revealed in DLS results (Figure 6.2(d)). Our results obtained using TEM (Figure 6.8) present that the presence of HA in the matrix stabilizes the AgNPs in the NP form preventing the release of ionic Ag for a considerable time. According to our results we can observe that the AgNPs become effectively stable after 70 days of incubation with HA.

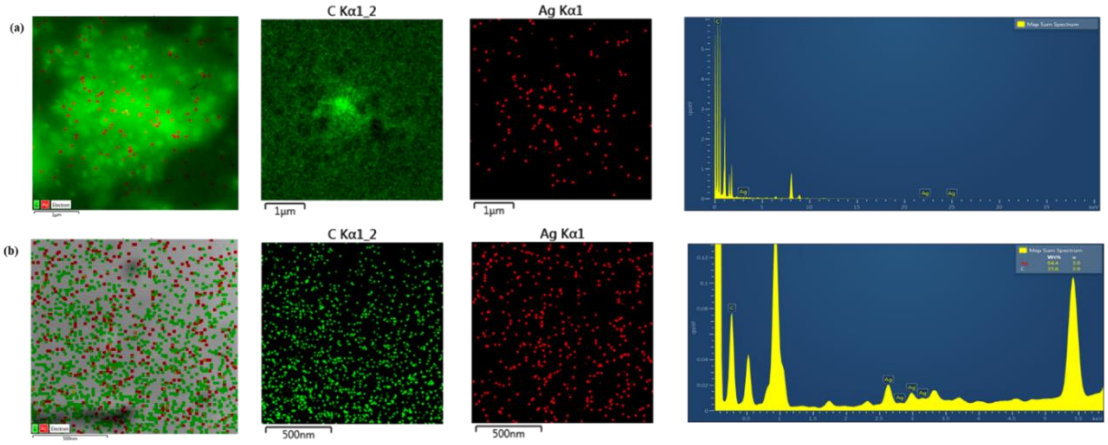

Figure 6.7 Elemental maps of AgNP solution incubated at different HA concentrations (a) 250 mg/L HA, (b) 10 mg/L HA; AgNP concentration: 5 mg/L.

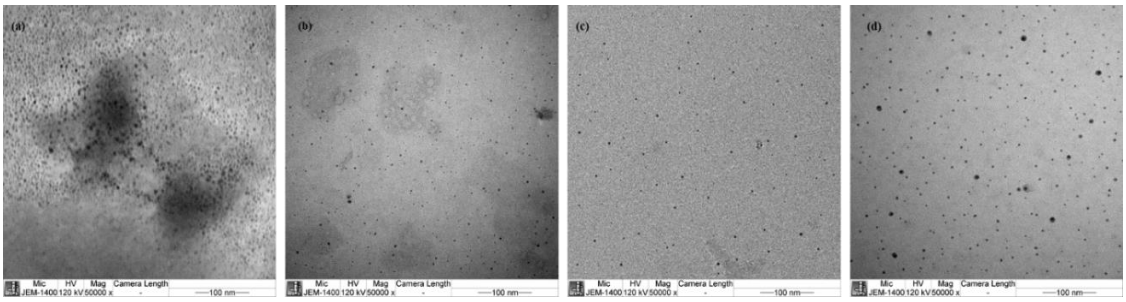

Figure 6.8 TEM images of AgNP incubated at different HA concentrations in the ambient environment (a) 1 mg/L (b) 10 mg/L (c) 100 mg/L and (d) 250 mg/L; AgNP concentration: 5 mg/L.

As reported previously, there were traces of smaller particles around 10 nm appeared over time (Figure 6.2(c) & Figure 6.6(a)). Interestingly, these small particles were considerably reduced in the presence of HA with long-term incubation and completely disappeared on day 150 (Figure 6.6(a)). The observed smaller particles were probably due to the initial dissolution (Figure 6.2(d)) of AgNPs. The dissolution of the AgNPs was gradually reduced and stabilized during the incubation with HA, while the particle size seems to be stabilized as well. The disappearance of small particles can be either due to the complete dissolution or reformation of larger AgNPs. It is noted that higher peak intensity was also observed on day 150 (Figure 6.6(a)). Thus, this observation can be attributed to the stabilization effect imposed by HA in reducing the dissolution [134]. Further discussion can be found in the next section on the concentration range of 1-20 mg/L HA.

6.3.3 The impact of sunlight on the HA - AgNPs mixtures

Exposure to the sunlight is a prominent environmental concern that affects the transformations of AgNPs, as it supplies energy ($h\nu$) that promotes conversion of ionic Ag to elemental Ag with the presence of natural organic matter [200], and also reduce the dissolution of AgNPs [193, 220]. The natural HA levels in the aquatic environment is in the range of 1-20 mg/L [221]. Therefore, the transformations of AgNPs in the lower range of HA concentration is reported here. The UV vis spectrum of the AgNPs with different HA concentrations in the presence and absence of sunlight is presented in Figure 4. In the absence of HA, the peak absorbance at the characteristic wavelength

(392 nm) gradually decreased with the time under the sunlight (Figure 6.10(a)), indicating the dissolution and/or aggregation of AgNPs. As a result, the colour of the AgNPs solution changed from dark yellow to almost no colour (Figure 6.9(b)). In the presence of 1 mg/L HA (Figure 6.10(b)), the peak absorbance at the characteristic wavelength exhibited a slight decrease in the beginning and no further decrease was observed with the time compared to the situation without HA. When the HA concentration is increased to 5, 10 and 20 mg/L (Figure 6.10(c), (d) & (e)), the reduction in the absorbance further decreased. There was almost no evident decrease in the peak absorbance at the characteristic wavelength at the HA concentration of 20 mg/L (Figure 6.10(e)) under the sunlight. Under dark conditions, there was almost no decrease in the absorbance without HA addition. This observation can be attributed to the fact that the AgNPs are deteriorated under the light irradiation and stays stable in the dark conditions.

In the presence of 1 mg/L HA (Figure 6.10(b) & (g)), the peak absorbance decreased in both light and dark conditions and the peak absorbance wavelength shifted above 400 nm. A higher concentration of AgNPs (10 mg/L) was applied with 1 mg/L HA under sunlight and the UV vis spectrum is shown in the Figure 6.10(h). The absorbance of AgNPs at the characteristic wavelength showed no obvious decrease during the incubation period of 14 days in the presence of 1 mg/L HA from the absorbance at the initial conditions.

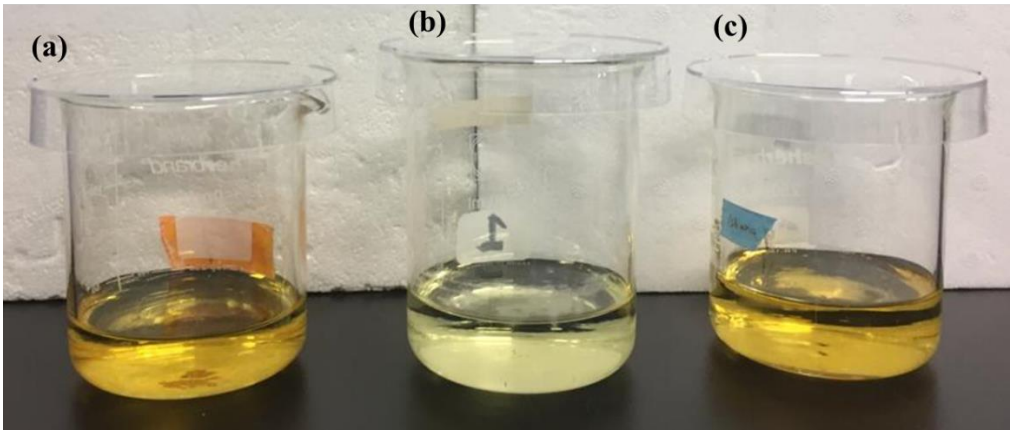

Figure 6.9 Photograph of the colour change of AgNP solutions after incubation for 14 days in the absence and presence of HA (a) original AgNP solution (b) AgNP solution after 14 days without HA (c) AgNP solution after 14 days with 1 mg/L HA

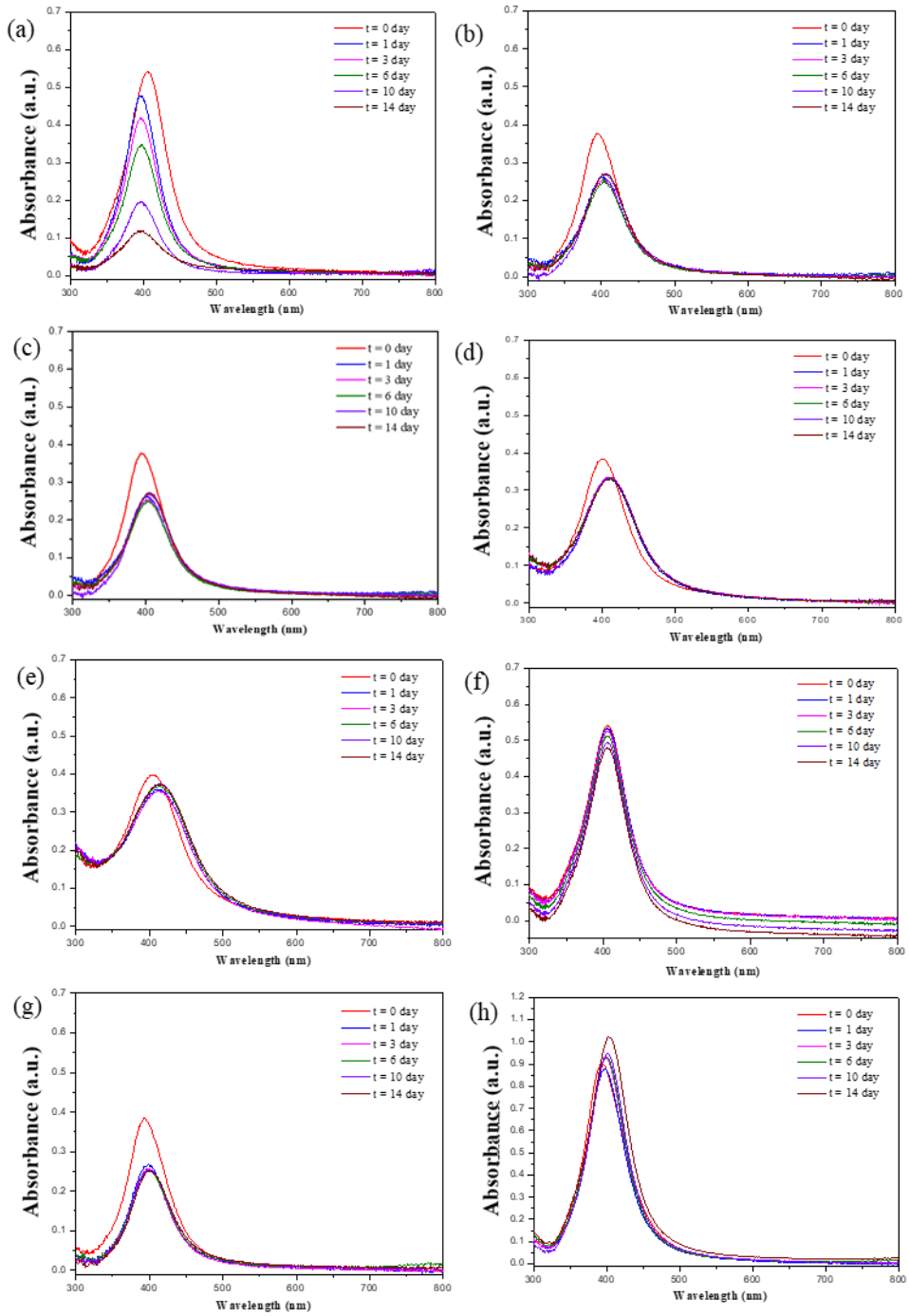

Figure 6.10 Change in the UV vis absorption spectrum of the AgNP solutions after incubation with different concentrations of HA for 14 days under sunlight (a) 0 mg/L HA, (b) 1 mg/L HA, (c) 5 mg/L HA, (d) 10 mg/L HA, and (e) 20 mg/L HA; in dark (f) 0 mg/L HA, (g) 1 mg/L HA with a AgNP concentration of 5 mg/L. (h) UV vis absorption spectrum for 10 mg/L AgNPs with 1 mg/L HA under sunlight.

The solution pH of the samples was stable during the period of incubation and the results are mentioned in the Figure 6.11. This ensures that there was no evident pH change took place during the experiment. TEM images (Figure 6.12) show that AgNPs aggregated after incubation for 14 days in the absence of HA, which can be correlated to the increase in the absorbance at 450-500 nm (Figure 6.10(a)). At a low concentration of HA (ex: 1 mg/L), the aggregation was inhibited with the smaller particles remaining in the solution. With the increase in the concentration of HA (ex: 20 mg/L), the aggregation of AgNPs was effectively inhibited without a remarkable change in the particle shape suggesting that HA can stabilize the AgNPs for a prolonged period.

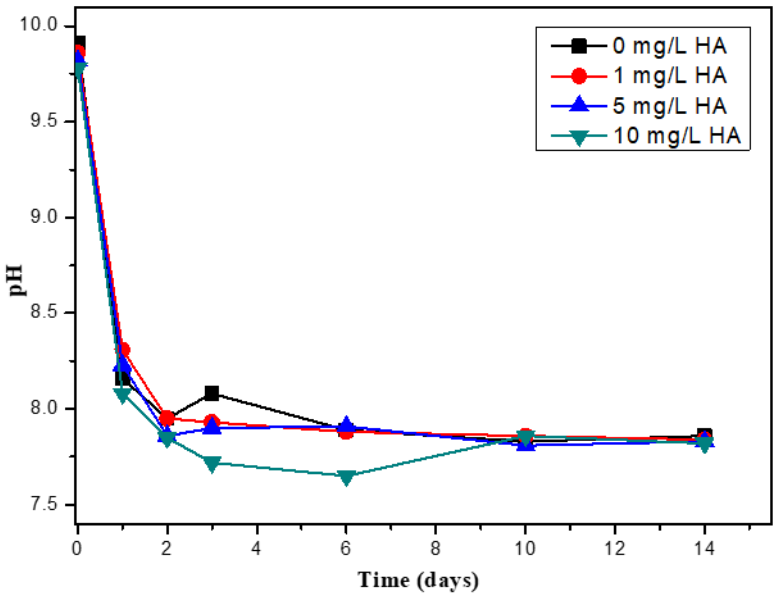

Figure 6.11 Change in the solution pH of the experimental solution during the incubation period at different HA concentration. AgNP concentration: 5 mg/L.

In addition, in the presence of HA, many smaller particles appeared with a mean particle diameter of 2.8 ± 1.1 nm and surrounded the original AgNPs (Figure 6.12). After 14 days of incubation, the particle size of these smaller particles increased, and it was observed to be 7.8 ± 0.3 nm. The growth in the particle size during the incubation period lead to the change in the PSD of the solution (Figure 6.12(b), (f) inset). High resolution TEM and EDX measurements were utilized to confirm that the newly formed particles were AgNPs and the results are shown in Figure 6.13. More results obtained using TEM and EDX at HA concentrations of 5 mg/L and 10 mg/L are mentioned in Figure 6.14. When ionic Ag was used instead of the AgNPs under the simulated sunlight, the ionic

Ag could be reduced to form secondary particles. This phenomenon was detected using UV vis absorption spectrum obtained with different HA concentrations incubated with 5 mg/L ionic Ag (Figure 6.15), TEM and EDX analysis (Figure 6.16).

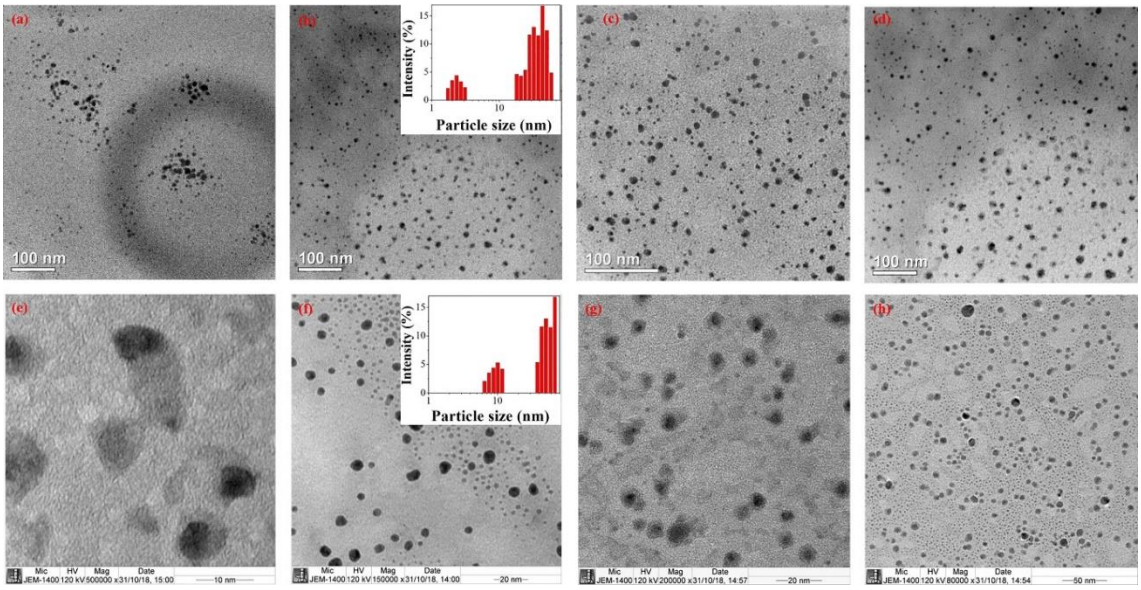

Figure 6.12 TEM images of the AgNP solutions after incubation with different concentrations of HA for 1 day and 14 days under sunlight (a, e) 0 mg/L HA, (b, f) 1 mg/L HA, (c,g) 5 mg/L HA and (d,h) 20 mg/L HA. (b, f-inset) PSD on day 1 and 14 at 1 mg/L HA. AgNP concentration: 5 mg/L.

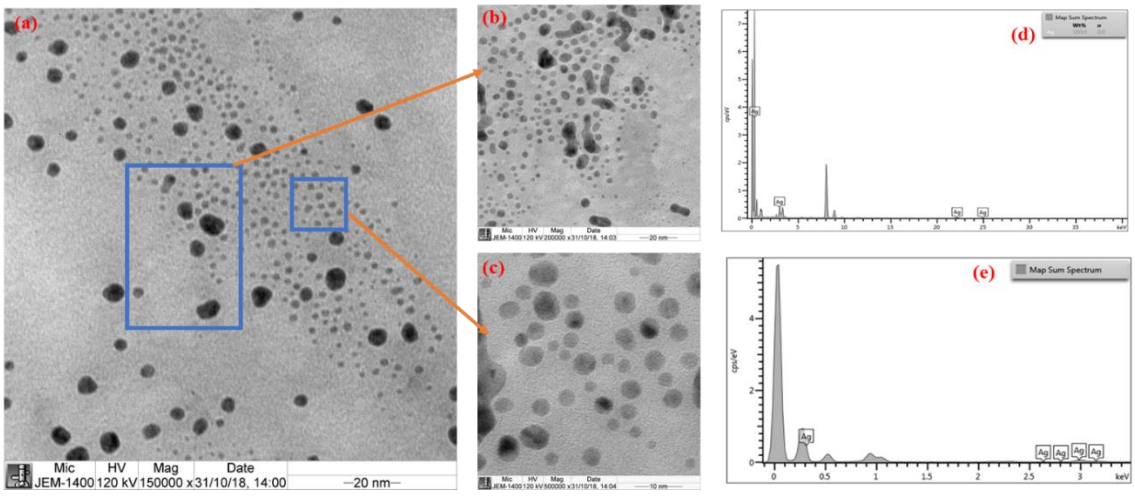

Figure 6.13 TEM images and the corresponding EDX spectra of AgNPs (5 mg/L) incubated with 1 mg/L HA for 14 days under the simulated sunlight. (a) TEM image of the AgNPs in the solution. (b) TEM image of the primary AgNPs and the corresponding (d) EDS spectrum. (c) TEM image of the secondary AgNPs and the corresponding (e) EDS spectrum.

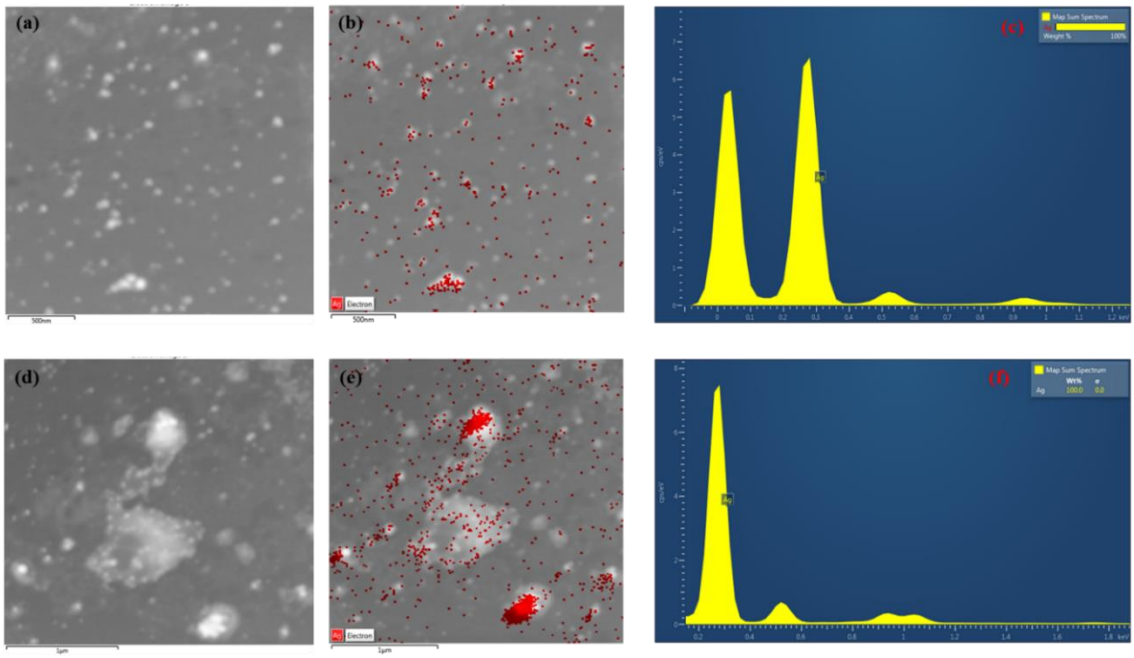

Figure 6.14 Elemental maps of AgNP solution incubated at different HA concentration (a-c) 5 mg/L HA, (d-f) 10 mg/L HA; AgNP concentration: 5 mg/L.

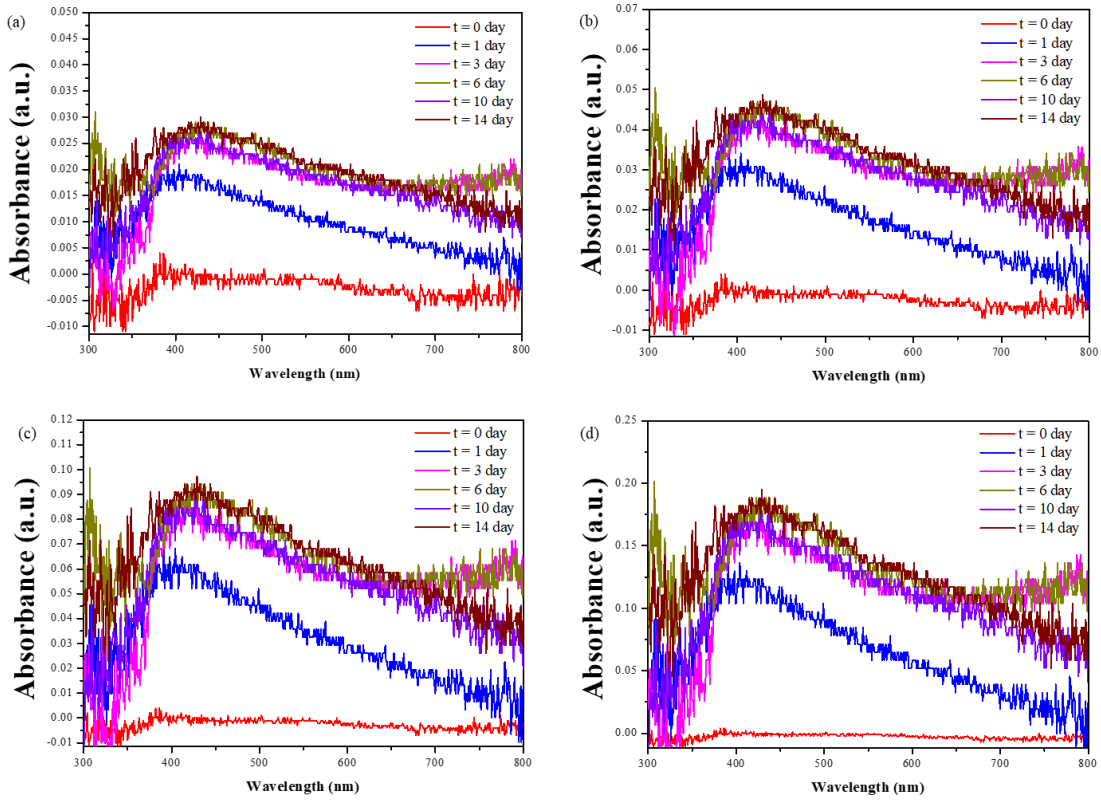

Figure 6.15 Change in the UV vis absorption spectrum of the Ag+ (5 mg/L) solution after incubation with different concentration of HA for 14 days under sunlight (a) 1 mg/L HA, (b) 5 mg/L HA, (c) 10 mg/L HA and (d) 20 mg/L HA.

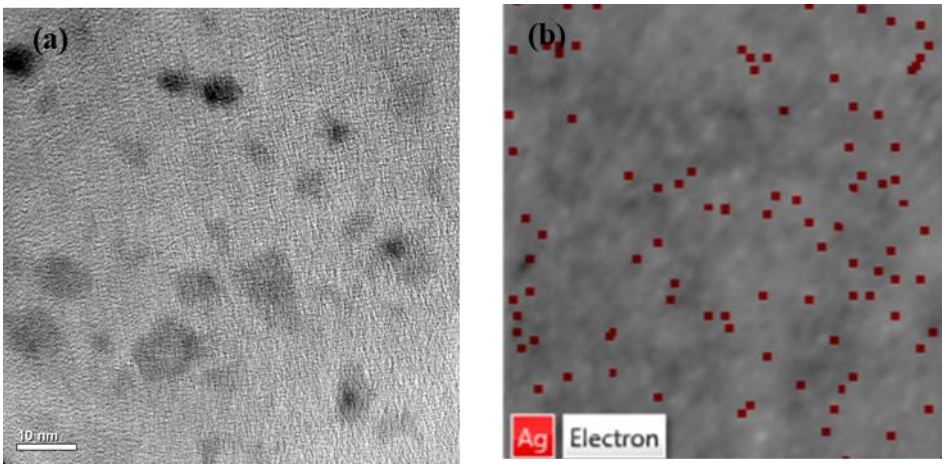

Figure 6.16 Elemental maps of Ag+ solution incubated with HA under sunlight (a) TEM image, (b) corresponding elemental map; Ag+ concentration: 5 mg/L. HA concentration: 1 mg/L.

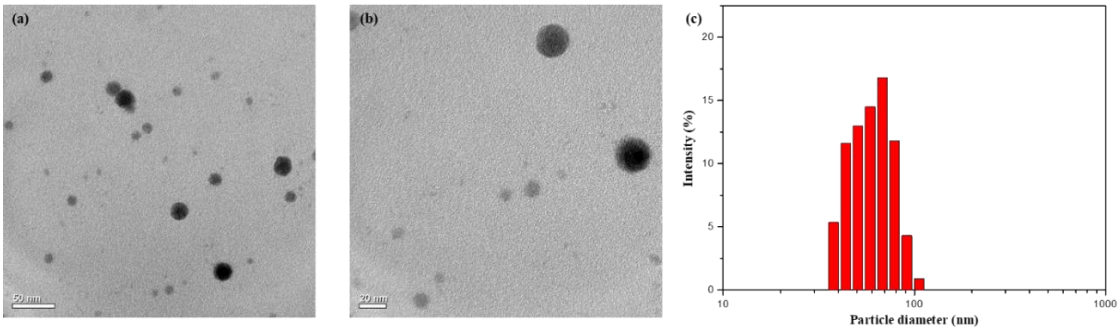

Figure 6.17 TEM images obtained of AgNP solution incubated in the dark (a) day 1 (b) day 14 (c) particle size distribution on the day 14; AgNP concentration: 5 mg/L HA concentration: 1 mg/L.

According to the UV vis spectrum obtained in the dark conditions (Figure 4(f) & (g)), it is evident that the peak absorbance reduced initially, but it did not shift remarkably compared to the light conditions (Figure 6.10(b-e)). This observation shows that the secondary particle formation due to the reduction of ionic Ag occurred in the presence of sunlight, did not take place in the dark conditions. The TEM images and the PSD on day 14 obtained in the dark conditions revealed that small particles were not formed in the solution (Figure 6.17). The release of ionic Ag at different HA concentrations in the presence and absence of sunlight is presented in Figure 6. Without HA, the ionic Ag

concentration increased in the first 6 days, and then remained almost stable during the rest of the incubation period. In the presence of HA (1 mg/L), the trend of release of ionic Ag is similar to that without HA up to 24 h, but gradually reduced afterwards. When the concentration of HA was further increased, the amount of ionic Ag released reduced greatly at a given time (Figure 6.18(a)). Compared to the conditions under sunlight, the amount of ionic Ag released in the dark conditions is presented in Figure 6.18(b). The amount of ionic Ag released in the dark conditions in the absence of HA was less than in the conditions under the sunlight. However, the ionic Ag released in the presence of HA was higher in the dark conditions compared to the results obtained at the conditions under sunlight. This observation further confirms that the reduction of ionic Ag occurred only in the presence of sunlight but not in the dark conditions.

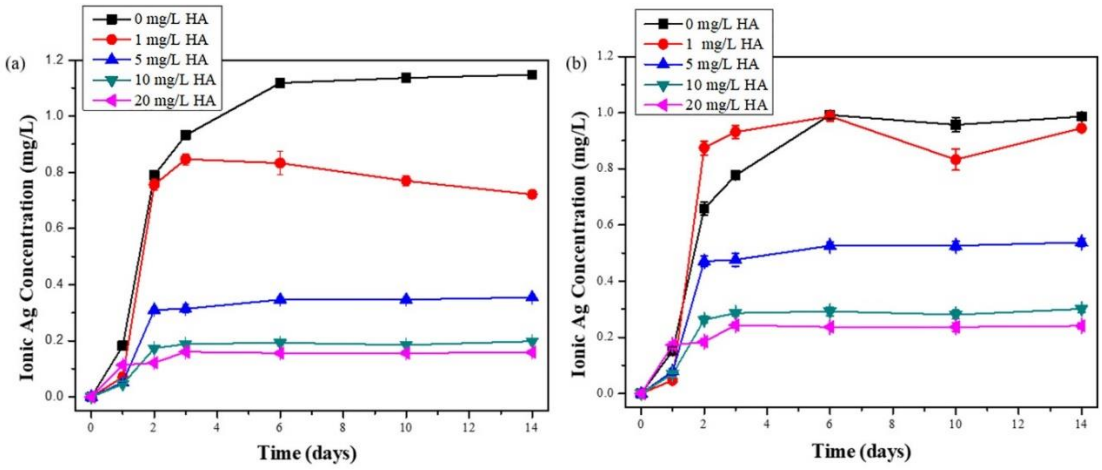

Figure 6.18 Change in the dissolved ionic Ag concentration of the experimental solutions after incubation with different concentrations of HA (a) under sunlight (b) in dark, AgNP concentration: 5 mg/L. The standard deviation from three parallel experiments is represented by the error bars.

6.3.4 Concentration dependent role of HA in the environment

This study presents the concentration dependent role of HA in the natural environment within the concentration range of 0 - 250 mg/L. The role of HA can be mainly explained in three parts as follows.

Firstly, in the absence of HA irrespective of the lighting level, the oxidative dissolution took place with the interaction of atmospheric and dissolved oxygen in the environment.

Simultaneously, the aggregation of AgNPs took place. Ultimately, these phenomena resulted in almost no or very less amount of AgNPs present in the aquatic phase in the NP form. This is evident with the results obtained using DLS (Figure 6.2(c)), TEM (Figure 6.12) and particularly with the colour change of the AgNP solution observed (Figure 6.9) and the disappearance of the characteristic peak in the UV vis spectrum (Figure 6.10).

Secondly, at the HA concentration of 1-20 mg/L, which is in accordance with the naturally occurring levels in the aquatic environment, HA stabilized the AgNPs. The stabilization occurred due to the inhibition of the release of the ionic Ag (Figure 6.18) and aggregation (Figure 6.10). Therefore, the AgNPs can persist stable for a longer period in the aquatic environment. In the presence of sunlight, which cannot be ignored when considering the natural aquatic environment, HA reduced the ionic Ag in the solution to form fresh, secondary AgNPs (Figure 6.15). Initially the secondary AgNPs formed near and around the primary AgNPs and then distributed to the bulk solution with a slight growth in their size. The secondary AgNPs were smaller than the primary AgNPs (Figure 6.12 & Figure 6.13), hence resulted in a redistribution of the PSD of the solution under the sunlight. This observation is also evident with the increase in the absorbance at the characteristic wavelength (Figure 6.10).

Thirdly, at higher concentrations of HA from 20 – 250 mg/L, which is observed in the soil environment, AgNPs were wrapped by the HA molecules (Figure 6.7), which resulted in an increase in the hydrodynamic diameter (Figure 6.2(b)). The coating of the AgNPs suppressed the dissolution of the AgNPs to ionic Ag as revealed by the concentration of dissolved Ag (Figure 6.6(b)). Therefore, the primary particles were stable in the environment for a prolonged period with no change in the primary particle size and morphology.

During the lifecycle of AgNPs, HA can be a critical factor in the aquatic environment that determine the fate of the AgNPs. Understanding the impacts of the HA on AgNPs can be crucial in predicting the transformations of AgNPs in these environments. The findings obtained during the study are significant when considering the environmental fate of the AgNPs. HA stabilizes the particles by reducing the possibility for the

dissociation of AgNPs and Ag dilution in the environment. Exposure to light resulted in the AgNP reduction and secondary particle formation.

7 Interactive influence of the EPS and electrolytes on the colloidal stability of AgNPs

This chapter discusses about the interactive influence of EPS and electrolytes on the colloidal stability of AgNPs. Section 7.1 provides a brief introduction about the study and the section 7.2 describes the experimental methods used during the study. The results obtained and the findings from the study are vividly discussed in the section 7.3 with the conclusions mentioned in the section 7.4.

7.1 Introduction

AgNPs are among the most widely used type of engineered NPs due to its unique physical and chemical properties and especially the antibacterial activity. Wastewater treatment plants are the most prominent distribution pathway among the multiple pathways that AgNPs enter the aquatic matrices [54]. Many research focused on understanding the factors including solution pH, ionic strength, valence of the electrolyte and the particle size which govern the transport and fate of AgNPs in the aquatic environment [199]. For example, increasing ionic strength can result in enhanced aggregation as divalent cations are more effective in facilitating aggregation than mono valent cations [45].

When the AgNPs are discharged into the wastewater treatment system, they interact with the organic matter, for instance, humic substances (HS) like humic acids (HA) and fluvic acids (FA), and non humic substances consisting of biological macromolecules like proteins and polysaccharides. Organic matter absorbed onto NPs can change the surface charge of the particles, thereby altering the colloidal stability [94]. Different structures and components of organic matter can result in diverse impacts on the aggregation of NPs. Some studies have reported that protein molecules are effective in stabilizing the AgNPs [222] whereas polysaccharides hinder the stability of AgNPs [202, 223]. On the other hand, aromatic rich HA are effective in stabilizing NPs compared to aliphatic rich HA [224].

According to the previous studies, a considerable amount of NPs entering into the biological wastewater treatment system are absorbed by activated sludge, which reduces the concentration of NPs in the effluent [55, 225]. The predicted average concentration of Ag in the sludge is in the range of 7-39 mg/kg [226]. AgNPs absorbed on to the sludge will be embedded in the sludge and form new products such as silver sulphide (Ag_2S) [55, 227]. However, the removal mechanism of NPs by the activated sludge is not comprehensively investigated.

Extracellular polymeric substances (EPS) is a heterogeneous mixture in the activated sludge, which is continuously secreted by the microorganisms during their growth and metabolic activities[228]. EPS is mainly a mixture of polysaccharides and proteins with

different functional groups including amide, amino, carboxyl, hydroxyl and phosphoryl groups [229-231]. EPS in the biological wastewater treatment system consists of different EPS fractions, predominantly soluble EPS (SB- EPS), loosely bound EPS (LB-EPS) and tightly bound EPS (TB-EPS) [232]. EPS plays important role in protecting the bacterial cell against the environmental stress [233]. The composition of EPS secreted by bacteria will be changed in order to respond the changes in the matrix they are present hence their adhesion capabilities. When present in the wastewater treatment system, EPS tends to interact with different types of electrolytes present in the wastewater [234, 235] which could play a pivotal role in the cohesiveness of the microbial aggregates as evaluated in different studies [236], by bridging the negatively charged sites of EPS to create stable, inter molecular and cell-EPS links. Meantime, it may also interact with NPs in the wastewater. It is highly possible that the interaction will start from SB-EPS, and then LB-EPS and finally TB-EPS given the layered structure of EPS in biomass. When present in the solution, NPs tend to release ions (i.e AgNPs release ionic Ag) which are harmful to the bacteria. The distribution and the composition of EPS vary in such a way to provide maximum protection against the toxic substances [237]. To our best knowledge, only a few studies attempted to understand the role of EPS on the aggregation and the colloidal stability of NPs [238, 239] and they barely considered AgNPs. The complex environment with the presence of both EPS and ions and their interactive behavior is even rarely investigated.

The objective of this study is to explore the impact of the EPS on the colloidal stability and the aggregation kinetics of AgNPs in the presence of $NaNO_3$ or $Ca(NO_3)_2$ through time resolved dynamic light scattering (TR-DLS). In addition, several other techniques such as Fourier transform infrared (FTIR) spectroscopy, electrophoretic mobility (EPM) and dissolved ionic Ag concentration were used to quantitatively and qualitatively analyze the constituents and the functional groups of fractionalized EPS components, i.e. SB- EPS, LB-EPS and TB-EPS. This study provides an overview with fundamental understanding on the colloidal stability of AgNPs in the presence of both inorganic and organic matters.

7.2 Experimental methods

7.2.1 EPS extraction

Raw wasted activated sludge from a local wastewater treatment plant in Singapore was obtained and stored at 4 °C prior to use. EPS extracted from the sludge samples was analyzed according Zhou et al. [240]. Initially, 15 ml of the sludge sample was centrifuged for 15 mins at 4 °C and 4,000 g and the supernatant was separated as SB-EPS. The remaining sludge pellet was re-suspended in 0.05% sodium chloride (NaCl) solution. Then the mixture was vortexed and incubated in a water bath at 70 °C for 1 min, followed by the centrifugation at 4 °C for 10 min at a speed of 4,000 g. Then the supernatant was separated as LB-EPS. The residue of the suspension pellet was re-suspended to its original volume by adding 0.05% NaCl solution, placed in a 60 °C water bath for 30 min, and centrifuged at 4,000 g for 15 min at 4 °C. After that the supernatant was washed and separated as TB-EPS. All the EPS fractions were filtered using membrane filters with a pore size of 0.45 µm. Na^+ and Cl^- ions in the solution were removed via ultra-centrifugation of the EPS solution using the 3 kDa membrane centrifugal filters (Millipore Inc.) at 5,000 g for 30 min at 4 °C.

7.2.2 Characterization of EPS

The Total organic carbon (TOC), polysaccharide and protein content in the different EPS fractions were measured according to the methods described by Li et al. [241]. A TOC/TN analyzer (Shimadzu, Japan) was used to determine the organic carbon and nitrogen content. Total polysaccharide content was measured using the phenol-sulphuric acid method as described in Dubois et al.[242]. Modified Lowry method [243] was used to determine the protein content in the samples. Major soluble organic fractions with different chemical functions and sizes in EPS were measured using size-exclusion chromatography, combined with organic carbon and nitrogen detection (LC-OCD-OND) as described in Xiao et al. [244]. The biopolymers, high molecular weight (HMW) protein, building blocks, low molecular weight (LMW) neutrals, LMW acids and HMW polysaccharide were quantified using LC-OCD-OND [245]. LMW polysaccharide and LMW protein concentrations were obtained by subtracting HMW polysaccharide and HMW protein from the total polysaccharide and protein concentrations determined through the spectrometer method respectively.

7.2.3 Determination of aggregation kinetics

The variation in the intensity weighted average hydrodynamic diameter of the experimental solutions with time was measured using a Zetasizer Nano (ZEN 3600, Malvern, UK). Aggregation kinetics of AgNPs was recorded at different $NaNO_3$ (0 – 500 mM) and $Ca(NO_3)_2$ (0 – 40 mM) concentrations in the presence and absence of EPS using time resolved DLS. The range of electrolyte concentration was selected to mimic the levels of electrolytes in the wastewater [246]. Since the dissolved organic carbon (DOC) concentration in the wastewater treatment system varies within the range of 10 – 90 mg/L [247], all the working solutions of the different EPS fractions was maintained at 50 mg/L of TOC during the AgNP aggregation experiments. The solution pH and the temperature were maintained at 8.0 and 25 ºC respectively.

To initiate the experiments, aliquots of pure AgNPs solution was added to the electrolyte solution or mixture of EPS and electrolyte solution up to a final volume of 1.2 mL. Final concentration of AgNPs in the experimental samples was kept at 5 mg/L. The solution mixture in the cuvette was vortexed for 5s to ensure proper mixing prior to the measurement. The hydrodynamic diameter of AgNPs in the mixture was recorded during a period of 60 mins. A photodetector at a scattering angle of 173º was used to detect the intensity of the scattered light during the measurements. Each measurement auto correlation function was accumulated for 10 s with a stability period of 3 s. All the experiments were performed for three replicates of the same condition sample and the results present the average of the three values.

EPM of the samples in the absence and presence of EPS was measured using a Malvern Zetasizer Nano. An incubation time of one hour was used during the measurement to allow the sample to be stabilized to meet the measurement quality criteria. Dissolved ionic Ag concentration of the experimental samples after one hour of incubation and the FTIR spectrum was obtained using the method mentioned previously [248].

Certain volume of AgNP suspension and EPS solution was mixed with $NaNO_3$ and $Ca(NO_3)_2$ solutions to make the final concentration. The mixture was gently shaken at 25 ℃ for 2 h and centrifuged at 20,000 g for 30 min. The total organic C of SB-EPS, LB-EPS and TB-EPS in the supernatant were determined using a TOC analyzer (multi

N/C 3100, Analytik Jena, Germany). The amount of EPS-C adsorbed was calculated by the difference between the amount of EPS added and that remaining in the supernatant.

The initial rate of increase in the hydrodynamic diameter (D_h) with time measured using TR-DLS, is expressed as aggregation kinetics. The aggregation rate constant (k) varies proportionally with the initial rate of increase in the hydrodynamic diameter. k is inversely proportional to the initial concentration of AgNPs in the solution which is denoted by (N_0) [93, 249]. It can be determined by the Eqn. (7.1).

$$k \propto \frac{1}{N_0}\left(\frac{dD_h(t)}{dt}\right)_{t\to 0} \tag{7.1}$$

The initial increase in the hydrodynamic diameter of AgNPs with time was calculated until the time that the hydrodynamic diameter becomes 1.5 times of the initial value. The method proposed by Huangfu et al. [250] was used in determining these time points. $D_h(t)/dt$ was calculated using linear least square regression analysis. The relationship used in this study has been tested and widely used in studying the aggregation kinetics of different types of NPs [93, 231, 251, 252].

The attachment efficiency (AE) (α), in the range of 0 to 1 was calculated by the ratio between the k quantified under different solution conditions and the k_{fast} quantified under fast or favourable aggregation conditions [93]. The AE is used as a tool in quantifying the aggregation kinetics of NPs according to the DLVO theory [83]. The described relationship is showed in the Eqn. (7.2) mentioned below.

$$\alpha = \frac{k}{k_{fast}} = \frac{\frac{1}{N_0}\left(\frac{dD_h(t)}{dt}\right)_{t\to 0}}{\frac{1}{(N_0)_{fast}}\left(\frac{dD_h(t)}{dt}\right)_{t\to 0,fast}} \tag{7.2}$$

Since the initial AgNP concentration in the solutions was maintained constant during the measurements under different solution conditions, Eqn. (7.2) can be simplified by neglecting the N_0, and calculating the AE as shown in Eqn. (7.3).

$$\alpha = \frac{\left(\frac{dD_h(t)}{dt}\right)_{t\to 0}}{\left(\frac{dD_h(t)}{dt}\right)_{t\to 0,fast}} \quad (7.3)$$

When calculating the AE in the presence of different EPS fractions, $(dD_h(t)/dt)_{t\to 0,fast}$ was obtained from the average values of $(dD_h(t)/dt)_{fast}$in the diffusion limited regime where the ionic strength is higher than the CCC in the presence of different electrolytes.

7.2.4 Statistical Analysis

Pearson's correlation was utilized to assess the linear correlation between the AE, adsorbed carbon and the dissolved organic matter using the software, SPSS version 19.0 [253]. The degree of correlation among the considered factors was evaluated using the Pearson's correlation coefficient (*R*), which is in the range of -1 to +1 with +1 denoting a perfect positive correlation, -1 denoting a perfect negative correlation and 0 denoting no correlation. A two-tailed t-test for the null hypothesis was carried out to determine the *p* value where the regression slope is zero. A statistically significant correlation is obtained with a probability (*p* value) less than 0.05.

7.3 Results and Discussion

7.3.1 AgNP and EPS characterization

7.3.1.1 AgNP characterization

According to the TEM results, the particles were spherical and well dispersed in the parent solution (Figure 7.1 (a)) with an average diameter of 23 ± 0.574 nm. A peak absorbance of 0.926 at the characteristic wavelength of 392 ± 2 nm in the UV-Vis absorption spectrum was observed for the synthesized AgNPs in the parent solution. The intensity weighted average hydrodynamic diameter obtained using DLS was 31.72 ± 2.114 nm (Figure 7.1 (b)). The total Ag concentration of the parent solution was 5.829 ± 0.015 mg/L with a dissolved ionic Ag concentration of 2.072 ± 0.002 mg/L. The pH and the zeta potential of the parent solution was 8.02 and -28.4 ± 1.6 mV respectively. The iso-electric point of AgNPs was approximately 4.03 (Figure 7.1 (c)).

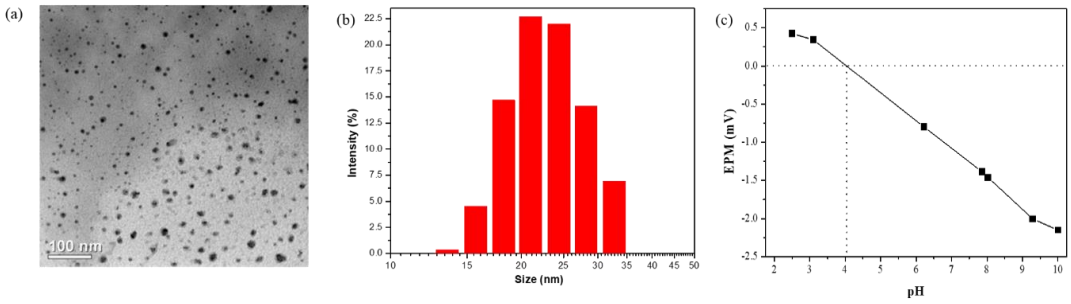

Figure 7.1 (a) Morphology of AgNPs in parent solution observed by TEM; b) Particle Size distribution of the AgNPs in parent solution (c) EPM of AgNPs as a function of pH

7.3.1.2 Characteristics of EPS

The variation in the constituents of different types of EPS, namely, SB-EPS, LB-EPS and TB-EPS are illustrated in Figure 7.2. The three types of EPS consisted primarily of organic carbon and nitrogen. Polysaccharides and protein in the three types of EPS followed the sequence of SB-EPS < LB-EPS < TB-EPS. However, the variation in the protein content among the three different fractions of EPS is higher than that of polysaccharides. The constituents in the DOC was further assessed and the results are mentioned in the Table 7.1. Amount of dissolved polysaccharides, protein and amino sugars in the EPS fractions are indicated by the concentration of bio polymers. The biopolymers and dissolved protein content in the three types of EPS varied in the sequence of TB-EPS < LB-EPS < SB-EPS which is in contrast with the variation in polysaccharides and protein in the EPS fractions.

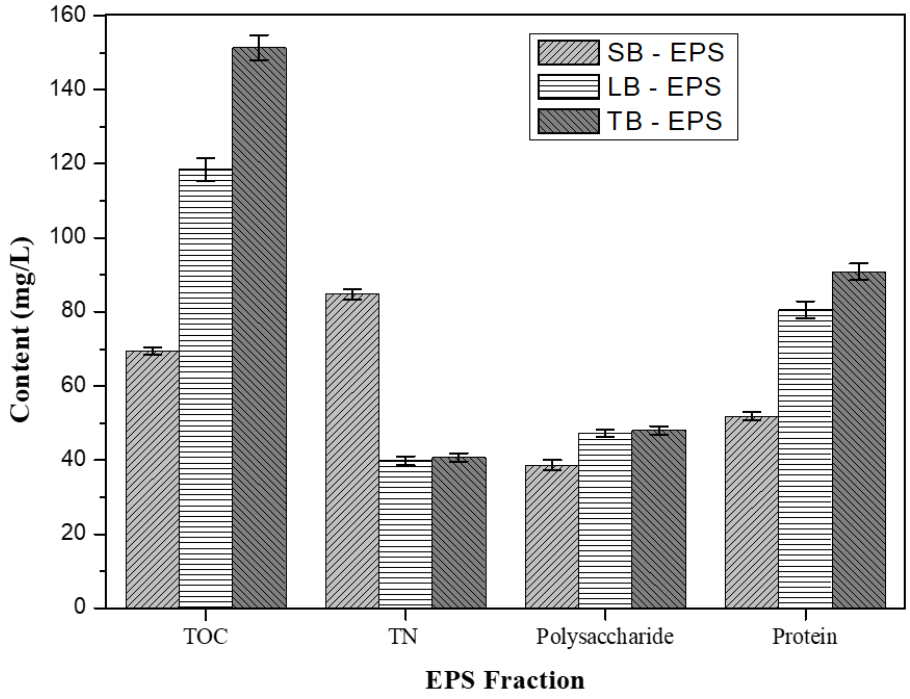

Figure 7.2 Variation in the concentration of Total Organic Carbon (TOC), Total Nitrogen (TN), polysaccharide and protein in SB-EPS, LB-EPS and TB-EPS.

Table 7.1 Fractions of dissolved organic matter (mg/L–C) in the different types of EPS.

EPS	Bio Polymers	PN	HMW PN	LMW PN	PS	HMW PS	LMW PS	HA	Building blocks	LMW Neutrals	LMW acids
SB	23.88	25.72	11.23	14.49	17.12	12.66	4.46	nq.	25.89	4.07	0.83
LB	9.68	40.03	3.97	36.06	20.97	5.71	15.27	nq.	19.97	26.01	4.19
TB	5.29	45.14	3.278	41.86	21.31	2.01	19.30	nq.	21.11	33.93	5.94

*PN- Protein, PS – Polysaccharide, HA – Humic acid.

7.3.2 Aggregation kinetics of AgNPs in different electrolyte solutions

The AE of AgNPs as a function of the electrolyte concertation ($NaNO_3$ or $Ca(NO_3)_2$) are presented in Figure 7.3. Hydrodynamic diameter profiles of AgNPs in the presence of the electrolyte are presented in Figure 7.4. At relatively low concentration of the electrolyte (<10 mM for $NaNO_3$ and <0.8 mM for $Ca(NO_3)_2$), the increase in the electrolyte concentration elevated the degree of charge screening [231] and led to an

increase in the rate of aggregation, as revealed by the increase in the AE. This is known as reaction limited aggregation where α <1. At higher electrolyte concentrations, i.e. 10 - 500 mM for $NaNO_3$ and 10 - 40 mM for $Ca(NO_3)_2$, the charge of AgNPs was completely screened. Hence, the energy barrier between the AgNPs was eliminated, enabling the NPs to aggregate in the diffusion limited regime (α ≥1).

This observed behavior of aggregation of AgNPs in the electrolyte solutions is consistent with the DLVO theory. The aggregation kinetics reaches the maximum in the diffusion limited regime and is independent of the electrolyte concentration. The CCC of an electrolyte is the concentration at which the reaction limited and diffusion limited regimes intersect [249]. The CCC for the AgNPs was determined to be 12 mM in $NaNO_3$, which was much higher than that in $Ca(NO_3)_2$ (0.8 mM). According to the Schulze-Hardy rule, for a negatively charged surface, the CCC ratio of the cations of valences 2 and 1 should be in the range of z^{-6} to z^{-2}, where z is the higher valence among the cations [254, 255]. The ratio of CCC values we obtained (0.8/12) is proportional to $z^{-3.9068}$, where z is the valence of the calcium counter ion, which is in accordance with the Schulze-Hardy rule.

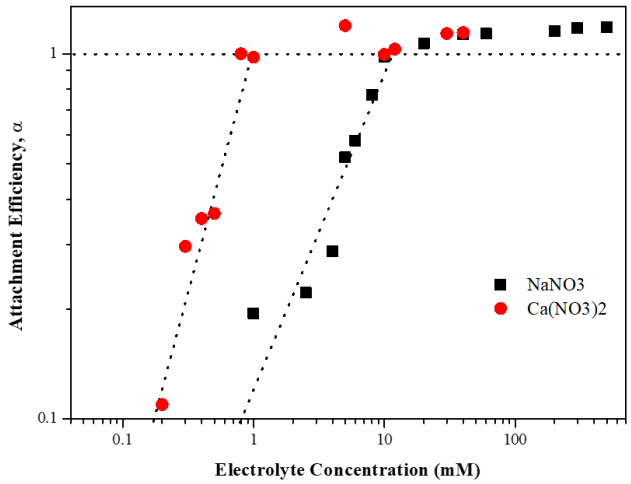

Figure 7.3 Change in the attachment efficiencies of AgNPs as a function of $NaNO_3$ and $Ca(NO_3)_2$ concentrations.

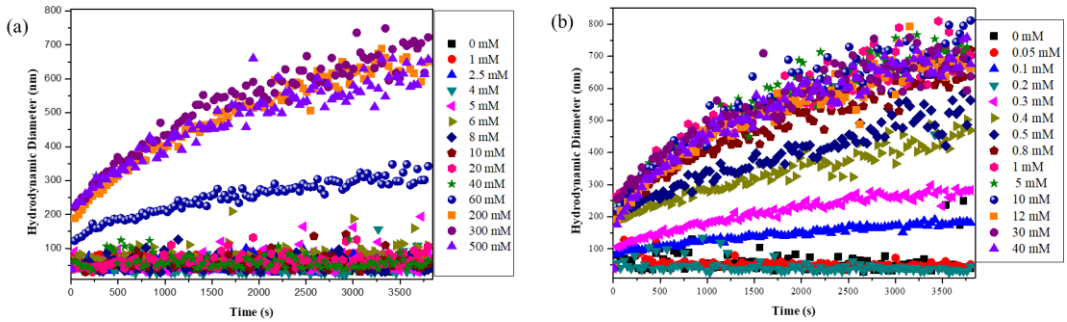

Figure 7.4 Aggregation profiles of AgNPs in (a) $NaNO_3$ and (b) $Ca(NO_3)_2$ solution

7.3.3 Effects of SB-EPS, LB-EPS and TB-EPS on the colloidal stability of AgNPs in monovalent cations

To explore the effects of different EPS fractions on the rate of aggregation of AgNPs, the AE in the presence of SB-EPS, LB-EPS and TB-EPS as a function of $NaNO_3$ concentration was examined (Figure 7.5(a)). Overall, the addition of EPS resulted in much lower AE compared to the EPS-free solution, indicating that EPS hindered the aggregation of AgNPs. The results obtained during this study are consistent with the previous research exploring the effect of biological macromolecules such as NOM, alginate and BSA on the stability of different types of NPs [93, 94, 231, 256]. Interestingly, only minor difference in the EPM of AgNPs was observed in the presence and absence of EPS in the $NaNO_3$ solution as shown in Figure 7.5(c). These results indicate that despite a significantly affected AE, EPS did not have a considerable effect on the EPM. Hence, the change in the rate of aggregation of AgNPs in this condition can be caused due to some other reasons, which can be mainly due to the steric repulsion induced from the adsorption of EPS molecules onto the AgNPs, which effectively stabilized the system. The percentage mass fractions of SB-EPS, LB-EPS and TB-EPS adsorbed on to the AgNPs as a function of $NaNO_3$ concentration is presented in Figure 7.6(a). The results obtained for the adsorption demonstrate the presence of steric hindrance induced by the adsorbed EPS during the aggregation of AgNPs in the $NaNO_3$ solution.

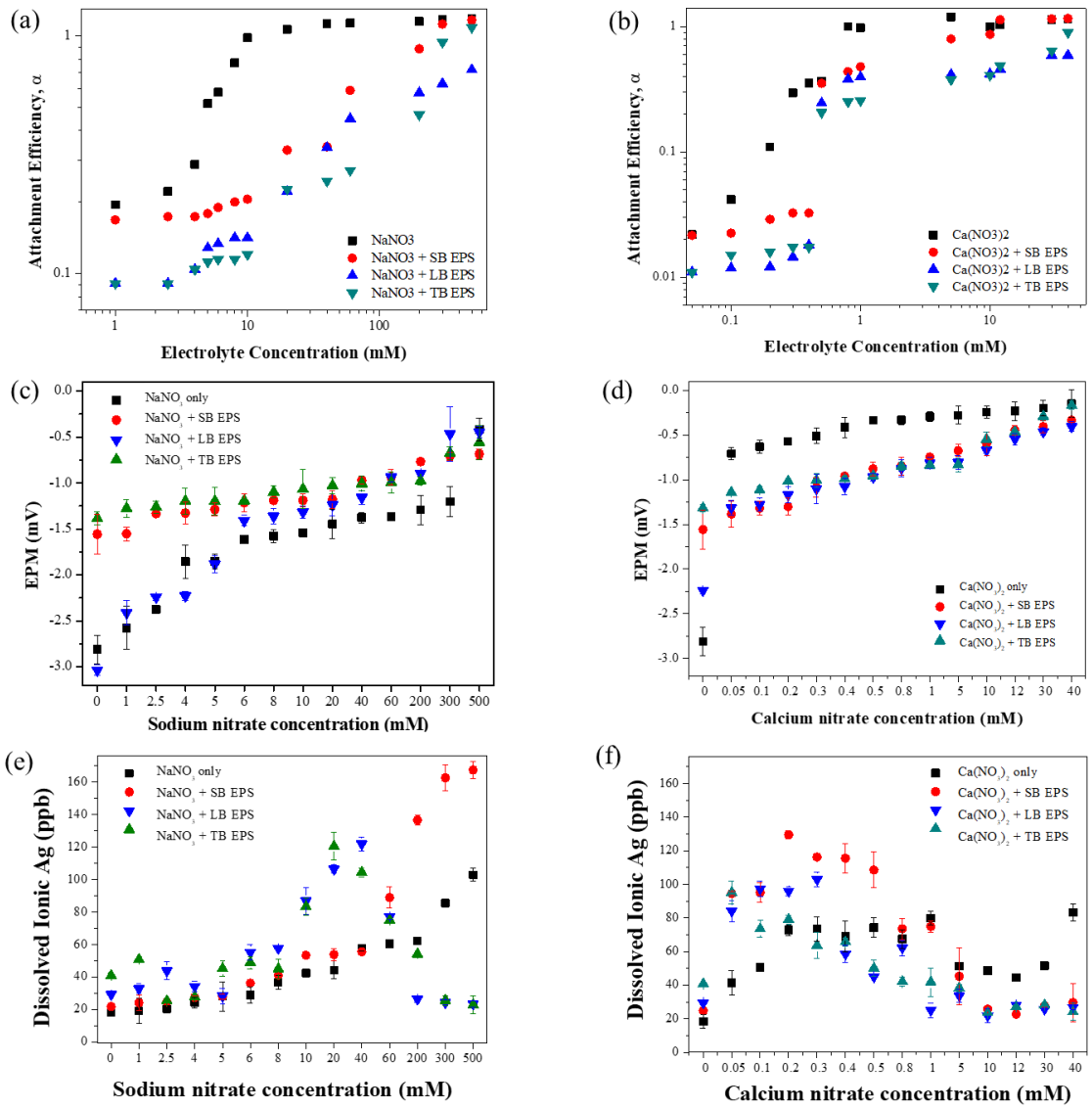

Figure 7.5 Change in the attachment efficiencies of AgNPs as a function of (a)$NaNO_3$ and (b) $Ca(NO_3)_2$ concentration, change in the Electrophoretic mobility (EPM) of AgNPs as a function of (c) $NaNO_3$ and (d) $Ca(NO_3)_2$ concentration after 1 hour of incubation and change in the dissolved ionic Ag concentration of the AgNPs as a function of (e) $NaNO_3$ and (f) $Ca(NO_3)_2$ concentration after 1 hour of incubation in the presence of SB-EPS, LB-EPS and TB-EPS.

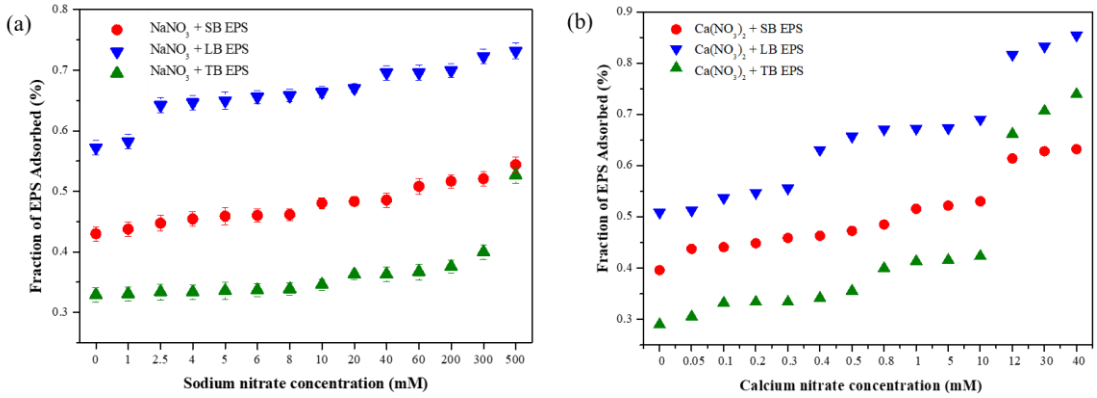

Figure 7.6 The mass fraction of EPS-C adsorbed by AgNPs as a function of (a) $NaNO_3$ and (b) $Ca(NO_3)_2$ concentration.

The dissolved ionic Ag concentration of the experimental samples gradually increased with the electrolyte concentration in the absence of EPS (Figure 7.5(e)). The trend observed in the ionic Ag concentration in the presence of SB-EPS is similar to the EPS free condition. However, the amount of ionic Ag released in the presence of SB-EPS is higher than in the absence of EPS, especially when $NaNO_3$ concentration is high. In the presence of LB-EPS and TB-EPS, the ionic Ag concentration increased up to 120 ppb, which doubled the ionic Ag concentration compared to the other two cases, and then decreased to the lower values with the further increase in the electrolyte concentration. The decrease observed in the ionic Ag concentration can be attributed to the coating effect induced by the higher amount of DOC (Figure 7.2 & Table 7.1), present in the LB-EPS and TB-EPS solutions which inhibited the dissolution of AgNPs to ionic Ag.

In the presence of SB-EPS, LB-EPS and TB-EPS, the CCC increased from 12 mM (no EPS) to 250 mM, 982.4 mM and 376.7 mM for $NaNO_3$, respectively (Figure 7.5(a)). This suggests that LB-EPS stabilized AgNPs more effectively than SB-EPS and TB-EPS. This again can be reflected in the aggregation profiles of AgNPs in the presence and absence of SB-EPS, LB-EPS and TB-EPS (Figure 7.7), which shows the change in the hydrodynamic diameter of the solution with time. According to Figure 7.7, the hydrodynamic diameter of the AgNPs remained almost constant in the presence of LB-EPS, in a constant electrolyte concentration, where as it changed differently in the presence of SB-EPS and TB-EPS. In these conditions, the adsorbed EPS (Figure 7.6) on

the hydrophobic AgNP surfaces induce long range steric repulsive forces, hence promoting the stability of AgNPs.

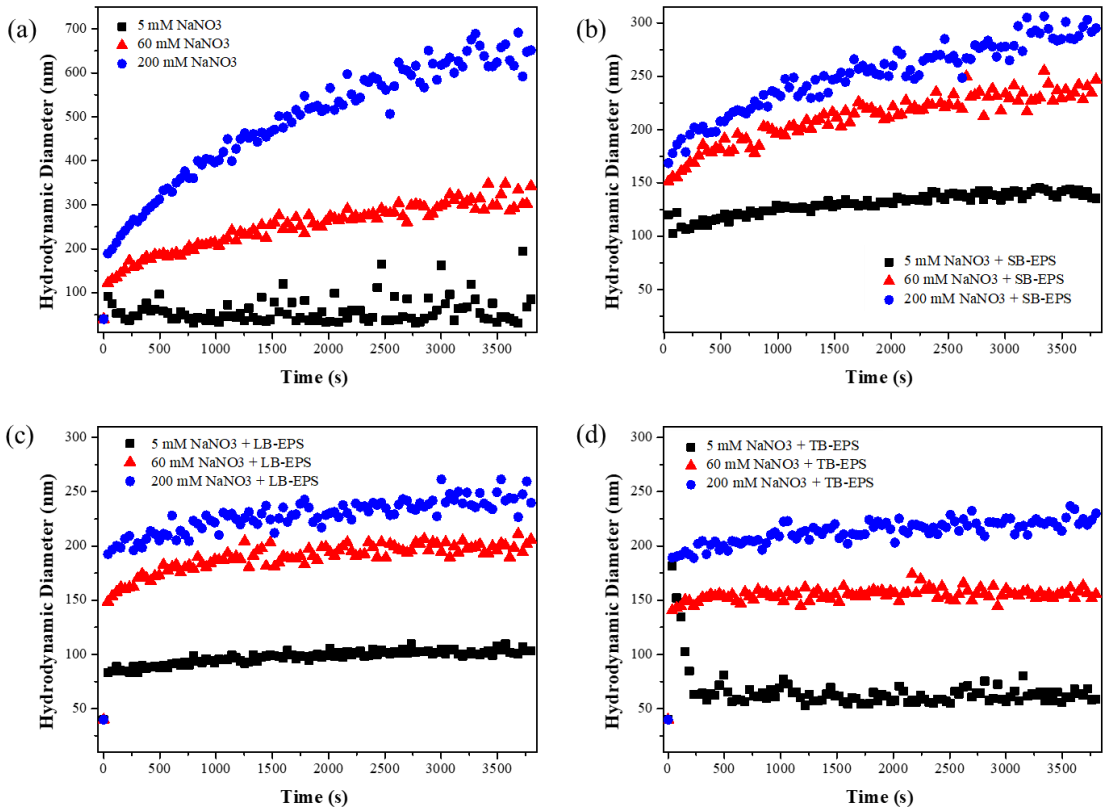

Figure 7.7 Aggregation profiles of AgNPs in various $NaNO_3$ solutions in the absence and presence of (a) SB-EPS, (b) LB-EPS and (c) TB-EPS

7.3.4 Effects of SB-EPS, LB-EPS and TB-EPS on the colloidal stability of AgNPs in divalent cations

Figure 7.5(b) presents the variation in the AE of the AgNPs in the presence and absence of EPS factions as a function of the $Ca(NO_3)_2$ concentration. At relatively low $Ca(NO_3)_2$ concentration, the AgNPs were stable in the presence of different EPS fractions. This stabilization can be caused due to the steric effect induced by the adsorbed EPS on the AgNPs as shown in Figure 7.6(b). Nevertheless, the AE of the AgNPs increased with the increasing $Ca(NO_3)_2$ concentration in the presence of EPS. When the $Ca(NO_3)_2$ concentration is increased above 10 mM, the AE, was greater than 1, in the presence of SB-EPS, which further increased with the $Ca(NO_3)_2$ concentration. The AE was almost constant up to 0.4 mM and beyond 5 mM $Ca(NO_3)_2$ in the presence of LB-EPS and TB-

EPS. The CCC values of AgNPs in $Ca(NO_3)_2$ changed from 0.8 mM (no EPS) to 11 mM, 1452.3 mM, and 44.1 mM in the presence of SB-EPS, LB-EPS and TB-EPS respectively. Even though the CCC values increased compared to the no EPS condition, the value obtained in the LB-EPS again shows a drastic difference. Furthermore, the CCC value obtained in the presence of LB-EPS in $Ca(NO_3)_2$ was higher than that in $NaNO_3$. This shows that irrespective of the electrolyte LB-EPS stabilized the AgNPs suspension effectively than the other EPS fractions. Representative aggregation profiles of AgNPs in the presence and absence of different EPS fractions in $Ca(NO_3)_2$ solutions are presented in Figure 7.8, which also shows a similar observation as in the presence of $NaNO_3$. Even though the change in the hydrodynamic diameter of AgNPs in the presence of LB-EPS and TB-EPS is similar and lower compared to the SB-EPS and EPS free condition, the variation in the hydrodynamic diameter of LB-EPS is less compared to that of TB-EPS.

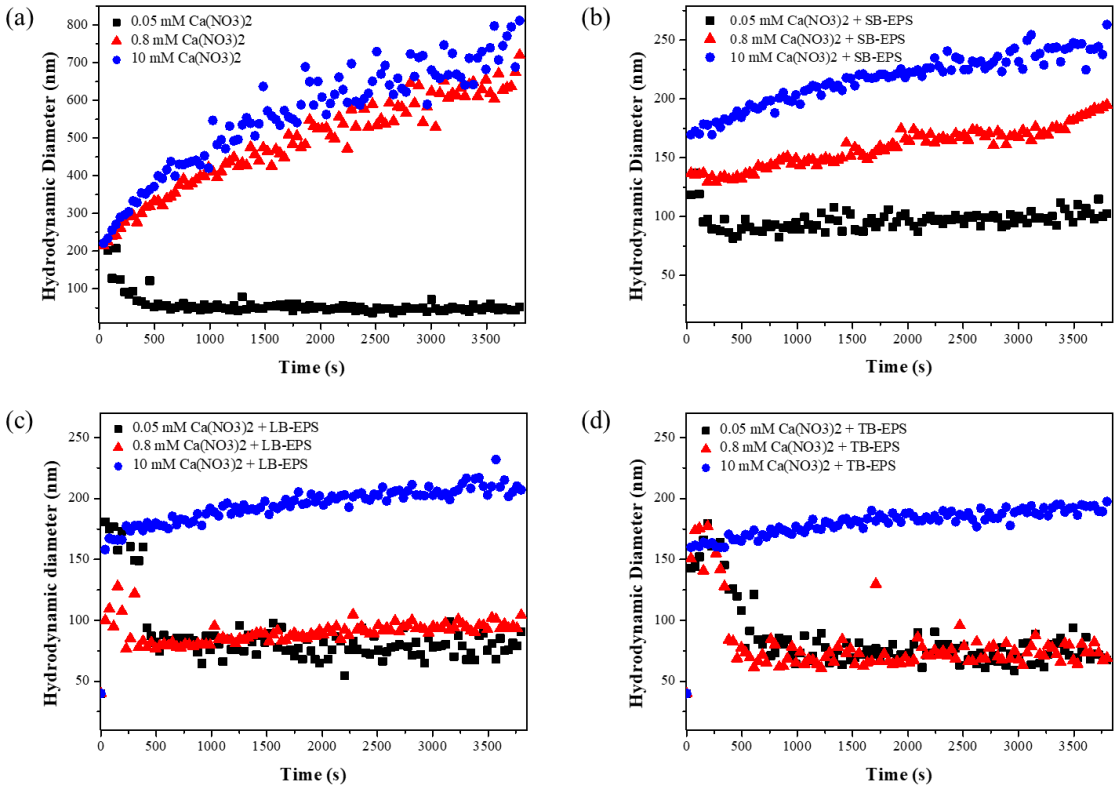

Figure 7.8 Aggregation profiles of AgNPs in various $Ca(NO_3)_2$ solutions in the absence and presence of (a) SB-EPS, (b) LB-EPS and (c) TB-EPS

The enhanced aggregation of AgNPs in the presence of SB-EPS compared to the other types of EPS in $Ca(NO_3)_2$ solutions could be due to the composition of SB-EPS with the formation of intermolecular bridging between Ca^{2+} and the COO^- in the macromolecules [231]. This phenomenon was verified through the results obtained for the z-average diameters of AgNPs in different EPS fractions in the presence of varying $Ca(NO_3)_2$ concentrations. As shown in Figure 7.9(b), the z-average diameters of AgNPs in the presence of EPS increased with the $Ca(NO_3)_2$ concentration after 12 mM.

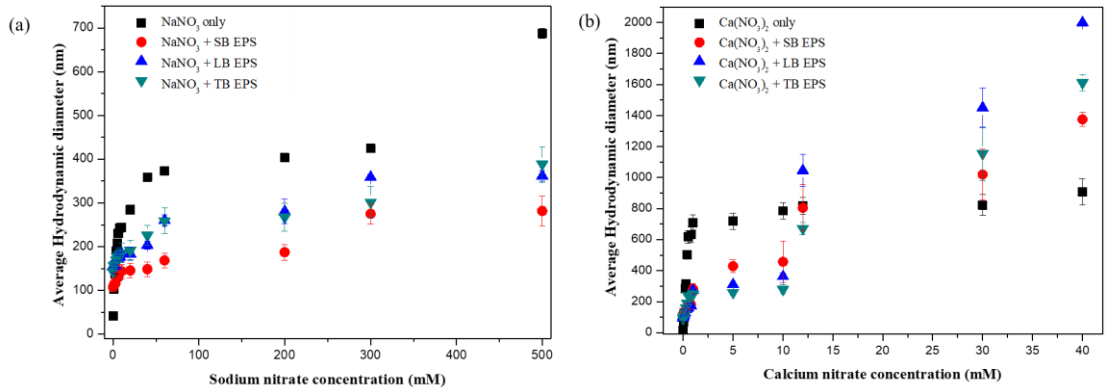

Figure 7.9 Z-average diameter of AgNPs with and without SB-EPS, LB-EPS and TB-EPS as a function of (a) $NaNO_3$ and (b) $Ca(NO_3)_2$ concentration.

The EPM values became less negative as the concentration of $Ca(NO_3)_2$ increased (Figure 7.5(d)), which was probably due to the charge screening reduced from the compression of the double layer or the neutralization of charge with the adsorption of Ca^{2+} [257] on the AgNP surface. Upon mixing with EPS, a similar increase in EPM with Ca^{2+} concentration was observed, but with a smaller amount than in the absence of EPS. This indicates the complexation of Ca^{2+} and EPS, forming EPS functional groups such as ionic carboxylates and phosphoryl which are negatively charged [258] and increasing the negative EPM of AgNPs. Decreasing EPM values suggests that electrostatic forces may be prominent among the interactions between negatively charged AgNPs and EPS, which is similar to the observations by Mosley et al. [259]. Hence, the impact of EPS on the aggregation of AgNPs can be due to the combined impact of inter particle bridging and electrostatic forces, while the stability induced by EPS on the AgNPs can be caused due to the cumulative effect of electrostatic and steric repulsion.

The dissolved ionic Ag concentration in $Ca(NO_3)_2$ solution in the absence and presence of EPS (Figure 7.5(f)), increased with the electrolyte concentration and started to decrease at some point. This point of trend reversal was different in various EPS types. When comparing this result with the other results obtained using different techniques, the release of ionic Ag was inhibited at higher electrolyte concentrations in the presence of EPS. This also may be a consequence of the enhanced aggregation of AgNPs followed with the coating by the biological macromolecules present in the matrix.

The FTIR spectra of the three types of EPS in the absence and presence of AgNPs was analyzed to qualitatively assess the impact of biochemical components of the EPS (Figure 7.10). From Figure 7.10(a), it can be observed that the peak at 3353 cm^{-1} (the red line) is assigned to -OH and $-NH_2$ [260-262]. The peaks at 2920 and 2854 cm^{-1} can be attributed to asymmetric stretching vibrations and symmetric stretching of $-CH_2$, respectively [263, 264] [186]. The peak at 1643 cm^{-1} is assigned to the stretching vibration of –COOH [260, 265]. The broad peak at 1355 cm^{-1} is the overlapped peak of symmetric deformation of $-CH_3$ and $-CH_2$ in protein and symmetric stretching of –COOH [266]. The peak at 1064 cm^{-1} is derived from the symmetric stretching of the phosphodiester backbone of nucleic acids [266]. Upon mixing of SB-EPS with AgNPs (the blue line), some of the above-mentioned peaks disappear, and the intensities of the peaks at 2920, 1643 and 1064 cm^{-1} increased, which could be caused by the increased symmetric vibrations of CH_2, vibrations of the C-N bond in the proteins and the stretching vibrations of O-H. This observation suggests that the stability of AgNPs induced by the SB-EPS can be linked mainly to the presence of hydroxyl groups in the solution.

In the FTIR spectrum obtained for LB-EPS (the red line in Figure 7.10(b)), peaks are observed at 3709 cm^{-1}(-OH and $-NH_2$)[260-262], 2932 cm^{-1} (asymmetric stretching vibrations of $-CH_2$)[263, 264], 1639 cm^{-1} (stretching vibration of -COOH)[260, 265], 1260 cm^{-1} (stretching vibration of C-O)[267], and 1022 cm^{-1} (stretching vibration of C=C and asymmetric stretching vibration of -C-O-C-) [268, 269](Figure 7.10(b)). Due to the interaction with AgNPs (blue line), the peak at 3709 cm^{-1} disappears and the intensities at 2932 and 1639 cm^{-1} increased. The peak at 1022 cm^{-1} in LB-EPS blue-shifts to 979 cm^{-1} and the peak at 1260 cm^{-1} red-shifts to 1419 cm^{-1}, suggesting that the

functional groups in the LB-EPS attach on to the surface of AgNPs forming attractive coulombic interactions [202] between the AgNPs and LB-EPS.

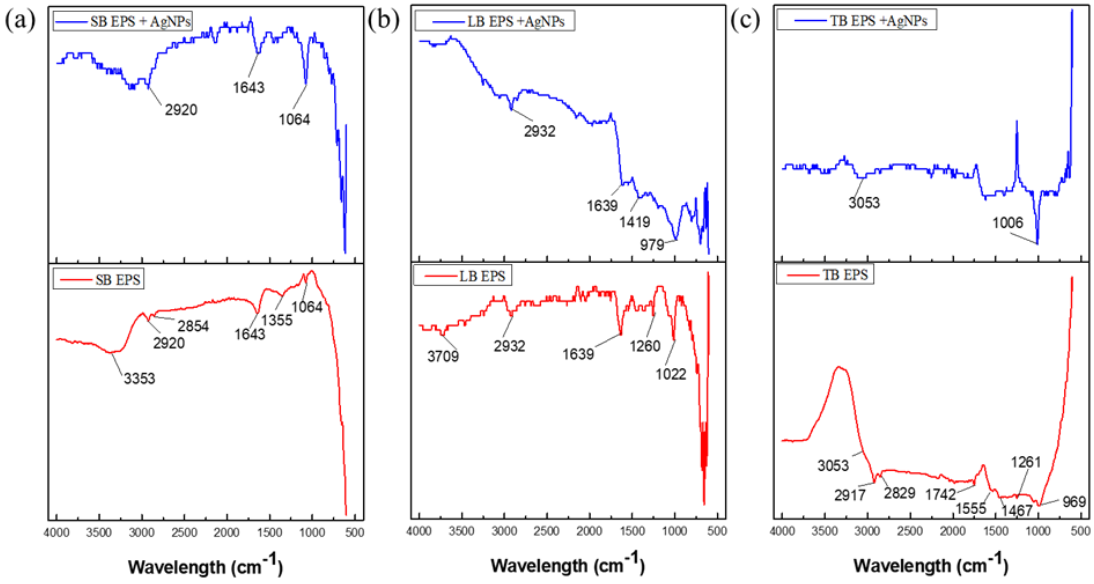

Figure 7.10 FTIR spectra of (a) SB-EPS, (b) LB-EPS and (c) TB-EPS in the absence and presence of AgNPs

In Figure 7.10(c) (red line), the peaks at 2917 and 2829 cm^{-1} belong to the asymmetric stretching vibration and symmetric stretching of -CH_2 [263, 264][1] [186]. The peak at 1742 cm^{-1} was attributed to the C=O stretch of ester groups in lipids and fatty acids [266]. The peak at1555 cm^{-1} was attributed to the stretching vibration of C–N and deformation vibration of N–H of amide II in protein [265, 269]. The peaks at 1467, 1261, and 969 cm^{-1} are assigned to asymmetric deformation of CH_3 and CH_2 of proteins [266, 270] , stretching vibration of C-O arising from polysaccharides and nucleic acids [267]. Most of these peaks disappeared due to the interaction with AgNPs. 1006 cm^{-1}(red shifted peak of 969 cm^{-1}) with increased intensity can be observed in the mixture of AgNPs and TB-EPS, which could be caused by the bonding of C-O of the carboxylic groups and the C-O-C in the polysaccharides in the TB-EPS onto the AgNPs.

When comparing the interactions of the three types of the EPS with the AgNPs, the functional groups in the TB-EPS were more tolerant to the presence of AgNPs owing to the protective role of the outer layers [271]. The differences between the FTIR spectra

suggest that the different functional groups present in the EPS fractions interacted differently with AgNPs.

Table 7.2 Pearson's correlation coefficients (R) between the attachment efficiency (AE), the adsorbed carbon (AC) and the available DOMs in all types of EPS.

	Bio polymer	PN	HMW PN	LMW PN	PS	HMW PS	LMW PS
AE	-	-0.445**	-	-0.433**	-0.436**	-	-0.415**
AC	0.573**	0.789**	0.547**	0.689**	0.869**	0.589**	0.607**

	Electrolyte Conc.	Building blocks	LMW neutrals	LMW acids	TN	TOC
AE	0.505**	-0.359**	-0.397**	-0.395**	-0.216*	-0.435**
AC	-	0.828**	0.541**	0.524**	0.658**	0.709**

**Correlation is significant at the 0.01 level (2-tailed).
*Correlation is significant at the 0.05 level.
"-" denotes correlation is insignificant ($p > 0.05$).

To investigate the correlation between DOMs abundance and AE as well as the adsorbed carbon, the Pearson's Correlation Coefficients were calculated (Table 7.2

Table 7.2). The amount of adsorbed carbon (AC) was strongly positive ($p < 0.01$) correlated to the concentrations of biopolymers, HMW PN, PN, LMW PN, PS, HMW PS, LMW PS, Building blocks, LMW neutrals, LMW acids, TN and TOC. This reveals that the adsorption of carbon to the AgNPs strongly depends on the amount of DOMs present in the EPS. Among them, PS showed the highest correlation ($R=0.869$, $p < 0.01$) followed by building blocks. On the other hand, the AE had a strong negative correlation with the PN, LMW PN, PS, LMW PS, Building blocks, LMW neutrals, LMW acids and TOC. This reveals the fact the AE is reduced due to the presence of these dissolved organic matter, while decreasing the potential for the aggregation of AgNPs. AE shows a weak or moderate negative correlation with TN concentration ($R=-0.216$, $p < 0.05$). In addition, AE shows a strong positive correlation with the electrolyte concentration, which depicts that the AgNP aggregation is facilitated by the electrolytes present in the matrix. There was nearly no correlation between the AE and the biopolymers, HMW

PN and HMW PS, which is reasonable that they are less reactive to interact with the AgNPs due to their inherently neutral behavior [272].

Improved stabilization of AgNPs in the presence of LB-EPS irrespective of the electrolyte was observed (Figure 7.5(a) & (b)). This can be due to several factors, such as the increase in the concentration of protein compared to SB-EPS and the change in the hydrophobic-hydrophilic interactions which is governed by the different fractions of organic matter. The predominant factor was due to the lowest amount of building blocks present in the LB-EPS compared to the other three types of EPS. Building blocks in the EPS denotes the hydrophilic DOC with a molecular weight of 300-500 g/mol [245, 273]. Therefore, the less amount of hydrophilic parts (Table 7.1) present in the LB-EPS, help in improving the stability of AgNPs and reducing the aggregation [274]. This is confirmed by the correlation between the building blocks and AE and AC, which is significantly negative and positive respectively.

When present together with the biomass in the wastewater treatment system, AgNPs tend to interact with the SB-EPS first as they would be available in abundance due to their solubility. According to the results in this study, interactions with the SB-EPS would result in the release of ionic Ag. The amount of ionic Ag released in the presence of SB-EPS is higher than the amount released in the absence of EPS (Figure 7.5(e) & (f)). The released ionic Ag and the remaining AgNPs would then interact with the LB-EPS. Even though the amount of ionic Ag released in the presence of LB-EPS is lower than that of SB-EPS (Figure 7.5(e) & (f)), the cumulative amount of ionic Ag released in the presence of both SB-EPS and LB-EPS can adversely affect the biomass. Due to the dissolved organic compounds present and the stabilizing capability in LB-EPS, the adverse impacts of the ionic Ag affecting the bacteria will be reduced as shown in higher CCC, lower AE (Figure 7.5(a) & (b)), FTIR spectrum (Figure 7.10 (b)) and the correlation results (Table 7.2). Hence, with the prior interaction of LB-EPS, the TB-EPS, which is attached to the cell wall, would have minimal interaction with the ionic Ag released and AgNPs. Furthermore, higher proportion of hydrophobic groups, i.e., protein related N-H, were present in the TB-EPS (Figure 7.2 & Figure 7.10(c)), which explains its role in increasing the surface hydrophobicity of the sludge [275] with a higher concentration of protein like substances protecting the bacteria.

On the other hand, in the presence of Na^+ and low concentration of Ca^{2+}, EPS stabilizes the AgNPs with extracellular protein playing a dominant role in the stabilization process. Therefore, EPS may enhance the toxicity of AgNPs towards the bacteria and decrease the removal efficiency of AgNPs under this condition. However, at higher Ca^{2+} concentrations, dissolved exopolysaccharide molecules formulate polysaccharide aggregates via intermolecular bridging and calcium complexation. Eventually, these aggregates bridge the AgNP aggregates together resulting in an increase in the overall size of the aggregates reducing the toxicity towards the bacteria and increasing the removal efficiency of the AgNPs. The concentration of electrolytes in the wastewater usually falls within the higher range of the studied concentration range[246]. When present together with EPS and electrolytes in the wastewater treatment systems, AgNPs tend to aggregate due to the impact of electrolytes reducing the dissolution. The AgNP aggregates formed will then be coated by the EPS present further stabilizing the AgNPs and reducing their capability of releasing ionic Ag. The decrease in the release of ionic Ag reduces the toxicity of AgNPs towards the bacteria. The trapped AgNPs may finally end up in the downstream sludge system and eventually anaerobic digestion. Hence the presence of EPS in activated sludge will help in removing the AgNPs from the wastewater and reduce their negative impact towards the environment. However, the concentration of EPS and the characteristics of the wastewater will determine the final fate of AgNPs present in the wastewater.

7.4 Conclusions

The presence of EPS and various types of cations in the wastewater treatment system would have different impact on the transformations of AgNPs. This study reports the impact of EPS on the colloidal stability of AgNPs in the presence of the electrolytes, $NaNO_3$ and $Ca(NO_3)_2$. The results demonstrate that EPS effectively stabilize the AgNPs in the presence of $NaNO_3$ and low concentration of $Ca(NO_3)_2$. However, it enhanced the rate of aggregation at higher $Ca(NO_3)_2$ concentration, as a result of the aggregation of the dissolved EPS with AgNPs through inter molecular bridging, connecting the AgNPs and forming aggregates. Among the three types of EPS, LB-EPS showed promising effects in improving the stabilization of AgNPs, mainly due to the less hydrophilic constituents present therein. Hence, the results of this study are useful in understanding

the impact of EPS on the aggregation and colloidal stability of negatively charged NPs, which is important in assessing the transformations of NPs, eventually determining their transport and final fate in the wastewater treatment system.

8 Impact of Polysaccharides and Protein on the colloidal stability of silver nanoparticles

This chapter presents the details of the study conducted to investigate the impact of polysaccharides and protein on the colloidal stability of AgNPs. A brief introduction about the study is mentioned in the section 8.1, followed by the experimental methods used in the section 8.2. The results obtained and the findings from the study are vividly discussed in the section 8.3. Finally, the conclusions derived from the study are mentioned in the section 8.4.

8.1 Introduction

The interactions of AgNPs with different compounds in the environment can have varying effects on the rate of dissolution, toxicity and stability of AgNPs[36, 103]. A wide range of environmental parameters present in the aquatic system can influence the transformation of the AgNPs including the ligands that bind Ag^{+} such as NH_3, Cl^{-}, S^{2-} and thiols, cations (monovalent or divalent) that can destabilize the AgNPs such as Mg^{2+} and Ca^{2+} as well as the biological macromolecules such as humic acid, proteins and polysaccharides which can stabilize the AgNPs [103, 201-205].

Protein comprises roughly 50% of the organic compounds found in the wastewater[276]. Model protein also have been able to show various interactions with AgNPs in experimental conditions and affect both their rate of dissolution and colloidal stability in the presence of destabilizing divalent cations[203, 277]. These interactions eventually determine the fate and the transformation of the AgNPs when present with these compounds.

Polysaccharides are also a major compound in the wastewater, which can interact with AgNPs and hinder their stability in different ways [202, 223]. The interactions of polysaccharides with the AgNPs can affect the toxicity of AgNPs towards the biomass in the biological wastewater treatment system. Even though there have been several studies on the impact of protein and polysaccharides on the toxicity of AgNPs towards bacteria [222, 278-280], their impact towards the colloidal stability of AgNPs has been barely investigated, and this information is essential to understand the cause of toxicity.

This study was designed to understand the impact of the biological macromolecules, especially protein and polysaccharides on the temporal changes in the colloidal stability and dissolution of AgNPs. The experiments were carried out for a period of 150 days with freshly synthesized uncoated AgNPs, sodium alginate (SA) and bovine serum albumin (BSA). Alginate and BSA were used as a model polysaccharide and protein respectively. BSA is a model protein that is used in studies examining the fouling of reverse osmosis (RO) membranes during wastewater reclamation and the production of energy from wastewater proteins in microbial fuel cells [256]. Alginate is a model

polysaccharide used in studies evaluating RO membrane fouling and is a naturally secreted lipopolysaccharide that plays a prominent role in biofilm formation [281].

The changes in the hydrodynamic diameter, zeta potential and the localized surface plasmonic resonance was measured to assess the colloidal stability of uncoated AgNPs in the presence of the above-mentioned organic compounds. The release of ionic Ag in the previously mentioned conditions were also monitored to understand the potential impacts of the organic compounds on the dissolution of AgNPs. Understanding the influence of biological macromolecules on the colloidal stability of AgNPs and the resulting potential toxicity towards the biomass will be important in predicting the transformations of AgNPs in the natural and engineering system.

8.2 Experimental methods

8.2.1 Stability experiments

To assess the influence of the individual organic compounds, different concentration of SA (3, 6, 15, 30, 45, 60 and 75 mg/L) and BSA (6, 12, 30, 60, 90, 120 and 150 mg/L) were prepared respectively, from the stock solutions as described in SI. The concentration range of the organic matter used during the experiments was selected to match the levels in wastewater[276]. AgNP stock solutions with a concentration of 5 mg/L was added into the SA or BSA solutions with different concentrations as mentioned above. The sample mixtures were sealed and stored under the ambient environmental conditions during the experimental period.

The interactions of protein and polysaccharides with the AgNPs induce changes in the absorption spectra of AgNPs [282]. The changes in the UV vis absorption spectra can be used to assess the bonding of protein and polysaccharides with the AgNPs[283, 284]. The shift and broadening of the absorption spectra in the AgNP solutions with protein and polysaccharides depend on the size and the state of aggregation of AgNPs. Hence, to evaluate the stability of AgNPs, UV vis absorption spectrum of the experimental solutions was recorded on 0, 1 hr, 1, 6, 14, 21, 35, 40, 48, 70, 100 and 150 days. In order to measure the size of the AgNPs in the experimental solutions, Dynamic Light Scattering (DLS) was used. DLS gives the hydrodynamic diameter of the AgNPs in the experimental solutions [282]. In order to track the changes in the particle size due to the

interactions with other compounds, DLS measurement was performed on 0, 1, 24 hr, 6, 14, 21, 35, 70, 100 and 150 days.

8.3 Results and Discussion

8.3.1 Characterization of the synthesized AgNPs

The average size of the synthesized AgNPs was 26 ± 1.248 nm. TEM results show that the diameters of more than 84% of the AgNPs ranged between 10-50 nm. The particles were reasonably monodispersed in the suspension and had a spherical shape (Figure 8.1(a)). The size value obtained using DLS was the peak size based on the intensity distribution (36.76 ± 5.172 nm) (Figure 8.1(b)). The synthesized AgNPs showed a characteristic peak at the wavelength of 392 ± 2 nm in the UV-Vis absorption spectrum with a peak-absorbance of 0.926. The total Ag concentration of the synthesized AgNPs was 5.829 ± 0.031 mg/L with a dissolved ionic Ag concentration of 2.268 ± 0.002 mg/L. The pH and zeta potential of the AgNP stock solution was reported to be 8.03 and -28.3 ± 1.7 mV respectively.

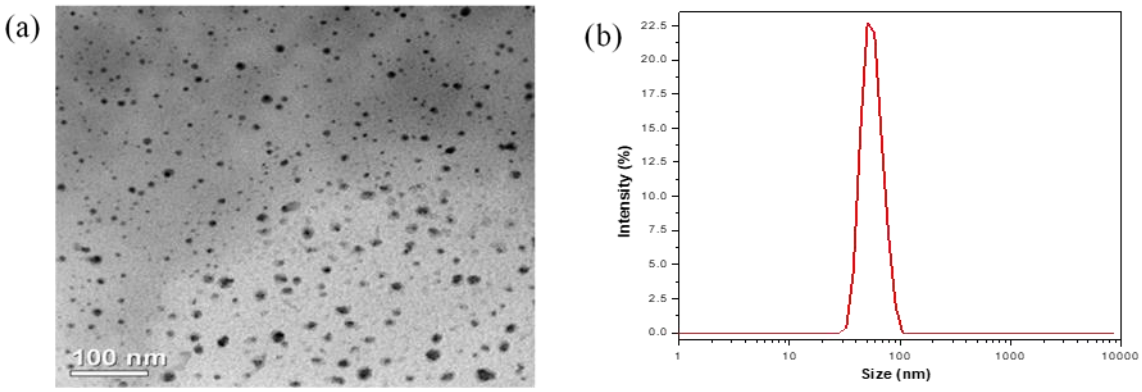

Figure 8.1 Characterization of the synthesized particles (a) Morphology by the TEM (b) Size distribution of the suspension by DLS

8.3.2 Modulation of the AgNP stability by SA and BSA

Increasing SA concentration reduced the peak absorbance at the characteristic wavelength and red shifted the localized SPR peak (Figure 8.2(a)). The peak absorbance wavelength initially shifted from 392 nm to 399 nm upon addition of SA. It was further shifted to 405 nm with the increase in the SA concentration. The absorbance slightly

increased from 0.325 to 0.37 (Figure 8.3 (a)) with the increase in the SA concentration. This observation suggests that the addition of SA alter the characteristics at the AgNP dielectric surface [285]. The change in the absorbance of the characteristic peak can be attributed to the decrease in the AgNP concentration upon addition of SA. The red shift in the characteristic wavelength can be attributed to the surface modification induced by SA on AgNPs. The increase in the absorbance at the red shifted wavelength with the increased SA concentration verifies the SA induced surface modification of AgNPs.

Upon the addition of BSA, the peak absorbance wavelength of AgNPs shifted from 392 nm to 401 nm, and further to 407 nm when BSA concentration increased. Affinity with the AgNP surface, interacting and binding on to the AgNPs as a protein [222] can be the reason for the observation of the slight red shift of the SPR peak in the presence of BSA. The absorbance at the characteristic wavelength also gradually decreased with the BSA concentration. Thus, it can be attributed to the surface modification of the AgNPs with the increasing BSA concentration. However, the peak absorbance observed at 407 nm at the BSA concentration of 150 mg/L is higher than that at 60 mg/L. This observation shows that the particles were stabilized under higher BSA concentrations. This can be attributed to the BSA induced masking of the SPR absorbance of AgNPs in a concentration dependent manner. Furthermore, there was no peak observed at the wavelength around 500 nm, which is the characteristic wavelength for AgNP aggregates. This observation depicts that the reducing absorbance was not caused due to aggregation, but due to the BSA induced surface modification.

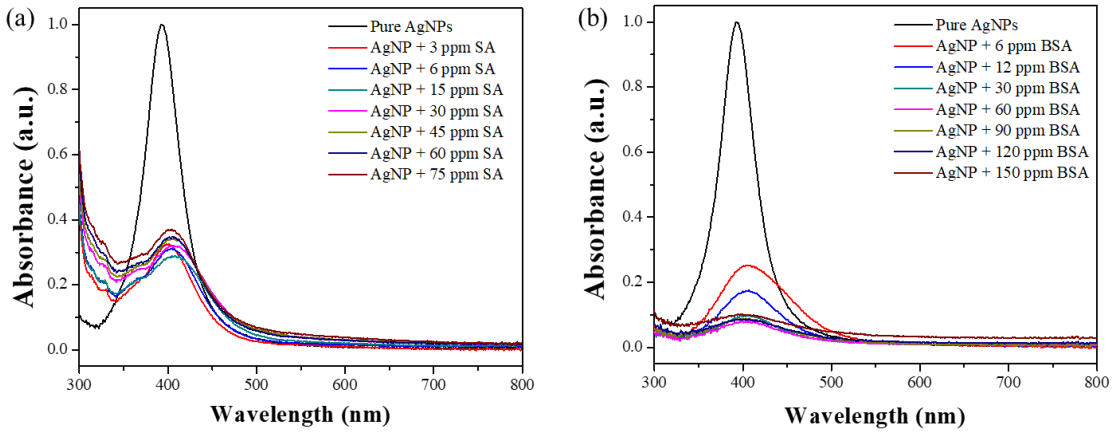

Figure 8.2 Change in the UV Vis absorption spectra of AgNP solutions with variable concentrations of (a) SA and (b) BSA after 1h of incubation. AgNP concentration: 5 mg/L.

DLS measurements revealed an increase in the average hydrodynamic diameter with the increasing SA concentration (Figure 8.4(a)). This observation can be attributed to the increasing ionic strength upon the addition of SA. The interactions between SA and AgNPs changed the electrical double layer as the SA molecules compete with the counter ions in the suspension [7, 215]. The increase in the hydrodynamic diameter observed with the increasing SA concentration suggests potential agglomeration of AgNPs at higher SA concentrations.

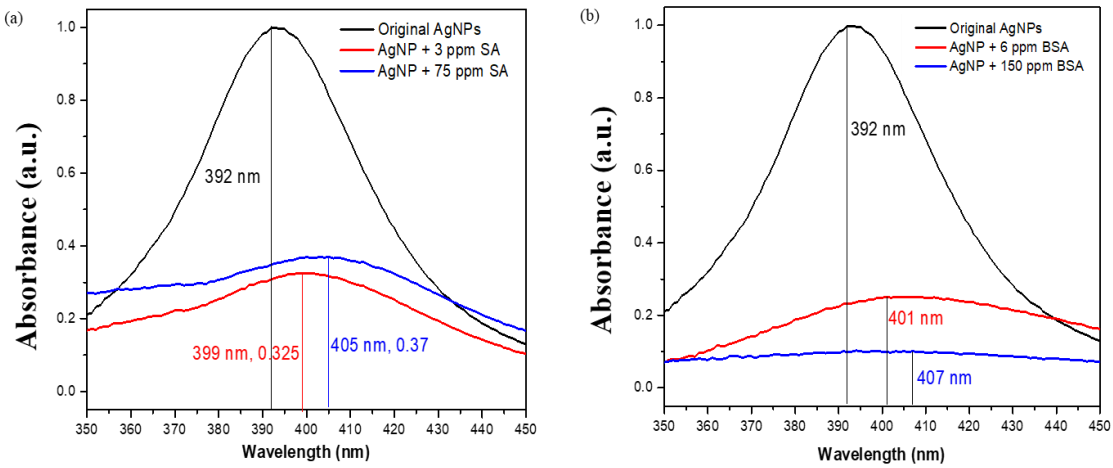

Figure 8.3 Peak shift in the localized surface plasmon resonance (SPR) spectra of AgNPs with variable concentrations of (a) SA and (b) BSA

Similar results were obtained in the presence of BSA. Up to the BSA concentration of 12 mg/L, the increase in the hydrodynamic diameter was not prominent. However, a significant increase can be observed when the BSA concentration was higher than 90 mg/L. It is clear that an obvious increase in the hydrodynamic diameter was observed in the presence of SA compared to BSA (Figure 8.4). This observation indicates that the particles were stabilized in the presence of protein compared to the polysaccharides.

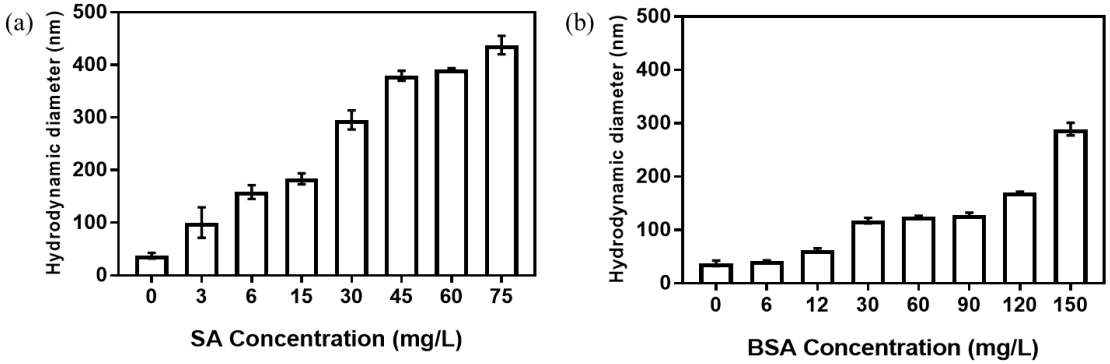

Figure 8.4 Change in the average hydrodynamic diameter of AgNPs with variable concentrations of (a) SA and (b) BSA after 1h of incubation. AgNP concentration: 5 mg/L.

As described previously, at the low concentrations of SA (0-15 mg/L) the particle size does not change significantly. In order to represent the different concentration ranges of 0-15 mg/L and 15-75 mg/L, 6 mg/L and 60 mg/L were selected respectively as the short-term behaviour of the other concentrations in the respective region were similar to the representative concentrations. Since the variation in the PSD with time changes in a similar pattern over different concentrations, 6 mg/L was selected as the representative concentration of alginate to discuss the results. With the increase in the concentration, there was a shift in the intensity peak in the PSD, suggesting the presence of larger particles (Figure 8.5(a)). Furthermore, the shift in the intensity peak in the PSD with time suggests that the presence of alginate results in larger particles in the beginning, which eventually breaks on to smaller particles and become stable over time (Figure 8.5(c)). At a constant concentration of SA, the average hydrodynamic diameter of the AgNPs increased with time. This observation can be due to the absorption of SA chemically onto the AgNP surface and remain as a coating for the AgNPs. These results are confirmed with the red shift occurred in the UV vis spectrum in the AgNP solutions in the presence of SA with time (Figure 8.6(a)). The red shift observed in the UV vis absorption spectrum is indicative of a surface modification of the AgNPs. Our observations can be further explained with the TEM images obtained (Figure 8.7) and the zeta potential results (Figure 8.8). According to the TEM images obtained there was no possible aggregation of AgNPs observed in the presence of alginate. Instead individual particles of different sizes can be observed (Figure 8.7 (a) & (c)). Furthermore, when we consider the TEM images obtained at different time intervals,

the number of particles in one frame reduced, suggesting that the particles were further stabilized with time (Figure 8.7(b) & (d)). The zeta potential of the AgNPs (-28.3 ± 1.7 mV) became further negative (-32.4 ± 1.3 mV) upon the addition of 6 mg/L SA. With the increase in the SA concentration to 60 mg/L, the negative zeta potential of the AgNPs further increased (-51.6 ± 2.1 mV), depicting the colloidal stability of AgNPs induced by SA (Figure 8.12). These observations further support the proposed mechanism of surface modification of AgNPs induced by alginate.

In order to represent the different concentration ranges of 0-30 mg/L and 30-150 mg/L, 12 mg/L and 120 mg/L were selected respectively as the short-term behaviour of the other concentrations in the respective region were similar to the representative concentrations. Since the variation in the PSD with time changes in a similar pattern over different concentrations, 12 mg/L was selected as the representative concentration of BSA to discuss the results. According to the Figure 8.5(b), the peak size of the AgNP solutions, did not change much upon the addition of 12 mg/L of BSA. But when the concentration of BSA increased up to 120 mg/L, a peak above 100 nm appeared showing an increase in the hydrodynamic diameter. When considering the change in the PSD with time in the presence of BSA, the particle size increased with small peaks appearing above 100 nm (Figure 8.5 (d)). Even though there was an increase in the hydrodynamic diameter, no evidence of aggregation was observed in the TEM images obtained at different time points with varying concentration of BSA (Figure 8.9). Stable, individual AgNPs can be visualized in the TEM images obtained under different solution conditions. This observation verifies the colloidal stability of AgNPs induced by BSA as a protein. In the presence of BSA, the zeta potential distribution remains almost mono modal irrespective of the BSA concentration even though the peak intensity changed with the concentration. Furthermore, the negative zeta potential of the AgNPs (-28.3 ± 1.7 mV) slightly increased to -29.6 ± 1.7 mV upon mixing with 12 mg/L BSA. Added to that the zeta potential distribution become mono modal upon the addition of 12 mg/L BSA depicting the stability of AgNPs induced by BSA (Figure 8.8). When the BSA concentration further increased to 120 mg/L, the peak intensity of the zeta potential distribution increased depicting the increased colloidal stability of AgNPs (Figure 8.8). Our observations using different analytical techniques suggest that the surface coating induced by the BSA molecules on the AgNPs increased the colloidal stability of AgNPs in the presence of BSA. (Figure 8.8).

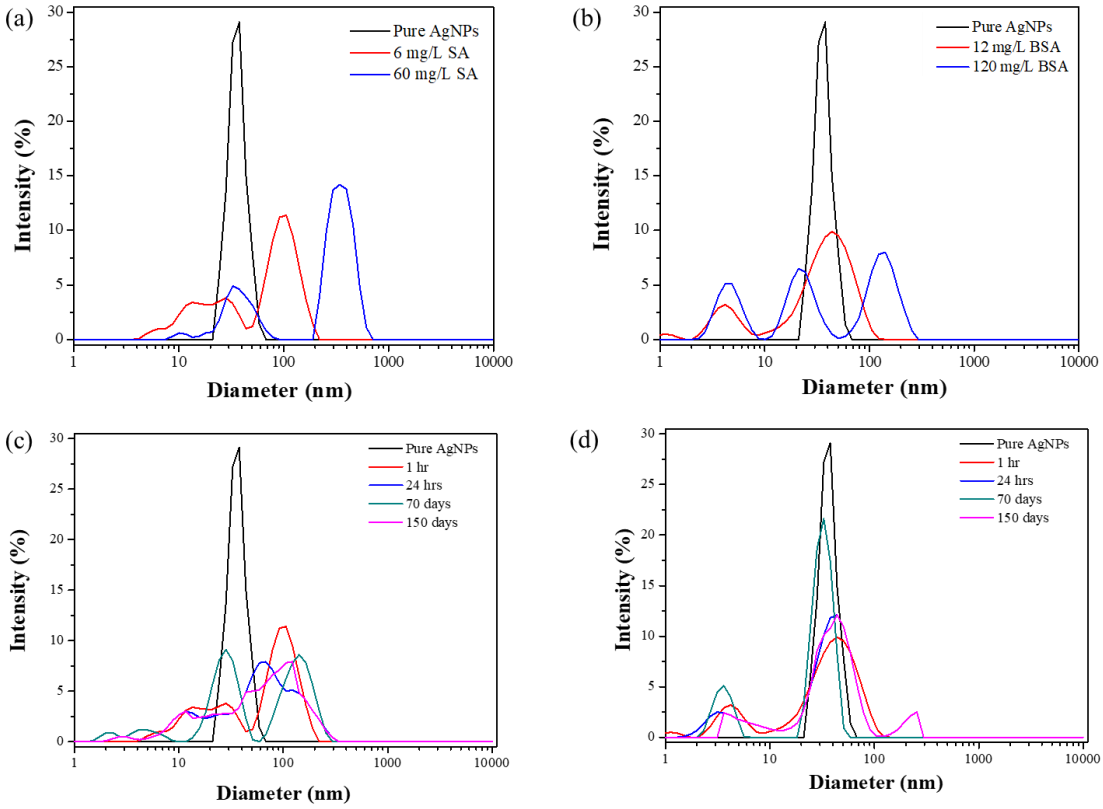

Figure 8.5 Change in the particle size distribution for (a) SA & (b) BSA with concentration after 1 h of incubation and change in the particle size distribution for (c) SA (6 mg/L) & (d) BSA (12 mg/L) with time. AgNP concentration: 5 mg/L.

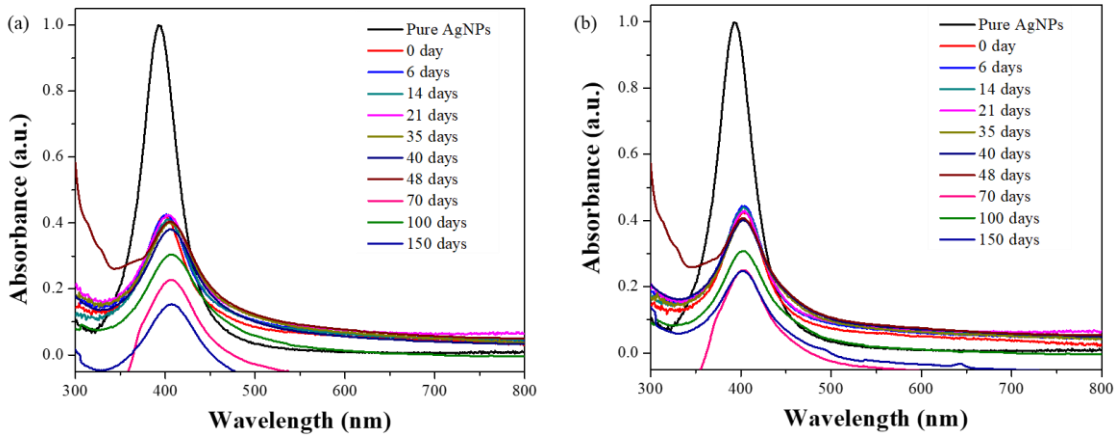

Figure 8.6 Change in the UV vis spectrum with time in the presence of (a) SA – 6 mg/L and (b) BSA – 12 mg/L.

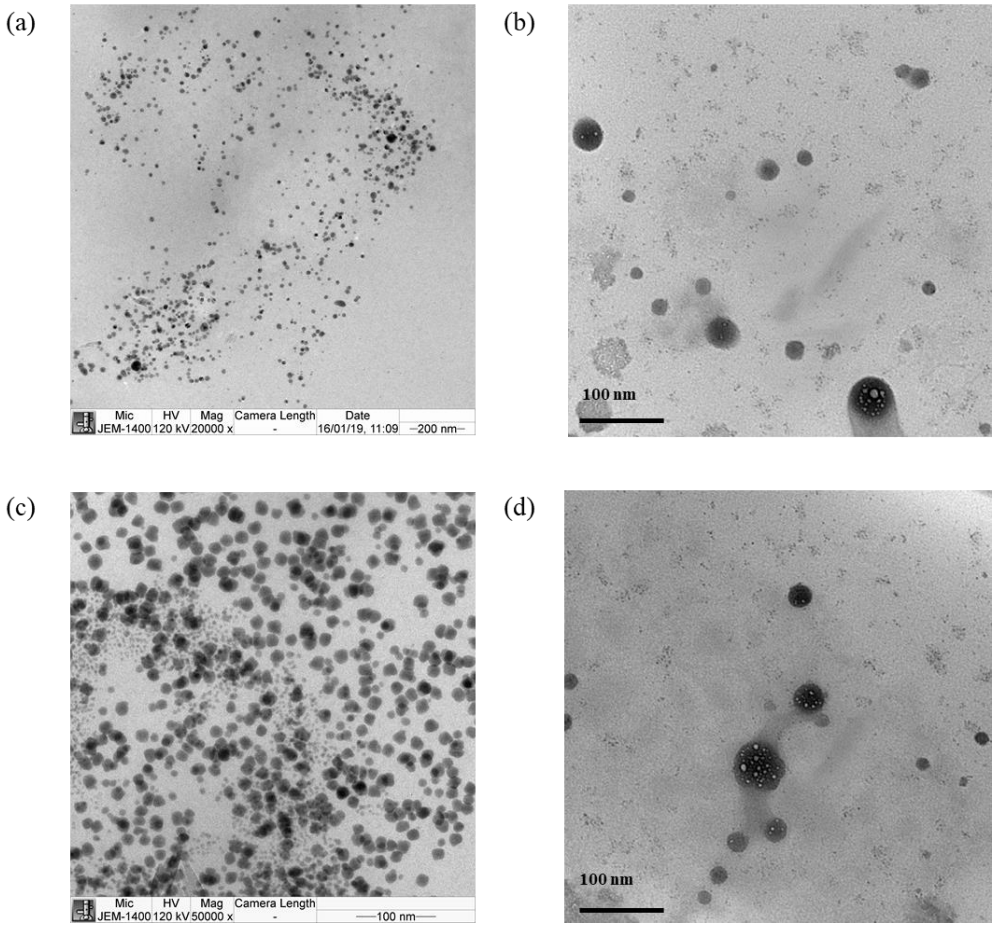

Figure 8.7 TEM images obtained at different time intervals (a) SA – 6 mg/L – 1 hr (b) SA – 6 mg/L – 70 days (c) SA – 60 mg/L – 1 hr and (d) SA – 60 mg/L- 70 days.

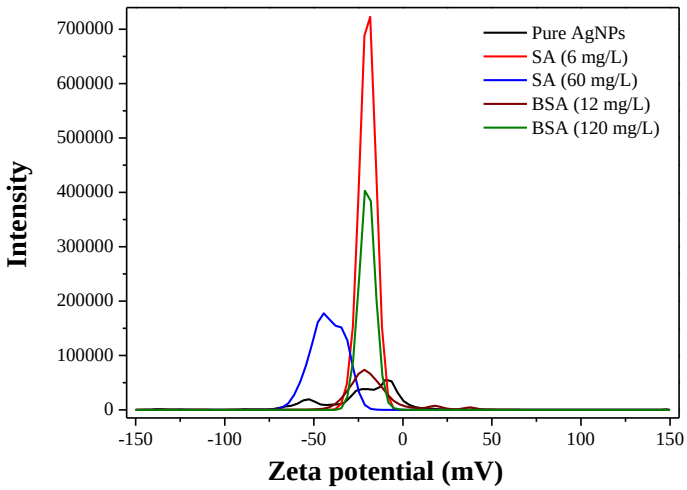

Figure 8.8 Zeta potential distribution of the AgNP solutions in the absence and presence of SA and BSA.

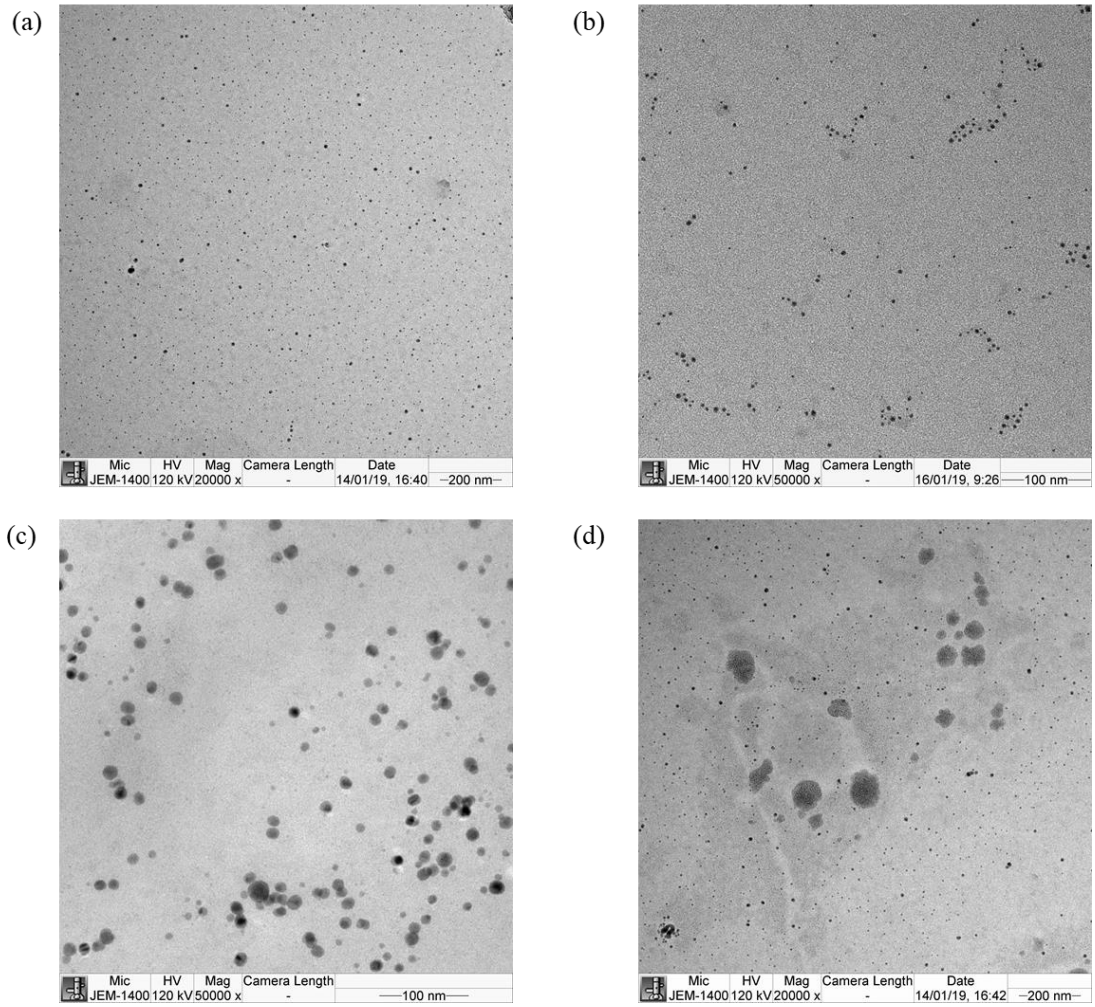

Figure 8.9 TEM images obtained at different time intervals (a) BSA – 12 mg/L – 1 hr (b) BSA – 12 mg/L – 70 days (c) BSA – 120 mg/L – 1 hr and (d) BSA – 120 mg/L- 70 days.

8.3.3 Modulation of the rate of ionic silver release by SA and BSA

Variations in the rate of AgNP dissolution were observed during the incubation with SA or BSA (Figure 8.10). The amount of ionic Ag released, increased with the SA concentration at a constant time. The concentration of the ionic Ag released at a constant SA concentration increased with the time except at higher SA concentrations (45-75 mg/L) (Figure 8.10(a)). At 45-75 mg/L SA, the amount of ionic Ag released fluctuated differently. The ionic Ag concentration recorded at 150 days was lower than that recorded at 70 days. This observation suggests that higher SA concentrations (45-75 mg/L) could, in fact inhibit Ag release, verifying the role of SA as an antioxidant. SA scavenges the reactive oxygen species present or otherwise formed in the test

matrix[256], thus providing a less conducive condition for the oxidative dissolution of AgNPs to occur from pure AgNP surfaces.

The amount of ionic Ag released upon the addition of BSA (6 mg/L BSA) is indicative of a favorable environment for pure AgNPs to dissociate into ionic Ag (Figure 8.10(b)). Bonding of BSA with the cations in the water, interacting with the pure AgNPs might facilitate the higher dissolution of AgNPs in the presence of BSA. The concentration of the ionic Ag released fluctuated with the BSA concentration, with an overall increase observed at the highest concentration (150 mg/L) after 1 hour of incubation. The concentration of ionic Ag increased up to 30 mg/L and decreased thereafter at a prolonged period (Figure 8.10(b)). Since there has not been any measurable amount of Ag detected in the highest concentrations of the organic compounds used in this study, this can be justified that the source of released ionic Ag under the evaluated conditions are solely due to the addition of pure AgNPs and not SA or BSA itself.

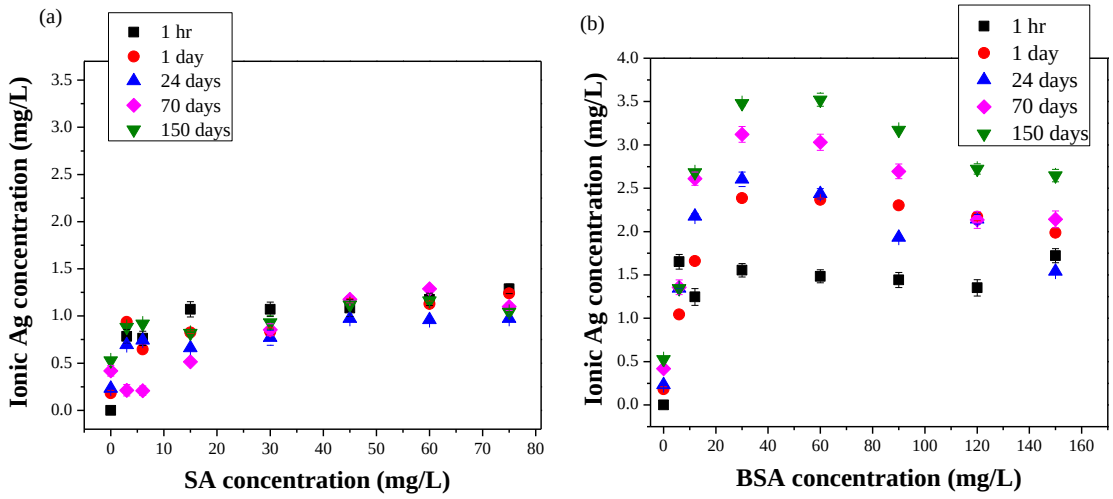

Figure 8.10 Change in the ionic Ag concentration with time at different concentrations of (a) SA and (b) BSA. AgNP concentration: 5 mg/L.

There is a clear increase in the peak intensity upon the addition of either SA or BSA in the zeta potential distribution (Figure 8.8). This implies the increase in the colloidal stability of AgNPs due to interactions in the presence of SA or BSA. As mentioned previously, zeta potential results further explain the stability induced by SA and BSA following a mechanism of surface modification of AgNPs resulting in more stable suspensions. In order to understand the coating mechanism of AgNPs in the presence of

SA and BSA, FTIR spectrum of the SA and BSA solutions were analyzed in the presence and absence of AgNPs and the results are mentioned in the Figure 8.11.

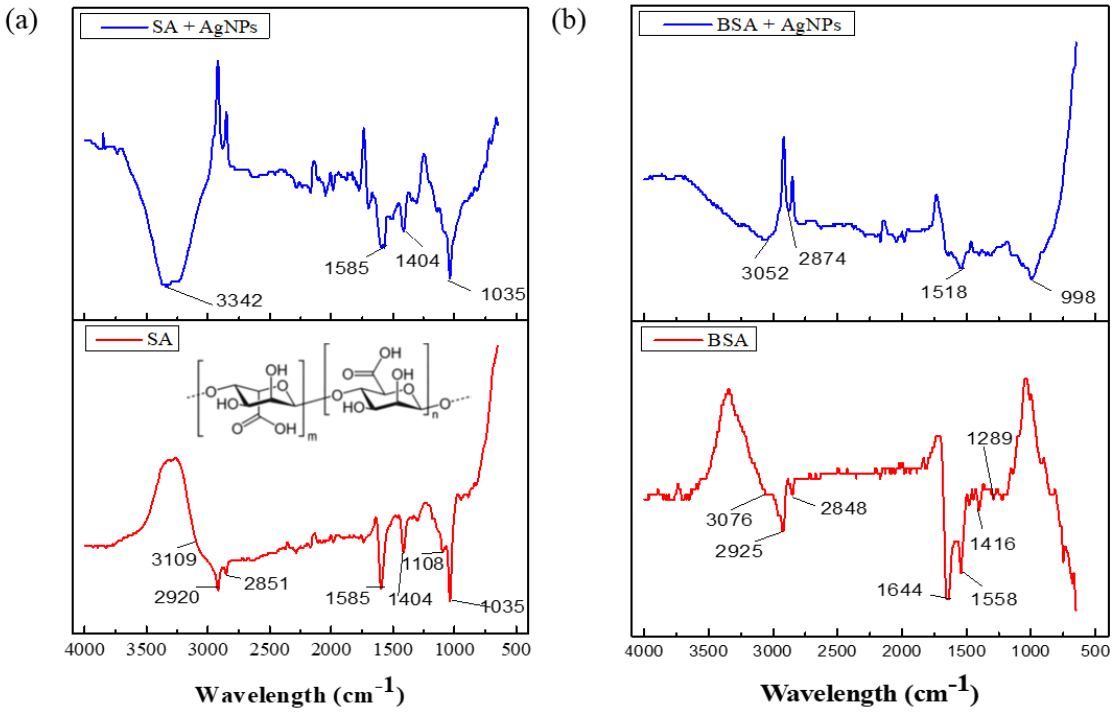

Figure 8.11 Change in the FTIR spectrum of (a) SA and (b) BSA in the presence and absence of AgNPs. AgNP concentration: 5 mg/L.

Absorption peak observed in the FTIR spectrum of SA at 3109 cm^{-1} (the red line) is assigned to the stretching vibrations of -OH groups[286]. The peaks observed at 2929 cm^{-1} and 2851 cm^{-1} are attributed to the asymmetric stretching vibrations[263, 264] and symmetric stretching of $-CH_2$[186]. The peak at 1585 cm^{-1} is assigned to the asymmetric stretching vibrations of –COOH [287]. The peak observed at 1404 cm^{-1} is due to the -COO- symmetric stretching. Characteristic peak of natural polysaccharides is observed at the wavelength 1108 cm^{-1}[287] and 1035 cm^{-1} is assigned to the -C-O-C- stretching mode arising from the glucosidic units [288] (Figure 8.11(a)). Upon mixing of SA with AgNPs (the blue line), some of the above-mentioned peaks disappeared and peaks with increased intensity can be observed at the wavelengths of 1585, 1404 and 1035 cm^{-1}. Furthermore the peak at 3109 cm^{-1} red shifted to 3342 cm^{-1} confirming that the hydroxyl groups can be responsible for the stabilization of AgNPs induced by alginate [288].

In the FTIR spectrum obtained for BSA (the red line), peak observed at 3076 cm^{-1} is assigned to the characteristic stretching vibrations of $-NH_2$ and -OH groups [289].

Absorption peaks at 2925 cm^{-1} and 2848 cm^{-1} are attributed to the symmetric stretching vibrations and symmetric stretching of -CH_2. The peak at 1644 cm^{-1} is due to stretching of amide I, α-helix [186, 290] and 1555 cm^{-1} is due to the stretching of amide II [291]. The peak observed at 1416 cm^{-1} is assigned to the wagging and twisting vibrations of -CH_2[289] and 1289 cm^{-1} is assigned to the amide III band, α-helix [186] (Figure 8.11(b)). Due to the interactions with AgNPs (the blue line), peak at 3076 cm^{-1} slightly blue shifted to 3052 cm^{-1}. The peaks at 2925 and 2848 cm^{-1} in BSA merged into one peak at 2874 cm^{-1} in the presence of AgNPs. The peak at 1644 cm^{-1} shifted to 1518 cm^{-1} in the BSA and AgNP mixture suggesting that BSA adsorbs to the AgNPs through the exposed α-helices [290, 291]. Furthermore, a red shift in the peak 921cm^{-1} to 998 cm^{-1} was also noted in the BSA and AgNP mixture.

8.3.4 SA and BSA induced stability of AgNPs

The impact of SA and BSA used during the experiments, reflects their ability to adsorb onto AgNPs [216], and to bind with and modify the AgNP surface in order to increase the colloidal stability of AgNPs. The presence of alginate resulted in a decrease in the concentration of the ionic Ag compared to BSA (Figure 8.10). This observation can be a result of the decreased dissolution of AgNPs in the presence of SA. The reason for this phenomenon can be proposed as the chemical adsorption of ionic Ag onto the AgNP surface. Unlike BSA, alginate did not dominate the rate of dissolution of AgNPs. Thus, alginate can reduce the inhibition effect of AgNPs through a mechanism of coating the AgNP surface. Surface modification of the AgNPs induced by SA directly prevent the interactions with the other compounds, as clearly depicted by the red shift in the peak absorbance wavelength (Figure 8.3(a)). However, once the ionic Ag is released from the AgNPs, alginate is unable to mitigate its toxicity [256]. SA tends to form a coating on the AgNP surface hence resulting in lower AgNP inhibition. But SA was unable to completely inhibit the dissolution of AgNPs due to its low affinity towards ionic Ag. The proposed mechanism of SA in stabilizing AgNPs is illustrated in Figure 8.12. Due to the coordination at an oxygen site of the SA molecule, cations interact with the negative charges available on the AgNP surface. The interactions between SA and AgNPs are influenced by the planar benzene ring in the SA molecule[207].

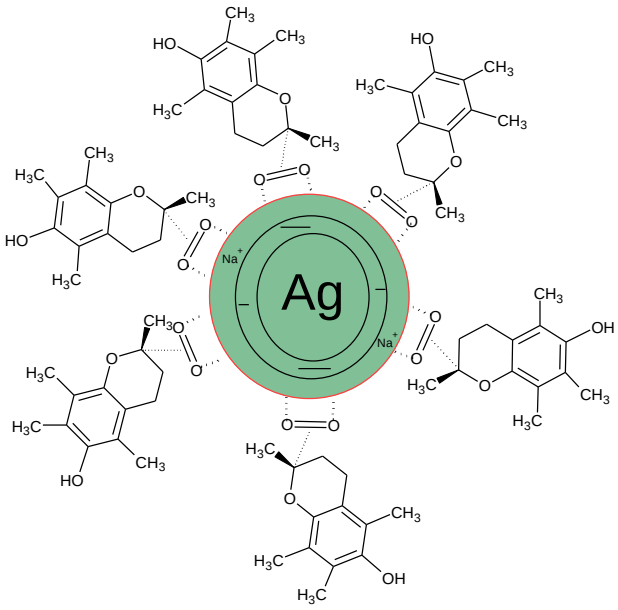

Figure 8.12 Proposed reaction mechanism of alginate molecules with AgNPs

Protein proved to be a dominant constituent determining the transformations of AgNPs [103]. BSA acted as an agent in stabilizing the AgNPs through a dual mechanism of chelation with the thiol groups and then binding on to the AgNP surface. The binding of BSA to the AgNP surface was stronger compared to the binding induced by the alginate. This resulted in higher stability in the presence of proteins compared to the polysaccharides.

According to the previous studies, the proteins present in the aquatic matrices can bind in to the noble metal NPs[203]. The lattice model of proteins binding to the NPs [292, 293] can be successfully applied to model the binding of BSA onto the AgNPs. This model predicts that low BSA concentration will bind BSA onto the NP surface in a side-on mode, forming many low energy bonds. This was observed among the interactions of BSA with AgNPs as shown in the FTIR spectrum (Figure 8.11(b)). These interactions will result in reduced release of ionic Ag in low BSA concentrations due to the adsorption of BSA to the AgNP surface (Figure 8.10(b)). The increased release of ionic Ag with the increasing BSA concentration can be due to the sequestration of ionic Ag chemically absorbed on the AgNP surface to the thiol groups present in BSA. These groups such as cysteine possess a higher binding affinity for metal cations [126, 203, 256]. BSA reduces the AgNP inhibition by a dual mechanism. This occurs, firstly, chelating the released ionic Ag by the Ag ligand group present within the BSA molecule

and then, coating the AgNPs to prevent direct interactions with the other compounds in the matrix as shown by the red shift in the peak absorbance wavelength (Figure 8.3(b)). The mechanism of BSA induced stability of AgNPs is illustrated in
Figure 8.13.

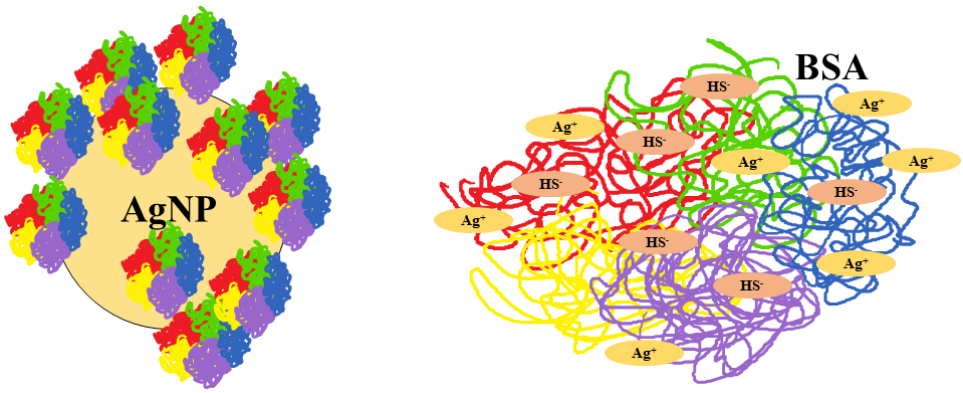

Figure 8.13 Proposed reaction mechanism of BSA with AgNPs

Interestingly, while increasing the colloidal stability, BSA itself catalyzed the dissolution of the AgNPs. Higher dissolution of the AgNPs was observed in the presence of the BSA and can be attributed to the extraction of chemically adsorbed ionic Ag on the AgNP surface by the thiols present within BSA. Therefore, it can be expected that the toxicity of AgNPs in the environments with a higher protein content is limited. But the same environment can pave way to the dissolution of the AgNPs via protein-induced dissolution. The toxicity of AgNPs would be reduced due to the decrease in the dissolution of polysaccharide coated AgNPs, in the environments with an increased polysaccharide content as in biofilms. However, the toxicity induced by the ionic Ag that have been released from the AgNPs before encountering with the polysaccharides would not be decreased as most of the polysaccharides are poor in ionic Ag binding ligands.

8.4 Conclusion

Our results present that SA stabilized the AgNPs through a singular mechanism by coating the AgNP surface. The coating induced by SA on the AgNPs, reduced the dissolution of AgNPs to ionic Ag. However, this phenomenon is not permanent, as once

the ionic Ag is released, SA is not able to reduce ionic Ag concentration. On the other hand, BSA uses a dual mechanism in protecting the biomass from AgNPs : (1) chelation of the ionic Ag by the Ag-ligand groups within BSA and (2) coating the AgNPs.

The findings are significant when considering the transformations of AgNPs in the biological wastewater treatment system. SA and BSA followed a mechanism of stabilizing the AgNPs in the matrix via chemically coating the AgNPs. The transformations observed under these types of organic matter can be affected by the other environmental factors as well. Future studies are envisioned to examine how the coatings induced by the proteins or polysaccharides on the AgNPs may affect their adsorption onto bacterial biomass, which is another important process determining the fate and transport of AgNPs in the wastewater.

9 pH induced interactions of AgNPs in the aquatic matrices observed using in situ LCTEM

This chapter presents a brief introduction about the study in the section 9.1, followed by the detailed methods used in the LCTEM experiments in the section 9.2. The results obtained and the findings from the study are vividly discussed in the section 9.3 with a short summary in the end.

9.1 Introduction

Interactions between NPs in solutions play an important role in understanding their transformations and subsequent fate in the engineered systems. They are responsible for the colloidal stability[203], aggregation[7], dissolution[294] and the reactions with biological macromolecules[103]. The interactions between the NPs in solution are regulated by the attractive and repulsive hydration forces between two interactive surfaces in water[295]. It is known that these short-range forces may prevent the surfaces from approaching closer than several water molecules[170]. However, the exact origin of these forces is still not fully understood, an example would be the classical continuum models that account only for a repulsive diffuse double layer and the attractive van der Waals (vdW) forces in the matrix[296]. While at short distances between two macroscopic hydrophilic surfaces, these forces may dominate over other intermolecular forces[297, 298]. However, it is unclear how repulsive hydration forces affect the interaction dynamics of NPs. As a result, the impact of the intermolecular forces in the solution layers on the NP interactions remain experimentally unresolved.

The size and structure of silver NPs (AgNPs) has a significant impact on various interactions, such as absorption, oxidation reactions, and dissolution. Hence, determining the transport and transformations of AgNPs in the aquatic environment is critical. Therefore, the modern research yearns for novel techniques to determine the evolution of the size and morphology of NPs in order to integrate the state of aggregation of NPs with their impact on the environment.

Recently, observing the interactions of NPs directly in solution matrices has been made possible using in situ liquid cell transmission electron microscopy (LCTEM), which can be a potential technique to be applied geochemical and environmental studies. LCTEM helps directly to quantify and structure the NPs dispersed in the solutions, as well as to simplify real-time interaction tracking between individual particles. This capability of LCTEM allows to automate dynamic processes depending on the total number of NPs. It also allows to explore how liquid flows through the cell and how the properties of the solution affect the interactions of NPs with high precision electron microscopy revealing that the presence of the electrostatic forces between the NPs play a crucial role in the attachment[198], growth[299] and the assembly[300] of NPs. In these studies, tracking

the movement of interacting NPs within few nanometers, showed that dipolar interactions facilitate the pairwise approach and the subsequent alignment of NPs. The LCTEM provides an opportunity to investigate the impact of an external stimuli directly on the interactions and the dynamics of NPs in a solution. Current studies have shown that the artefacts such as contamination, charging, unwanted crystallization and dissolution should be considered in the interpretation of the results.

The objectives of this study include (1) evaluating the mechanism of aggregation of AgNPs in water and acid with respect to the change in the interactive forces, (2) assessing the impact of short range and long-range intermolecular forces on the interactions of NPs and (3) appraising the suitability of LCTEM as a technique for in situ studies in environment related subjects. Here, using dynamic, in situ LCTEM imaging [301-304], we visualized the time resolved pH induced interactions of AgNPs in water, showing that their approach towards each other is hindered by the primary hydration shell of each individual AgNP. When contrasting the interactions of AgNPs, in the absence and presence of acid, we found that the presence of protons in the solution alter the surface charge of the AgNPs thereby resulting in a change in the electrostatic potential of the AgNPs. Our analysis reveals that these AgNPs jump to contact only when the charge cloud around the particles are altered.

9.2 Experimental Methods

The AgNPs used during the experiments were synthesized via oxidation-reduction of $AgNO_3$ using $NaBH_4$. Detailed procedure on the synthesis[305] and the reproducibility of this method is mentioned in Chapter 3. Synthesized AgNPs were characterized according to the methods mentioned in Fernando et al[248] and the typical size of the NPs used here were about 20-30 nm. Our experimental setup consisted of a thin layer of liquid specimen[306] (~50 nm) with AgNPs sandwiched between the two electron transparent Silicon Nitride (Si_3N_4) membranes (~50nm thick on each side) of a liquid cell with the help of the Au spacer, which essentially protects the liquid samples from the high vacuum of the TEM. The diffusion of NPs due to translation and rotation within these thin liquid films near liquid-solid interfaces is strongly suppressed[307, 308], which allows for the real time imaging and quantification of the interaction force fields of an otherwise rapid phenomenon. We carried out the flow experiment using the

Protochip Poseidon Liquid Cell Holder with two kinds of solutions; freshly synthesized, uncoated 10 mg/L AgNP solution (final pH ~8) and 10% (w/v %) Nitric (V) acid solution. Before loading the AgNPs onto the grids, they were adequately rinsed using acetone and methanol at least for 5 min respectively. This was mainly to eliminate the possible impurities and protective coatings, which was followed by immediate air-dry. Then, the e-chips were plasma cleaned (3:1Argon/Oxygen mixture) for about 5 min using the Fishione Plasma Cleaner Nanoclean Model 1070 for surface treatment to change the Si_3N_4 membranes from hydrophobic to hydrophilic and to remove possible organic contaminants on the surfaces [309]. The cleaner is set to 100% power using 75% Argon with 25% Oxygen. First, the AgNPs in the fluid cell e-chips was observed through the JEOL 2010 TEM with a high-resolution pole piece operated at 200 kV with electron doses ranging from 6 to 58.5 e/($Å^2$.s) and at a rate of 4-10 frames per second. Then the AgNPs was pumped through the liquid cell holder to the fluid cell using a syringe pump (Harvard Apparatus, Pump 11 Elite) at an infuse rate of 300 µl/h. After allowing ample time for the AgNPs to reach the fluid cell, the movement of AgNPs in the matrix was observed. Subsequently, Nitric (V) acid was pumped into the fluid cell using a syringe pump at an infuse rate of 150 µl/h. The impact of the beam on the movement of NPs in liquid cells due to heating or momentum transfer from energetic electrons is negligible under these imaging conditions, however charging during the imaging may enhance the movement of the NPs. The images obtained during different scenario were processed as mentioned below.

9.2.1 Image Processing - Nano particle Detection and Tracking

The proposed NP detection and tracking method is implemented using C++, using OpenCV [310] library. At each image frame particles were detected, and these detected particles were assigned unique identity to track them across the frames.

At detection stage, all processing was carried out in grey image space. Initial steps of the detection process were carried out following the method proposed in [170]. First the image was inverted, and Gaussian filtering was applied to reduce the noise effect from the camera. 8 is used as the standard deviation for the Gaussian kernel for both x and y directions. Then the Sobel operator was applied on the smoothed image to obtain the gradient image. The gradient image was converted to a binary image by assigning 1 to

the values of the gradient image (magnitude of the gradient) that are higher than a threshold, otherwise assigning 0. This threshold was calculated using the Otsu's threshold selection method [311]. Then morphological closing and opening operations were applied on the binary image to reduce the false positives. Kernal of 9x9 was used to perform morphological operations. At this stage, NPs were assigned 1 and the background was assigned 0. Then connected component analysis on this image provide an estimate on the boundary of each NP along with area covered by it. This process is visually presented in Figure 9.1. Then as a false positive removal process all the connected components smaller than a threshold were removed. This threshold was empirically set at 500 pixels, but this value should be set depending on the magnification of the images. At this stage, for each detected NP set of parameters are defined. These parameters are:

(a) center and radius: Since these NPs are circular in 2D shape, center and radius of the smallest circle that contain this NP are considered as the center and the radius of the particle.
(b) Perimeter and area: Arc length of the contour surrounding the NP is taken as the perimeter while number of pixels inside the contour is considered the area.

After the detection, set of particles were identified with above mentioned parameters. During tracking stage particle localization and size based matching criteria was used. Firstly, the particles in two adjacent frames (frame at time t and frame at time t+1) that are nearest to each other (i.e. in terms of the smallest distance between the centers of the particles) were grouped together. Then if the area difference between these two particles was less than 50% of the area of the particle of the initial frame (frame at time t,) the same track identity was assigned. This was repeated for all the frames. Comparing the area helps in assigning a new track identity when two particles attached as their area was most likely to double.

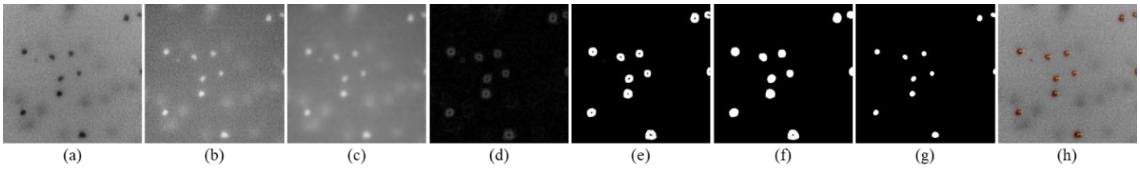

Figure 9.1 Nano particle detection process. (a) Original image, (b) Inverted image, (c) Gaussian smoothed image, (d) Sobel magnitude image, (e)Otsu threshold of (d), (f) Morphological closed image, (g) Morphological opened image and (h) Detected nano particles on top of original image.

9.3 Results and Discussion

The time resolved TEM images of the AgNPs interacting in water (Figure 9.2A) are compared with that in the presence of protons (Figure 9.2B).

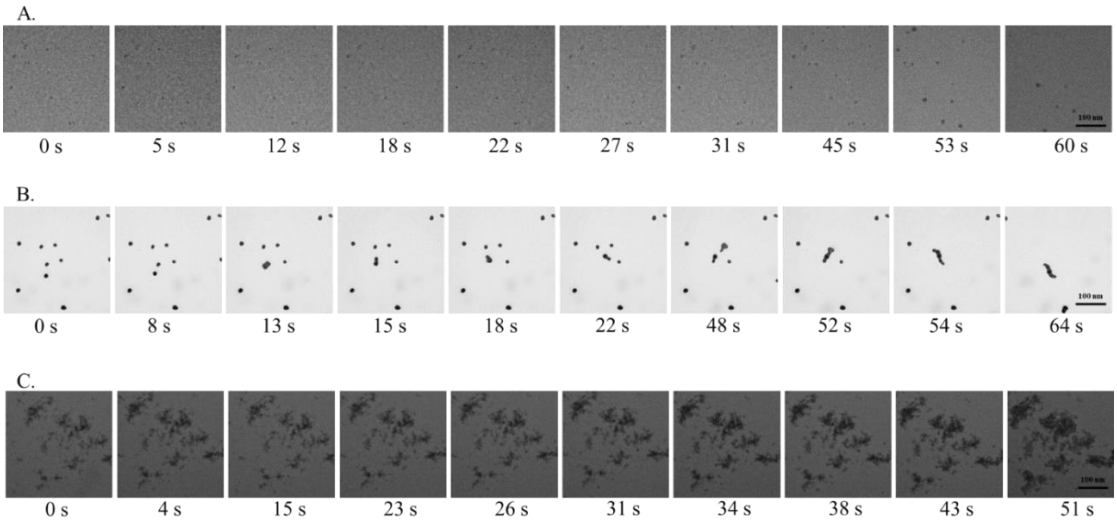

Figure 9.2 Time series images showing the interactions of AgNPs in the (A) DI water, (B) presence of protons and (c) time series images showing the interactions of AgNP aggregates in the acidic solution. AgNP concentration: 10 mg/L.

According to the Figure 9.2A, the distance between the single NPs as well as the clusters changed in an irregular manner with time, suggesting the random movement of AgNPs in the liquid. This is more apparent from the Movie S1 where it indicates that the movement of AgNPs in Figure 9.2A was non-directional. The randomly moving AgNPs jumped back and forth several times before the attachment. On the contrary, in Figure 9.2B, in the presence of acid, individual AgNPs moved directly towards the aggregates prior to the attachment (Figure 9.2B, Movie S2). In fact, the aggregation of AgNPs,

starts with the aggregation of two individual particles forming an aggregate. Subsequently the other particles attached to the previously formed aggregate to form bigger aggregates in the presence of protons (Movie S2). The initially formed aggregates rotate before aggregating with another NP or an aggregate. This further indicates the presence of directional interaction in a protonated environment. It is observed that as the distance between the AgNPs changed, only pairwise interaction can be observed. When the AgNPs interact in the presence of protons the pairwise distance (coupling proximity) changes differently depicting the change in the solution matrix affecting the interactions. A striking difference between Figure 9.2A & B is the time taken for the aggregation of AgNPs in the water and in the presence of protons. It takes longer time for aggregation between the particles in water as compared to those in protons. Furthermore, we observe that in the presence of the protons, the pairwise interaction which first promote the AgNPs to first form a few pairs is followed by a sudden jump allowing these paired AgNPs to contact each other, which result in the attachment of these pairs of AgNPs with each other. The difference in the time taken for the inter particle attachment in these two scenarios indicate that this jump to contact phenomenon that result in the particle attachment occur almost instantaneously after the electron layer around the AgNPs is affected, which is governed by the properties of the solution being either water or acid.

Variation in the solution pH changed the behavior of the AgNPs resulting in rapid attachment of smaller aggregates in forming larger aggregates. Figure 9.2C shows the growth of the aggregates of AgNPs in the presence of protons. The size of the AgNP aggregates change with the time resulting in larger aggregates as shown in Figure 9.2C. The distance between the single AgNPs and aggregates decreased with time in the presence of the protons (Figure 9.2B & C). The interaction forces between the membrane and the aggregates may directly influence the attachment of the AgNPs to the membrane in the acidic condition.

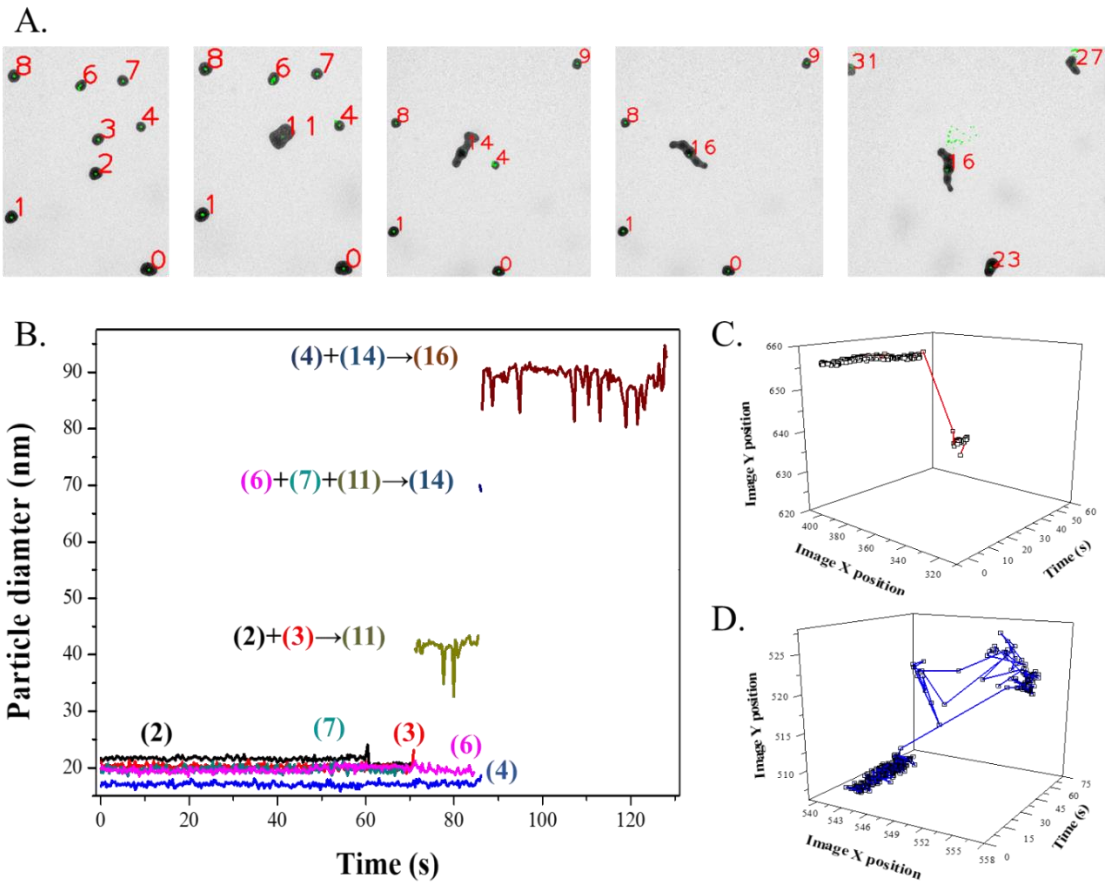

Figure 9.3 (A) Images with the tracking IDs showing movement of AgNPs in forming aggregates, (B) the change in the particle diameter of the AgNPs in (A) in the solution, (C) Mobility of the particle with the Track ID (2) in (A) and (D) Mobility of the particle with the Track ID (4) in (A). AgNP concentration: 10 mg/L.

The TEM images of the AgNPs with tracking IDs before and after the addition of HNO_3 acid are shown in Figure 9.3A. In the presence of the acid, initially the isolated NPs attracted to each other. Then the remaining particles started to attach to the aggregates formed resulting in larger aggregates with an increase in their overall diameter as shown in Figure 9.3B. AgNPs moved in random directions before the attachment, as shown in Figure 9.3C & D. According to the figures, different particles (track ID 2 & 4) mobilized in the solution in different ways finally attaching to the larger aggregates formed. According to the Figure 9.3C & D, the mobility exhibited by the particle with track ID (4) is higher than that of the particle with the track ID (2). Particle with the track ID (2), moved for a limited as an individual particle before the aggregation. However, the particle with the tracking ID (4) moved randomly for a considerable time before the aggregation as observed in Figure 9.3D.

In addition to the direct measurements obtained on the morphological features of the NPs, it is also possible to observe the movement of the NP aggregates in the solution using LCTEM. The random movements of the AgNPs and their attractive and repulsive interactions in the water can be seen in the Movie S1. Since the point of zero charge of bare Si_3N_4 is about pH 4.1, AgNPs initially adhered to the positively charged Si_3N_4 membrane[312] when they are in the DI water ($pH \approx 6.5$), via electrostatic attraction and vdW forces. After several seconds of exposure to the electron beam, some of the particles or aggregates detached from the Si_3N_4 membrane and moved in a quasi 2D plane closer to the membrane in the focal plane. With the increasingly negative electrical charges built up on the Si_3N_4 membrane due to the secondary emission of the electron beam irradiation, the negatively charged AgNPs repulsed and detached from the membrane. However, as the aggregates increase to a considerable size such as the one observed in Fig 1C, it the larger aggregates are attracted strongly towards the membrane. This can be described by the attractive forces between a membrane and the particles can be expressed as

$$F = -\frac{k_A R}{6z^2} \tag{9.1}$$

Where k_A is the Hamaker constant of water which is 1.5 x 10^{-19}, R is the radius of the AgNPs or the aggregates and z is the distance between the membrane and the aggregate. Larger aggregates (Figure 9.2C) were stationary during the time of observation. In this scenario, the electrostatic repulsive force between the Si_3N_4 membrane and AgNPs was lower than the vdW attractive force between the membrane and the particles. However, some AgNPs and smaller aggregates were observed moving continuously in a random manner (Figure 9.2C). Rotational and translational as well as translational-rotational coupled movements of these small AgNP aggregates were also observed (Movie 1 & 2).

Due to the formation of the aggregates in the acidic condition, the movements of the individual NPs and aggregates is lower compared to the movement in DI water under similar dose of irradiation. The fast movement of the NPs and aggregates in the water can be attributed to the charging of the Si_3N_4 membrane and NPs due to the electron beam induced irradiation. The electrostatic repulsion between the membrane and the charged AgNP aggregates can be the driving force for the fast movement of aggregates

in water (Figure 9.2A, Movie S1). Instead, the presence of protons can increase the conductivity of the solution and reduce the negative electrical charge built up by the membrane. Moreover, aggregates with an increased size were observed in the presence of protons, as the vdW attractive force between the AgNPs and Si_3N_4 increased (Eqn. (9.1)). This phenomenon suppressed the detachment and mobility of the AgNPs. Our findings imply that the immobility of the AgNPs in LCTEM studies could be a result of the increasing concentration of protons. Repulsion of free diffusive NPs instantly from the field of view[313] is a common artefact in the LCTEM studies. It is mitigated by adding other chemicals [309, 314], which was not used during our experiments to avoid interferences.

9.3.1 Interaction forces experienced by AgNPs in water

Electron beam irradiation can increase the electrostatic repulsive force between AgNPs and the membrane in water. The addition of protons weakens this electrostatic repulsive force and decrease the distance (z) between the AgNPs. The interactive force between the membrane and the particles/aggregates is inversely proportional to z^2 (Eqn. (9.1)). Therefore, the stronger traction from the membrane probably limits the random motion of aggregates in the acidic solution. Furthermore, the higher concentration of protons reduced the energy barrier for the aggregation of AgNPs. Each of the AgNP aggregates is enclosed in a repulsive and anisotropic charge cloud when they are in water. When the repulsive clouds of two AgNPs or aggregates overlap, they approach each other closely. According to the Movie S1 & Figure 9.2A, individual NPs moved nearer to the aggregates and approached them from different directions before the aggregation. The individual AgNPs will be further repulsed by the repulsive cloud of the aggregates, which will then try different ways to overcome the energy barrier for the interaction. The electrostatic repulsion was screened in the presence of protons (Fig 1B). The short-range interactions between the aggregates are dominated by the vdW attractions, which facilitated the final attachment process. On the other hand, the long-range attractions will take place when the distance between two AgNPs become larger than the range of the vdW forces. These long range attractions are usually observed between identically charged NPs in confined geometries[315] similar to the liquid cell used in the LCTEM study. Therefore, the long-range attractions between the NPs, can be the driving force

for two AgNPs or aggregates to move together. Yet, the mechanism of attraction of like charge particles remains unresolved. This could probably cause due to the redistribution of the ions and counter ions by the confining walls in the solution around AgNPs, mediating long-range attractions. Therefore, the long-range, like-charge attractions and the short-range vdW attractions worked together in governing the direct attachment of AgNPs and smaller aggregates to the larger aggregates in the presence of protons.

9.3.2 Interaction forces experienced by AgNPs in the presence of Protons

The observations made here show that the aggregation of individual AgNPs is increased in the presence of protons when the concentration of AgNPs is the same (Figure 9.2A vs Figure 9.2B), even though the mobility is reduced when the size of the aggregates increase (Figure 9.2B vs Figure 9.2C). This result demonstrates that the impact of presence of protons affect the aggregation state of the individual AgNPs and aggregates determining their interactions in the solution. Therefore, the surface area can be significantly limited in the compact and larger AgNP aggregates. The increase in the ionic forces not only stimulates large and complex aggregates, but also stimulates aggregation by changing the way they behave together. This finding is especially important in understanding the behavior of AgNPs in the surface and groundwater, as the pH induced aggregation and the interactions of AgNPs will govern their toxicity in the environmental matrices.

In summary our study reveals that AgNPs under the random motion in an aquatic matrix tend to aggregate due to the impact of steric repulsive and attractive vdW forces. The aggregation of AgNPs induced by the chemical composition of the solution matrix will have important implications on the kinetics of the transformations of the AgNPs when present in the aquatic environment. The formation of transient pairs before the direct contact may provide enough time for AgNPs to change their orientation and explore optimal configuration prior to complete attachment. This phenomenon may play a critical role in different processes such as the oriented attachment of crystals or site-specific binding between biological macromolecules. We believe that future studies exploiting the use of LCTEM will provide important insights on exploring the details of

interaction mechanisms among other properties of the solution matrix and the AgNPs, which will be important in the areas in environmental engineering.

10 Conclusions and Recommendations

This chapter presents the key conclusions derived during this study, followed by some recommendations which can be considered in designing future studies.

10.1 Conclusions

This thesis investigated several environmental parameters to evaluate the impact of these factors on the transformations of AgNPs and the key conclusions derived are listed below.

(1) Surfactants stabilized the AgNPs better than the polymers did and assisted in obtaining a monomodal particle size distribution. From the two surfactants used during the experiments, CTAB being a cationic surfactant showed promising characteristics as a suitable stabilizer which can preserve the synthesized AgNPs for an extended period.

(2) pH had a strong influence on the properties of the AgNPs, as it governed the surface charge of AgNPs hence aggregation and oxidative dissolution. At acidic and neutral pH, the particles were destabilized resulting in higher rate of aggregation. In the alkaline conditions, the particles were re-stabilized due to the presence of hydroxyl ions resulting in more stable suspensions. The short-term results reveal that the impact of DO on the fate of the AgNPs is negligible compared to the effect of pH, and aggregation dominate the initial transformation.

(3) The role of HA varies within the concentration range of 0-250 mg/L. Firstly, in the absence of HA irrespective of the lighting level, the oxidative dissolution and aggregation took place with the interaction of atmospheric and dissolved oxygen. Secondly, at the HA concentration of 1–20 mg/L, HA stabilized the AgNPs due to the inhibition of the release of the ionic Ag and aggregation. In the presence of sunlight, HA reduced the ionic Ag to form secondary AgNPs, hence resulted in a redistribution of the PSD of the solution under the sunlight. Thirdly, at higher concentrations of HA from 20 to 250 mg/L, AgNPs were wrapped by the HA molecules suppressing the dissolution.

(4) EPS effectively stabilize the AgNPs in the presence of $NaNO_3$ and low concentration of $Ca(NO_3)_2$. However, it enhanced the rate of aggregation at higher $Ca(NO_3)_2$ concentration, as a result of the aggregation of the dissolved EPS with AgNPs through inter molecular bridging, connecting the AgNPs and forming aggregates. Among the three types of EPS, LB-EPS showed promising effects in improving the stabilization of AgNPs, mainly due to the less hydrophilic constituents present therein.

(5) SA and BSA followed a mechanism of stabilizing the AgNPs in the matrix via chemically coating the AgNPs. The transformations observed under these types of organic matter can be affected by the other environmental factors as well.
(6) Finally, the suitability of using a novel technique, liquid cell transmission electron microscopy (LCTEM) to track the time resolved changes in the transformations of AgNPs was explored and it showed promising results that can be exploited in the future research.

10.2 Recommendations

Due to the abundant usage of AgNPs in the consumer products their presence in water bodies will be inevitable and probably increase in the future. Therefore, understanding the cumulative impact of different factors on the transformations of AgNPs and their long-term persistence in the aquatic matrices will be important. Furthermore, the transformations of AgNPs in the complex environments such as wastewater treatment systems also need to be considered. The mechanisms leading to the transformations of AgNPs will vary due to the multiple factors present in the wastewater which can determine their fate. On the other hand, the impact of the transformed AgNPs on the biomass and the microbial communities also need to be considered in order to predict possible remedial actions in removing the AgNPs.

When present in anaerobic conditions the transformations of AgNPs will vary due to the absence of oxygen with little or almost no oxidative dissolution. Since the antibacterial activity of AgNPs depends on its ability to produce ionic Ag, the toxicity of AgNPs in the anaerobic conditions may be reduced. Furthermore, if there are microorganisms present in those conditions, they can produce secondary AgNPs via reducing the ionic Ag, which depend on their capacity to transfer electrons. This phenomenon may differently affect the transformations of AgNPs in these conditions and understanding them will be important in predicting the behavior of AgNPs in the anaerobic digestion.

When the anaerobic digestion is considered, AgNPs will coexist with the microorganisms in those conditions, which will also secrete EPS and the characteristics of EPS in these conditions will vary from that of the aerobic conditions. Therefore, understanding the differential impacts of EPS secreted under such conditions will also be important in exploring the fate of AgNPs. In summary, understanding the water

chemistry conditions present in the real scenarios will provide insights to predict the aging process of AgNPs and eventually its transport and fate in the environment.

References

[1] S. J. Klaine *et al.*, "Nanomaterials in the environment: behavior, fate, bioavailability, and effects nanotechnology," *Environmental toxicology and chemistry*, Article no. 9, 2008.

[2] G. Liu, D. Wang, J. Wang, and C. Mendoza, "Effect of ZnO particles on activated sludge: Role of particle dissolution," *Science of the Total Environment*, Article vol. 409, pp. 2852-2857, 1/1/2011 2011.

[3] A. García *et al.*, "Effect of cerium dioxide, titanium dioxide, silver, and gold nanoparticles on the activity of microbial communities intended in wastewater treatment," *Journal of hazardous materials*, Article 2012.

[4] S. K. Brar, M. Verma, R. D. Tyagi, and R. Y. Surampalli, "Engineered nanoparticles in wastewater and wastewater sludge - Evidence and impacts," *Waste Management*, vol. 30, no. 3, pp. 504-520, 2010.

[5] B. Le Ouay and F. Stellacci, "ScienceDirect Antibacterial activity of silver nanoparticles: A surface science insight," *Nano Today*, vol. 10, pp. 339-354, 2015.

[6] A. P. Gondikas, A. Morris, B. C. Reinsch, S. M. Marinakos, G. V. Lowry, and H.-K. Heileen, "Cysteine-Induced Modifications of Zero-valent Silver Nanomaterials: Implications for Particle Surface Chemistry, Aggregation, Dissolution, and Silver Speciation," *Environmental Science & Technology*, Article vol. 46, no. 13, pp. 7037-7045, 2012.

[7] A. M. E. Badawy, T. P. Luxton, R. G. Silva, K. G. Scheckel, M. T. Suidan, and T. M. Tolaymat, "Impact of Environmental Conditions (pH, Ionic Strength, and Electrolyte Type) on the Surface Charge and Aggregation of Silver Nanoparticles Suspensions," *Environmental Science & Technology*, vol. 44, no. 4, pp. 1260-1266, 2010/02/15 2010.

[8] A. M. El Badawy, R. G. Silva, B. Morris, K. G. Scheckel, M. T. Suidan, and T. M. Tolaymat, "Surface charge-dependent toxicity of silver nanoparticles," *Environmental Science & Technology*, vol. 45, no. 1, pp. 283-287, 2011.

[9] R. A. Bell, N. Ogden, and J. R. Kramer, "The biotic ligand model and a cellular approach to class B metal aquatic toxicity," *Comparative Biochemistry and Physiology Part C: Toxicology & Pharmacology*, vol. 133, no. 1–2, pp. 175-188, 9// 2002.

[10] D. J. H., ""Heavy metals" a meaningless term? (IUPAC Technical Report)," in *Pure and Applied Chemistry* vol. 74, ed: pac.

[11] K.-H. Cho, J.-E. Park, T. Osaka, and S.-G. Park, "The study of antimicrobial activity and preservative effects of nanosilver ingredient," *Electrochimica Acta*, vol. 51, no. 5, pp. 956-960, 11/10/ 2005.

[12] T. Maneerung, S. Tokura, and R. Rujiravanit, "Impregnation of silver nanoparticles into bacterial cellulose for antimicrobial wound dressing," *Carbohydrate Polymers*, vol. 72, no. 1, pp. 43-51, 4/3/ 2008.

[13] O. Choi, K. K. Deng, N. J. Kim, L. Ross, R. Y. Surampalli, and Z. Hu, "The inhibitory effects of silver nanoparticles, silver ions, and silver chloride colloids on microbial growth," *Water Research*, vol. 42, no. 12, pp. 3066-3074, 2008.

[14] Y. Yang, Q. Chen, J. D. Wall, and Z. Hu, "Potential nanosilver impact on anaerobic digestion at moderate silver concentrations," *Water research*, vol. 46, no. 4, pp. 1176-1184, 2012.

[15] A. D. Tappin, J. L. Barriada, C. B. Braungardt, E. H. Evans, M. D. Patey, and E. P. Achterberg, "Dissolved silver in European estuarine and coastal waters," *Water Research,* vol. 44, no. 14, pp. 4204-4216, 7// 2010.
[16] B. S. Atiyeh, M. Costagliola, S. N. Hayek, and S. A. Dibo, "Effect of silver on burn wound infection control and healing: Review of the literature," *Burns,* vol. 33, no. 2, pp. 139-148, 3// 2007.
[17] F. Zhang *et al.*, "Degradable polyphosphoester-based silver-loaded nanoparticles as therapeutics for bacterial lung infections," *Nanoscale,* 10.1039/C4NR07103D vol. 7, no. 6, pp. 2265-2270, 2015.
[18] D. E. Marx and D. J. Barillo, "Silver in medicine: The basic science," *Burns,* vol. 40, pp. S9-S18.
[19] A. Melaiye and W. J. Youngs, "Silver and its application as an antimicrobial agent," *Expert Opinion on Therapeutic Patents,* vol. 15, no. 2, pp. 125-130, 2005/02/01 2005.
[20] S. Silver, L. T. Phung, and G. Silver, "Silver as biocides in burn and wound dressings and bacterial resistance to silver compounds," *Journal of Industrial Microbiology and Biotechnology,* vol. 33, no. 7, pp. 627-634, 2006// 2006.
[21] M. Ganguly, J. Pal, C. Mondal, A. Pal, and T. Pal, "Imine (-CH[double bond, length as m-dash]N-) brings selectivity for silver enhanced fluorescence," *Dalton Transactions,* 10.1039/C4DT04022H vol. 44, no. 9, pp. 4370-4379, 2015.
[22] S. Das, R. Raj, N. Mangwani, H. R. Dash, and J. Chakraborty, "2 Heavy Metals and Hydrocarbons: Adverse Effects and Mechanism of Toxicity," *Microbial Biodegradation and Bioremediation,* p. 23, 2014.
[23] T. J. Baker, C. R. Tyler, and T. S. Galloway, "Impacts of metal and metal oxide nanoparticles on marine organisms," *Environmental Pollution,* vol. 186, pp. 257-271, 2014.
[24] U. S. EPA. (2013). *Secondary Drinking Water Regulations: Guidance for NuisanceChemicals*.Available: http://water.epa.gov/drink/contaminants/secondarystandards.cfm#tabletop.
[25] R. J. Watts, "Hazardous wastes: sources, pathways, receptors," 1998.
[26] P. L. Drake and K. J. Hazelwood, "Exposure-related health effects of silver and silver compounds: a review," *Annals of Occupational Hygiene,* vol. 49, no. 7, pp. 575-585, 2005.
[27] J. L. Axson *et al.*, "Rapid Kinetics of Size and pH-Dependent Dissolution and Aggregation of Silver Nanoparticles in Simulated Gastric Fluid," *Journal of Physical Chemistry C,* 2015.
[28] M. Kooti, S. Gharineh, M. Mehrkhah, A. Shaker, and H. Motamedi, "Preparation and antibacterial activity of CoFe2O4/SiO2/Ag composite impregnated with streptomycin," *Chemical Engineering Journal,* vol. 259, pp. 34-42, 1/1/ 2015.
[29] Z.-m. Xiu, Q.-b. Zhang, H. L. Puppala, V. L. Colvin, and P. J. J. Alvarez, "Negligible Particle-SpecificAntibacterial Activityof Silver Nanoparticles," *Nano Letters,* Article vol. 12, no. 8, pp. 4271-4275, 2012.
[30] G. Research. (May,2015). *Silver Nanoparticles Market By Application (Electronics & Electrical, Healthcare, Food & Beverages, Textiles) And Segment Forecasts To 2022*. Available: http://www.grandviewresearch.com/industry-analysis/silver-nanoparticles-market

[31] A. Ivask *et al.*, "Size-dependent toxicity of silver nanoparticles to bacteria, yeast, algae, crustaceans and mammalian cells in vitro," *PloS one,* vol. 9, no. 7, p. e102108, 2014.
[32] Y. J. Lee *et al.*, "Ion ‐ release kinetics and ecotoxicity effects of silver nanoparticles," *Environmental toxicology and chemistry,* vol. 31, no. 1, pp. 155-159, 2012.
[33] J. K. Schluesener and H. J. Schluesener, "Nanosilver: application and novel aspects of toxicology," *Archives of toxicology,* vol. 87, no. 4, pp. 569-576, 2013.
[34] T. Benn, B. Cavanagh, K. Hristovski, J. D. Posner, and P. Westerhoff, "The release of nanosilver from consumer products used in the home," *Journal of environmental quality,* vol. 39, no. 6, pp. 1875-1882, 2010.
[35] D. E. Gorka *et al.*, "Reducing Environmental Toxicity of Silver Nanoparticles through Shape Control," 2015.
[36] T. M. Tolaymat, A. M. El Badawy, A. Genaidy, K. G. Scheckel, T. P. Luxton, and M. Suidan, "An evidence-based environmental perspective of manufactured silver nanoparticle in syntheses and applications: a systematic review and critical appraisal of peer-reviewed scientific papers," *Science of the Total Environment,* vol. 408, no. 5, pp. 999-1006, 2010.
[37] G. Wen, Y. Luo, A. Liang, and Z. Jiang, "Autocatalytic oxidization of nanosilver and its application to spectral analysis," *Scientific reports,* vol. 4, p. 3990, 2014.
[38] S. Saravanan, S. Nethala, S. Pattnaik, A. Tripathi, A. Moorthi, and N. Selvamurugan, "Preparation, characterization and antimicrobial activity of a bio-composite scaffold containing chitosan/nano-hydroxyapatite/nano-silver for bone tissue engineering," *International journal of biological macromolecules,* vol. 49, no. 2, pp. 188-193, 2011.
[39] S. Wageh, L. He, A. A. Al-Ghamdi, Y. Al-Turki, and S. Tjong, "Nano silver-anchored reduced graphene oxide sheets for enhanced dielectric performance of polymer nanocomposites," *RSC Advances,* vol. 4, no. 54, pp. 28426-28431, 2014.
[40] Y. Lee and S.-G. Oh, "Counter-ion effects of silver salt on the production yield of silver nanoparticles in alcohol reduction process," *Colloids and Surfaces A: Physicochemical and Engineering Aspects,* vol. 459, pp. 172-176, 2014.
[41] S. Prabhu and E. K. Poulose, "Silver nanoparticles: mechanism of antimicrobial action, synthesis, medical applications, and toxicity effects," *International Nano Letters,* vol. 2, no. 1, pp. 1-10, 2012.
[42] Y. Sun and Y. Xia, "Shape-controlled synthesis of gold and silver nanoparticles," *Science,* vol. 298, no. 5601, pp. 2176-2179, 2002.
[43] Y. Zhu, K. Morisato, W. Li, K. Kanamori, and K. Nakanishi, "Synthesis of silver nanoparticles confined in hierarchically porous monolithic silica: a new function in aromatic hydrocarbon separations," *ACS applied materials & interfaces,* vol. 5, no. 6, pp. 2118-2125, 2013.
[44] P. L. Freire *et al.*, "Action of silver nanoparticles towards biological systems: cytotoxicity evaluation using hen's egg test and inhibition of Streptococcus mutans biofilm formation," *International journal of antimicrobial agents,* vol. 45, no. 2, pp. 183-187, 2015.
[45] K. A. Huynh and K. L. Chen, "Aggregation kinetics of citrate and polyvinylpyrrolidone coated silver nanoparticles in monovalent and divalent electrolyte solutions," *Environmental science & technology,* vol. 45, no. 13, pp. 5564-5571, 2011.

[46] J. E. Skebo, C. M. Grabinski, A. M. Schrand, J. J. Schlager, and S. M. Hussain, "Assessment of metal nanoparticle agglomeration, uptake, and interaction using high-illuminating system," *International journal of toxicology,* vol. 26, no. 2, pp. 135-141, 2007.
[47] L. Rizzello and P. P. Pompa, "Nanosilver-based antibacterial drugs and devices: mechanisms, methodological drawbacks, and guidelines," *Chemical Society Reviews,* vol. 43, no. 5, pp. 1501-1518, 2014.
[48] M.-N. Croteau, A. D. Dybowska, S. N. Luoma, S. K. Misra, and E. Valsami-Jones, "Isotopically modified silver nanoparticles to assess nanosilver bioavailability and toxicity at environmentally relevant exposures," *Environmental Chemistry,* vol. 11, no. 3, pp. 247-256, 2014.
[49] Y. Zhang *et al.*, "Synthesis of silver nanoparticles via electrochemical reduction on compact zeolite film modified electrodes," *Chemical Communications,* no. 23, pp. 2814-2815, 2002.
[50] K. Bogle, S. Dhole, and V. Bhoraskar, "Silver nanoparticles: synthesis and size control by electron irradiation," *Nanotechnology,* vol. 17, no. 13, p. 3204, 2006.
[51] A. R. Shahverdi, S. Minaeian, H. R. Shahverdi, H. Jamalifar, and A.-A. Nohi, "Rapid synthesis of silver nanoparticles using culture supernatants of Enterobacteria: a novel biological approach," *Process Biochemistry,* vol. 42, no. 5, pp. 919-923, 2007.
[52] H. J. Lee, S. Y. Yeo, and S. H. Jeong, "Antibacterial effect of nanosized silver colloidal solution on textile fabrics," *Journal of Materials Science,* vol. 38, no. 10, pp. 2199-2204, 2003/05/01 2003.
[53] S. Siddhartha, B. Tanmay, R. Arnab, S. Gajendra, P. Ramachandrarao, and D. Debabrata, "Characterization of enhanced antibacterial effects of novel silver nanoparticles," *Nanotechnology,* vol. 18, no. 22, p. 225103, 2007.
[54] R. Kaegi *et al.*, "Fate and transformation of silver nanoparticles in urban wastewater systems," *Water Research,* vol. 47, no. 12, pp. 3866-3877, 2013.
[55] R. Kaegi, A. Voegelin, B. Sinnet, H. Hagendorfer, and M. Burkhardt. (2011) Behavior of Metallic Silver Nanoparticles in a Pilot Wastewater Treatment Plant. 3902-3908.
[56] S. Kittler, C. Greulich, J. Diendorf, M. Koller, and M. Epple, "Toxicity of silver nanoparticles increases during storage because of slow dissolution under release of silver ions," *Chemistry of Materials,* vol. 22, no. 16, pp. 4548-4554, 2010.
[57] J. Liu and R. H. Hurt, "Ion release kinetics and particle persistence in aqueous nano-silver colloids," *Environmental science & technology,* vol. 44, no. 6, pp. 2169-2175, 2010.
[58] E. V. Formo, C. B. Potterf, M. Yang, R. Unocic, D. N. Leonard, and M. Pawel, "How a Nanostructure ' s Shape Affects its Lifetime in the Environment : Comparing a Silver Nanocube to a Nanoparticle when Dispersed in Aqueous Media How a Nanostructure ' s Shape Affects its Lifetime in the Environment : Comparing a Silver Nanocube to a Nanoparticle when Dispersed in Aqueous Media," 2016.
[59] W. Zhang, Y. Yao, N. Sullivan, and Y. Chen, "Modeling the primary size effects of citrate-coated silver nanoparticles on their ion release kinetics," *Environmental science & technology,* vol. 45, no. 10, pp. 4422-4428, 2011.
[60] A. Despic and J. M. Bockris, "Kinetics of the Deposition and Dissolution of Silver," *The Journal of Chemical Physics,* vol. 32, no. 2, pp. 389-402, 1960.

[61] X. Yang *et al.*, "Mechanism of silver nanoparticle toxicity is dependent on dissolved silver and surface coating in Caenorhabditis elegans," *Environmental science & technology*, vol. 46, no. 2, pp. 1119-1127, 2011.
[62] S. Chen, T. Akai, K. Kadono, and T. Yazawa, "Reversible control of silver nanoparticle generation and dissolution in soda-lime silicate glass through x-ray irradiation and heat treatment," *Applied Physics Letters*, vol. 79, no. 22, pp. 3687-3689, 2001.
[63] S. o. things. (16.09.2016). *Ksp solubility constant for common salts*. Available: http://www.solubilityofthings.com/water/ions_solubility/ksp_chart.php
[64] D. D. Wagman, W. H. Evans, V. B. Parker, R. H. Schumm, and I. Halow, "The NBS tables of chemical thermodynamic properties. Selected values for inorganic and C1 and C2 organic substances in SI units," DTIC Document1982.
[65] J. Cox, D. D. Wagman, and V. A. Medvedev, *CODATA key values for thermodynamics*. Chem/Mats-Sci/E, 1989.
[66] T. M. Benn, P. Westerhoff, and P. Herckes, "Detection of fullerenes (C60 and C70) in commercial cosmetics," *Environmental Pollution*, vol. 159, no. 5, pp. 1334-1342, 5// 2011.
[67] R. Kaegi, A. Voegelin, B. Sinnet, S. Zuleeg, H. Siegrist, and M. Burkhardt, "Transformation of AgCl nanoparticles in a sewer system - A field study," *Science of the Total Environment*, vol. 535, pp. 20-27, 2014.
[68] E. Lombi *et al.*, "Transformation of four silver/silver chloride nanoparticles during anaerobic treatment of wastewater and post-processing of sewage sludge," *Environmental pollution*, vol. 176, pp. 193-197, 2013.
[69] J. Fabrega, S. N. Luoma, C. R. Tyler, T. S. Galloway, and J. R. Lead, "Silver nanoparticles: behaviour and effects in the aquatic environment," *Environment international*, vol. 37, no. 2, pp. 517-531, 2011.
[70] G. Maiorano *et al.*, "Effects of cell culture media on the dynamic formation of protein− nanoparticle complexes and influence on the cellular response," *ACS nano*, vol. 4, no. 12, pp. 7481-7491, 2010.
[71] J. Dai and M. L. Bruening, "Catalytic nanoparticles formed by reduction of metal ions in multilayered polyelectrolyte films," *Nano Letters*, vol. 2, no. 5, pp. 497-501, 2002.
[72] N. R. Panyala, E. M. Peña-Méndez, and J. Havel, "Silver or silver nanoparticles: a hazardous threat to the environment and human health," *J Appl Biomed*, vol. 6, no. 3, pp. 117-129, 2008.
[73] A. Kascatan-Nebioglu, M. J. Panzner, C. A. Tessier, C. L. Cannon, and W. J. Youngs, "N-Heterocyclic carbene–silver complexes: A new class of antibiotics," *Coordination Chemistry Reviews*, vol. 251, no. 5, pp. 884-895, 2007.
[74] L. Balogh, D. R. Swanson, D. A. Tomalia, G. L. Hagnauer, and A. T. McManus, "Dendrimer-silver complexes and nanocomposites as antimicrobial agents," *Nano Letters*, vol. 1, no. 1, pp. 18-21, 2001.
[75] C. A. Citadelle, E. Le Nouy, F. Bisaro, A. M. Slawin, and C. S. Cazin, "Simple and versatile synthesis of copper and silver N-heterocyclic carbene complexes in water or organic solvents," *Dalton Transactions*, vol. 39, no. 19, pp. 4489-4491, 2010.
[76] E. M. Hotze, T. Phenrat, G. V. Lowry, and C. Mellon, "Nanoparticle Aggregation : Challenges to Understanding Transport and Reactivity in the Environment," pp. 1909-1924, 2010.
[77] L. V. Stebounova, E. Guio, and V. H. Grassian, "Silver nanoparticles in simulated biological media: a study of aggregation, sedimentation, and

dissolution," *Journal of Nanoparticle Research,* vol. 13, no. 1, pp. 233-244, 2011.

[78] J. A. Brant, J. Labille, C. O. Robichaud, and M. Wiesner, "Fullerol cluster formation in aqueous solutions: Implications for environmental release," *Journal of Colloid And Interface Science,* Article vol. 314, pp. 281-288, 1/1/2007 2007.

[79] E. M. V. Hoek and G. K. Agarwal, "Extended DLVO interactions between spherical particles and rough surfaces," *Journal of Colloid and Interface Science,* vol. 298, no. 1, pp. 50-58, 6/1/ 2006.

[80] E. M. Hotze, T. Phenrat, and G. V. Lowry, "Nanoparticle Aggregation: Challenges to Understanding Transport and Reactivity in the Environment," (in English), *Journal of Environmental Quality,* vol. 39, no. 6, pp. 1909-1924, 2010.

[81] J. Buffle and G. G. Leppard, "Characterization of aquatic colloids and macromolecules. 1. Structure and behavior of colloidal," *Environmental Science & Technology,* Article vol. 29, no. 9, p. 2169, 1995.

[82] E. Barbot, P. Dussouillez, J. Y. Bottero, and P. Moulin, "Coagulation of bentonite suspension by polyelectrolytes or ferric chloride: Floc breakage and reformation," *Chemical Engineering Journal,* Article vol. 156, pp. 83-91, 1/1/2010 2010.

[83] B. Derjaguin and L. Landau, "Theory of the stability of strongly charged lyophobic sols and of the adhesion of strongly charged particles in solutions of electrolytes," *Progress in Surface Science,* Article vol. 43, pp. 30-59, 1/1/1993 1993.

[84] J. J. M. Werner Stumm, *Aquatic Chemistry: Chemical Equilibria and Rates in Natural Waters, 3rd Edition*. 1996, p. 1040.

[85] S. M. Gatica, M. W. Cole, and D. Velegol, "Designing van der Waals Forces between Nanocolloids," *Nano Letters,* vol. 5, no. 1, pp. 169-173, 2005/01/01 2005.

[86] P. Graf *et al.*, "Peptide-coated silver nanoparticles: synthesis, surface chemistry, and pH-triggered, reversible assembly into particle assemblies," (in eng), no. 1521-3765 (Electronic), 20090601 DCOM- 20090701 2009.

[87] T. Phenrat, N. Saleh, K. Sirk, R. D. Tilton, and G. V. Lowry, "Aggregation and Sedimentation of Aqueous Nanoscale Zerovalent Iron Dispersions," *Environmental Science & Technology,* vol. 41, no. 1, pp. 284-290, 2007/01/01 2007.

[88] W. Wu, R. F. Giese, and C. J. van Oss, "Stability versus flocculation of particle suspensions in water—correlation with the extended DLVO approach for aqueous systems, compared with classical DLVO theory," *Colloids and Surfaces B: Biointerfaces,* vol. 14, no. 1–4, pp. 47-55, 8// 1999.

[89] G. Fritz, V. Schädler, N. Willenbacher, and N. J. Wagner, "Electrosteric Stabilization of Colloidal Dispersions," *Langmuir,* vol. 18, no. 16, pp. 6381-6390, 2002/08/01 2002.

[90] J. L. Ortega-Vinuesa, A. Martín-Rodríguez, and R. Hidalgo-Álvarez, "Colloidal Stability of Polymer Colloids with Different Interfacial Properties: Mechanisms," *Journal of Colloid and Interface Science,* vol. 184, no. 1, pp. 259-267, 1996/12/01 1996.

[91] T. Phenrat, N. Saleh, K. Sirk, H.-J. Kim, R. D. Tilton, and G. V. Lowry, "Stabilization of aqueous nanoscale zerovalent iron dispersions by anionic polyelectrolytes: adsorbed anionic polyelectrolyte layer properties and their

effect on aggregation and sedimentation," *Journal of Nanoparticle Research,* vol. 10, no. 5, pp. 795-814, 2008// 2008.
[92] M. S. Romero-Cano, A. Martín-Rodríguez, and F. J. de las Nieves, "Electrosteric Stabilization of Polymer Colloids with Different Functionality," *Langmuir,* vol. 17, no. 11, pp. 3505-3511, 2001/05/01 2001.
[93] K. L. Chen and M. Elimelech, "Influence of humic acid on the aggregation kinetics of fullerene (C60) nanoparticles in monovalent and divalent electrolyte solutions," *Journal of Colloid and Interface Science,* vol. 309, no. 1, pp. 126-134, 5/1/ 2007.
[94] R. F. Domingos, N. Tufenkji, and K. J. Wilkinson, "Aggregation of Titanium Dioxide Nanoparticles: Role of a Fulvic Acid," *Environmental Science & Technology,* vol. 43, no. 5, pp. 1282-1286, 2009/03/01 2009.
[95] M. F. Hochella *et al.*, "Nanominerals, Mineral Nanoparticles, and Earth Systems," *Science,* 10.1126/science.1141134 vol. 319, no. 5870, p. 1631, 2008.
[96] F. He, D. Zhao, J. Liu, and C. B. Roberts, "Stabilization of Fe−Pd Nanoparticles with Sodium Carboxymethyl Cellulose for Enhanced Transport and Dechlorination of Trichloroethylene in Soil and Groundwater," *Industrial & Engineering Chemistry Research,* vol. 46, no. 1, pp. 29-34, 2007/01/01 2007.
[97] H. W. D. Fennell Evans, *The Colloidal Domain: Where Physics, Chemistry, Biology, and Technology Meet, 2nd Edition*. 1999.
[98] S. Y. Moon, T. Kusunose, and T. Sekino, "CTAB-Assisted Synthesis of Size- and Shape-Controlled Gold Nanoparticles in SDS Aqueous Solution," *Materials Letters,* vol. 63, no. 23, pp. 2038-2040, 9/30/ 2009.
[99] S. Bhattacharjee and M. Elimelech, "Surface Element Integration: A Novel Technique for Evaluation of DLVO Interaction between a Particle and a Flat Plate," *Journal of Colloid and Interface Science,* vol. 193, no. 2, pp. 273-285, 1997/09/15 1997.
[100] S. W. Montgomery, M. A. F. A. U. G. Franchek, and V. W. Goldschmidt, "Analytical Dispersion Force Calculations for Nontraditional Geometries," (in Eng), no. 1095-7103 (Electronic), 20000629 2000.
[101] J. T. K. Milton J. Rosen, *Surfactants and Interfacial Phenomena, 4th Edition*. 2012, p. 616.
[102] T. C. Prathna, N. Chandrasekaran, and A. Mukherjee, "Studies on aggregation behaviour of silver nanoparticles in aqueous matrices: Effect of surface functionalization and matrix composition," *Colloids and surfaces,* Article no. 1-3, 2011.
[103] C. Levard, E. M. Hotze, G. V. Lowry, and G. E. Brown Jr, "Environmental transformations of silver nanoparticles: impact on stability and toxicity," *Environmental Science & Technology,* vol. 46, no. 13, pp. 6900-6914, 2012.
[104] S. Elzey and V. H. Grassian, "Agglomeration, isolation and dissolution of commercially manufactured silver nanoparticles in aqueous environments," *Journal of Nanoparticle Research,* 2010.
[105] J. T. Tai *et al.*, "Protein Silver Nanoparticle Interactions to Colloidal Stability in Acidic Environments," *LANGMUIR,* vol. 30, no. 43, pp. 12755-12764, 2014.
[106] T. S. Peretyazhko, Q. B. Zhang, and V. L. Colvin, "Size-Controlled Dissolution of Silver Nanoparticles at Neutral and Acidic pH Conditions: Kinetics and Size Changes," *Environmental Science & Technology,* vol. 48, no. 20, pp. 11954-11961, 2014.

[107] M. Iggland and M. Mazzotti, "Population balance modeling with size-dependent solubility: Ostwald ripening," *Crystal Growth & Design,* vol. 12, no. 3, pp. 1489-1500, 2012.
[108] J. Fabrega, S. R. Fawcett, J. C. Renshaw, and J. R. Lead, "Silver nanoparticle impact on bacterial growth: effect of pH, concentration, and organic matter," *Environmental science & technology,* vol. 43, no. 19, pp. 7285-7290, 2009.
[109] B. Reidy, A. Haase, A. Luch, K. A. Dawson, and I. Lynch, "Mechanisms of silver nanoparticle release, transformation and toxicity: A critical review of current knowledge and recommendations for future studies and applications," *Materials,* vol. 6, no. 6, pp. 2295-2350, 2013.
[110] R. Saini, A. Srivastava, P. Gupta, and K. Das, "pH dependent reversible aggregation of Chitosan and glycol-Chitosan stabilized silver nanoparticles," *Chemical Physics Letters,* vol. 511, no. 4, pp. 326-330, 2011.
[111] M. Singh, I. Sinha, and R. Mandal, "Role of pH in the green synthesis of silver nanoparticles," *Materials Letters,* vol. 63, no. 3, pp. 425-427, 2009.
[112] G. Wang, Y. Zhang, Y. Cui, M. Duan, and M. Liu, "Study on the non-linear refraction of silver nanoparticles with aggregation effect," *Optics communications,* vol. 249, no. 1, pp. 311-317, 2005.
[113] X. Jiang and A. Yu, "Silver nanoplates: a highly sensitive material toward inorganic anions," *Langmuir,* vol. 24, no. 8, pp. 4300-4309, 2008.
[114] L. Li and Y.-J. Zhu, "High chemical reactivity of silver nanoparticles toward hydrochloric acid," *Journal of colloid and interface science,* vol. 303, no. 2, pp. 415-418, 2006.
[115] X. Li, J. J. Lenhart, and H. W. Walker, "Aggregation Kinetics and Dissolution of Coated Silver Nanoparticles," 2011.
[116] B. Derjaguin and L. Landau, "Theory of the stability of strongly charged lyophobic sols and of the adhesion of strongly charged particles in solutions of electrolytes," *Acta physicochim. URSS,* vol. 14, no. 6, pp. 633-662, 1941.
[117] E. Werway and J. T. G. Overbeek, "Theory of Stability of Lyophobic ColloidsElsevier," *Amsterdam-New York,* p. 34, 1948.
[118] S. Botasini and E. Méndez, "Silver nanoparticle aggregation not triggered by an ionic strength mechanism," *Journal of Nanoparticle Research,* vol. 15, no. 4, pp. 1-7, 2013// 2013.
[119] A. M. El Badawy, K. G. Scheckel, M. Suidan, and T. Tolaymat, "The impact of stabilization mechanism on the aggregation kinetics of silver nanoparticles," *Science of the total environment,* vol. 429, pp. 325-331, 2012.
[120] J. Gao *et al.*, "Influence of Suwannee River humic acid on particle properties and toxicity of silver nanoparticles," *Chemosphere,* vol. 89, no. 1, pp. 96-101, 2012.
[121] N. Akaighe *et al.*, "Humic acid-induced silver nanoparticle formation under environmentally relevant conditions," *Environmental science & technology,* vol. 45, no. 9, pp. 3895-3901, 2011.
[122] M. Baalousha, Y. Nur, I. Römer, M. Tejamaya, and J. Lead, "Effect of monovalent and divalent cations, anions and fulvic acid on aggregation of citrate-coated silver nanoparticles," *Science of the Total Environment,* vol. 454, pp. 119-131, 2013.
[123] L. Kaplan and J. Newbold, "The role of monomers in stream ecosystem metabolism," *Aquatic ecosystems: interactivity of dissolved organic matter. Academic Press, New York,* pp. 97-119, 2003.

[124] S.-j. Yu, Y.-g. Yin, J.-b. Chao, M.-h. Shen, and J.-f. Liu, "Highly dynamic PVP-coated silver nanoparticles in aquatic environments: chemical and morphology change induced by oxidation of Ag0 and reduction of Ag+," *Environmental Science & Technology,* vol. 48, no. 1, pp. 403-411, 2013.
[125] B. M. Angel, G. E. Batley, C. V. Jarolimek, and N. J. Rogers, "The impact of size on the fate and toxicity of nanoparticulate silver in aquatic systems," *Chemosphere,* vol. 93, no. 2, pp. 359-365, 2013.
[126] L. R. Pokhrel, B. Dubey, and P. R. Scheuerman, "Impacts of select organic ligands on the colloidal stability, dissolution dynamics, and toxicity of silver nanoparticles," *Environmental Science and Technology,* 2013.
[127] I. L. Gunsolus, M. P. S. Mousavi, K. Hussein, P. Bühlmann, and C. L. Haynes, "Effects of Humic and Fulvic Acids on Silver Nanoparticle Stability, Dissolution, and Toxicity," *Environmental Science & Technology,* vol. 49, no. 13, pp. 8078-8086, 2015.
[128] S. M. Wirth, G. V. Lowry, and R. D. Tilton, "Natural organic matter alters biofilm tolerance to silver nanoparticles and dissolved silver," *Environmental science & technology,* vol. 46, no. 22, pp. 12687-12696, 2012.
[129] P. Borm *et al.*, "Research strategies for safety evaluation of nanomaterials, part V: role of dissolution in biological fate and effects of nanoscale particles," *Toxicological Sciences,* vol. 90, no. 1, pp. 23-32, 2006.
[130] J. Liu, D. A. Sonshine, S. Shervani, and R. H. Hurt, "Controlled release of biologically active silver from nanosilver surfaces," *ACS nano,* vol. 4, no. 11, pp. 6903-6913, 2010.
[131] R. Ma *et al.*, "Size-controlled dissolution of organic-coated silver nanoparticles," *Environmental science & technology,* vol. 46, no. 2, pp. 752-759, 2011.
[132] G. A. Sotiriou and S. E. Pratsinis, "Antibacterial activity of nanosilver ions and particles," *Environmental science & technology,* vol. 44, no. 14, pp. 5649-5654, 2010.
[133] S. Deb and M. Shukla, "A review of dissolved organic matter transport processes affecting soil and environmental quality," *J Environment Analytic Toxicol,* vol. 1, no. 2, p. 106, 2011.
[134] C. J. Milne, D. J. Lapworth, D. C. Gooddy, C. N. Elgy, and É. Valsami-Jones, "Role of Humic Acid in the Stability of Ag Nanoparticles in Suboxic Conditions," *Environmental Science & Technology,* vol. 51, no. 11, pp. 6063-6070, 2017/06/06 2017.
[135] Y. Yin, J. Liu, and G. Jiang, "Sunlight-Induced Reduction of Ionic Ag and Au to Metallic Nanoparticles by Dissolved Organic Matter," *ACS Nano,* vol. 6, no. 9, pp. 7910-7919, 2012/09/25 2012.
[136] W.-C. Hou, B. Stuart, R. Howes, and R. G. Zepp, "Sunlight-Driven Reduction of Silver Ions by Natural Organic Matter: Formation and Transformation of Silver Nanoparticles," *Environmental Science & Technology,* vol. 47, no. 14, pp. 7713-7721, 2013/07/16 2013.
[137] S.-j. Yu, Y.-g. Yin, J.-b. Chao, M.-h. Shen, and J.-f. Liu, "Highly Dynamic PVP-Coated Silver Nanoparticles in Aquatic Environments: Chemical and Morphology Change Induced by Oxidation of Ag0 and Reduction of Ag+," *Environmental Science & Technology,* vol. 48, no. 1, pp. 403-411, 2014/01/07 2014.
[138] L.-J. A. Ellis, E. Valsami-Jones, J. R. Lead, and M. Baalousha, "Impact of surface coating and environmental conditions on the fate and transport of silver

nanoparticles in the aquatic environment," *Science of the Total Environment,* vol. 568, pp. 95-106, 2016.
[139] G.-P. Sheng, H.-Q. Yu, and X.-Y. Li, "Extracellular polymeric substances (EPS) of microbial aggregates in biological wastewater treatment systems: a review," *Biotechnology advances,* vol. 28, no. 6, pp. 882-894, 2010.
[140] K. Czaczyk and K. Myszka, "Biosynthesis of extracellular polymeric substances (EPS) and its role in microbial biofilm formation," *Polish Journal of Environmental Studies,* vol. 16, no. 6, p. 799, 2007.
[141] T. More, J. Yadav, S. Yan, R. Tyagi, and R. Surampalli, "Extracellular polymeric substances of bacteria and their potential environmental applications," *Journal of environmental management,* vol. 144, pp. 1-25, 2014.
[142] G. M. Teitzel and M. R. Parsek, "Heavy Metal Resistance of Biofilm and Planktonic Pseudomonas aeruginosa," *Applied & Environmental Microbiology,* Article vol. 69, no. 4, p. 2313, 2003.
[143] N. P. Ivleva, M. Wagner, H. Horn, R. Niessner, and C. Haisch, "In Situ Surface-Enhanced Raman Scattering Analysis of Biofilm," *Analytical Chemistry,* Article vol. 80, no. 22, pp. 8538-8544, 2008.
[144] B. Vu, C. Miao, R. J. Crawford, and E. P. Ivanova, "Bacterial Extracellular Polysaccharides Involved in Biofilm Formation," *Molecules,* Article vol. 14, no. 7, pp. 2535-2554, 2009.
[145] F. Kang, P. J. Alvarez, and D. Zhu, "Microbial extracellular polymeric substances reduce Ag+ to silver nanoparticles and antagonize bactericidal activity," *Environmental science & technology,* vol. 48, no. 1, pp. 316-22, 2014.
[146] K. Zhou, Y. Hu, L. Zhang, K. Yang, and D. Lin, "The role of exopolymeric substances in the bioaccumulation and toxicity of Ag nanoparticles to algae," *Scientific Reports,* vol. 6, p. 32998, 2016.
[147] P. Wang *et al.*, "Silver Nanoparticles Entering Soils via the Wastewater − Sludge − Soil Pathway Pose Low Risk to Plants but Elevated Cl Concentrations Increase Ag Bioavailability," 2016.
[148] B. Carr and M. Wright, "Nanoparticle tracking analysis," *Innovations in Pharmaceutical Technology,* vol. 26, pp. 38-40, 2008.
[149] Q. Tu *et al.*, "Microfluidic Device: A Miniaturized Platform for Chemical Reactions," *Chinese Journal of Chemistry,* vol. 31, no. 3, pp. 304-316, 2013.
[150] R. Daw and J. Finkelstein, "Lab on a chip," *Nature,* vol. 442, no. 7101, pp. 367-367, 2006.
[151] S. Kazim *et al.*, "Morphology and Kinetics of Aggregation of Silver Nanoparticles Induced with Regioregular Cationic Polythiophene," *Langmuir,* vol. 32, no. 1, pp. 2-11, 2016/01/12 2016.
[152] L. Mulfinger, S. D. Solomon, M. Bahadory, A. V. Jeyarajasingam, S. A. Rutkowsky, and C. Boritz, "Synthesis and Study of Silver Nanoparticles," *Journal of Chemical Education,* vol. 84, no. 2, p. 322, 2007/02/01 2007.
[153] D. L. Van Hyning and C. F. Zukoski, "Formation Mechanisms and Aggregation Behavior of Borohydride Reduced Silver Particles," *Langmuir,* vol. 14, no. 24, pp. 7034-7046, 1998/11/01 1998.
[154] D. K. Carpenter, "Dynamic Light Scattering with Applications to Chemistry, Biology, and Physics (Berne, Bruce J.; Pecora, Robert)," *Journal of Chemical Education,* vol. 54, no. 10, p. A430, 1977/10/01 1977.
[155] B. Michen *et al.*, "Avoiding drying-artifacts in transmission electron microscopy: Characterizing the size and colloidal state of nanoparticles," *Scientific Reports,* Article vol. 5, p. 9793, 05/12/online 2015.

[156] K. Mehrabi, B. Nowack, Y. Arroyo Rojas Dasilva, and D. M. Mitrano, "Improvements in Nanoparticle Tracking Analysis To Measure Particle Aggregation and Mass Distribution: A Case Study on Engineered Nanomaterial Stability in Incineration Landfill Leachates," *Environmental Science & Technology,* vol. 51, no. 10, pp. 5611-5621, 2017/05/16 2017.
[157] R. J. R. J. Hunter, *Foundations of Colloid Science*, 2nd ed ed. Oxford University Press, 2001.
[158] K.-S. Chou and Y.-S. Lai, "Effect of polyvinyl pyrrolidone molecular weights on the formation of nanosized silver colloids," *Materials Chemistry and Physics,* vol. 83, no. 1, pp. 82-88, 2004/01/15/ 2004.
[159] F. J. H., "The colloidal domain: Where physics, chemistry, biology, and technology meet. By D. Fennell Evans and Hakån Wennerström. VCH Publishers, New York 1994, XXXII, 515 pp., hardcover, $65.00, DM 980, ISBN 1–56081–525–6," *Advanced Materials,* vol. 8, no. 3, pp. 260-260, 1996.
[160] M. Popa, T. Pradell, D. Crespo, and J. M. Calderón-Moreno, "Stable silver colloidal dispersions using short chain polyethylene glycol," *Colloids and Surfaces A: Physicochemical and Engineering Aspects,* vol. 303, no. 3, pp. 184-190, 2007/08/15/ 2007.
[161] K.-S. Chou and C.-Y. Ren, "Synthesis of nanosized silver particles by chemical reduction method," *Materials Chemistry and Physics,* vol. 64, no. 3, pp. 241-246, 2000/05/15/ 2000.
[162] H. H. Huang *et al.*, "Photochemical Formation of Silver Nanoparticles in Poly(N-vinylpyrrolidone)," *Langmuir,* vol. 12, no. 4, pp. 909-912, 1996/01/01 1996.
[163] Z. Zhang, B. Zhao, and L. Hu, "PVP Protective Mechanism of Ultrafine Silver Powder Synthesized by Chemical Reduction Processes," *Journal of Solid State Chemistry,* vol. 121, no. 1, pp. 105-110, 1996/01/05/ 1996.
[164] M. Chen, L.-Y. Wang, J.-T. Han, J.-Y. Zhang, Z.-Y. Li, and D.-J. Qian, "Preparation and Study of Polyacryamide-Stabilized Silver Nanoparticles through a One-Pot Process," *The Journal of Physical Chemistry B,* vol. 110, no. 23, pp. 11224-11231, 2006/06/01 2006.
[165] H. Huey-Shan and H. Shan-hui, "Biological performances of poly(ether)urethane–silver nanocomposites," *Nanotechnology,* vol. 18, no. 47, p. 475101, 2007.
[166] L. M. Liz-Marzán and I. Lado-Touriño, "Reduction and Stabilization of Silver Nanoparticles in Ethanol by Nonionic Surfactants," *Langmuir,* vol. 12, no. 15, pp. 3585-3589, 1996/01/01 1996.
[167] M.-H. Lee, S.-G. Oh, K.-D. Suh, D.-G. Kim, and D. Sohn, "Preparation of silver nanoparticles in hexagonal phase formed by nonionic Triton X-100 surfactant," *Colloids and Surfaces A: Physicochemical and Engineering Aspects,* vol. 210, no. 1, pp. 49-60, 2002/10/16/ 2002.
[168] F. Mafuné, J.-y. Kohno, Y. Takeda, T. Kondow, and H. Sawabe, "Structure and Stability of Silver Nanoparticles in Aqueous Solution Produced by Laser Ablation," *The Journal of Physical Chemistry B,* vol. 104, no. 35, pp. 8333-8337, 2000/09/01 2000.
[169] D. Yu and V. W.-W. Yam, "Hydrothermal-Induced Assembly of Colloidal Silver Spheres into Various Nanoparticles on the Basis of HTAB-Modified Silver Mirror Reaction," *The Journal of Physical Chemistry B,* vol. 109, no. 12, pp. 5497-5503, 2005/03/01 2005.

[170] U. Anand, J. Lu, D. Loh, Z. Aabdin, and U. Mirsaidov, "Hydration Layer-Mediated Pairwise Interaction of Nanoparticles," *Nano Letters,* vol. 16, no. 1, pp. 786-790, 2016/01/13 2016.
[171] X. Zheng, L. Zhu, A. Yan, X. Wang, and Y. Xie, "Controlling synthesis of silver nanowires and dendrites in mixed surfactant solutions," *Journal of Colloid and Interface Science,* vol. 268, no. 2, pp. 357-361, 2003/12/15/ 2003.
[172] Y.-H. Chen and C.-S. Yeh, "Laser ablation method: use of surfactants to form the dispersed Ag nanoparticles," *Colloids and Surfaces A: Physicochemical and Engineering Aspects,* vol. 197, no. 1, pp. 133-139, 2002/02/04/ 2002.
[173] S. Skoglund *et al.*, "Effect of Laundry Surfactants on Surface Charge and Colloidal Stability of Silver Nanoparticles," *Langmuir,* vol. 29, no. 28, pp. 8882-8891, 2013/07/16 2013.
[174] Y. Zhang, J. Xia, J. Xu, B. Sun, W. Wu, and L. Zhu, "Impacts of surfactants on dissolution and sulfidation of silver nanowires in aquatic environments," *Environmental Science: Nano,* 10.1039/C8EN00898A vol. 5, no. 10, pp. 2452-2460, 2018.
[175] Y. Liang, S. A. Bradford, J. Simunek, H. Vereecken, and E. Klumpp, "Sensitivity of the transport and retention of stabilized silver nanoparticles to physicochemical factors," *Water Research,* vol. 47, no. 7, pp. 2572-2582, 2013/05/01/ 2013.
[176] V. Shah, B. Bharatiya, M. K. Mishra, D. Ray, and D. O. Shah, "Molecular insights into sodium dodecyl sulphate mediated control of size for silver nanoparticles," *Journal of Molecular Liquids,* vol. 273, pp. 222-230, 2019/01/01/ 2019.
[177] L. Kvítek *et al.*, "Effect of Surfactants and Polymers on Stability and Antibacterial Activity of Silver Nanoparticles (NPs)," *The Journal of Physical Chemistry C,* vol. 112, no. 15, pp. 5825-5834, 2008/04/01 2008.
[178] W. Zhang, B. Xiao, and T. Fang, "Chemical transformation of silver nanoparticles in aquatic environments: Mechanism, morphology and toxicity," *Chemosphere,* vol. 191, pp. 324-334, 2018/01/01/ 2018.
[179] R. A. Campbell, S. R. W. Parker, J. P. R. Day, and C. D. Bain, "External reflection FTIR spectroscopy of the cationic surfactant hexadecyltrimethylammonium bromide (CTAB) on an overflowing cylinder," *Langmuir,* vol. 20, no. 20, pp. 8740-8753, 2004/09/01 2004.
[180] G. Su, C. Yang, and J.-J. Zhu, "Fabrication of gold nanorods with tunable longitudinal surface plasmon resonance peaks by reductive dopamine," *Langmuir,* vol. 31, no. 2, pp. 817-823, 2015.
[181] R. M. El-Shishtawy, A. M. Asiri, and M. M. Al-Otaibi, "Synthesis and spectroscopic studies of stable aqueous dispersion of silver nanoparticles," *Spectrochimica Acta Part A: Molecular and Biomolecular Spectroscopy,* vol. 79, no. 5, pp. 1505-1510, 2011.
[182] M. Ortiz-Tafoya and A. Tecante, "Physicochemical characterization of sodium stearoyl lactylate (SSL), polyoxyethylene sorbitan monolaurate (Tween 20) and κ-carrageenan," *Data in brief,* vol. 19, pp. 642-650, 2018.
[183] A. C. Borges, A. Jayakrishnan, P.-E. Bourban, C. J. Plummer, D. P. Pioletti, and J.-A. E. Månson, "Synthesis and photopolymerization of tween 20 methacrylate/N-vinyl-2-pyrrolidone blends," *Materials Science and Engineering: C,* vol. 32, no. 8, pp. 2235-2241, 2012.

[184] E. Silva, S. M. Saraiva, S. P. Miguel, and I. J. Correia, "PVP-coated silver nanoparticles showing antifungal improved activity against dermatophytes," *Journal of Nanoparticle Research*, vol. 16, no. 11, p. 2726, 2014.
[185] R. Bryaskova, D. Pencheva, S. Nikolov, and T. Kantardjiev, "Synthesis and comparative study on the antimicrobial activity of hybrid materials based on silver nanoparticles (AgNps) stabilized by polyvinylpyrrolidone (PVP)," *Journal of Chemical Biology*, vol. 4, no. 4, p. 185, 2011.
[186] G. Socrates, *Infrared and Raman characteristic group frequencies: tables and charts*. John Wiley & Sons, 2004.
[187] K. Shameli *et al.*, "Synthesis and characterization of polyethylene glycol mediated silver nanoparticles by the green method," *International Journal of Molecular Sciences*, vol. 13, no. 6, pp. 6639-6650, 2012.
[188] T. C. Prathna, N. Chandrasekaran, and A. Mukherjee, "Studies on aggregation behaviour of silver nanoparticles in aqueous matrices: Effect of surface functionalization and matrix composition," *Colloids and Surfaces A: Physicochemical and Engineering Aspects*, vol. 390, no. 1, pp. 216-224, 2011/10/20/ 2011.
[189] Y. Zheng, M. Zheng, Z. Ma, B. Xin, R. Guo, and X. Xu, "Sugar Fatty Acid Esters," in *Polar Lipids*, M. U. Ahmad and X. Xu, Eds.: Elsevier, 2015, pp. 215-243.
[190] M. Takeo, "Disperse systems," *Disperse Systems, by Makoto Takeo, pp. 328. ISBN 3-527-29458-9. Wiley-VCH, March 1999.*, p. 328, 1999.
[191] Z. Fereshteh, R. Rojaee, and A. Sharifnabi, "Effect of different polymers on morphology and particle size of silver nanoparticles synthesized by modified polyol method," *Superlattices and Microstructures*, vol. 98, pp. 267-275, 2016/10/01/ 2016.
[192] R. M. Pashley and M. E. Karaman, *Applied Colloid and Surface Chemistry*. John Wiley & Sons, 2005.
[193] Y. Li, W. Zhang, J. Niu, and Y. Chen, "Surface-Coating-Dependent Dissolution, Aggregation, and Reactive Oxygen Species (ROS) Generation of Silver Nanoparticles under Different Irradiation Conditions," *Environmental Science & Technology*, vol. 47, no. 18, pp. 10293-10301, 2013/09/17 2013.
[194] S. K. Mwilu *et al.*, "Changes in silver nanoparticles exposed to human synthetic stomach fluid: Effects of particle size and surface chemistry," *Science of The Total Environment*, vol. 447, pp. 90-98, 2013/03/01/ 2013.
[195] J. Liu, Z. Wang, A. Sheng, F. Liu, F. Qin, and Z. L. Wang, "In Situ Observation of Hematite Nanoparticle Aggregates Using Liquid Cell Transmission Electron Microscopy," 2016.
[196] P. Mulvaney, "Surface Plasmon Spectroscopy of Nanosized Metal Particles," *Langmuir*, vol. 12, no. 3, pp. 788-800, 1996/01/01 1996.
[197] D. Paramelle, A. Sadovoy, S. Gorelik, P. Free, J. Hobley, and D. G. Fernig, "A rapid method to estimate the concentration of citrate capped silver nanoparticles from UV-visible light spectra," *Analyst*, 10.1039/C4AN00978A vol. 139, no. 19, pp. 4855-4861, 2014.
[198] Q. Chen, H. Cho, K. Manthiram, M. Yoshida, X. Ye, and A. P. Alivisatos, "Interaction Potentials of Anisotropic Nanocrystals from the Trajectory Sampling of Particle Motion using in Situ Liquid Phase Transmission Electron Microscopy," *ACS Central Science*, vol. 1, no. 1, pp. 33-39, 2015/03/25 2015.
[199] W. Zhou, Y.-L. Liu, A. M. Stallworth, C. Ye, and J. J. Lenhart, "Effects of pH, Electrolyte, Humic Acid, and Light Exposure on the Long-Term Fate of Silver

Nanoparticles," *Environmental Science & Technology,* vol. 50, no. 22, pp. 12214-12224, 2016/11/15 2016.
[200] X. Zou, J. Shi, and H. Zhang, "Morphological evolution and reconstruction of silver nanoparticles in aquatic environments: the roles of natural organic matter and light irradiation," *J Hazard Mater,* vol. 292, no. Supplement C, pp. 61-9, Jul 15 2015.
[201] C. Kostigen Mumper, A.-K. Ostermeyer, L. Semprini, and T. S. Radniecki, "Influence of ammonia on silver nanoparticle dissolution and toxicity to Nitrosomonas europaea," *Chemosphere,* vol. 93, no. 10, pp. 2493-2498, 2013/11/01/ 2013.
[202] S. S. Khan, A. Mukherjee, and N. Chandrasekaran, "Impact of exopolysaccharides on the stability of silver nanoparticles in water," *Water Research,* vol. 45, no. 16, pp. 5184-5190, 2011/10/15/ 2011.
[203] R. I. MacCuspie, "Colloidal stability of silver nanoparticles in biologically relevant conditions," *Journal of Nanoparticle Research,* vol. 13, no. 7, pp. 2893-2908, 2011/07/01 2011.
[204] H. Zhang, J. A. Smith, and V. Oyanedel-Craver, "The effect of natural water conditions on the anti-bacterial performance and stability of silver nanoparticles capped with different polymers," *Water Research,* vol. 46, no. 3, pp. 691-699, 2012/03/01/ 2012.
[205] T. Ung, L. M. Liz-Marzán, and P. Mulvaney, "Controlled Method for Silica Coating of Silver Colloids. Influence of Coating on the Rate of Chemical Reactions," *Langmuir,* vol. 14, no. 14, pp. 3740-3748, 1998/07/01 1998.
[206] T. Zhang *et al.,* "Role of Secondary Particle Formation in the Persistence of Silver Nanoparticles in Humic Acid Containing Water under Light Irradiation," *Environmental Science & Technology,* vol. 51, no. 24, pp. 14164-14172, 2017/12/19 2017.
[207] L. R. Pokhrel, B. Dubey, and P. R. Scheuerman, "Impacts of Select Organic Ligands on the Colloidal Stability, Dissolution Dynamics, and Toxicity of Silver Nanoparticles," *Environmental Science & Technology,* vol. 47, no. 22, pp. 12877-12885, 2013/11/19 2013.
[208] Y. Yin *et al.,* "Water chemistry controlled aggregation and photo-transformation of silver nanoparticles in environmental waters," *Journal of Environmental Sciences,* vol. 34, pp. 116-125, 2015.
[209] T. Silva, L. R. Pokhrel, B. Dubey, T. M. Tolaymat, K. J. Maier, and X. Liu, "Particle size, surface charge and concentration dependent ecotoxicity of three organo-coated silver nanoparticles: comparison between general linear model-predicted and observed toxicity," *Science of the total environment,* vol. 468, pp. 968-976, 2014.
[210] Z.-m. Xiu, Q.-b. Zhang, H. L. Puppala, V. L. Colvin, and P. J. Alvarez, "Negligible particle-specific antibacterial activity of silver nanoparticles," *Nano letters,* vol. 12, no. 8, pp. 4271-4275, 2012.
[211] H. Liu *et al.,* "Threshold Concentrations of Silver Ions Exist for the Sunlight-Induced Formation of Silver Nanoparticles in the Presence of Natural Organic Matter," *Environmental Science & Technology,* vol. 52, no. 7, pp. 4040-4050, 2018/04/03 2018.
[212] J. Buffle, K. J. Wilkinson, S. Stoll, M. Filella, and J. Zhang, "A Generalized Description of Aquatic Colloidal Interactions: The Three-colloidal Component Approach," *Environmental Science & Technology,* vol. 32, no. 19, pp. 2887-2899, 1998/10/01 1998.

[213] G. Cornelis, C. DooletteMadeleine Thomas, M. J. McLaughlin, J. K. Kirby, D. G. Beak, and D. Chittleborough, "Retention and Dissolution of Engineered Silver Nanoparticles in Natural Soils," (in English), *Soil Science Society of America Journal,* vol. 76, no. 3, pp. 891-902, 2012.
[214] W. Lu *et al.*, "Effect of surface coating on the toxicity of silver nanomaterials on human skin keratinocytes," *Chemical Physics Letters,* vol. 487, no. 1, pp. 92-96, 2010/02/25/ 2010.
[215] N. Akaighe, S. W. Depner, S. Banerjee, V. K. Sharma, and M. Sohn, "The effects of monovalent and divalent cations on the stability of silver nanoparticles formed from direct reduction of silver ions by Suwannee River humic acid/natural organic matter," *Science of The Total Environment,* vol. 441, pp. 277-289, 2012/12/15/ 2012.
[216] M. Delay, T. Dolt, A. Woellhaf, R. Sembritzki, and F. H. Frimmel, "Interactions and stability of silver nanoparticles in the aqueous phase: Influence of natural organic matter (NOM) and ionic strength," *Journal of Chromatography A,* vol. 1218, no. 27, pp. 4206-4212, 2011/07/08/ 2011.
[217] D. G. Kinniburgh, W. H. van Riemsdijk, L. K. Koopal, and M. F. Benedetti, "Chapter 23 - Ion Binding to Humic Substances: Measurements, Models, and Mechanisms," in *Adsorption of Metals by Geomedia,* E. A. Jenne, Ed. San Diego: Academic Press, 1998, pp. 483-520.
[218] R. Kretzschmar, H. Holthoff, and H. Sticher, "Influence of pH and humic acid on coagulation kinetics of kaolinite: a dynamic light scattering study," *Journal of colloid and interface science,* vol. 202, no. 1, pp. 95-103, 1998.
[219] D. Lu, Q. Liu, T. Zhang, Y. Cai, Y. Yin, and G. Jiang, "Stable silver isotope fractionation in the natural transformation process of silver nanoparticles," *Nature Nanotechnology,* vol. 11, p. 682, 06/20/online 2016.
[220] P. V. Kamat, M. Flumiani, and G. V. Hartland, "Picosecond Dynamics of Silver Nanoclusters. Photoejection of Electrons and Fragmentation," *The Journal of Physical Chemistry B,* vol. 102, no. 17, pp. 3123-3128, 1998/04/01 1998.
[221] C.-N. Lok *et al.*, "Silver nanoparticles: partial oxidation and antibacterial activities," *JBIC Journal of Biological Inorganic Chemistry,* vol. 12, no. 4, pp. 527-534, 2007/05/01 2007.
[222] J.-T. Tai *et al.*, "Protein–Silver Nanoparticle Interactions to Colloidal Stability in Acidic Environments," *Langmuir,* vol. 30, no. 43, pp. 12755-12764, 2014/11/04 2014.
[223] S. Sudheer Khan, A. Mukherjee, and N. Chandrasekaran, "Interaction of colloidal silver nanoparticles (SNPs) with exopolysaccharides (EPS) and its adsorption isotherms and kinetics," *Colloids and Surfaces A: Physicochemical and Engineering Aspects,* vol. 381, no. 1, pp. 99-105, 2011/05/20/ 2011.
[224] Y. Li, C. Yang, X. Guo, Z. Dang, X. Li, and Q. Zhang, "Effects of humic acids on the aggregation and sorption of nano-TiO2," *Chemosphere,* vol. 119, pp. 171-176, 2015.
[225] M. Kiser, P. Westerhoff, T. Benn, Y. Wang, J. Perez-Rivera, and K. Hristovski, "Titanium nanomaterial removal and release from wastewater treatment plants," *Environmental science & technology,* vol. 43, no. 17, pp. 6757-6763, 2009.
[226] S. A. Blaser, M. Scheringer, M. MacLeod, and K. Hungerbühler, "Estimation of cumulative aquatic exposure and risk due to silver: contribution of nano-functionalized plastics and textiles," *Science of the total environment,* vol. 390, no. 2-3, pp. 396-409, 2008.

[227] B. Kim, C.-S. Park, M. Murayama, and M. F. Hochella, "Discovery and Characterization of Silver Sulfide Nanoparticles in Final Sewage Sludge Products," *Environmental Science & Technology,* vol. 44, no. 19, pp. 7509-7514, 2010/10/01 2010.
[228] Z. Wei, S. Huang, Y. Zhang, H. Li, and S. Zhou, "Characterization of extracellular polymeric substances produced during nitrate removal by a thermophilic bacterium Chelatococcus daeguensis TAD1 in batch cultures," *RSC Advances,* vol. 7, no. 70, pp. 44265-44271, 2017.
[229] A. Omoike and J. Chorover, "Adsorption to goethite of extracellular polymeric substances from Bacillus subtilis," *Geochimica et Cosmochimica Acta,* vol. 70, no. 4, pp. 827-838, 2006.
[230] M. Hoffman and A. W. Decho, "Extracellular enzymes within microbial biofilms and the role of the extracellular polymer matrix," in *Microbial extracellular polymeric substances*: Springer, 1999, pp. 217-230.
[231] D. Lin, S. Drew Story, S. L. Walker, Q. Huang, and P. Cai, "Influence of extracellular polymeric substances on the aggregation kinetics of TiO2 nanoparticles," *Water Research,* vol. 104, pp. 381-388, 2016/11/01/ 2016.
[232] G.-H. Yu, P.-J. He, L.-M. Shao, and P.-P. He, "Stratification structure of sludge flocs with implications to dewaterability," *Environmental science & technology,* vol. 42, no. 21, pp. 7944-7949, 2008.
[233] R. Weiner, S. Langille, and E. Quintero, "Structure, function and immunochemistry of bacterial exopolysaccharides," *Journal of industrial microbiology,* vol. 15, no. 4, pp. 339-346, 1995.
[234] C. Mayer *et al.*, "The role of intermolecular interactions: studies on model systems for bacterial biofilms," *International journal of biological macromolecules,* vol. 26, no. 1, pp. 3-16, 1999.
[235] X.-M. Liu *et al.*, "Contribution of extracellular polymeric substances (EPS) to the sludge aggregation," *Environmental science & technology,* vol. 44, no. 11, pp. 4355-4360, 2010.
[236] F. Ahimou, M. J. Semmens, G. Haugstad, and P. J. Novak, "Effect of protein, polysaccharide, and oxygen concentration profiles on biofilm cohesiveness," *Appl. Environ. Microbiol.,* vol. 73, no. 9, pp. 2905-2910, 2007.
[237] P. Lembre, C. Lorentz, and P. Di Martino, "Exopolysaccharides of the biofilm matrix: a complex biophysical world," *The complex world of polysaccharides,* pp. 371-392, 2012.
[238] J. Labille, F. Thomas, M. Milas, and C. Vanhaverbeke, "Flocculation of colloidal clay by bacterial polysaccharides: effect of macromolecule charge and structure," *Journal of colloid and interface science,* vol. 284, no. 1, pp. 149-156, 2005.
[239] B. Koukal *et al.*, "Effect of Pseudokirchneriella subcapitata (Chlorophyceae) exudates on metal toxicity and colloid aggregation," *Water research,* vol. 41, no. 1, pp. 63-70, 2007.
[240] X. Zhou, Q. Wang, G. Jiang, P. Liu, and Z. Yuan, "A novel conditioning process for enhancing dewaterability of waste activated sludge by combination of zero-valent iron and persulfate," *Bioresource technology,* vol. 185, pp. 416-420, 2015.
[241] D. Li, Y. Zhou, Y. Tan, S. Pathak, M. bin Abdul Majid, and W. J. Ng, "Alkali-solubilized organic matter from sludge and its degradability in the anaerobic process," *Bioresource technology,* vol. 200, pp. 579-586, 2016.

[242] M. Dubois, K. A. Gilles, J. K. Hamilton, P. t. Rebers, and F. Smith, "Colorimetric method for determination of sugars and related substances," *Analytical chemistry,* vol. 28, no. 3, pp. 350-356, 1956.
[243] B. Fr, T. Griebe, and P. Nielsen, "Enzymatic activity in the activated-sludge floc matrix," *Applied microbiology and biotechnology,* vol. 43, no. 4, pp. 755-761, 1995.
[244] K. Xiao *et al.*, "Variations in physical, chemical and biological properties in relation to sludge dewaterability under Fe (II)–Oxone conditioning," *Water research,* vol. 109, pp. 13-23, 2017.
[245] S. A. Huber, A. Balz, M. Abert, and W. Pronk, "Characterisation of aquatic humic and non-humic matter with size-exclusion chromatography–organic carbon detection–organic nitrogen detection (LC-OCD-OND)," *Water research,* vol. 45, no. 2, pp. 879-885, 2011.
[246] L. Varden and F. Bou-Abdallah, "Detection and separation of inorganic cations in natural, potable, and wastewater samples using capillary zone electrophoresis with indirect UV detection," *American journal of analytical chemistry,* vol. 8, no. 1, p. 81, 2017.
[247] A. Katsoyiannis and C. Samara, "The fate of dissolved organic carbon (DOC) in the wastewater treatment process and its importance in the removal of wastewater contaminants," *Environmental Science and Pollution Research-International,* vol. 14, no. 5, pp. 284-292, 2007.
[248] I. Fernando and Y. Zhou, "Concentration dependent effect of humic acid on the transformations of silver nanoparticles," *Journal of Molecular Liquids,* vol. 284, pp. 291-299, 2019/06/15/ 2019.
[249] K. L. Chen and M. Elimelech, "Aggregation and Deposition Kinetics of Fullerene (C60) Nanoparticles," *Langmuir,* vol. 22, no. 26, pp. 10994-11001, 2006/12/01 2006.
[250] X. Huangfu, J. Jiang, J. Ma, Y. Liu, and J. Yang, "Aggregation Kinetics of Manganese Dioxide Colloids in Aqueous Solution: Influence of Humic Substances and Biomacromolecules," *Environmental Science & Technology,* vol. 47, no. 18, pp. 10285-10292, 2013/09/17 2013.
[251] N. B. Saleh, L. D. Pfefferle, and M. Elimelech, "Influence of Biomacromolecules and Humic Acid on the Aggregation Kinetics of Single-Walled Carbon Nanotubes," *Environmental Science & Technology,* vol. 44, no. 7, pp. 2412-2418, 2010/04/01 2010.
[252] W. Zhang, U. s. Rattanaudompol, H. Li, and D. Bouchard, "Effects of humic and fulvic acids on aggregation of aqu/nC60 nanoparticles," *Water Research,* vol. 47, no. 5, pp. 1793-1802, 2013/04/01/ 2013.
[253] D. Lu, K. Xiao, Y. Chen, Y. N. A. Soh, and Y. Zhou, "Transformation of dissolved organic matters produced from alkaline-ultrasonic sludge pretreatment in anaerobic digestion: From macro to micro," *Water Res,* vol. 142, pp. 138-146, May 25 2018.
[254] J. T. G. Overbeek, "The rule of Schulze and Hardy," *Pure and Applied Chemistry,* vol. 52, no. 5, pp. 1151-1161, 1980.
[255] A. R. Petosa, D. P. Jaisi, I. R. Quevedo, M. Elimelech, and N. Tufenkji, "Aggregation and deposition of engineered nanomaterials in aquatic environments: role of physicochemical interactions," *Environmental science & technology,* vol. 44, no. 17, pp. 6532-6549, 2010.
[256] A.-K. Ostermeyer, C. Kostigen Mumuper, L. Semprini, and T. Radniecki, "Influence of Bovine Serum Albumin and Alginate on Silver Nanoparticle

Dissolution and Toxicity to Nitrosomonas europaea," *Environmental Science & Technology,* vol. 47, no. 24, pp. 14403-14410, 2013/12/17 2013.
[257] X. Liu, M. Wazne, Y. Han, C. Christodoulatos, and K. L. Jasinkiewicz, "Effects of natural organic matter on aggregation kinetics of boron nanoparticles in monovalent and divalent electrolytes," *Journal of colloid and interface science,* vol. 348, no. 1, pp. 101-107, 2010.
[258] Q. Li and M. Elimelech, "Organic fouling and chemical cleaning of nanofiltration membranes: measurements and mechanisms," *Environmental science & technology,* vol. 38, no. 17, pp. 4683-4693, 2004.
[259] L. M. Mosley, K. A. Hunter, and W. A. Ducker, "Forces between colloid particles in natural waters," *Environmental science & technology,* vol. 37, no. 15, pp. 3303-3308, 2003.
[260] Y. Zhou, S. Xia, J. Zhang, B. T. Nguyen, and Z. Zhang, "Insight into the influences of pH value on Pb (II) removal by the biopolymer extracted from activated sludge," *Chemical Engineering Journal,* vol. 308, pp. 1098-1104, 2017.
[261] G. Guibaud, N. Tixier, A. Bouju, and M. Baudu, "Relation between extracellular polymers' composition and its ability to complex Cd, Cu and Pb," *Chemosphere,* vol. 52, no. 10, pp. 1701-1710, 2003.
[262] Y. Zhou, S. Xia, Z. Zhang, J. Zhang, and S. W. Hermanowicz, "Associated adsorption characteristics of Pb (II) and Zn (II) by a novel biosorbent extracted from waste-activated sludge," *Journal of Environmental Engineering,* vol. 142, no. 7, p. 04016032, 2016.
[263] Y. Zhou, S. Xia, J. Zhang, Z. Zhang, and S. W. Hermanowicz, "Adsorption characterizations of biosorbent extracted from waste activated sludge for Pb(II) and Zn(II)," *Desalination and Water Treatment,* vol. 57, no. 20, pp. 9343-9353, 2016/04/26 2016.
[264] M. Iqbal, A. Saeed, and S. I. Zafar, "FTIR spectrophotometry, kinetics and adsorption isotherms modeling, ion exchange, and EDX analysis for understanding the mechanism of Cd2+ and Pb2+ removal by mango peel waste," *Journal of hazardous materials,* vol. 164, no. 1, pp. 161-171, 2009.
[265] G. Guibaud, S. Comte, F. Bordas, and M. Baudu, "Metal removal from single and multimetallic equimolar systems by extracellular polymers extracted from activated sludges as evaluated by SMDE polarography," *Process Biochemistry,* vol. 40, no. 2, pp. 661-668, 2005.
[266] B. Cao *et al.*, "Extracellular polymeric substances from Shewanella sp. HRCR‐1 biofilms: characterization by infrared spectroscopy and proteomics," *Environmental Microbiology,* vol. 13, no. 4, pp. 1018-1031, 2011.
[267] L. Wei *et al.*, "Adsorption of Cu2+ and Zn2+ by extracellular polymeric substances (EPS) in different sludges: Effect of EPS fractional polarity on binding mechanism," *Journal of hazardous materials,* vol. 321, pp. 473-483, 2017.
[268] G. Guibaud, S. Comte, F. Bordas, S. Dupuy, and M. Baudu, "Comparison of the complexation potential of extracellular polymeric substances (EPS), extracted from activated sludges and produced by pure bacteria strains, for cadmium, lead and nickel," *Chemosphere,* vol. 59, no. 5, pp. 629-638, 2005.
[269] Y. Liu, W. Lv, Z. Zhang, and S. Xia, "Influencing characteristics of short-time aerobic digestion on spatial distribution and adsorption capacity of extracellular polymeric substances in waste activated sludge," *RSC Advances,* vol. 8, no. 56, pp. 32172-32177, 2018.

[270] F. Brian-Jaisson *et al.*, "Characterization and anti-biofilm activity of extracellular polymeric substances produced by the marine biofilm-forming bacterium Pseudoalteromonas ulvae strain TC14," *Biofouling*, vol. 32, no. 5, pp. 547-560, 2016.
[271] G. You *et al.*, "Effects of CeO2 nanoparticles on production and physicochemical characteristics of extracellular polymeric substances in biofilms in sequencing batch biofilm reactor," *Bioresource Technology*, vol. 194, pp. 91-98, 2015/10/01/ 2015.
[272] D. K. Božanić, S. Dimitrijević-Branković, N. Bibić, A. Luyt, and V. Djoković, "Silver nanoparticles encapsulated in glycogen biopolymer: Morphology, optical and antimicrobial properties," *Carbohydrate polymers*, vol. 83, no. 2, pp. 883-890, 2011.
[273] S. A. Huber, "Evidence for membrane fouling by specific TOC constituents," *Desalination*, vol. 119, no. 1-3, pp. 229-234, 1998.
[274] M. Luo *et al.*, "Properties of different natural organic matter influence the adsorption and aggregation behavior of TiO2 nanoparticles," *Journal of Saudi Chemical Society*, vol. 22, no. 2, pp. 146-154, 2018.
[275] X. Guo, X. Wang, and J. Liu, "Composition analysis of fractions of extracellular polymeric substances from an activated sludge culture and identification of dominant forces affecting microbial aggregation," *Scientific reports*, vol. 6, p. 28391, 2016.
[276] I. Metcalf & Eddy, *Wastewater engineering : treatment, disposal, and reuse*. New York: McGraw-Hill, 1991.
[277] J. Zook, S. E Long, D. Cleveland, C. Lay A Geronimo, and R. Maccuspie, *Measuring silver nanoparticle dissolution in complex biological and environmental matrices using UV-visible absorbance*. 2011, pp. 1993-2002.
[278] R. D. Vasquez *et al.*, "Polysaccharide-mediated green synthesis of silver nanoparticles from Sargassum siliquosum JG Agardh: Assessment of toxicity and hepatoprotective activity," *OpenNano*, vol. 1, pp. 16-24, 2016.
[279] S. Sanyasi *et al.*, "Polysaccharide-capped silver Nanoparticles inhibit biofilm formation and eliminate multi-drug-resistant bacteria by disrupting bacterial cytoskeleton with reduced cytotoxicity towards mammalian cells," *Scientific reports*, vol. 6, p. 24929, 2016.
[280] L. Guerrini, R. Alvarez-Puebla, and N. Pazos-Perez, "Surface modifications of nanoparticles for stability in biological fluids," *Materials*, vol. 11, no. 7, p. 1154, 2018.
[281] W. S. Ang, A. Tiraferri, K. L. Chen, and M. Elimelech, "Fouling and cleaning of RO membranes fouled by mixtures of organic foulants simulating wastewater effluent," *Journal of Membrane Science*, vol. 376, no. 1, pp. 196-206, 2011/07/01/ 2011.
[282] M. Mahmoudi, I. Lynch, M. R. Ejtehadi, M. P. Monopoli, F. B. Bombelli, and S. Laurent, "Protein− nanoparticle interactions: opportunities and challenges," *Chemical reviews*, vol. 111, no. 9, pp. 5610-5637, 2011.
[283] D. C. António, C. Cascio, D. Gilliland, A. J. Nogueira, F. Rossi, and L. Calzolai, "Characterization of silver nanoparticles-alginate complexes by combined size separation and size measurement techniques," *Biointerphases*, vol. 11, no. 4, p. 04B309, 2016.
[284] S. Khan, A. Gupta, N. Verma, and C. Nandi, "Kinetics of protein adsorption on gold nanoparticle with variable protein structure and nanoparticle size," *The Journal of chemical physics*, vol. 143, no. 16, p. 164709, 2015.

[285] Z. Nie *et al.*, "Enhanced radical scavenging activity by antioxidant-functionalized gold nanoparticles: A novel inspiration for development of new artificial antioxidants," *Free Radical Biology and Medicine*, vol. 43, no. 9, pp. 1243-1254, 2007/11/01/ 2007.
[286] R. Sukirtha *et al.*, "Cytotoxic effect of Green synthesized silver nanoparticles using Melia azedarach against in vitro HeLa cell lines and lymphoma mice model," *Process Biochemistry*, vol. 47, no. 2, pp. 273-279, 2012.
[287] F. Foliatini, Y. Yulizar, and M. A. E. Hafizah, "The synthesis of alginate-capped silver nanoparticles under microwave irradiation," *Journal of Mathematical and Fundamental Sciences*, vol. 47, no. 1, pp. 31-50, 2015.
[288] Y. Shao *et al.*, "Green synthesis of sodium alginate-silver nanoparticles and their antibacterial activity," *International journal of biological macromolecules*, vol. 111, pp. 1281-1292, 2018.
[289] D.-P. Yang *et al.*, "Highly sensitive electrochemiluminescence biosensor for cholesterol detection based on AgNPs-BSA-MnO2 nanosheets with superior biocompatibility and synergistic catalytic activity," *Sensors and Actuators B: Chemical*, vol. 260, pp. 642-649, 2018.
[290] N. Dasgupta, S. Ranjan, D. Patra, P. Srivastava, A. Kumar, and C. Ramalingam, "Bovine serum albumin interacts with silver nanoparticles with a “side-on” or “end on” conformation," *Chemico-biological interactions*, vol. 253, pp. 100-111, 2016.
[291] A. Rajeshwari, S. Pakrashi, S. Dalai, V. Iswarya, N. Chandrasekaran, and A. Mukherjee, "Spectroscopic studies on the interaction of bovine serum albumin with Al2O3 nanoparticles," *Journal of Luminescence*, vol. 145, pp. 859-865, 2014.
[292] S. M. Ricci, J. Talbot, P. Schaaf, B. Senger, and J. C. Voegel, "A Lattice Model for the Adsorption Kinetics of Proteins on Solid Surfaces," *The Journal of Physical Chemistry*, vol. 98, no. 18, pp. 4906-4912, 1994/05/01 1994.
[293] K. Rezwan, L. P. Meier, M. Rezwan, J. Vörös, M. Textor, and L. J. Gauckler, "Bovine Serum Albumin Adsorption onto Colloidal Al2O3 Particles: A New Model Based on Zeta Potential and UV−Vis Measurements," *Langmuir*, vol. 20, no. 23, pp. 10055-10061, 2004/11/01 2004.
[294] X. Li and J. J. Lenhart, "Aggregation and Dissolution of Silver Nanoparticles in Natural Surface Water," *Environmental Science & Technology*, vol. 46, no. 10, pp. 5378-5386, 2012/05/15 2012.
[295] J. Israelachvili and H. Wennerström, "Role of hydration and water structure in biological and colloidal interactions," *Nature*, vol. 379, no. 6562, p. 219, 1996.
[296] V. Parsegian and T. Zemb, "Hydration forces: Observations, explanations, expectations, questions," *Current opinion in colloid & interface science*, vol. 16, no. 6, pp. 618-624, 2011.
[297] J. P. Cleveland, T. Schäffer, and P. K. Hansma, "Probing oscillatory hydration potentials using thermal-mechanical noise in an atomic-force microscope," *Physical Review B*, vol. 52, no. 12, p. R8692, 1995.
[298] J. I. Kilpatrick, S.-H. Loh, and S. P. Jarvis, "Directly probing the effects of ions on hydration forces at interfaces," *Journal of the American Chemical Society*, vol. 135, no. 7, pp. 2628-2634, 2013.
[299] J. E. Evans, K. L. Jungjohann, N. D. Browning, and I. Arslan, "Controlled growth of nanoparticles from solution with in situ liquid transmission electron microscopy," *Nano letters*, vol. 11, no. 7, pp. 2809-2813, 2011.

[300] Y. Liu, X.-M. Lin, Y. Sun, and T. Rajh, "In situ visualization of self-assembly of charged gold nanoparticles," *Journal of the American Chemical Society,* vol. 135, no. 10, pp. 3764-3767, 2013.
[301] M. Williamson, R. Tromp, P. Vereecken, R. Hull, and F. Ross, "Dynamic microscopy of nanoscale cluster growth at the solid–liquid interface," *Nature materials,* vol. 2, no. 8, p. 532, 2003.
[302] H. Zheng, R. K. Smith, Y.-w. Jun, C. Kisielowski, U. Dahmen, and A. P. Alivisatos, "Observation of single colloidal platinum nanocrystal growth trajectories," *Science,* vol. 324, no. 5932, pp. 1309-1312, 2009.
[303] N. De Jonge and F. M. Ross, "Electron microscopy of specimens in liquid," *Nature nanotechnology,* vol. 6, no. 11, p. 695, 2011.
[304] B. H. Kim, J. Yang, D. Lee, B. K. Choi, T. Hyeon, and J. Park, "Liquid‐phase transmission electron microscopy for studying colloidal inorganic nanoparticles," *Advanced Materials,* vol. 30, no. 4, p. 1703316, 2018.
[305] I. Fernando and Y. Zhou, "Impact of pH on the stability, dissolution and aggregation kinetics of silver nanoparticles," *Chemosphere,* vol. 216, pp. 297-305, 2019/02/01/ 2019.
[306] J. Lu, Z. Aabdin, N. D. Loh, D. Bhattacharya, and U. Mirsaidov, "Nanoparticle dynamics in a nanodroplet," *Nano letters,* vol. 14, no. 4, pp. 2111-2115, 2014.
[307] E. White, M. Mecklenburg, B. Shevitski, S. Singer, and B. Regan, "Charged nanoparticle dynamics in water induced by scanning transmission electron microscopy," *Langmuir,* vol. 28, no. 8, pp. 3695-3698, 2012.
[308] E. A. Ring and N. de Jonge, "Video-frequency scanning transmission electron microscopy of moving gold nanoparticles in liquid," *Micron,* vol. 43, no. 11, pp. 1078-1084, 2012.
[309] J. Liu, Z. Wang, A. Sheng, F. Liu, F. Qin, and Z. L. Wang, "In Situ Observation of Hematite Nanoparticle Aggregates Using Liquid Cell Transmission Electron Microscopy," *Environmental Science & Technology,* vol. 50, no. 11, pp. 5606-5613, 2016/06/07 2016.
[310] G. Bradski, "The opencv library," *Dr Dobb's J. Software Tools,* vol. 25, pp. 120-125, 2000.
[311] N. Otsu, "A threshold selection method from gray-level histograms," *IEEE transactions on systems, man, and cybernetics,* vol. 9, no. 1, pp. 62-66, 1979.
[312] P. Ngabonziza, M. Stehno, G. Koster, and A. Brinkman, *In-Situ Characterization Techniques for Nanomaterials*, 1 ed. Springer, 2018.
[313] T. J. Woehl, K. L. Jungjohann, J. E. Evans, I. Arslan, W. D. Ristenpart, and N. D. Browning, "Experimental procedures to mitigate electron beam induced artifacts during in situ fluid imaging of nanomaterials," *Ultramicroscopy,* vol. 127, pp. 53-63, 2013.
[314] H. Zheng, S. A. Claridge, A. M. Minor, A. P. Alivisatos, and U. Dahmen, "Nanocrystal diffusion in a liquid thin film observed by in situ transmission electron microscopy," *Nano letters,* vol. 9, no. 6, pp. 2460-2465, 2009.
[315] W. R. Bowen and A. O. Sharif, "Long-range electrostatic attraction between like-charge spheres in a charged pore," *Nature,* vol. 393, no. 6686, p. 663, 1998.